# Metastasis of Pancreatic Cancer:

# Influence of the hepatic microenvironment on the growth behavior of pancreatic ductal epithelial cells

**Dissertation**

Zur Erlangung des Doktorgrades der
Mathematisch-Naturwissenschaftlichen Fakultät der
Christian-Albrechts-Universität zu Kiel

vorgelegt von
**Lennart Terje Niklas Lenk**
aus Hamburg

Kiel im August 2017

Erste Gutachterin: Prof. Dr. rer. nat. Susanne Sebens

Zweiter Gutachter: Prof. Dr. rer. nat. Thomas Roeder

Tag der mündlichen Prüfung: 16. Oktober 2017

Zum Druck genehmigt: 16. Oktober 2017

Parts of this thesis have been published elsewhere:

**Lenk L**, Pein M, Will O, Gomez B, Viol F, Hauser C, Egberts JH, Gundlach JP, Helm O, Tiwari S, Weiskirchen R, Rose-John S, Röcken C, Mikulits W, Wenzel P, Schneider G, Saur D, Schäfer H, Sebens S. The hepatic microenvironment essentially determines tumor cell dormancy and metastatic outgrowth of pancreatic ductal adenocarcinoma. *OncoImmunology* (In press)

Für meine Familie

# Summary

Pancreatic ductal adenocarcinoma (PDAC) represents the fourth common cause of cancer-related deaths worldwide. Most PDACs are diagnosed at advanced stage when distant metastasis already emerged. Even patients successfully undergoing complete resection of the primary tumor usually develop distant metastasis shortly after surgery. PDAC metastases mostly form in the liver, whereas recent studies suggest that dissemination of pancreatic ductal epithelial cells (PDECs) to this site may already occur prior to primary tumor formation. Yet, it remains widely unclear how the hepatic microenvironment and its condition impact on metastatic outgrowth of disseminated PDECs. Therefore, this study aimed at elucidating the impact of a physiological liver microenvironment, characterized by hepatic stellate cells (HSCs) and an inflammatory hepatic microenvironment, featuring high abundance of hepatic myofibroblasts (HMFs), on growth behavior of premalignant and malignant PDECs.

Characterization of liver metastases in PDAC bearing mice unveiled the emergence of micrometastases with low amounts of proliferating tumor cells in HSCs-rich microenvironments, whereas macrometastases with significantly higher quantities of proliferating tumor cells were detected in HMFs-rich areas. To examine if inflammatory conditions in the liver promote growth of disseminated PDAC cells, a syngeneic mouse model was deployed for which aging was selected as inflammatory stimulus. Two weeks after orthotopic injection of R254 PDAC cells, aged mice exposed significantly higher amounts of proliferating disseminated tumor cells (DTCs) in the liver than young mice whereas primary tumor size of both groups was comparable. Gene expression analysis of liver tissues showed higher expression of HMFs-related genes including vascular endothelial growth factor (VEGF) in aged mice while young animals showed higher expression of functional homologues of human interleukin-8 (IL-8). Importantly, four weeks after tumor cell injection, micrometastases were exclusively detected in livers of aged mice.

To examine underlying mechanisms of these findings, an indirect coculture system was utilized in which premalignant H6c7-kras cells or malignant Panc1 cells were cultured in presence of HSCs or HMFs. In line with *in vivo* findings, presence of HSCs resulted in a significantly lower amount of proliferative H6c7-kras and Panc1 cells compared to HMFs coculture. Interestingly, HSCs coculture induced a quiescence-associated phenotype (QAP) in both PDEC lines, characterized by flattened and enlarged morphology, absence of Ki67, low phosphorylated (p)-ERK/p-p38 ratio, accompanied by higher p21 protein levels and senescence-associated β-galactosidase activity than HMFs cocultured PDECs. Of note, HSCs-mediated growth arrest could be identified as a state of dormancy. When

cultivating HSCs cocultured Panc1 cells in presence of HMFs for further 6 days, a significant amount of Panc1 cells with QAP features regained proliferative activity. This effect was less pronounced in H6c7-kras cells, indicating a lower propensity of premalignant PDECs to escape dormancy. Importantly, IL-8 was identified as inducer of HSCs-mediated QAP, whereas VEGF could be identified as a factor by which HMFs promote growth and revert dormancy in PDECs.
Taken together, this work shows a striking impact of the hepatic microenvironment and its condition on the growth behavior of premalignant and malignant PDECs, thereby identifying HSCs and HMFs as components of a dormancy permissive or restrictive hepatic microenvironment, respectively. Moreover, this is the first study providing ample evidence that aging-related inflammation of the liver acts to promote metastatic outgrowth of dormant pancreatic DTCs.

# Zusammenfassung

Das duktale Adenokarzinom des Pankreas (PDAC) stellt die vierthäufigste Ursache krebsbedingter Todesursachen weltweit dar. Das PDAC wird meist in fortgeschrittenem Stadium diagnostiziert, wenn bereits Fernmetastasen entstanden sind. Sogar solche Patienten bei denen der Primärtumor vollständig reseziert werden kann, entwickeln gewöhnlich Fernmetastasen kurze Zeit nach dem Eingriff. PDAC-Metastasen bilden sich zumeist in der Leber, wobei neuere Studien darauf hinweisen, dass die Disseminierung von pankreatischen Duktusepithelzellen (PDEZ) in die Leber der vollständigen Entwicklung des Primärtumors vorausgehen kann. Jedoch ist bislang kaum bekannt, wie die hepatische Mikroumgebung und ihr Zustand das Auswachsen von disseminierten PDEZ zu Metastasen beeinflussen können. Das Ziel dieser Studie war es daher, den Einfluss einer physiologischen Leberumgebung, charakterisiert durch hepatische Sternzellen (HSZ), und einer entzündlichen Mikroumgebung, charakterisiert durch hepatische Myofibroblasten (HMF), auf das Wachstumsverhalten von prämalignen und malignen PDEZ aufzuklären.

Die Charakterisierung von Lebermetastasen in einem endogenen PDAC-Mausmodell deckte das Aufkommen von Mikrometastasen mit einer geringen Anzahl an proliferierenden Tumorzellen in HSZ-reichen Mikroumgebungen auf, während Makrometastasen mit einer signifikant höheren Anzahl an proliferierenden Tumorzellen in HMF-reichen Mikroumgebungen festgestellt wurden. Um zu untersuchen, ob inflammatorische Bedingungen in der Leber das Wachstum disseminierter PDAC-Zellen fördern, wurde ein syngenes Mausmodell angewendet, für welches Altern als Entzündungs-stimulus gewählt wurde. Zwei Wochen nach der orthotopen Injektion von R254-PDAC-Zellen zeigten gealterte Mäuse eine signifikant höhere Anzahl an proliferierenden disseminierten Tumorzellen (DTZ) in der Leber als junge Mäuse, wobei Primärtumoren vergleichbare Größen aufwiesen. Genexpressionsanalysen von Lebergeweben zeigten eine deutlich höhere Expression von HMF-assoziierten Genen, einschließlich *Vascular Endothelial Growth Factor* (*VEGF*) in gealterten Mäusen, während junge Mäuse eine höhere Expression der funktionellen Homologe des humanen *Interleukin-8* (*IL-8*) aufwiesen. Hervorzuheben ist, dass vier Wochen nach Tumorzell-Injektion Mikrometastasen ausschließlich in älteren Mäusen detektiert wurden. Um die diesen Befunden unterliegenden Mechanismen aufzuklären, wurde ein indirektes Kokultur-System angewendet, in welchem prämaligne H6c7-kras-Zellen oder maligne Panc1-Zellen in Gegenwart von HSZ oder HMF kultiviert wurden. In Einklang mit den *in vivo* Befunden resultierte die Gegenwart von HSZ in einer signifikant niedrigeren Anzahl an proliferierenden H6c7-kras- und Panc1-Zellen. HSZ induzierten einen Quieszenz-assoziierten Phänotyp (QAP) in beiden PDEZ-Linien. Dieser zeich-

nete sich durch eine abgeflachte und vergrößerte Morphologie, die Abwesenheit von Ki67, einem niedrigen Verhältnis von phosphoryliertem (p-)ERK zu p-p38, begleitet von einer höheren p21 Proteinmenge und Seneszenz-assoziierter β-Galactosidase-Aktivität als in HMF-kokultivierten PDEZ aus. Zudem konnte dieser HSZ-vermittelte Wachstumsarrest als Zustand von Tumorzelldormanz identifiziert werden. Die Untersuchung HSZ-kokultivierter Panc1-Zellen, die anschließend in Gegenwart von HMF kultiviert wurden, zeigte die Wiedererlangung proliferativer Aktivität in einem deutlichen Anteil an Panc1-Zellen mit QAP-Eigenschaften. Dieser Effekt war weniger stark ausgeprägt in H6c7-kras-Zellen, was eine geringere Tendenz von prämalignen PDEZ, den Dormanz-Zustand zu verlassen, anzeigt. IL-8 konnte als Induktor des HSZ-vermittelten QAP bestimmt werden, während VEGF als Faktor identifiziert wurde, über den HMF das Wachstum und die Reversion von Dormanz in PDEZ fördern.
Zusammengenommen zeigen die Ergebnisse dieser Arbeit einen beachtlichen Einfluss der hepatischen Mikroumgebung und ihres Zustandes auf das Wachstumsverhalten von prämalignen und malignen PDEZ und identifizieren HSZ und HMF als Komponenten einer Dormanz-permissiven bzw. -restriktiven Leberumgebung. Dies ist die erste Studie, die zeigt, dass altersbedingte Entzündung in der Leber das Auswachsen ruhender pankreatischer DTZ begünstigt.

# List of Abbreviations

| | |
|---|---|
| **5-FU** | **5-F**luoro**u**racil |
| **(v/v)** | **v**olume/**v**olume percent |
| **(w/v)** | **w**eight/**v**olume percent |
| **°C** | **Degree Celcius** |
| **α-SMA** | **α-s**mooth-**m**uscle-**a**ctin |
| **µ** | **Micro** |
| **APS** | **A**mmonium **p**er**s**ulfate |
| **AT** | **A**us**t**ria |
| **ATRA** | **A**ll-**t**rans **r**etinoic **a**cid |
| **BPE** | **B**ovine **p**ituitary **e**xtract |
| **BSA** | **B**ovine **s**erum **a**lbumin |
| **BW** | **B**ody **w**eight |
| **CAF** | **C**ancer-**a**ssociated **f**ibroblast |
| **$C_t$** | **C**ycle **t**hreshold |
| **cDNA** | **C**omplementary **d**eoxyribonucleic **a**cid |
| **CH** | **Switzerland** |
| **CK** | **C**yto**k**eratin |
| **$CO_2$** | **C**arbon **di**hydr**o**xide |
| **Col** | **Col**lagen |
| **CPS** | **c**ounts **p**er **s**econd |
| **CT** | **C**omputed **t**omography |
| **CTCs** | **C**irculating **t**umor **c**ell**s** |
| **CXCR** | **CXC** chemokine **r**eceptor |
| **dd$H_2$O** | **D**ouble **d**istilled **w**ater |
| **DE** | **Germany** |
| **DDR** | **D**NA **d**amage **r**esponse |
| **DMEM** | **D**ulbecco's **M**odified **E**agle **M**edium |
| **DNA** | **D**eoxyribo**n**ucleic **a**cid |
| **dsDNA** | **D**ouble **s**tranded **d**eoxyribo**n**ucleic **a**cid |
| **dsRNA** | **D**ouble **s**tranded **r**ibo**n**ucleic **a**cid |
| **DTC** | **D**isseminated **t**umor **c**ell |
| **ECM** | **E**xtra**c**ellular **m**atrix |
| **EDTA** | **E**thylene**d**iamine**t**etraacetic **a**cid |
| **EGF** | **E**pidermal **g**rowth **f**actor |
| **EMT** | **E**pithelial **m**esenchymal **t**ransition |
| **ELISA** | **E**nzyme-**l**inked **I**mmuno**s**orbent **A**ssay |
| **FCS** | **F**etal **c**alf **s**erum |

| | |
|---|---|
| **FFPE** | **F**ormalin-**f**ixed **p**arrafin-**e**mbedded |
| **FGF** | **F**ibroblast **g**rowth **f**actor |
| **fw** | **F**or**w**ard |
| **g** | **G**ram |
| **GFP** | **G**reen **f**luorescent **p**rotein |
| **h** | **H**our |
| **$H_2O$** | **Water** |
| **HMFs** | **H**epatic **m**yo**f**ibroblast**s** |
| **HMF** | The **h**epatic **m**yo**f**ibroblast **c**ell line M-HT |
| **HPV-E6E7** | **H**uman **p**apilloma**v**irus **E6 E7** |
| **HRP** | **H**orse**r**adish **p**eroxidase |
| **HSCs** | **H**epatic **s**tellate **c**ell**s** |
| **HSC** | The **h**epatic **s**tellate **c**ell line M1-4HSC |
| **HSP** | **H**eat**s**hock **p**rotein |
| **HNSC** | **H**ead and **n**eck **s**quamous **c**arcinoma |
| **ICC** | **I**mmuno**c**yto**c**hemistry |
| **IGF** | **I**nsulin **g**rowth **f**actor |
| **IL** | **I**nter**l**eukin |
| **KC** | **K**eratinocyte **c**hemoattractant |
| **l** | **L**iter |
| **L-Gln** | **L-Gl**utami**n**e |
| **LIX** | **L**ipopolysaccharide-**i**nduced C**X**C chemokine |
| **m** | **M**eter |
| **MAPK** | **M**itogen **a**ctivated **p**rotein **k**inases |
| **M** | **M**olar |
| **MET** | **M**esenchymal **e**pithelial **t**ransition |
| **mA** | **M**illi**a**mpere |
| **mg** | **M**illi**g**ram |
| **MHz** | **M**ega**h**ert**z** |
| **min** | **Min**ute |
| **ml** | **M**illi**l**iter |
| **mm** | **M**illi**m**eter |
| **MIF** | **M**acrophage migration **i**nhibitory **f**actor |
| **MIP** | **M**acrophage **i**nflammatory **p**rotein |
| **MMPs** | **M**atrix **m**etallo**p**roteinase**s** |
| **M-MuLV** | **M**oloney **M**urine **L**eukemia **V**irus |
| **MRD** | **M**inimal **r**esidual **d**isease |

| | |
|---|---|
| **mRNA** | **M**essenger **r**ibo**n**ucleic **a**cid |
| **n** | **N**ano |
| **NaPyr** | **N**atrium **pyr**vate |
| **OD** | **O**ptical **d**ensity |
| **OIS** | **O**ncogene-**i**nduced **s**enescence |
| **One-way RM ANOVA** | **R**epeated **m**easures **an**alysis **o**f **va**riance |
| **PanIN** | **Pan**creatic **i**ntraepithelial **n**eoplasia |
| **PBS** | **P**hosphate-**b**uffered **s**aline |
| **Pen/Strep** | **Pen**icillin and **strep**tomycin |
| **PDAC** | **P**ancreatic **d**uctal **a**deno**c**arcinoma |
| **PDEC** | **P**ancreatic **d**uctal **e**pithelial **c**ell |
| **PDGF** | **P**latelet-**d**erived **g**rowth **f**actor |
| **PFA** | **P**ara**f**orme**a**ldehyde |
| **ph** | **Ph**oton |
| **Phosphorylated-ERK** | **p-ERK** |
| **Phosphorylated-p38** | **pp38** |
| **PVDF** | **P**oly**v**inyli**d**ene **f**luoride |
| **QAP** | **Q**uiescence-**a**ssociated **p**henotype |
| **qRT-PCR** | **Q**uantitative **r**eal**t**ime **p**olymerase **c**hain **r**eaction |
| **r** | **r**ecombinant |
| **Rb** | **R**etino**b**lastom protein |
| **RNA** | **R**ibo**n**ucleic **a**cid |
| **RNAi** | **R**ibo**n**ucleic **a**cid **i**nterference |
| **RPMI** | **R**oswell **P**ark **m**emorial **i**nstitute |
| **RT** | **R**oom **t**emperature |
| **rv** | **R**e**v**erse |
| **SABG** | **S**enescence-**a**ssociated β-**g**alactosidase |
| **SASP** | **S**enescence-**a**ssociated **s**ecretory **p**henotype |
| **SD** | **S**tandard **d**eviation |
| **SDF-1** | **S**tromal **d**erived **f**actor **1** |
| **SDS** | **S**odium **d**odecyl **s**ulfate |
| **SDS-PAGE** | **S**odium **d**odecyl **s**ulfate **p**olyacrylamide **g**el **e**lectrophoresis |
| **sec** | **Sec**onds |
| **shRNA** | **S**hort **h**airpin **r**ibo**n**ucleic **a**cid |
| **siRNAs** | **S**mall **i**nterfering **r**ibo**n**ucleic **a**cid |
| **SIS** | **S**tress-**i**nduced **s**enescence |

| | |
|---|---|
| **TAMs** | **T**umor-**a**ssociated **m**acrophage**s** |
| **TBS** | **T**ris **b**ase **s**odium chloride |
| **TBS-T** | **TBS-T**ween |
| **TEMED** | **Te**tra**m**ethyl**e**thylene**d**iamine |
| **TGF-β** | **T**ransforming **g**rowth **f**actor **beta** |
| **TNF-α** | **T**umor **n**ecrosis **f**actor **alpha** |
| **U** | Enzyme **u**nit |
| **UK** | **U**nited **k**ingdom |
| **US** | **U**nited **s**tates |
| **UV** | **U**ltra **v**iolet |
| **VEGF** | **V**ascular **e**ndothelial **g**rowth **f**actor |
| **WB** | **W**estern **b**lot |
| **Wks** | **w**eeks |
| **xg** | **G**ravitational force |

# Contents

# 1. Introduction

## 1.1. The pancreatic ductal adenocarcinoma (PDAC)

### 1.1.1. Epidemiology and etiology

The pancreatic ductal adenocarcinoma (PDAC) is characterized by an aggressive biology and a particularly poor prognosis. About 18.600 new cases of PDAC were predicted for the year 2016 in Germany [1]. Despite its low incidence of 14.3 per 100.000 male inhabitants and 11.3 per 100.000 female inhabitants PDAC is ranked the fourth leading cause of cancer-related deaths in Germany and the most fatal malignancy of the gastrointestinal tract [1, 2]. PDAC has a 5 year survival rate of solely 8 % and a 10 year survival rate of 7 % whereas most patients will succumb to the disease within the first 12 months after prognosis [1, 3]. Accordingly, the count of new cases of PDAC nearly equals the number of PDAC-related deaths. Whereas significant effort has been invested in the exploration of PDAC in the last decades, no evident progress regarding the curability of this disease has been made. A recent report accordingly predicted that by 2030 PDAC will be the second leading cause of cancer-related deaths worldwide [4]. PDAC is a disease of elderly patients. The median age upon diagnosis is 71 for male and 75 for female patients while the lifetime risk to develop PDAC is 1.49 % [5]. PDAC makes itself felt by unspecific symptoms, which mostly emerge in the late stage of carcinogenesis. Upon diagnosis 80 % of PDAC patients present with an advanced stage of the disease, commonly when metastatic spread has already occurred. In this case, a curative therapy is no longer feasible and patients will be subjected to palliative care [6]. To date, full resection of the tumor represents the only curative therapy option for PDAC patients in Germany [6]. Perfidiously, even patients who successfully undergo complete tumor resection without detectable PDAC cells in the tumor margin (R0) commonly develop local recurrences or metastases within months after surgical intervention [7, 8]. In the consequence, 80 % of PDAC patients being treated after curative therapy schemes will also die within the first 2 years after diagnosis [9, 10]

To date only a few risk factors for PDAC development are ensured. Most of these

factors are attributable to lifestyle and hence represent modifiable risk factors. Foremost smoking accounts for 20 % - 35 % of PDAC cases and increases the disease risk about 2.2-fold [11, 12]. The risk to develop PDAC is still modestly elevated even 10 years after smoking cessation [11]. Excessive alcoholic abuse is recognized as a further lifestyle factor promoting the development of PDAC. An increased and dose dependent disease risk was assessed for the consumption of more than three drinks a day [13]. Furthermore, alcohol and its metabolites were shown to exhibit direct carcinogenic potential and represent the main factors to drive pancreatitis [14]. Accordingly, chronic pancreatitis, among other sustained inflammatory conditions, is assumed to pave the ground for PDAC development [15]. Moreover, a correlation between diabetes mellitus type 1 and type 2 and PDAC carcinogenesis has been reported [16, 17]. Further studies accordingly suggest that dietary factors and obesity increase the PDAC disease risk. For instance, a prospective study with adult U.S. citizens associated a body mass index (BMI) higher than 40 $kg/m^2$ with a relative disease risk of 1.49 for men and 2.76 for women [18].

About 10 % of all PDAC cases are based on a hereditary background. Various genetic conditions have been linked to PDAC carcinogenesis, among them Peutz-Jeghers syndrome, hereditary pancreatitis and cystic fibrosis. The penetration of these predispositions is commonly high and raises the risk to develop PDAC by 2-fold to 132-fold [5, 19, 20]. A better understanding of the causes and risks that promote the development of PDAC is needed to improve patient prognosis. To date, only a conscious lifestyle or a lifestyle change regarding the above mentioned factors are considered to lower the chance of developing PDAC. Next to regular physical activity, fat-reduced nutrition and the consumption of fruits, vegetables and whole grains represent accepted beneficial lifestyle components [21, 22].

### 1.1.2. Pathology

The pancreas is a glandular organ compartmentalized into an exocrine and endocrine gland [23]. The exocrine serous tissue produces bicarbonate-rich digestive juice which is drained into the duodenum via acinus ducts [24]. The endocrine pancreas is formed by islets of Langerhans. Latter ones produce glucagon, insulin, somatostatin, pancreatic polypeptide and ghrelin which are directly released into the blood circulation [25]. Both parts of the pancreas can give rise to tumors. Tumors of the exocrine pancreas tissue represent 95 % of all cancers of the pancreas. Among these, PDAC exposes the highest prevalence and accounts for 90 % of all cases [9]. Other malignancies of the exocrine pancreas like the mucinous cystadenocarcinoma or the acinar adenocarcinoma as well as tumors of the endocrine pancreas expose a superior prognosis to PDAC due to the earlier emergence of

symptoms and better therapy response [26, 27].
The PDAC is assumed to emerge by stepwise progression from precursor lesions like the intraductal papillary mucinous neoplasia (IPMN), mucinous cystic neoplasia (MCN) or pancreatic intraepithelial neoplasia (PanIN) [28]. More recently, the acinoductal compartment has been established as a potential origin of PDAC [29]. Acinoductal structures may undergo acinar to ductal metaplasia (ADM) and subsequently develop to tubular complexes (TC) and atypical flat lesions (AFL). This process may lead to PanIN formation or represent and independent progenitor of PDAC [30]. Among the potential precursor lesions of PDAC the highest significance is accredited to PanINs. These represent asymptomatic lesions composed of mucinous columnar and cuboidal cells. They are categorized into different stages according to the degree of hyperplasia and dysplasia [31]. In contrast to the physiological pancreas duct which exhibits a monolayered, highly prismatic and polarized epithelium, PanIN-1 lesions expose low grade mucinous dysplasia (PanIN-1a) or papillary duct structures (PanIN-1b) with a basal polarization of nuclei [32]. PanIN-2 lesions are characterized by nuclear pleomorphism and high amounts of papillae [33]. Finally, PanIN-3 lesions show a high grade of dysplasia and hyperplasia while epithelial cells in contrast to carcinoma maintain their contact to the basement membrane and are non-invasive. They are hence referred to as *carcinoma in situ* [32].
The multistep progression from a healthy pancreatic ductal epithelium to PDAC via PanIN lesions is hallmarked by common genetic and epigenetic alterations. Most abundant and detected in about 95 % of all PDAC cases is the $KRAS^{G12D}$ point mutation [34, 35]. This mutation is already detectable in most PanIN-1 lesions [36]. The gene product of the *KRAS* proto-oncogene interacts with several signaling molecules with implications in cellular proliferation, survival, differentiation and migration [37]. *KRAS* mutations are hence recognized as the main driver mutations of PanIN initiation and progression [36]. Further common mutations detectable already at the early PanIN stage are *P16/CDKN2A*, *GNAS* and *BRAF* [36]. Later mutational events in the pathogenesis of PDAC are loss of function of *TP53* and *SMAD4* which are reported to occur at the PanIN-3 stage [38]. Mutations in *TP53* are found in 75 % of all PDAC [39]. The most common mutational events accompanying PanIN progression are depicted in **Figure 1.1**.

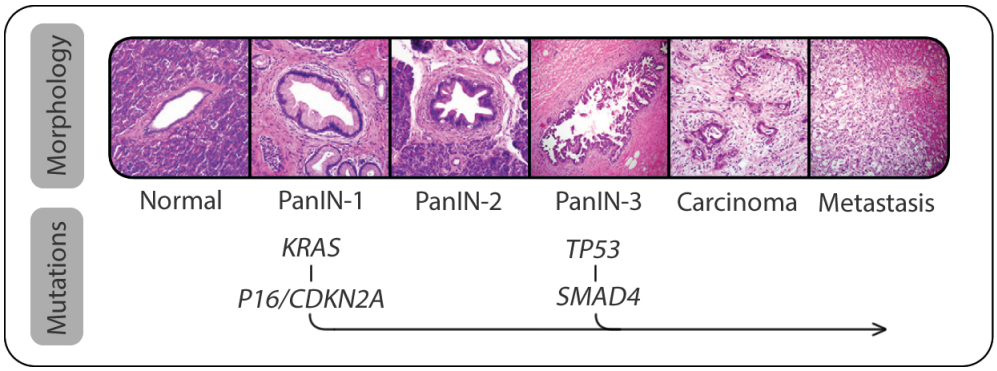


**Figure 1.1.: Development of primary PDAC.** A normal pancreas duct develops to PDAC via stepwise progression of pancreatic intraepithelial neoplastia (PanIN) lesions. PanIN progression is accompanied by the frequent accumulation of mutations. Upper panel: Hematoxilin eosin (HE) stainings of pancreas sections (adapted from Han and Hoff, 2013). Lower panel: The four most common driver mutations of PDAC.

A distinctive pathologic hallmark of PDAC is its pronounced desmoplastic reaction. Unlike most other cancer entities, PDAC tumors comprise a vast amount of non-neoplastic cells and corresponding extracellular matrix (ECM). The activated profound tumor stroma of PDAC can make up to 80 % of the entire tumor volume [40]. A plethora of different non-neoplastic cells contribute to the desmoplastic reaction. Immune cells like mast cells, macrophages, lymphocytes and plasma cells as well as adipocytes and endothelial cells can be found in the PDAC stroma [41–43]. Cancer-associated fibroblasts (CAFs) represent the predominant cellular component of the PDAC stroma. These emerge from pancreatic stellate cells (PSC) and represent the source of the majority of ECM molecules in the tumor mass. Hence, increasing amounts of type I, type III and type V collagen (col) and fibronectin can be detected during PDAC progression [42, 44]. Furthermore, PSCs and CAFs produce various cytokines, chemokines and growth factors which support primary tumor progression [45]. The recruitment and activation of PSCs was shown to occur already at the PanIN stage [46]. While a tumor promoting impact of the PDAC stroma was considered as ensured, recent studies challenged this dogma and claimed that the stroma may act to restrain tumor progression [47, 48]. In fact, compelling evidence for either mode of action of the tumor stroma was brought forward. On the one hand various studies accordingly support the view that the desmoplastic reaction represents the basis for the profound chemoresistance of PDAC [49, 50]. On the other hand it was recently shown that depletion of CAFs can result in more dedifferentiated and aggressive PDAC tumors [47, 48].

### 1.1.3. Therapy and clinical challenges

Various clinical factors contribute to the aggravated treatability and corresponding dismal prognosis of PDAC. Foremost the late occurrence of symptoms and their ambiguity narrow the timeframe for a potential curative clinical intervention [5]. Moreover, due to its posterior position in the abdomen the pancreas itself is difficult to access by most imaging modalities [6]. Common imaging techniques like sonography, computed tomography or magnetic resonance imaging (MRI) are only feasible to detect primary tumors which exceed a certain size [51]. Furthermore, the close proximity of the pancreas to truncus coeliacus, duodenum, common bile duct, arteria mesenterica superior and hepatic portal vein render the resection of PDAC a most challenging and time consuming surgical intervention [6, 9]. Concurrently, invasion of local lymph nodes is commonly observed in PDAC [52]. As a result of the entirety of these clinical factors, a successful R0 resection is only achieved in about 30 – 50 % of operated PDAC patients [53]. Compared to R0 resection, R1 resection status represents a negative prognostic factor and commonly leads to local recurrence [54]. However, as mentioned above, even patients who underwent R0 resection present with a local relapse and/or liver metastases within the first months after surgery [7, 8, 53]. A further challenge oncologists have to face is PDAC's profound chemoresistance [6]. In fact, the spectrum of potential adjuvant and neo-adjuvant chemotherapy approaches to prolong PDAC patient survival is nearly exhausted. In the curative and palliative setting gemcitabine is the common drug of choice and increases the overall survival to about 6 months [55]. More recently, the addition of nab-paclitaxel to gemcitabine treatment has been approved as beneficial and was shown to lead to an increased overall survival of 8.5 months compared to gemcitabine monotherapy [56]. Patients in palliative care can be treated after the polychemotherapeutical FOLFIRINOX therapy scheme. This comprises folinic acid, 5-fluoruracil (5-FU), irinotecan as well as oxaliplatin and leads to an overall survival of 11 months. However, albeit enhanced progression free survival this treatment exhibits a considerable toxicity profile and is only applicable to patients in an adequate general condition [57]. Finally, even the curative approach, encompassing surgical resection and adjuvant gemcitabine treatment, achieves an overall survival of 12-19 months [58]. Hence, novel curative and palliative therapy approaches as well as more sensitive detection techniques are urgently needed to oppose the aggressive nature of PDAC. In the last years, the tumor stroma shifted into the focus of attention of PDAC research as it comprises several potential targets of therapeutical intervention [59].

## 1.2. Metastasis

The vast majority of cancer patients does not die in the wake of the primary tumor but metastatic disease [60]. Yet, current therapy options are not fitted to particularly target PDAC metastases whereas the resistance mechanisms of primary and secondary lesions to chemotherapy may differ fundamentally. To achieve success in the treatment of metastatic disease, a better understanding of the various steps of metastatic progression is urgently demanded.

### 1.2.1. The invasion-metastasis cascade in carcinoma

A tumor cell has to acquire certain genetic alterations and morphologic features to successfully leave the primary organ and form a metastatic lesion at the secondary site. The microenvironment and the condition of the neoplastic cell itself determine the success of this process [61].

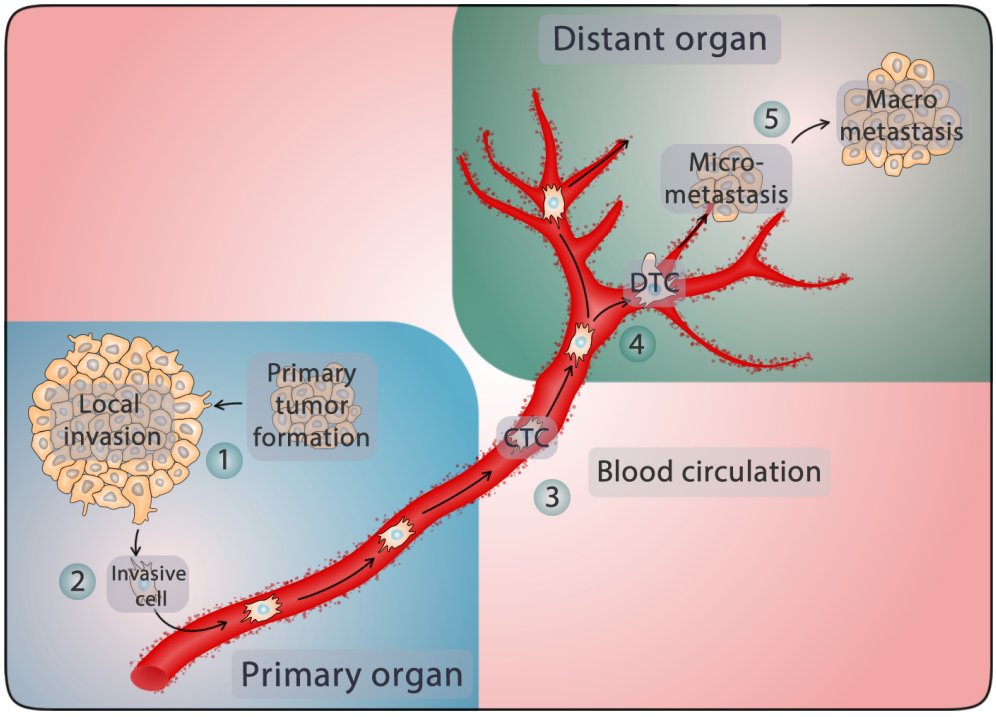


**Figure 1.2.: The invasion-metastasis cascade of malignant carcinoma.** A primary tumor forms (1) and cells from this tumor invade the local tissue (2). Some cells manage to intravasate into newly formed blood vessels and to survive as circulating tumor cell (CTC) in the blood circulation (3). At the distant organ, some cells adhere to the endothelial surface and extravasate into the organ (4). Disseminated tumor cells (DTCs) form a micrometastasis which later on outgrows to an overt and clinically detectable metastasis (5).

As the first step of malignant progression, neoplastic cells need to acquire invasive features enabling them to perforate the basement membrane and penetrate the surrounding tissue [62]. In order to evade the primary context, invasive cells

must intravasate into the blood circulation or infest the lymphatic system [63]. Neoplastic cells are then transported to distant organs as single or clustered circulating tumor cells (CTCs) and subsequently extravasate at the secondary site [63]. Cells which successfully migrated into a distant compartment or organ are termed disseminated tumor cells (DTCs). If single DTCs or DTC clusters possess an adequate equipment to survive and proliferate in the secondary microenvironment they may outgrow to overt metastases [61]. A graphic scheme of the invasion-metastasis cascade of carcinoma is depicted in **Figure 1.2**.
The basement membrane represents an organised scaffold that separates epithelia and endothelia from the underlying connective tissue [62]. Neoplastic cells express various proteases like metalloproteases (MMPs) which facilitate the penetration of this scaffold and digestion of the dense ECM of the microenvironment [64]. Moreover, epithelial to mesenchymal transition (EMT) is considered an important prerequisite in this context [65]. During EMT, epithelial cells lose their polarity and acquire a motile mesenchymal phenotype. This process is promoted by transcription factors like Slug, Snail, Twist and ZEB-1 which initiate the downregulation of epithelial molecules, e.g. E-cadherin, occludin and cytokeratins and upregulation of mesenchymal markers like vimentin [66]. In the consequence, the intercellular contact is disrupted and cells may leave the epithelial context to invade the surrounding tissue. The microenvironment plays a crucial role in the induction of EMT in neoplastic cells as stromal cells may release EMT promoting factors. For example macrophages, myofibroblasts and other stromal cells are reported sources of tumor necrosis factor-$\alpha$ (TNF -$\alpha$) and transforming growth factor-$\beta$ (TGF-$\beta$), both of which are potent inducers of EMT processes [67–69]. In this fashion, a desmoplastic stroma encompassing a primary lesion may further boost the invasive behavior and aggressiveness of cells which successfully left their epithelial context. Moreover, the process of EMT has been linked to the acquisition of cancer stemness features. This includes an enhanced self-renewal capacity and the initiation of survival pathways which are mandatory to overcome apoptosis cues elicited by immune cells [70]. The major route of metastatic spread is the haematogenous circulation [71]. The intravasation of neoplastic cells into the circulation is supported by angiogenesis processes accompanying primary tumor progression [71]. In contrast to normal vessels, those emerging during angiogenesis expose a diffuse growth and morphology and exhibit increased permeability which facilitates the entry of invasive cells into the circulation [72]. However, once entered the bloodstream CTCs need to evade prevailing shear forces and the elimination by immune cells. By the expression of tissue factor (TF) which acts as an initiator of platelet coagulation, CTCs gain a significant advantage for survival. The TF-mediated accumulation of platelets around the CTC protects

the cell of physical stress and concurrently impedes CTC lysis by NK cells [73, 74]. Once arrived at the secondary organ, CTCs must attach to the luminal side of vascular endothelial cells and breach the sub-epithelial ECM [75]. The extravasation of CTCs is facilitated by platelet-mediated upregulation of CCL2 which promotes monocyte recruitment and vascular permeability [76]. Furthermore, recent *in vitro* and *in vivo* studies suggest that the reversion of EMT and newly acquisition of an epithelial phenotype during mesenchymal to epithelial transition (MET) may increase the chance for carcinoma cells to successfully seed in the secondary organ [77]. Finally, cells which successfully disseminated need to establish a growth promoting niche to eventually outgrow to clinical relevant metastases. It his hence assumed that pre-existing inflammatory conditions in the secondary environment increase the likelihood of successful metastatic progression. However, which cell entities of the secondary microenvironment are involved in this process and the mechanisms by which they impact on DTCs is poorly understood.

### 1.2.2. Limiting steps in the metastatic cascade

The various steps a neoplastic cell has to take in order to evade the primary epithelium and to colonize a distant organ represent stochastic events and are all connected with a significant risk of elimination [78]. The initial loss of contact to the basement membrane represents one of the first apoptotic stimuli a neoplastic cell has to overcome [79]. In the blood circulation, CTCs are constantly exposed to numerous immune regulatory components and distinct physical stress cues [71]. A high proportion of CTCs falls a victim to apoptosis while being trapped in the branches of the secondary vasculature since CTCs have a diameter which is 3 to 4 times larger than the pores of capillaries in distant organs [80]. Importantly, most of the cells which manage to seed the secondary organ are poorly adapted to the prevalent conditions in the microenvironment they encounter and are consequently growth arrested [81]. In a pioneering mouse study the highest number of tumor cells failed to initiate growth after successful dissemination to the secondary organ [82]. Further clinical data suggest that the process of colonization may occur with a notable delay since breast cancer patients develop metastases up to decades after initial treatment even in the absence of a detectable primary tumor [83]. These data indicate that colonization of the secondary organ may indeed represent the most rate-limiting step in the metastatic cascade. Overall, cancer metastasis is a highly inefficient process. Mathematical modelling of the metastatic cascade predicted that less than 0.01 % of CTCs shed into the circulation effectively form a clinical relevant metastatic lesion [84, 85]. However, parameters leading to this low value may fundamentally differ between different cancer entities since some cancer entities like lung cancer or PDAC expose a

particular rapid occurrence of metastasis after initial diagnosis [86].

### 1.2.3. Metastasis in PDAC

Gaining a profound understanding of the metastatic progression of PDAC is of particular significance as the presence of metastases by the time of diagnosis impedes a curative therapy attempt. The hallmark genetic alterations of PDAC may represent distinct components of the disease's metastatic propensity as mutations in *KRAS*, *P16/CDKN2A*, *TP53* and *SMAD4* have been implicated in metastatic processes in PDAC mouse models as well as patient samples, respectively [60]. Historically, the prevalent opinion on PDAC metastasis was that neoplastic cells demand the entirety of these mutations to escape the primary context and disseminate to distant organs. Tumor cell dissemination and metastasis formation were accordingly recognized as late events in the evolution of PDAC and other cancer entities. In fact, Yachida *et al.* could show that the development from a normal cell to a neoplastic cell with metastatic capacity takes nearly 20 years and that metastasis occurs in the last 3 years before patient's decease [87]. However, more recent reports argue that PDAC dissemination may occur concomitantly to primary tumor progression when only few genetic alterations have been acquired [88]. This hypothesis is partially based on the clinical observation that the majority of PDAC patients who undergo surgical resection and show no signs of metastasis succumb to metastatic disease within 5 years [8]. Further support for this hypothesis was recently brought forward by Rhim *et al.* who provided experimental evidence for the early dissemination of pancreatic ductal epithelial cells (PDECs). Using fluorescence based lineage tracing they detected PDECs in the circulation and livers of mice carrying pancreas duct specific *KRAS* and *TP53* mutations (KPC) that harbored only PanIN lesions. These cells exposed a mesenchymal phenotype and markers of cancer-initiating cells. Importantly, circulating PDECs isolated from *KRAS* mutated mice (KC) exposed poor colony formation capacity *in vitro* indicating that further intrinsic alterations or environmental cues are necessary for successful colonization [89]. Interestingly, the same group was able to detect circulating PDECs in blood samples of patients with pancreatic cystic lesions strongly indicating clinical relevance of early dissemination of PDECs from precancerous lesions [90]. The current view on the invasion and metastasis cascade of PDAC under particular consideration of the early dissemination model is schematically depicted in **Figure 1.3**.

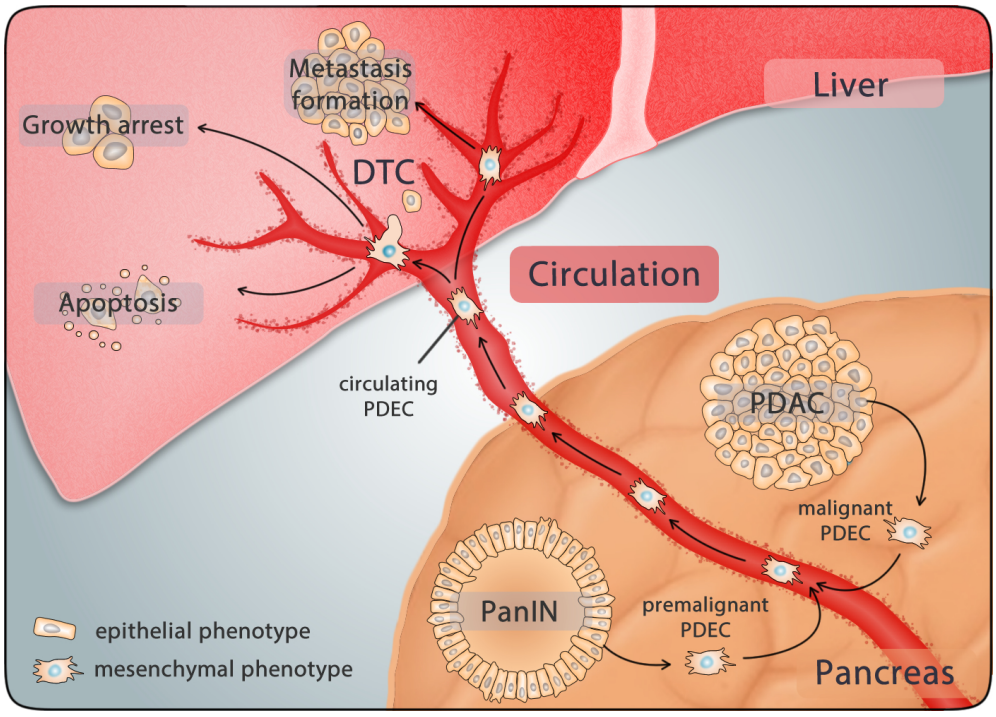


**Figure 1.3.: The invasion-metastasis cascade in PDAC.** Pancreatic ductal epithelial cells (PDECs) first invade the surrounding connective tissue. PDECs may derive from an established primary tumor or, as more recent reports suggest, also from precancerous lesions like PanIN [89, 90]. In this case, epithelial-to-mesenchymal transition may precede the complete acquisition of PDAC hallmark mutations. After intravasation, premalignant PDECs from PanIN lesions or malignant PDAC cells may similarly be found in the circulation as circulating PDECs. After reaching the liver, disseminated PDECs are confronted with conditions of the secondary foreign microenvironment that may determine if these cells may go into apoptosis, become growth arrested or outgrow to overt metastases.

## 1.3. Role of the cellular hepatic microenvironment in PDAC metastasis

PDAC cells comprise the propensity to metastasize to various organs including the peritoneum, lungs, bones and lymph nodes [91]. However 80 % of PDAC patients develop metastases in the liver rendering it the predominant site of metastatic spread in PDAC [92]. A particular understanding of the organ as well as the interplay of cell types it encompasses with DTCs is mandatory to identify potential novel targets for therapeutical intervention [93]. The liver is the central metabolic organ in vertebrates. It is located in the right epigastrium in close proximity to pancreas, bile, stomach, duodenum and colon [94]. Its central physiologic tasks are the detoxification of detrimental compounds and metabolites as well as the production of bile. Furthermore, the liver is critically involved in the biosynthesis of amino acids and clotting factors as well as the storage of glycogen [95]. The organ's haemal supply is provided by hepatic sinusoids which distribute blood inflowing from the vena portae (75 %) and ar-

teria hepatica propria (25 %) whereas both vessels represent potential entrance routes for CTCs [93]. It is hence assumed that the liver is predominantly seeded by PDECs due to its direct circulatory conjunction with the pancreas via the vena portae [96]. However, the poor efficiency of metastatic processes described above strongly indicates that additional cellular adaption processes are required to effectively colonize the hepatic microenvironment [96]. In 1889, Stephen Paget formulated the 'seed and soil theory' claiming that a DTC of a certain tumor entity ('seed') demands the interplay with a particular secondary environment ('soil') for successful metastatic colonization [97]. This theory, describing a process also referred to as tumor cell homing was validated by various studies which demonstrated that DTCs of different cancer entities selectively seed in specific target organs [97, 98]. Hence, the unique composition of the liver may represent a particular sanctuary for DTCs of pancreas duct origin. The predominant cell type endemic to the liver is the parenchymatic hepatocyte occupying about 80 % of the organ's volume [99]. Non-parenchymatic cells represent 40 % of the hepatic cell repertoire [99]. Among non-parenchymatic cells Kupffer cells are the most abundant ones. They represent a specialized type of macrophages which differentiate in the liver and are detectable along the sinusoidal walls [100]. Kupffer cells are among other functions responsible for the phagocytosis of e.g. bacteria and aged erythrocytes in the hepatic blood circulation [101]. A particular role in the context of inflammation assume hepatic stellate cells (HSCs) which represent the second most abundant non-parenchymatic cell entity in the liver. In a physiological liver, quiescent HSCs represent 5 % - 8 % of the cellular hepatic composition and reside in the space of Disse [102]. HSCs are characterized by the occurrence of the intermediate filament desmin and the deposition of cytoplasmic droplets storing vitamin A in form of retinoic esters [102]. They expose a slow cycling phenotype and slight cytokine secretion [103]. Furthermore, HSCs may directly contribute to immune responses as they are reported to exhibit an antigen presenting capacity [104]. Albeit their low abundance, HSCs represent the key effector cell entity of inflammatory processes and other function impairing stimuli in the liver [103]. After perceiving activation cues like inflammation, injury, infection or chemotherapy, HSCs cease the storage of retinoic acids and transdifferentiate into hepatic myofibroblasts (HMFs*) [103, 105]. HMFs expose a high abundance of $\alpha$-smooth muscle actin ($\alpha$-SMA) and release a plethora of growth factors, including TGF-$\beta$, platelet derived growth factor (PDGF), vascular endothelial growth factor (VEGF) and stromal derived factor-1 (SDF-1) [105–107].

*In the literature the nomenclature for hepatic stellate cells at different degrees of transdifferentiation is used inconsistently. In this thesis, the term hepatic stellate cells (HSCs) represents the stage of quiescence or early activation while the designation hepatic myofibroblasts (HMFs) is used to describe HSCs at an advanced state of activation.

Moreover, HMFs are the main source of ECM molecules like type I and type III collagens [103, 108]. As such, HMFs on the one hand determine and preserve the architecture of the organ upon injury whereas on the other hand their dysregulated propagation may lead to chronic fibrosis and cancer progression. **Figure 1.4** schematically demonstrates the localization and transdifferentiation of HSCs in the space of Disse [109].

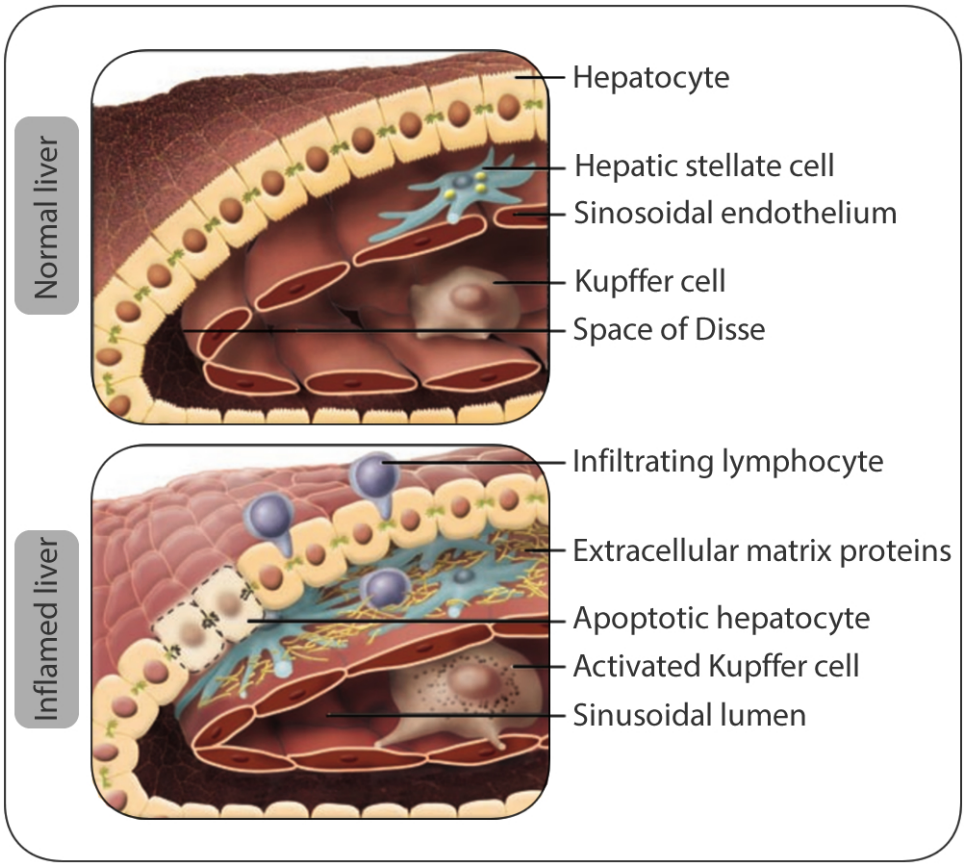


**Figure 1.4.: The activation of hepatic stellate cells (HSCs).** HSCs are located in the space of Disse and represent a quiescent cell population. Upon activation stimuli like e.g. inflammation or injury, HSCs cease their lipid storing function and transdifferentiate into hepatic myofibroblasts (HMFs). Latter ones release a plethora of extracellular matrix molecules and determine the architecture of the liver (adapted from [109]).

Importantly, it has lately been shown that HMFs are critically involved in homing processes of PDAC cells to the liver and the formation of a growth and survival promoting microenvironment, termed a pre-metastatic niche [110, 111]. However the entire spectrum of HSC activation cues and the fashion by which HMFs contribute to liver metastasis in PDAC and other types of cancer are yet insufficiently investigated. Moreover, it is not known which cells in the liver contribute to the poor efficiency of metastases and determine if DTCs may outgrow to overt metastases or remain in a growth arrested condition.

## 1.4. The different shapes of growth arrest

The dysregulation of growth control is a key feature of cancer cells. The acquisition of replicative immortality, the ability to evade growth suppressors and the sustainment of proliferative signaling are accordingly recognized as hallmarks of cancer [112]. Most chemotherapeutical agents are hence designed to target highly proliferative cells [113]. Concomitantly, eradicating non-proliferative tumor cells is mandatory to prevent tumor recurrence and to fully cure cancer diseases. This is since some tumor cells may persist in the organism after treatment in a state of growth arrest. As such tumor cells are not affected by most chemotherapeutic agents and may hence be the source of relapse after treatment [114]. Various reports support the view that DTCs acquire a state of growth arrest when having infiltrated distant organs as they lack adequate adhesion and growth signaling [115, 116]. The ability of neoplastic cells to enter and escape cellular growth arrest may hence represent a crucial step in metastatic evolution [117]. However, the detection of growth arrested tumor cells is particularly challenging as these are clinically unobtrusive [118]. Furthermore, the acquisition of growth arrest in neoplastic cells can manifest in different shapes and phenotypes which may, however, encompass distinct relevance for cancer progression and recurrence [119]. Thus, understanding and characterizing the different mechanisms of growth arrest in cancer cells and PDECs specifically is mandatory to identify novel markers for their detection in order to prevent tumor relapse and metastatic progression.

### 1.4.1. Quiescence

Cellular quiescence is defined as a state in which cells are non-dividing but uphold their proliferative potential [120]. Quiescent cells are captured in the $G_0$-phase and are hence situated outside the cell cycle which applies to most cells of adult mammalian organisms [121]. In comparison to $G_1$ cells, $G_0$ cells may re-enter the S-phase with a distinct lag of variable duration [122]. Quiescence mechanisms are mandatory for the physiological function of various tissues. For example, immune competent cell populations like lymphocytes demand a tight regulation of the balance between quiescence and proliferation to ensure a spatiotemporally controlled immune response [123]. Furthermore, quiescent cells are provided with the ability to survive stress and detrimental cues which is of particular importance for long-living cells like stem cells. When situated in a quiescent state, cells cease various basic cellular processes like metabolism and are generally refractory to differentiation cues [124]. Quiescence *in vitro* is acquired when cells lack mitotic signals, normally received by e.g serum growth factors and nutrients [125] It was hence long time assumed that quiescence represents a passive state whereas

the more recent view sees quiescence as a condition that is actively maintained by various cell entities via induction of corresponding signaling pathways [122]. Among these particular significance is attributed to the retinoblastoma (Rb)-E2F pathway. Proteins of the Rb family including Rb, p130 and p107 promote quiescence by binding and repressing E2F transcription factors which regulate a plethora of genes involved in DNA replication and cell cycle progression [122, 126, 127]. The Rb-E2F pathway is mutated in most, possibly in all cancer cells [128]. It is considered a bistable switch determining if quiescent cells overcome the rescue-point (R-point) which sentinels the cell's entry into the cell cycle [129]. A further critical regulator of cellular quiescence is p53 which was shown to maintain quiescence in fibroblasts and hematopoietic stem cells via promotion of its downstream targets Gfi-1 and Necdin [130, 131]. Of note, p53 also regulates the cyclin dependent kinase (CDK) inhibitor p21. Latter protein is found in higher abundances in quiescent cells and is also an integral component of the Rb-E2F pathway [132]. It could be shown that normal fibroblasts induced to quiescence fail to enter growth arrest when p21 is compromised [133]. The lack of proliferative signaling in quiescent cells can be utilized to detect these *in vitro* and *in vivo*. For this purpose, bromodeoxyuridine (BrdU) labelling as well as Ki67 stainings can be employed [134]. Moreover, the upregulation of above-mentioned signaling molecules like p53 and p21 can be documented via immuno-histological and cytological stainings as well as western blot analysis.

### 1.4.2. Senescence

Historically, cellular senescence was demarcated from quiescence by a final loss of proliferative potential [125]. Senescent cells, in contrast to quiescent cells, are captured while being situated inside the $G_1$ or $G_2$ phase of the cell cycle and remain metabolically active [125]. Cellular senescence occurs when cells receive growth promoting signals while their proliferation is halted [125]. It is considered a critical protective mechanism to ensure tissue function and to separate out dysfunctional, aging and stressed cells [135, 136]. Consequently, senescent cells can be observed in patient tissues after treatment with chemotherapeutic agents or radiation [137]. The initial observation of cellular senescence traces back to Leonard Hayflick who described in 1961 that the number of deviations a cell may undergo in culture is confined and that cells are irreversibly growth arrested after exceeding this limit (Hayflick limit) [138]. This mechanism of senescence induction is termed replicative senescence. It is a consequence of the DNA polymerase's disability to replicate the lagging strand of the DNA at the 3' end which results in shortening of telomeres at a rate of 100 – 120 nucleotides per cycle [139, 140]. Once telomeres reach a critical length, a DNA damage response (DDR) is induced

[141]. The DDR manifests in the emergence of histone y-H2AX foci as well as activation of the kinases ATM and ATR [142, 143]. Furthermore, this process is highly dependent on p53 and p21 which are downstream targets of ATM and ATR [135, 144]. P21 activation leads to the inhibition of CDK2 which in turn results in a cease of Rb-mediated proliferation cues and subsequent growth arrest [144, 145]. If the DDR trespasses a certain threshold, it will not lead to DNA damage repair but either to apoptosis or senescence [136]. Senescence can also occur as a result of cellular stress cues albeit functional telomeres and persistent telomerase activity. Potent triggers of the so called stress-induced senescence (SIS) can be epigenetic stress and reactive oxygen species (ROS) but also the loss of tumor suppressors and activation of oncogenes [144, 146]. In contrast to replicative senescence, SIS is achieved via ARF or p16 signaling. The ARF kinase fulfills its function via the p53-p21 axis similar to ATM and ATR while p16-mediated senescence is achieved via CDK4/6- and Rb-inhibition [144, 147, 148]. Oncogene induced senescence (OIS) represents a subform of SIS in which the *KRAS* oncogene plays a particular role. Mutations in the *KRAS* gene like the $KRAS^{G12D}$ mutation can on the one hand cause enhanced proliferation but also hyperreplication and consequent growth arrest due to replicative and oxidative stress [144, 149]. OIS hence represents a further crucial checkpoint neoplastic cells need to escape in order to successfully form a tumor. It was recently demonstrated that mutant p53 promotes the overcoming of *KRAS*-mediated OIS in premalignant PDECs and fosters their malignant progression [150].

Senescent cells expose a particular phenotype including a flattened and enlarged morphology with a diminished nucleoplasmatic ratio *in vitro* and are often multinucleated [151]. Irrespective of the senescence induction cue a common feature of senescent cells is the release of various pro- and anti-inflammatory cytokines. This senescence-associated secretory phenotype (SASP) is a consequence of the DDR and encompasses factors like Interleukin (IL)-6, IL-8, IL-1 as well as various chemokines of the CXCL and CCL families [152]. The SASP can be utilized as surrogate marker for the detection of senescent cells *in vivo* and *in vitro*. The common increase in p16/CDKN2a, p21 and p53 may also help to identify senescent cells [136]. Yet, the most accepted marker for the detection of senescent cells is an increased activity of acid β-Galactosidase [153]. Acid β-Galactosidase is located in the lysosome, which experiences a marked increase during senescence induction, and can be detected at high levels in senescent cells at pH 6.0. It is hence termed senescence-associated β-galactosidase (SABG). However, the concomitant detection of SABG and other senescence markers like heterochromartin foci or γ-H2AX is recommended to precisely characterize senescent cells [136].

The predominant view that senescence represents an irreversible growth arrest

has been challenged by different observations published in the last years. For example, the inhibition of p53 or the mTOR-pathway was able to restore the proliferative capacity of cells which exposed a senescent phenotype [154, 155]. Furthermore, some breast cancer patients harbored SABG and p16 positive cells after receiving neoadjuvant therapy indicating that senescent cells could represent a source of tumor relapse *in vivo* [135].

### 1.4.3. Dormancy

In general, the biological term dormancy describes a condition in which an organism or a cell temporarily ceases its physiological functions and growth. It can be observed in various biological systems e.g. in plant seeds that fail to germinate or in animals as a delay of development also termed diapause [156, 157]. However, dormancy has particular implications in cancer. In this context, the term dormancy is mostly used to describe a period following treatment during which patients remain asymptomatic before they expose local tumor recurrence and/or metastasis [158]. Cancer dormancy encompasses the absence or cessation of growth on two levels: The level of a tumor cell population (tumor mass dormancy) or on the cellular level (cellular dormancy). Tumor mass dormancy covers mechanisms that restrain the propagation of a tumor cell population. Such populations may contain proliferative cells but do not expose spatial expansion due to the concomitant elimination of a corresponding amount of cells [118]. One mechanism counteracting growth may be active immune surveillance by innate and adaptive immune effector mechanisms resulting in immune-mediated dormancy [119]. Moreover, growing tumors rely on the recruitment of vessels to ensure nutrient and oxygen supply. If proangiogenic factors like VEGF and antiangiogenic factors like thrombospondin (TSP) balance each other, tumors are caught in angiogenic dormancy [159]. Similar to cellular quiescence cellular dormancy describes cells which exist in a reversible $G_0$ -$G_1$ arrest and expose diminished metabolic activity. Additionally, the definition of cellular dormancy includes that in contrast to quiescence a certain trigger stimulus is required to revert it [119]. The induction of dormancy can be a result of disturbed growth factor and adhesion signaling. Two pioneering studies by Aguirre-Ghiso and Liu *et al.* showed that disruption of EGFR-mediated urokinase plasminogen activator receptor (uPAR) signaling causes diminished ERK activation and proliferation and a dormant phenotype in head and neck squamous carcinoma (HNSC) cells [115, 160]. These findings were supported by more recent studies which showed that restoration of VCAM-1 adhesion signaling represents a potent trigger to counteract the dormant phenotype of breast cancer cells [119, 161]. Aguirre-Ghiso *et al.* were able to show that the ratio of phosphorylated (p-) ERK and

p-p38 helps to identify cells and tumors in a state of dormancy. In their hands, sustained ERK activity favored a proliferative phenotype in cells of different cancer entities whereas a low p-ERK/p-p38 signaling ratio correlated with cellular dormancy [160]. Furthermore, ERK signaling is negatively regulated by p-p38 and hence inhibition of p38 in dormant cells is sufficient to bring back proliferative activity of some cancer cells [162]. Meanwhile, few stimuli which may act to revert tumor mass dormancy and cellular dormancy could be identified. Sustained proangiogenic VEGF signaling helps to induce the angiogenic switch which promotes blood supply of tumorous lesions thereby restraining angiogenic dormancy [163]. Furthermore, diminished TGF-β signaling was reported to promote reactivation of dormant metastatic breast cancer cells [164].

Tumor mass dormancy and cancer cell dormancy are considered the basis for different important clinical observations like minimum residual disease (MRD) [114]. MRD occurs when a therapeutical intervention fails to fully eradicate all cells of a tumor. As a consequence, some cells may survive in the patient's organs and eventually give rise to tumor relapse after concluded treatment [114]. This is also relevant for PDAC where remaining vital tumor cells are commonly observed in the bone marrow, lymph nodes, blood and peritoneum [165]. Lin *et al.* recently delivered experimental evidence that the dysregulation of the c-Myc oncogene may be critically involved in the induction and maintenance of this process [166]. Due to the rapid disease process of PDAC dormancy processes appear less important than in other cancer entities like e.g. breast or prostate cancer where recurrence could be observed years or sometimes even decades after treatment [167]. Yet, the concept of dormancy could help to explain the emergence of metastases shortly after therapy despite full removal of the primary tumor [8]. Of note, the early dissemination model proposed for some cancer entities including PDAC only gains clinical relevance when assuming that early DTCs may survive in distant organs for longer periods [117, 167]. Hence, the concept of early dissemination is probable to strongly depend on dormancy processes.

Yet, it is not fully understood whether cellular dormancy indeed represents a distinct phenotype and mechanism independent of cellular quiescence and senescence. As noted above, all three mechanisms of growth arrest are achieved by similar key molecules and pathways. Accordingly, their phenotypic and morphologic features overlap. Whereas irreversible senescence is not likely to represent a mechanism underlying tumor recurrence and metastatic spread, reversible senescence may be a mechanistic fit for the latter processes. Since cellular senescence comprises the pro-inflammatory SASP as additional feature it may be relevant for the detection and eradication of tumor cells which kind of growth arrest underlies MRD and occult metastasis.

### Role of the microenvironment in the induction and reversion of dormancy

The observation that adhesion and growth factor signaling influence the dormant phenotype of neoplastic cells implies that additional to cell intrinsic factors the microenvironment represents a crucial determinant for the acquisition and maintenance of a dormant phenotype in neoplastic cells [168]. Some organs comprise a relatively high ability to support the growth of DTCs and are hence classified as 'dormancy permissive' microenvironments [119]. The bone marrow is considered a dormancy permissive environment as it exhibits high amounts of factors like growth arrest specific protein 6 (GAS 6), bone morphogenetic proteins 4 and 7 (BMP4 and BMP7) as well as TGF-β2, all of which were shown to induce cellular dormancy in different cancer entities [169–172]. In accordance with the seed and soil hypothesis, some organs provide conditions which promote the escape from dormancy and are hence termed 'dormancy restrictive' [119]. Bragado *et al.* were able to show that the relatively low levels of TGF-β2 in the lungs allow for dormancy escape and metastasis formation of HNSC DTCs in a p38 dependent manner [171]. Importantly, the induction and reversion of dormancy may also rely on inflammatory processes. Utilizing an experimental model of breast cancer metastasis, Barkan *et al.* showed that inflammation of pulmonary tissue, manifesting in enhanced collagen-1 release, may drive DTCs to escape cellular dormancy [173, 174].

## 1.5. Aim of the study

Despite extensive research efforts undertaken in the last decades and significant progress in the understanding of the pathological events underlying its development, PDAC remains a widely incurable malignancy. This is mainly owed to the frequent occurrence of metastatic disease which commonly manifests prior to diagnosis or even subsequent to successful resection of the primary tumor [6–8]. Since the liver is colonized in 80 % of all PDAC patients, understanding of mechanisms which underlie the outgrowth of disseminated PDECs in the liver may reveal promising novel targets for PDAC treatment [92]. However, the pathological events promoting PDAC liver metastasis as well as their chronology are poorly understood. The link between primary PDAC progression and inflammation is to date well established and the tumor stroma is shifting into the centre of attention of PDAC therapy research [175]. However, the poor availability of patient material aggravates the characterization of PDAC liver metastasis, particularly in the early course of metastatic disease [6]. Hence, it remains widely unclear how inflammatory cues in the hepatic microenvironment may impact on the accretion and progression of disseminated PDECs. Studies from HNSC and

mammary carcinoma support the view that inflammatory conditions in the secondary organ promote the escape of DTCs from growth arrest and foster their outgrowth to metastases [171, 173]. It was therefore hypothesized that the condition of the hepatic microenvironment – physiological versus inflamed – may critically determine the fate and proliferative behavior of disseminated PDECs. In the liver, HSCs and thereof transdifferentiated HMFs are the main effector cell population of inflammatory processes [105]. Accordingly, inflamed livers expose a high amount of HMFs (**cf. Chapter 1.3**). Hence, in this study HSCs and HMFs were regarded as representative of a physiological or inflamed liver microenvironment, respectively.

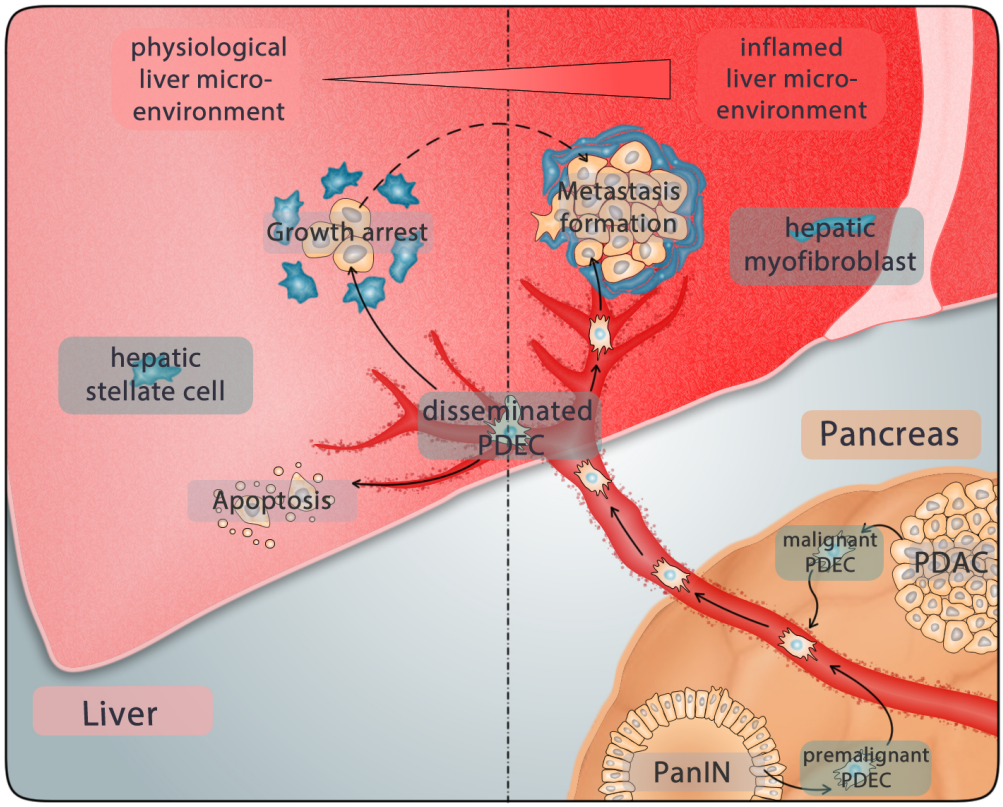


**Figure 1.5.: Working hypothesis.** HSCs are a characteristic of a physiological liver whereas an inflamed liver is characterized by higher amounts of HMFs. It was recently reported that besides malignant PDAC cells, also premalignant PDECs may disseminate to the liver [89]. It was hence hypothesized that the condition of the liver – physiological versus inflamed – determines the likelihood of succesfull outgrowth of dissemintated PDECs from PanINs or PDAC to overt metastases.

In a first step, it was sought to characterize PDAC metastases with particular regard to tumor cell proliferation and the abundance of HSC and HMF in the direct microenvironment. For this approach, liver sections of the well-established KPC mouse model of PDAC were analyzed for tumor cell proliferation and stromal composition via immunohistological methods [176].
Aging is an accepted risk factor for PDAC onset [5]. It was previously shown that

aging is associated with various systemic alterations including cellular senescence and altered intercellular communication which manifest in a state of subclinical inflammation also referred to as smouldering inflammation or 'inflammaging' [177]. Accordingly, some studies report that HMFs emerge concomitantly with proceeding age [103]. It was hence hypothesized that inflammaging fosters the outgrowth of metastases in the liver. To study the impact of aging-related smouldering inflammation on the proliferation of disseminated PDECs, a syngeneic mouse model was used. Therefore, C57Bl/J mice 8 weeks or 52 of age were injected orthotopically with KPC derived PDAC cells. These animals were analyzed regarding primary and secondary tumor progression via *in vivo* imaging modalities and *ex vivo* via immunohistological stainings.

*In vitro* coculture systems were demonstrated to be useful tools for examining the mutual impact of stromal cells and tumor cells and to determine underlying mechanisms of intercellular communication [178, 179]. In previous own work, an indirect coculture system could be established which is feasible to examine the impact of HSCs and HMFs on PDECs [180, 181]. This model relies on the murine cell line M1-4HSC which exhibits various features of HSCs, including desmin-positivity and TGF-β responsivity [182]. Under substantial administration of exogenous TGF-β, M1-4HSC acquire an HMFs-like phenotype, termed M-HT, which manifests in a spindle-shaped morphology and diminished amounts of intracellular desmin [182]. Hence, the M1-4HSC cell line was utilized representative of HSCs and M-HT cells were applied representative of HMFs to model a physiological or an inflamed hepatic microenvironment, respectively. Representative of disseminated PDECs deriving from PanIN lesions the premalignant PDEC line H6c7-kras was used whereas the malignant cell line Panc1 was utilized to model DTCs from established PDAC. The indirect coculture of M1-4HSC or M-HT with premalignant and malignant PDECs ought to provide indications for the behavior of DTCs in the liver. Overall, this work aimed at gaining a better understanding of the mechanisms underlying the outgrowth of liver metastasis in PDAC.

# 2. Materials

## 2.1. Laboratory devices

| Device | Manufacturer |
|---|---|
| **Centrifuges** | |
| Heraeus Fresco 17 | Thermo Scientific, Schwerte, DE |
| Heraeus Multifuge 3 S-R | Thermo Scientific, Schwerte, DE |
| Heraeus Multifuge X1 | Thermo Scientific, Schwerte, DE |
| Heraeus Pico 17 | Thermo Scientific, Schwerte, DE |
| Rotina 420 R | Hettich, Tuttlingen, DE |
| Sprout mini centrifuge | Heathrow Scientific, Vernon Hills, US |
| **Incubators** | |
| BBD 6220 CO2 incubator | Thermo Scientific, Schwerte, DE |
| GyroTwister 3D shaker | Labnet, Woodbridge, US |
| HERA Cell 240 incubator | Thermo Scientific, Schwerte, DE |
| PMS 1000 Microplate Shaker | Grant bio, Essex, UK |
| QBA1 table incubator | Grant, Cambridge, UK |
| Stuart SRT9 roll mixer | Bibby Scientific Ltd., Stone, UK |
| WNB 7-45 water bath | Memmert, Schwabach, DE |
| WTC ED-53 incubator | Binder, Tuttlingen, DE |
| **Measuring Devices** | |
| Fusion SL detection system | Vilber Lourmat, Eberhardzell, DE |
| LightCycler 480 II | Roche, Basel, CH |
| Infinite® 200 PRO, plate reader | Tecan, Crailsheim, DE |
| NanoQuant Plate | Tecan, Crailsheim, DE |
| NightOWL LB 983 | Berthold Technol., Bad Wildbad, DE |
| Neubauer counting chamber | Marienfeld, Lauda-Koenigshofen, DE |
| pH 7110 pH-meter | inoLab, Weilheim, DE |
| Vevo770® | FujiFilm VisualSonics, Toronto, CAN |

| **Histology devices** | |
|---|---|
| FS20 MultiGourmet | Braun, Aschaffenburg, DE |
| HM430 Microtome | Thermo Fisher, Darmstadt, DE |
| Heating Plate 100 °C | Jürgens, Bremen, DE |
| Paraffin stretch bath | Medax, Neumünster, DE |
| TES 99 Paraffin embedding system | Medite, Burgdorf, DE |

| **Microscopes** | |
|---|---|
| AE2000 | Motic, Wetzlar, DE |
| Axiovert 25 | Zeiss, Jena, DE |
| Axio Scope-A1 | Zeiss, Jena, DE |
| BZ-9000 II | Keyence, Osaka JPN |
| Evos XL Core Cell Imaging System | AMG, Bothell, US |

| **Other devices** | |
|---|---|
| ARPEGE 110 nitrogen tank | AirLiquide, Paris, FR |
| CS-300V Power supply | Cleaver Scientific, West Sussex, UK |
| Freezer | Liebherr, Ochsenhausen, DE |
| Fridge | Liebherr, Ochsenhausen, DE |
| HERAfreeze Basic freezer | Thermo Scientific, Schwerte, DE |
| Laboport vacuum pump | KNF Neuberger, Freiburg, DE |
| MILLI-Q Reagent Water System | Merck Millipore, Billerica, US |
| MR Hei-Mix S magnetic stirrer | Heidolph Instruments, Schwabach, DE |
| OmniPAGE VS10D gel chamber | Cleaver Scientific, West Sussex, UK |
| SD20 Semi Dry Maxi transfer chamber | Cleaver Scientific, West Sussex, UK |
| Sonicator Sonoplus | Bandelin, Berlin, DE |
| Sunrise remote control | Tecan, Crailsheim, DE |
| Vortex Genius 3 vortex shaker | IKA-Werke, Staufen, DE |

| | |
|---|---|
| **Pipettes** | |
| Finnpipette F1 0.2-2 µl | Thermo Scientific, Schwerte, DE |
| Finnpipette F1 1-10 µl | Thermo Scientific, Schwerte, DE |
| Finnpipette F1 2-20 µl | Thermo Scientific, Schwerte, DE |
| Finnpipette F1 20-200 µl | Thermo Scientific, Schwerte, DE |
| Finnpipette F1 100-1000 µl | Thermo Scientific, Schwerte, DE |
| Macro pipette controller | Brand, Wertheim, DE |
| Pipetboy acu | Integra Biosciences, Fernwald, DE |
| **Sterile benches** | |
| HERA Safe | Thermo Scientific, Schwerte, DE |
| HERA Safe KS | Thermo Scientific, Schwerte, DE |
| **Scales** | |
| Precisa BJ 2100D | Precisa Gravimetrics, Dietikon, CH |
| Precisa XB120A | Precisa Gravimetrics, Dietikon, CH |

## 2.2. Consumables

| Consumable | Manufacturer |
|---|---|
| 0.1 - 10 µl, 10 - 200 µl, 100 - 1000 µl pipette tips | Sarstedt, Nuembrecht, DE |
| 1.25 mL, 5.0 mL Ritips | Ritter, Schwabmuenchen, DE |
| 1.5 mL, 2 mL Eppendorf tubes | Eppendorf, Hamburg, DE |
| 15 mL, 50 mL centrifuge tubes | Sarstedt, Nuembrecht, DE |
| 18 mm coverslips | Menzel, Braunschweig, DE |
| 5 mL, 10 mL, 50 mL serological pipettes | greiner bio-one, Frickenhausen, DE |
| 6-/12-/96-well flat-bottom plates | greiner bio-one, Frickenhausen, DE |
| 6-/12-well transwell inserts, pore size 0.4 µm | greiner bio-one, Frickenhausen, DE |
| 75 $cm^2$ cell culture flasks | greiner bio-one, Frickenhausen, DE |
| 96-well PCR plates, white | Roche, Basel, CH |
| Cell Scraper 25 cm | Sarstedt, Nuembrecht, DE |
| CryoPure tube, 1.0 mL, white | Sarstedt, Nuembrecht, DE |
| Micro-Touch nitrile examination gloves | Ansell, Muenchen, DE |
| Nalgene rapid-flow sterile disposable filter with SFCA membrane (pore size 0.2 µm) | Thermo Scientific, Schwerte, DE |
| Nunc® CryoTube® 1.8 ml | Sigma Aldrich, Muenchen, DE |
| Parafilm M sealing film | Brand, Wertheim, DE |
| RA Lamb Coverglass and Coverslip Staining Rack | Thermo Scientific, Schwerte, DE |
| SuperFrost object slide 76 x 26 mm | Menzel, Braunschweig, DE |
| Transfer pipettes 3.5 ml | Sarstedt, Nuembrecht, DE |
| WatchMaker Forcep No. 6 | Thermo Scientific, Schwerte, DE |
| Westran polyvinylidene fluoride (PVDF) membrane 0.45 µm | Th.Geyer GmbH, Renningen, DE |
| Whatmann-3MM filter paper FE | Healthcare, Buckinghamshire, UK |

## 2.3. Kit systems

| Kit | Manufacturer |
|---|---|
| Bio-Plex® Pro Assay | Bio-Rad Laboratories, Muenchen, DE |
| DC™ Protein Assay | Bio-Rad Laboratories, Muenchen, DE |
| Lab Vision™ MultiVision Polymer Detection System | Thermo Fisher, Darmstadt, DE |
| MycoAlert™ Mycoplasma Detection Kit | Lonza Group, Basel, CH |
| NucleoSpin RNA/Protein | Macherey-Nagel, Düren, DE |
| RevertAid First Strand cDNA Synthesis Kit | Thermo Scientific, Schwerte, DE |
| Senescence β-Galactosidase Staining Kit | New England Biolabs GmbH, Frankfurt(Main), DE |

## 2.4. Software

| Software | Manufacturer |
|---|---|
| Axiovision 4.6 | Carl Zeiss AG, Jena, DE |
| BIOREVO | Keyence, Osaka, JPN |
| Citavi | Swiss Academic Software GmbH, Wädenswil, CH |
| Fireworks CS6 | Adobe |
| FUSION-CAPT 16.06 | Vilber Lourmat, Eberhardzell, DE |
| ImageJ 1.47v | Wayne Rasband, National Institute of Health, Bethesda, Maryland, US |
| LightCycler480 Software | Roche, Basel, CH |
| i-control™Microplate Reader Software | Tecan, Crailsheim, DE |
| Microsoft Excel 2010 | Microsoft Corporation, Redmond, US |
| SigmaPlot 12.5 | Systat Software Inc., Chicago, US |
| Vevo® software | FujiFilm VisualSonics, Toronto, CAN |

## 2.5. Chemicals, buffers and reagents

### 2.5.1. Chemicals

| Chemical | Manufacturer |
|---|---|
| 2-mercaptoethanol | Sigma-Aldrich, Muenchen, DE |
| 6-aminocaproic acid | Sigma-Aldrich, Muenchen, DE |
| Accutase solution | EMD Millipore Corporation, Temecula, California, US |
| Acetic acid, 10 % | Carl Roth GmbH, Karlsruhe, DE |
| AEC substrate-Chromogen Ready-to-Use | Dako Diagnostika, Hamburg, DE |
| All-trans-Retinoic acid (ATRA) | Sigma Aldrich, Muenchen, DE |
| AMD3100 (Plerixafor) | Kindly provided by PD Dr. Kirsten Hattermann-Koch, Kiel, DE |
| Ammonium persulfate (APS) | Merck Millipore, Darmstadt, DE |
| Bovine pituitary extract (BPE) | Life Technologies, Darmstadt, DE |
| Bovine serum albumin (BSA), fraction V | Biomol, Hamburg, DE |
| Bromphenol blue ACS Reag., Ph Eur | Merck Millipore, Darmstadt, DE |
| Clarity Western ECL substrate | Bio-Rad Laboratories, Muenchen, DE |
| Dithiothreitol (DTT) | Sigma-Aldrich, Muenchen, DE |
| Dulbecco's Modified Eagle Medium (DMEM) | PAA, Pasching, AT |
| EnVision + system-HRP labelled polymer anti-mouse | Dako Diagnostika, Hamburg, DE |
| Ethanol | Merck Millipore, Darmstadt, DE |
| Fetal calf serum (FCS) | Biochrom, Berlin, DE |
| FluorSave$^{TM}$ Reagent | Merck Millipore, Darmstadt, DE |
| Glycerol | Sigma-Aldrich, Muenchen, DE |
| Hydrogen peroxide 30 % | Th.Geyer GmbH, Renningen, DE |
| Keratinocyte serum-free medium | Life Technologies, Darmstadt, DE |
| L-glutamine (L-Gln) | PAA, Pasching, AT |

| | |
|---|---|
| LightCycler480 SYBR Green I Master | Roche, Basel, Switzerland |
| Mayer's Haemalaun | Applichem, Darmstadt, DE |
| Methanol | Th.Geyer GmbH, Renningen, DE |
| Milk powder | Carl Roth GmbH, Karlsruhe, DE |
| PageRuler prestained protein ladder | Thermo Scientific, Schwerte, DE |
| Paraformaldehyde (PFA) 4.5 % (w/v) | BUEFA Chemikalien GmbH Co. KG, Hude, DE |
| Penicillin-streptomycin (Pen/Strep) | PAA, Pasching, AT |
| Phosphate buffered saline (PBS) | PAA, Pasching, AT |
| Ponceau S | Carl Roth GmbH, Karlsruhe, DE |
| Richard-Allan Scientific™ Mounting Medium | Thermo Scientific, Schwerte, DE |
| Roswell Park Memorial Institute (RPMI) 1640 medium | Biochrom, Berlin, DE |
| Rotiphorese gel 40 acrylamide/ bisacrylamide 40 % solution | Carl Roth GmbH, Karlsruhe, DE |
| Sodium chloride | Carl Roth GmbH, Karlsruhe, DE |
| Sodium dodecyl sulfate (SDS) ultra-pure | Carl Roth GmbH, Karlsruhe, DE |
| Sodium orthovanadate | Santa Cruz Biotech., Heidelberg, DE |
| Sodium pyruvate 100 mM | Biochrom, Berlin, DE |
| SteCM Medium | provitro AG, Berlin, DE |
| Sudan Black B | Sigma-Aldrich, Muenchen, DE |
| Tris base | Carl Roth GmbH, Karlsruhe, DE |
| Triton X-100 | Sigma-Aldrich, Muenchen, DE |
| Trypan blue solution Fluka 0.4 % | Sigma-Aldrich, Muenchen, DE |
| Trypsin-EDTA | PAA, Pasching, AT |
| Tween 20 | Serva, Heidelberg, DE |

### 2.5.2. Buffers and formulations

| **Western blotting** | |
|---|---|
| Blot buffer A | 300 mM Tris base<br>20 % (v/v) methanol<br>pH 11 |
| Blot buffer B | 25 mM Tris base<br>20 % (v/v) methanol<br>pH 10.6 |
| Blot buffer C | 25 mM Tris base<br>20 % (v/v) methanol<br>40 mM aminocaproid acid<br>pH 10.6 |
| Blotto | 50 g/l milk powder<br>in TBS-T (1x) |
| Laemmli buffer (2x) | 128 mM Tris base<br>4.6 % (w/v) SDS<br>10 % (v/v) glycerol<br>1 mM sodium orthovanadate<br>pH 7.6 |
| Loading Dye (4x) | 50 ml Laemmli buffer (2x)<br>0.005 % (w/v) bromphenol blue<br>2.5 % (v/v) 2-mercaptoethanol |
| Separation gel buffer | 1.5 M Tris base<br>0,4 % (w/v) SDS<br>pH 8,8 |
| Stacking gel buffer | 0.5 M Tris base<br>0.4 % (w/v) SDS<br>pH 6,8 |
| TBS (10x) | 20 mM Tris base<br>140 mM sodium chloride<br>pH 7.6 |

| | |
|---|---|
| TBS-Tween (TBS-T) | 1798 ml $ddH_2O$<br>200 ml TBS (10x)<br>1000 l Tween 20 |
| Western blot running buffer | 5000 mL $ddH_2O$<br>25 mM Tris base<br>192 mM glycin<br>0.1 % (w/v) SDS |

## 2.6. Material for in vivo experiments

### 2.6.1. Tools and consumables

| **Article** | **Manufacturer** |
|---|---|
| Insulin syringe U-40, 1 ml, 29,5 GA/0,33 x 12,7 mm | Becton Dickinson, USA |
| Bepanthen® | Bayer Vital, Leverkusen DE |
| Gauze compress $10 * 10$ cm | Hartmann, Heidenheim, DE |
| Gauze compress $6 * 6$ cm | NOBA Verbandmaterial, Wetter, DE |
| Kodan® | Schülke & Mayr GmbH, Norderstedt, DE |
| Micro needleholder after Müller FM 061 R | Aesculap, Tuttlingen, DE |
| Micro tweezers with 1 x 2 teeth after Müller FM034R | Aesculap, Tuttlingen, DE |
| Micro tweezers with ring (diameter 1.2 mm) | Aesculap, Tuttlingen, DE |
| Veet depilation creme | Reckitt Benckiser, Slough, UK |
| Vicryl 6-0 | Ethicon Inc., Somerville, USA |
| Scissors, fine, straight, BC 060 R | Aesculap, Tuttlingen, DE |
| sterile cotton buds | Beese, Barsbüttel, DE |

### 2.6.2. Injection solutions for in vivo experiments

| Solution | Manufacturer |
|---|---|
| Glucose 5% B.Braun solution | Braun, Melsungen, DE |
| Anexate® (Flumazenil, 0,1 mg/ml) | Roche, Grenzach-Wyhen, DE |
| Antisedan® (Atipamezol, 5 mg/ml) | Pfizer, Karlsruhe, DE |
| D-Luciferin Firefly (XR-1001) | Xenogen Corp., Alameda, USA |
| Dormitor® (Medetomidin, 1 mg/ml) | Pfizer, Karlsruhe, DE |
| Fentanyl® (0,05 mg/ml) | Janssen-Cilag, Neuss, DE |
| Isotonic sodiumchloride sol. 0,9 % | Braun, Melsungen, DE |
| Midazolam® (1 mg/ml) | Roche, Grenzach-Wyhen, DE |
| Naloxon® (0,4 mg/ml) | CuraMed, Karlsruhe, DE |
| Temgesic® (0,3 mg/ml) | Reckitt Benckiser, Slough, UK |

## 2.7. Cell biological material

### 2.7.1. Cell lines

| Cell line | Information / Source |
|---|---|
| **A) Premalignant pancreatic ductal epithelial cells** | |
| H6c7eR-Kr<br>(referred to as H6c7-kras) | HPDE cell line immortalized with HPV16-E6E7 genes and transduced with the viral vector pBabepuro-K-Ras$^{G12V}$ [183]<br>PDAC relevant mutations: *KRAS* |
| **B) Malignant pancreatic ductal epithelial cells** | |
| R254 | PDAC cell line isolated from a pancreas of a KPC mouse carrying an fLuc/GFP-reporter cassette [184]<br>PDAC relevant mutations:<br>*KRAS*, *P16/CDKN2A*, *TP53* |
| Panc1 | Cell line generated from a 56-year-old male with an adenocarcinoma in the head of the pancreas [185]<br>PDAC relevant mutations:<br>*KRAS*, *P16/CDKN2A*, *TP53* |
| **C) Hepatic stromal cells** | |
| M1-4HSC | HSCs line isolated from p19$^{ARF}$ null mice in an early activation stage [182] |
| M-HT | M1-4HSC cells that have transdifferentiated into myofibroblasts after minimum 3 weeks exposure to 1 ng/ml exogenous TGF-β1 [182] |
| HHSteC | Human hepatic stellate cells isolated from the liver of a 3 years old male infant (SC-5300; provitro AG,<br>Berlin, DE) |

### 2.7.2. Culture media and additives

| Cell line | culture media |
|---|---|
| **Routine cell culture** | |
| R254 | DMEM High Glucose<br>(10 % (v/v) FCS, 1 %(v/v) L-Gln,<br>1 % (v/v) Pen/Strep) |
| H6c7-*kras* | 50 % (v/v) keratinocyte-serumfree-medium<br>(50 µg/ml bovine pituitary extract, 5 ng/ml EGF, 1 µg/ml puromycin),<br>50 % (v/v) RPMI 1640<br>(10 % (v/v) FCS, 1 % (v/v) L-Gln) |
| Panc1 | RPMI 1640<br>(10 % (v/v) FCS, 1 %(v/v) L-Gln,<br>1 % (v/v) NaPyr) |
| M1-4HSC | MI-Medium<br>(DMEM High Glucose<br>10 % (v/v) FCS, 1 % (v/v) NaPyr,<br>1 % (v/v) Glut, 1 % (v/v) Pen/Strep) |
| M-HT | MI-Medium (1 ng/ml TGF-β1) |
| HHSteC | SteC-Medium<br>(2% FCS + SteC-Medium supplements) |
| **Coculture and blocking experiments** | |
| H6c7-*kras*<br>co<br>M1-4HSC<br>M-HT<br>HHSteC-HSC | RPMI 1640<br>(10 % (v/v) FCS, 1 % (v/v) L-Gln |
| Panc1<br>co<br>M1-4HSC<br>M-HT<br>HHSteC-HMF | 1:1 RPMI 1640 : DMEM High Glucose<br>(10 % (v/v) FCS, 1 % (v/v) L-Gln) |

## 2.8. PCR-Primer

| Gene | 5' - 3' Sequence | Annealing temp. |
|---|---|---|
| **Purchased from Eurofins genomics** | | |
| m β-Actin | fw-AAGAGCTATGAGCTGCCT<br>rv-TACGGATGT CAACGTCAC | 58 °C |
| m FGF2 | fw-AGAGCGACCCACACGTCAAAC<br>rv-CCAACTGGAGTATTTCCGTGACC | 58 °C |
| m/h GAPDH | fw-TCCATGACAACTTTGGTATCGTGG<br>rv-GACGCCTGCTTCACCACCTTCT | 58 °C |
| m TGF-β1 | fw-GCTGAACCAAGGAGACGGAA<br>rv-AGAAGTTGGCATGGTAGCCC | 58 °C |
| m VEGF-A | fw-ACTGGACCCTGGCTTTACTG<br>rv-TCTGCTCTCCTTCTGTCGTG | 58 °C |
| **Purchased from realtimeprimers.com** | | |
| m α-SMA | fw-ATGCAGAAGGAGATCACAGC<br>rv-CAGCTTCGTCGTATTCCTGT | 58 °C |
| m Col-1A1 | fw-ATGATGCTAACGTGGTTCGT<br>rv-TGGTTAGGGTCGATCCAGTA | 58 °C |
| m Desmin | fw-CAGGAGATGGAATACCG<br>rv-GGCCATCTCATCCTTTAGGT | 58 °C |
| m IL-6 | fw-TAGTCCTTCCTACCCCAATTTCC<br>rv-TTGGTCCTTAGCCACTCCTTC | 58 °C |
| m KC | fw-CCAGAGCTTGAAGGTGTTGC<br>rv-TCTGAACCAAGGGAGCTTCA | 58 °C |
| m LIX | fw-CAGAAGGAGGTCTGTCTGGA<br>rv-TGGTTTCCCTTTTCTCATCA | 58 °C |
| m MIP-2 | fw-CAGACTCCAGCCACACTTCA<br>rv-TTCAGGGTCAAGGCAAACTT | 58 °C |
| m TNF-α | fw-CCCACTCTGACCCCTTTACT<br>rv-TTTGAGTCCTTGATGGTGGT | 58 °C |
| **Purchased from Biometra** | | |
| m IL-1β | fw-ATCCTCTGTGACTCATGGGATG<br>rv-GATCCACACTCTCCAGCTGCA | 55 °C |

## 2.9. Biochemical Material

### 2.9.1. Antibodies

**Primary antibodies**

| Specificity (Clone) | Host Isotype | Stock Concentration | Dilution / Application | Manufacturer |
|---|---|---|---|---|
| α-Smooth muscle actin (1A4) | mouse IgG1 | 2-6 mg/ml | 1:200 (IHC-p, IF)<br>1:2000 (WB) | Sigma Aldrich, Munich, DE |
| Desmin (D93F5) | rabbit IgG | - | 1:1000 (WB)<br>1:50 (IHC-p, IF) | Cell Signaling, Frankfurt, DE |
| Ki67 (B56) | mouse IgG1 | 0.5 mg/ml | 1:200 (IHC-p)<br>1:100 (IHF)<br>1:250 (ICC) | BD Biosciences, Heidelberg, DE |
| Cytokeratin-19 (10712-1-AP) | rabbit IgG | 100 µg/ml | 1:200 (IHC-p) | Proteintech EU, Manchester, UK |
| GFP Tag (A-11122) | rabbit IgG | 2 mg/ml | 1:100 (IHF) | Thermo Fisher, Darmstadt, DE |
| HSP90 (H-114) | rabbit IgG | 200 µg/ml | 1:2000 (WB) | Santa Cruz, Heidelberg, DE |
| p21 (187) | mouse IgG1 | 200 µg/ml | 1:250 (WB) | Cell Signaling, Frankfurt, DE |
| p38 MAPK | rabbit IgG | 27 µg/ml | 1:1000 (WB) | Cell Signalling, Frankfurt, DE |
| p44/42 ERK1/2 | rabbit IgG | 7.6 µg/ml | 1:1000 (WB) | Cell Signalling, Frankfurt, DE |
| phospho-p38 MAPK (D3F9) | rabbit IgG | 78 µg/ml | 1:1000 (WB) | Cell Signalling, Frankfurt, DE |
| phospho-p44/42 ERK1/2 | rabbit IgG | 150 µg/ml | 1:1000 (WB) | Cell Signalling, Frankfurt, DE |
| COL1A1 (C-18)-R | rabbit IgG | 200 µg/ml | 1:1000 (WB) | Santa Cruz, Heidelberg, DE |

**Isotype control antibodies**

| Name | Host / Isotype | Stock Concentration | Dilution / Application | Manufacturer |
|---|---|---|---|---|
| Isotype (MAB002) | mouse IgG1 | 0.5 mg/ml | - | R&D Systems, Abingdon, UK |
| Normal Rabbit IgG Control | rabbit IgG1 | 1.0 mg/ml | - | R&D Systems, Abingdon, UK |

**Secondary antibodies**

| Name | Host / Isotype | Stock Concentration | Dilution / Application | Manufacturer |
|---|---|---|---|---|
| mouse IgG H&L | horse | 170 µg/ml | 1:2000 (WB) | Cell Signalling, Frankfurt, DE |
| rabbit IgG H&L | goat | 83 µg/ml | 1:2000 (WB) | Cell Signalling, Frankfurt, DE |
| mouse IgG H&L Alexa fluor® 488 | goat IgG | 2 mg/ml | 1:400 (IHF) | Life Technologies, Darmstadt, DE |
| rabbit IgG H&L DyLight® 594 | goat IgG | 2 mg/ml | 1:400 (IHF) | Thermo Fisher, Darmstadt, DE |

| **Blocking antibodies** | | | |
|---|---|---|---|
| **Antibody** | **Target** | **Final Concentration** | **Manufacturer** |
| Tocilizumab | h IL-6R | 10 µg/ml | kindly provided by Prof. Dr. Stefan Rose-John, Kiel, DE |
| sgp130Fc | IL-6/IL-6R-complex | 10 µg/ml | kindly provided by Conaris Research Institute AG, Kiel, DE |
| MAB208 | h IL-8 (CXCL8) | 2.5 µg/ml | R&D Systems, Abingdon, UK |
| Bevacizumab | h VEGF-A | 10 µg/ml | Roche, Basel, CH |
| Aflibercept | h/m VEGF-A/B + PGF | 10 µg/ml | provided by Prof. Dr. Alexa Klettner, Kiel, DE |
| **Control antibodies** | | | |
| **Antibody** | **Isotype control for** | **Final Concentration** | **Manufacturer** |
| Rituximab | Tocilizumab Bevacizumab Aflibercept | 10 µg/ml | kindly provided by Prof. Matthias Peipp, Kiel, DE |
| control Fc | sgp130Fc | 10 µg/ml | kindly provided by Conaris Research Institute AG, Kiel, DE |
| Isotype (MAB002) | MAB208 | 2.5 µg/ml | R&D Systems, Abingdon, UK |

### 2.9.2. Growth factors and cytokines

| **Factor** | **Manufacturer** |
|---|---|
| human Epidermal growth factor | BioLegend, Fell, DE |
| human Transforming growth factor-β1 | BioLegend, Fell, DE |
| human Stromal Derived Factor-1α | PeproTech, Hamburg, DE |
| human Interleukin-6 | BioLegend, Fell, DE |
| murine Interleukin-6 | BioLegend, Fell, DE |
| human Interleukin-8 | BioLegend, Fell, DE |

# 3. Methods

## 3.1. In situ characterization of liver metastases in an endogenous PDAC mouse model

For the initial screening of liver metastases in a stroma-related context, livers of the established KPC mouse model (Pdx1-Cre; LSL-Kras$^{G12D/+}$; LSL-Trp53$^{R172H/+}$) [176] were examined (**Figure 3.1**). Formalin-fixed paraffin-embedded (FFPE) liver tissues were kindly provided by Prof. Dr. Dieter Saur and Prof. Dr. Günter Schneider (II. Medizinische Klinik und Poliklinik, Klinikum Rechts der Isar, Technical University Munich, Munich, Germany). Corresponding animal experiments were executed in compliance with European guidelines for care and use of laboratory animals and approved by local authorities (Az. 55.2-1-54-2532-31-11).

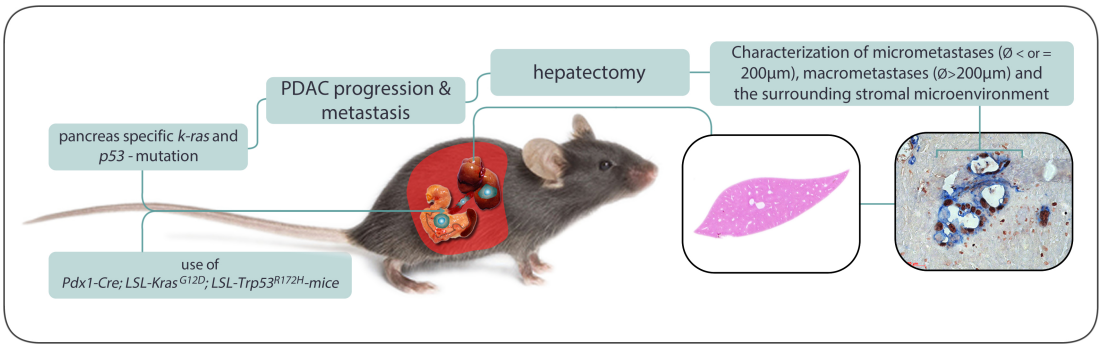


**Figure 3.1.: Experimental setup for the characterization of liver metastases in an endogenous PDAC mouse model**

### 3.1.1. Immunohistochemistry

FFPE liver tissue blocks were cut into serial sections of 3 µm slices and dried overnight in an incubator at 37 °C. Tissue specimens were deparaffinized and rehydrated with xylene and graded ethanol baths in slide staining dishes containing 200 ml of the particular solution. Tissue slices were incubated in xylene twice for 10 min, respectively, following two incubation steps for 10 min in 100% ethanol. Five min incubation in 95% ethanol including 1.5% $H_2O_2$ were affiliated in order to quench the activity of endogenous peroxidases. Then, tissue sections were

transferred into 70% ethanol, following incubations in 50% ethanol and dd$H_2O$ for 2 minutes (min), respectively. The rehydration of tissue sections was completed by a 5 min washing step in PBS. Next, tissue sections were subjected to antigen retrieval, which was performed at pH 6.0 for 20 min at subboiling temperature. Sections were cooled at room temperature (RT) for another 20 min and washed three times in PBS and a subsequent blocking step was performed. Therefore, sections were transferred into a wet chamber and 100 µl of a 4% BSA/PBS solution with 0.3% Triton X-100 were pipetted onto the specimens before being covered with parafilm in order to provide equal distribution of the blocking solution. In the following, tissue sections were incubated overnight in primary antibody solution in a wet chamber. Primary antibody solutions contained either rabbit anti-mouse-cytokeratin-19 (CK-19) antibodies mixed with mouse anti-mouse-α-smooth muscle actin (α-SMA) antibodies or rabbit anti-mouse-desmin antibodies mixed with mouse anti-mouse-Ki67 antibodies diluted in 100 µl 1% BSA in PBS solution with 0.3% Triton X-100, respectively. Detection of antibody-binding was performed with the Lab Vision$^{TM}$ MultiVision Polymer Detection System according to the manufacturer's instructions. Tissue slices were therefore washed three times in TBS-T + 0.3% Triton X-100 before one drop MultiVision Polymer Cocktail: anti-mouse/HRP + anti-rabbit/AP was added to the sections, which were then incubated for 1 h at RT. Specimens were again washed 3 times in TBS-T + 0.3% Triton X-100 and chemical detection of HRP- or AP-antibody-complexes was affiliated. For this purpose, 100 µl of freshly prepared LVblue solution were pipetted onto the tissue slices and covered with parafilm for 10 min, followed by three further washing steps in TBS-T + 0.3% Triton X-100. Subsequently, 100 µl of freshly prepared LVred solution were added to the slides for 10 min under parafilm. Tissue sections were washed with dd$H_2O$ twice and afterwards dried at RT. Finally, stained tissue sections were mounted with xylene-substitute mounting medium provided in the kit.

For detailed morphologic analysis of tissue sections, haematoxylin and eosin (HE) stainings were done on corresponding serial sections to visualize cell nuclei and cytoplasm. Following deparaffinization and rehydration, tissue specimens were therefore incubated for 10 seconds in haematoxylin solution and subsequently rinsed in tab water for 5 min. Sections were then incubated in eosin for 5 min and again rinsed in tab water for another 5 min. A dehydration via respective 2 min incubation steps in 50% ethanol, 70% ethanol and 100% ethanol was affiliated for long-term maintenance of staining intensity and sections were mounted with Richard-Allan Scientific$^{TM}$ Mounting Medium.

Stained sections were evaluated using a Zeiss Axiovert 25 microscope equipped with an Axiocam-503 color (Zeiss). The specificity of all stainings was verified

performing parallel negative control stainings with corresponding IgG-control antibodies. Identified liver metastases were verified by Prof. Dr. Christoph Röcken (Institute of Pathology; UKSH Campus Kiel; Kiel, Germany) on a sample basis. The sizes of detected metastases were determined using the proprietary measuring tool of the Zeiss AxioVision software. Ki67 scoring of CK-19-positive cells/areas was done according to a pathologically validated 5-tiered scoring system adapted from [186]**(Table 3.1)**.
For stroma characterization, the CK-19-positive area plus 2 cell diameter was defined as region of interest. α-SMA- and desmin-immunostaining was assessed using a 4 tiered scoring system **(Table 3.1)**

**Table 3.1.: Scoring system for PDEC-proliferation and surrounding stroma**

| **PDEC-proliferation scoring (Number of Ki67-positive cells)** | | | | |
|---|---|---|---|---|
| **Score 0** | **Score 1** | **Score 2** | **Score 3** | **Score 4** |
| negative | <10 % | 10 - 50 % | 50 - 99% | 100 % |
| **Stroma scoring (Intensity of α-SMA or desmin staining)** | | | | |
| **Score 0** | **Score 1** | **Score 2** | **Score 3** | |
| no staining | weak staining | intermediate staining | strong staining | |

## 3.2. Analysis of pancreatic and hepatic tumor growth in an age-related syngeneic PDAC mouse model

### 3.2.1. Animal care and tumor cell application

To determine the impact of inflammation on PDEC proliferation in an aging-related *in vivo* inflammation model, C57BL/6J wild type mice, either 8 weeks or 52 weeks of age, were obtained from Charles River Germany (Sulzfeld, Germany). Animal experiments and care were carried out in accordance with European guidelines for care and use of laboratory animals and approved by local authorities (V242-77326/2015 (123-10/11). Mice were allowed to acclimatize and kept in a sterile S1-environment in the central animal husbandry of UKSH Campus Kiel (Kiel, Germany) at 22°C ± 2°C and 55 ± 10% relative humidity in

adherence to a 12 h light- and dark rhythm. Bedding, food and water were autoclaved in order to achieve specific pathogen-free conditions in accordance with FELASA-guidelines. All animals were exclusively fed with chlorophyll-free food to minimize tissue autofluorescence, which compromises bioluminesence detection. Mice were kept in Macrolon®-cages type III with filtertops in Lamina-Flow-cabinets in groups of up to 5 animals. For both age groups, Twenty animals were used per age group and 10 mice per age group were sacrificed after 2 weeks and 4 weeks, respectively (**Figure 3.2**).

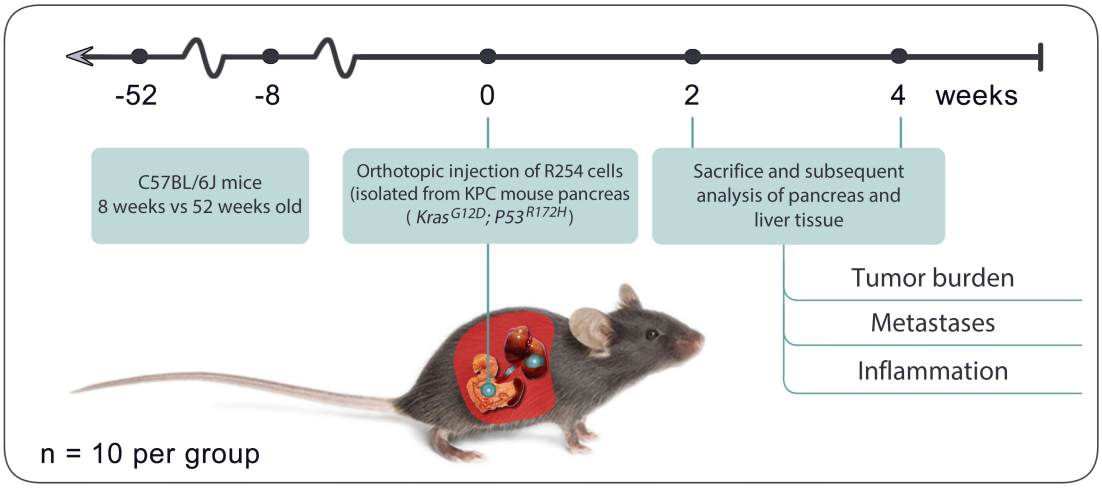


**Figure 3.2.: Experimental setup for the analysis of pancreatic and hepatic tumor growth in an age-related syngeneic PDAC mouse model.**

For the preparation of tumor cells, $3*10^4$ R254 cells (**cf. Chapter 2.7.1**), cultured and detached as described in **Chapter 3.3.1** were suspended in 25 µl DMEM supplied with 10% FCS and placed on ice until application. Abdominal surgery was performed as described previously [187] by Prof. Dr. Jan-Hendrik Egberts, Dr. Charlotte Hauser and Dr. Jan-Paul Gundlach (Department of General, Visceral-, Thoracic-, Transplantation- and Pediatric Surgery, UKSH Campus Kiel, Kiel, Germany). For this purpose, mice received general anaesthesia via intra-peritoneal injection of 5 µl/kg bodyweight (BW) combination-narcosis composed of Midazolam (5 mg/kg BW), Fentanyl (0.05 mg/kg BW) and Dormitor (0.5 mg/kg BW), which were mixed under sterile conditions. The absence of paw withdrawal reflexes was verified and animals were weighed before mouse abdomina were sterilized and shaved. A median-laparotomy was performed, the pancreas identified and 25 µl of R254 cell suspension were injected into the pancreas head. The abdominal wall was immediately closed using Vicryl 6-0 suture. As control treatments, one animal per group received an injection of 25 µl cell-free medium while a second animal was completely excluded from the surgical intervention. To avoid cooling, animals were placed on a heating mat during the time of surgery. The

anesthesia was antagonized via subcutaneous injection of a mixed combination of Anexate (0.1 mg/ml BW), Naloxon (0.4 mg/ml BW) and Antisedan (5 mg/ml BW). The animal recovery was carefully supervised with red light rewarming and supported with subcutaneous injection of Temgesic (0.1 mg/kg BW) and Glucose 5% B.Braun solution (0.025 mg/kg BW). All animals survived the respective treatment.

### 3.2.2. Determination of PDAC growth via ultrasound imaging

*In vivo* monitoring of primary and secondary tumor growth as well as the collection of tissues was carried out 2 weeks and 4 weeks post-operation. For this approach, operated animals as well as respective control animals were anesthetized as described above and abdominal hair was removed with depilation creme. Before, during and between examination events, animals were placed on heating mats to avoid cooling. After preparation, mice underwent abdominal ultrasound screening using a Vevo770® high-resolution *in vivo* micro-imaging system which exhibits a resolution of 30 µm. An RMV706 ultrasound transducer (20 - 60 MHz) was used and signals recorded in sagittal and transversal direction. After 3-dimensional image acquisition via the Vevo®-Software, volumetric analysis of tumors was performed applying the ellipsoid-formula:

$$tumor\ volume\ (mm^3) = \frac{tumor\ length\ (mm) * tumor\ width\ (mm) * tumor\ depth\ (mm)}{2}$$

Ultrasound examinations as well as primary tumor size measurements were carried out by Dr. Olga Will (Molecular Imaging North Competence Center, Clinic of Radiology and Neuroradiology, CAU and UKSH Campus Kiel, Kiel, Germany)

### 3.2.3. Determination of PDAC growth via detection of bioluminescence

The expression of luciferase reporter-constructs by R254 cells allows for specific identification of tumors in mice via detection of bioluminescence signals. Furthermore, the utilization of luciferase expressing cells delivers a control for successful tumor cell accretion since only vital cells express luciferase and are therefore able to process and activate exogenously supplied luciferin-substrate. Luciferase-activity was measured in a NightOWL LB 983 *in vivo* Imaging System. For this procedure, animals received an intraperitoneal injection of 10 µl/kg

BW a D-Luciferin Firefly solution. After 15 min, mice were transferred into the NightOWL LB 983 imaging device and a picture was taken to document the position of the animal. Subsequently, the bioluminescence signal was measured with a 550 nm excitation filter and a 605 nm emission filter with the exposure time set to 3 seconds. Signals were measured in photons per second (ph/s) and quantified using the proprietary WinLight 32-Software®. The examination and analysis of *in vivo* bioluminscence imaging was supervised by Dr. Sanjay Tiwari (Molecular Imaging North Competence Center, Clinic of Radiology and Neuroradiology, CAU and UKSH Campus Kiel, Kiel, Germany).

### 3.2.4. Tissue collection and storage

Following *in vivo* imaging, mice were euthanised and fixed on polystyrene-panels in supine position. Abdomina were then opened along the *linea alba* and pancreata as well as livers were carefully removed. In the following, organs were bisected.
One half of the organ was transferred into a 1.8 ml Nunc® CryoTube®, snap-frozen in liquid nitrogen and stored at -80°C for PCR-based analysis. The other half of the respective tissue specimen was fixed in 4.5% PBS-buffered formalin before it was dehydrated and transferred into a paraffin-block for immunohistological analysis. The dehydration and paraffinization procedure was carried out at the Institute of Pathology, UKSH Campus Kiel (Kiel, Germany).

### 3.2.5. Immunofluorescence

Besides an fLuc-gene cassette, the reporter-construct of R254 cells also contains an enhanced green fluorescent protein (EGFP)-gene cassette allowing specific detection of R254 cells in tissues via antibody based visualization of expressed GFP-Tags. For this approach, FFPE liver tissue blocks were cut into serial sections of 3 µm, which until incubation in primary antibody solution underwent preparation steps as described in **Chapter 3.1.1**. The incubation in primary antibody solution was carried out overnight at 4°C in a humidified chamber. The applied solution consisted of rabbit anti-GFP-Tag antibodies mixed with mouse anti-mouse-Ki67 antibodies diluted in 100 µl 1% BSA/PBS solution with 0.3% Triton X-100. Following this step, tissue sections were washed in PBS with 0.3% Triton X-100 three times and incubated in 70% ethanol supplied with 0.1% Sudan Black-B for 20 min. Sudan Black-B was used to diminish tissue autofluorescence which is particularly pronounced in FFPE liver tissues. After three further washing steps in PBS +0.3% Triton X-100, tissue slides were incubated in 100 µl 1% BSA/PBS solution with 0.3% Triton X-100, supplied with Alexa Fluor 488

goat anti-mouse IgG H+L and goat anti-rabbit IgG H+L DyLight 594 for primary antibody visualization. Hoechst 33258 was added to the solution in 1:500 dilution in order to stain nuclei. Sections were washed in PBS 3 times and subsequently mounted in FluorSave Reagent. Visualization and evaluation of tissue sections was performed using a Zeiss Axiovert 25 microscope equipped with an Axiocam-503 color. For characterization of DTCs in the liver, ten view fields were photographed at 200-fold magnification and the median number of GFP-positive DTCs and their Ki67 status were determined. Liver micrometastases were defined as clusters of more than 5 GFP-positive DTCs. For the detection and quantification of DTCs and micrometastases in the liver, one entire liver section per animal was screened. Detected DTCs and micrometastases were photographed at 200-fold magnification.

### 3.2.6. RNA-isolation of whole-tissue specimens

For PCR-based analysis of liver tissues, the cryo-preserved half of the respective extracted organ was used. The tissue specimen was removed from the cryotube and transferred into a plastic dish. A piece of probe was cut out without allowing thawing of tissue. The cut section was immediately transferred into a ceramic mortar which was filled with liquid nitrogen and stored on ice. The tissue was then disrupted and homogenized into fine powder by grinding with a pestle while liquid nitrogen was allowed to vaporize completely. In the following, total RNA of up to 40 mg of tissue homogenizate was isolated using the peqGOLD Total RNA Kit according to manufacturer's instructions. Then, isolated RNA was eluted in 40 µl of nuclease-free dd$H_2O$ and collected in a 1.5 ml reaction tube. Nucleic acid concentration was measured using an Infinite 200 PRO spectrophotometer and the RNA was stored at -80°C.

### 3.2.7. cDNA synthesis

Complementary DNA (cDNA) was generated from isolated RNA using the RevertAid First Strand cDNA Synthesis Kit according to the manufacturer's guidelines. For this process, up to 500 ng of RNA were mixed with 1 µl of oligo$(dT)_{18}$ primers and filled up with nuclease-free dd$H_2O$ to a total volume of 12.5 µl. Following mixing, the solution was incubated at 65°C for 5 min to assure optimal annealing of primers to the template RNA. After cooling on ice, samples were briefly spinned down and the following components were added to the respective RNA probe:

| Components per RNA sample | |
|---|---|
| 5.0 µl | 5x SybR Reaction Buffer |
| 0.5 µl | Ribolock RNase Inhibitor (20 U/µl) |
| 2.0 µl | 10 mM dNTP Mix |
| 1.0 µl | M-MuLV Reverse Transcriptase (200 U/µl) |
| 8.5 µl | Total volume |

After gentle mixing, probes were incubated at 42°C for 1 h. Finally, the reaction was stopped by a 5 min incubation step at 70°C. Samples were diluted 1:4 and kept at -20°C for long-term storage.

### 3.2.8. Quantitative realtime-polymerase chain reaction (qRT-PCR)

For the implementation of qRT-PCR, 2.5 µl of synthesized cDNA were pipetted into a white 96-well microtiter plate, which was stored on ice. Subsequently, each probe was filled up to a total volume of 10 µl according to the reaction mixture specified in the table below. The microtiter plate was then sealed with a translucent foil and the plate centrifuged at 400 g for 2 min. The qRT-PCR was carried out according to the program listed in the table below applying annealing temperatures as listed in **Chapter 2.8**. A melting curve analysis was affiliated for PCR quality control. All probes were pipetted and measured in duplicates using a maximum cycle amount of 50 cycles in a Light Cycler 480 II. Template-free $ddH_2O$ was measured as a negative control. The qRT-PCR evaluation was performed using the proprietary Light Cycler 480 software (Version 1.5) and Microsoft Excel. The relative gene expression was determined using the $2^{\Delta\Delta}$-method and the mean of m β-Actin- and m GAPDH expression as normalization reference.

| Reaction mixture per probe | |
|---|---|
| 2.5 µl | 1:4 diluted cDNA sample |
| 5.0 µl | Light Cycler Sybr Green I Master |
| 0.1 µM | Forward primer |
| 0.1 µM | Reverse primer |
| 0.5 µl | nuclease free $ddH_2O$ |
| 10 µl | Total volume |

| QRT-PCR protocol | | | |
|---|---|---|---|
| 1 | Denaturing | 10 sec | 95°C |
| 2 | Annealing | 20 sec | **Cf. 2.8** |
| 3 | Amplification | 30 sec | 72°C |
| 4 | -50 cycles 1-3 | | |
| 5 | Final extension | | |
| 6 | Melting curve | | |
| 7 | Cooling | | |

# 3.3. Cell biological methods

## 3.3.1. Cell cultivation

All following cell culturing procedures were conducted under sterile conditions in a laminar-flow cabinet. Autoclaved material was used and cells were regularly examined with a MycoAlert$^{TM}$ PLUS Mycoplasma Detection Kit to assure *mycoplasma*-free conditions.

### Thawing cells

In order to take cells into culture after long term storage at -196 °C in liquid nitrogen, cryo vials containing the cells in suspension were removed from a nitrogen tank and prewarmed in a water bath at 37 °C. The cells were then carefully resuspended in 5 ml prewarmed medium in a 50 ml centrifuge tube and centrifuged for 5 min at 400 xg. Subsequently, the cell pellet was resuspended in 10 ml of the respective cell culture medium (**cf. Chapter 2.7.2**) and transferred into a 75 $cm^2$ cell culture flask and stored in an incubator at 37 °C, 86% humidity and 5% $CO_2$. The next day, the cell culture medium was aspirated and exchanged for fresh prewarmed medium. At this step, external factors for cell stimulation were pipetted into the medium (**cf. Chapter 2.7.2**).

### Cultivation

If not indicated otherwise, all cells were cultivated in 10 ml of their respected culture medium (**cf. Chapter 2.7.2**) in 75 $cm^2$ culture flasks at 37 °C, 86% humidity and 5% $CO_2$. Twice a week, or whenever cultured cells showed a confluence of about 70% - 80%, passaging was performed. For this purpose, the medium was carefully aspirated, substituted by 5 ml of prewarmed PBS and the flask gently pivoted. The PBS was aspirated and 5 ml of prewarmed Accutase were pipetted into the cell culture flask, following 20 min incubation at 37 °C, 86% humidity and 5% $CO_2$. The cell suspension was subsequently transferred into a 50 ml centrifugation tube containing 5 ml of prewarmed cell culture medium and spinned down for 5 min at 400 xg. The medium was then aspirated and the obtained cell pellet resuspended in 10 ml of cell culture medium. The suspension was filled up with cell culture medium to a total amount of 30 ml, of which 10 ml were transferred into fresh culture flasks, respectively. If provided, additional factors for stimulation or maintenance of cell cultures (**cf. Chapter 2.7.2**) were pipetted into the medium and the flasks were incubated as described above. To avoid unintended activation of the M1-4HSC and HHSteC cells in culture, these cells were treated with particular carefulness and a number of 10 passages was

not exceeded. All other cell lines were cultured to a maximum passage number of 15.

#### Freezing cells

In order to freeze cells for long-term storage, these were washed with PBS and detached from 75 $cm^2$ culture flasks as described above. After 5 min centrifugation at 400 xg, the cell pellet was resuspended in prewarmed PBS and again spinned down. Finally, the pellet was resuspended in 10% sterile DMSO dissolved in FCS and transferred into a cryo vial. The latter one was then transferred into a cryo box and stored at -80 °C. After two days, cryo vials were conveyed into liquid nitrogen.

### 3.3.2. Determination of vital cell numbers

In order to seed defined amounts of cells and furthermore determine the vital cell number after a completed experiment, a Neubauer counting chamber was utilized. Following cell detachment as described above, a proportion of the respective cell suspension was diluted 1:10 in trypan blue solution. In the following, 10 µl of the solution were pipetted into the counting chamber. Only unstained cells were then included into the counting and the number of vital cells per ml was determined, applying the following formula:

$$\frac{cells}{ml} = \frac{vital\ cells * 10^4}{number\ of\ counted\ squares}$$

### 3.3.3. Coculture

To examine the impact of the hepatic microenvironment on the proliferation behavior of PDEC at different stages of malignant progression, indirect coculture systems were established and utilized. Representative of PDECs disseminating and seeding the liver at an early, premalignant stage of PDAC development the human PDEC line H6c7-kras [183] was used in this study. Dissemination from an already established malignant tumor was modelled using the malignant PDAC cell line Panc1 [185]. Different inflammatory conditions in the hepatic microenvironment were modelled using HSCs at different grades of activation and transdifferentiation. Representative of a physiological liver microenvironment HSC in an early activation stage, namely the murine cell line M1-4HSC [188], were utilized. To model an inflamed hepatic microenvironment, activated and transdiffentiated HMFs were applied in this study. The murine cell line M-HT [182], resulting of

M1-4HSC cells after 3 weeks of permanent exposure to 1 ng/ml TGF-β1, was thereby deployed. In order to reproduce key experiments in a human-human coculture system, human primary HSCs (HHSteC, **cf. Chapter 2.7.1**) at different degrees of transdifferentiation were utilized.

### Murine - human coculture system

For indirect cocultivation, hepatic stromal cells and PDECs were seeded separately before both cell compartments were combined in order to start the coculture. Therefore, $2 * 10^4$ H6c7-kras or $1 * 10^4$ Panc1 cells, cultured and detached as described (**cf. Chapter 3.3.1**), were seeded into the cavities of 6-well-plates in 2 ml of their respective medium (**cf. Chapter 2.7.2**). In parallel, M1-4HSC or M-HT cells were detached and resuspended in MI-medium free of exogenous TGF-β1 and Pen/Strep. The cavities of 6-well-plates were filled with 2 ml of MI-medium and corresponding transwell-inserts with 0.4 µ pores were placed therein. Then, $5 * 10^4$ M1-4HSC or M-HT cells, suspended in 1.5 ml medium were seeded into the transwell-inserts, respectively. After overnight incubation at 37 °C, 86% humidity and 5% $CO_2$, the medium of all wells was aspirated and substituted by the particular coculture medium (**cf. Chapter 2.7.2**). Subsequently, the coculture was started by transferring the transwell-inserts into the corresponding wells containing PDECs (**Figure 3.3**). The coculture conditions were maintained for 6 days at 37 °C, 86% humidity and 5% $CO_2$.

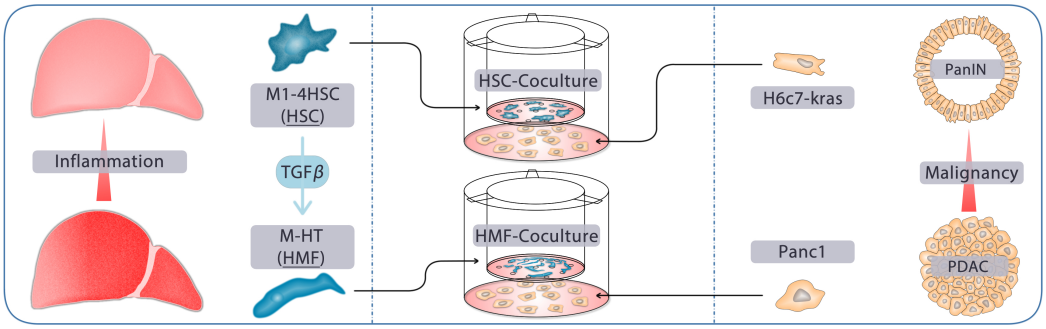


**Figure 3.3.: Settings for murine-human coculture systems.** M1-4HSC (HSC), representative of a physiological liver microenvironment, or M-HT (HMF), modelling an inflamed liver, were indirectly cocultured with premalignant H6c7-kras cells or malignant Panc1 cells for 6 days. HMF were generated by long-term exposure of HSC to 1 ng/ml TGF-β1. H6c7-kras cells were used to model the dissemination of PDECs at an early stage of PDAC pathogenesis while Panc1 cells were applied to model PDEC dissemination from an established PDAC primary tumor. Both compartments were connected by a membrane with 0.4 µm-pores which facilitates mutual influence by soluble factors.

### Human - human coculture system

HHSteC are primary HSCs isolated from human liver tissue and expose an advanced degree of transdifferentiation. To generate a human cell system exhibiting features corresponding to M1-4HSC and M-HT, respectively, human HHSteC

were cultured as described above (**cf. Chapter 3.3.2**) and particular factors were added into the medium upon cell passaging. A previous study reported that all-trans-retinoic acid (ATRA) reprograms pancreatic stellate cells (PSCs) to quiescence via retoinic acid receptor beta (RAR-γ)-mediated downregulation of actomyosin [189]. Accordingly, HHSteC were cultured in 2.5 µM ATRA to obtain cells with a phenotype corresponding to HSCs with a lower degree of trandifferentiation. In line with the generation of M-HT cells from M1-4HSC cells according to Proell *et al.* [182], HHSteC were weekly stimulated with 1 ng/ml TGF-β1 in order to promote transdifferentiation. Due to the light sensitivity of ATRA, all experiments were conducted under the exclusion of light.
HHSteC pretreated with ATRA or TGF-β1 were then cocultured with Panc1 and H6c7-kras cells, respectively, applying culture conditions and cell numbers corresponding to the above mentioned murin-human coculture system. All coculture experiments were conducted with with HHSteC at passage 5-8 to assure replicable conditions. The coculture setup is depicted in **Figure 3.4**.

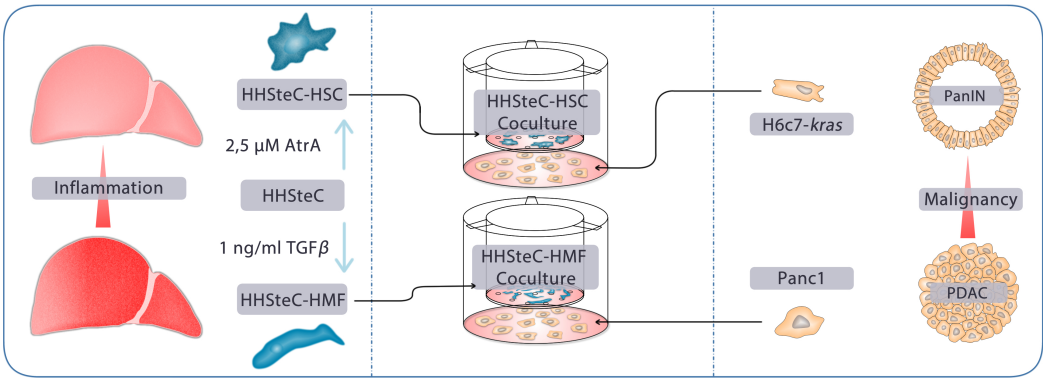


**Figure 3.4.: Settings for human-human coculture-systems.** HHSteC-HSC were generated by treatment of HHSteC with 2.5 µM all-trans-retinoic acid (ATRA) and used representative of a physiological liver microenvironment. HHSteC-HMF were produced by permanently exposing HHSteC to 1 ng/ml TGF-β1, modelling an inflamed liver. HHSteC-HSC and HHSteC-HMF were indirectly cocultured with premalignant H6c7-kras cells or malignant Panc1 cells for 6 days. H6c7-kras cells were used to model the dissemination of PDECs at an early stage of PDAC development while Panc1 cells were applied to model PDEC dissemination from an established PDAC primary tumor. Both compartments were connected by membranes with 0.4 µm-pores which facilitate mutual influence by soluble factors.

## 3.3.4. Immunocytochemical staining of Ki67

For immunocytochemical stainings of Ki67, H6c7-kras and Panc1 cells were cocultured as described in **Chapter 3.3.3**, while the cells were grown on glass coverslips, placed on the bottom of the respective well. After completed culture, transwells were discarded and the coverslips were transferred into the cavities of 12-well-plates, which were filled with 1 ml PBS. After 5 min incubation, coverslips were kept in 1 ml of a 4.5% paraformaldehyde solution for 10 min at RT. After 3 washing steps for 5 min in PBS, the coverslips were transferred into 0.3% $H_2O_2$

solved in methanol and incubated at -20 °C for 10 min to quench endogenous peroxidases. After 3 further PBS-washing steps for 5 min, blocking was done in 4% BSA/PBS for 60 min. Subsequently, 100 µl of mouse anti-human-Ki67 antibody, dissolved 1:250 in 1% BSA/PBS, were applied on the coverslips for 1 h at RT in a humid chamber. After 3 washing steps in PBS for 5 min, the coverslips were incubated on a drop of EnVision™ System HRP anti-mouse for 30 min at RT. Following 3 further 5 min washing steps in PBS, the immunostaining was visualized with AEC Substrate for 10 min. In the following, coverslips were repeatedly washed in PBS and a brief hematoxilin staining was affiliated. Finally, the coverslips were blued under floating tap water for 5 min, dried and subsequently sealed on microscope slides with Richard-Allan Scientific™ Mounting Medium. Evaluation and quantification of Ki67-stainings were carried out using an Evos XL Core Cell Imaging System. Therefore, 5 images per probe were captured at 280-fold magnification and cells staining positive for Ki67 were marked using Adobe Fireworks CS6. Stained and unstained cells were counted and the percentage ratio of positively stained cells was calculated before the mean percentage of Ki67-positive cells of 5 images was determined.

### 3.3.5. Immunocytofluorescence-staining of α-SMA and desmin

For immunofluorescence detection of α-SMA and desmin in HHSteC, these cells were detached and grown in accordance with the procedure described in **Chapter 3.3.1 and 3.3.3**. The coverslips were incubated in 1 ml of PBS in the cavities of 12-well-plates and fixed applying 1 ml of a 4.5% paraformaldehyde-solution. Before coverslips were incubated in 1 ml methanol for 10 min at -20 °C, they were washed 3 times with PBS. Blocking was performed incubating the coverslips in 1 ml of 4% BSA/PBS. The blocking solution and all following solutions contained 0.3% Triton X-100 to induce and maintain the permeabilization of cell membranes. For incubation of the coverslips in primary antibody solution, anti-mouse-α-SMA antibody was diluted 1:100 in 1% PBS/BSA and anti-rabbit-desmin antibody was added in 1:50 dilution. The staining specificity was validated using isotype control antibodies in corresponding dilutions. The coverslips were incubated in 100 µl of the prepared primary antibody solution in a humidified chamber overnight at 4 °C. Following 3 washing steps in PBS for 5 min, the secondary antibody solution was applied for 1 h at RT in a humidified chamber. This solution consisted of Alexa Fluor 488 goat anti-mouse IgG H+L and goat anti-rabbit IgG H+L DyLight 594 as well as Hoechst 33258 diluted 1:400, respectively, in 1% BSA/PBS + 0.3% Triton. The coverslips were subsequently washed 3 times for 5 min in PBS and mounted on microscope slides in FluorSave Reagent. Stained cells were evaluated using a BZ-9000 II microscope using the

proprietary BIOREVO software.

### 3.3.6. Staining of senescence-associated beta-galactosidase (SABG)

In order to determine the activity of SABG and visualize the lysomal compartment in H6c7-kras and Panc1 cells after coculture, the Senescence β-Galactosidase Staining Kit (Cell Signaling) was utilized according to manufacturer's instructions. For this purpose, transwell-inserts were removed after completed coculture and the culture medium was aspirated and replaced by PBS. After 5 min incubation, cells were fixed for 15 min at RT in a formaldehyde-based fixative solution. During 2 washing steps in PBS for 5 min, the staining solution, supplied with the kit was prepared and set to pH 5.9 - 6.1. Fixed cells were incubated in the staining solution overnight in a dry incubator at 37 °C. Cells were then washed with PBS 3 times for 5 min and covered with 2 ml 70% glycerol for long-term storage at 4 °C. An Evos XL Core Cell Imaging System (AMG) was applied for evaluating the stainings. For the quantification of SABG-positive cells, 5 view fields per probe were photographed at 280-fold magnification. Using Adobe Fireworks CS6, a horizontal centerline was projected into the obtained images. Stained and unstained cells along the line were counted and the percentage ratio of positively stained cells was calculated. The mean percentage of SABG-positive cells was then determined from 5 examined images.

### 3.3.7. Extended coculture and realtime Life Cell Imaging

In order to examine changes in the proliferation behavior of M1-4HSC cocultured H6c7-kras and Panc1 cells in presence of M1-4HSC or M-HT, the coculture was prolonged for further 6 days. For this approach, the cell number of H6c7-kras and Panc1 cells upon initial seeding was halved. Accordingly, $1 * 10^4$ H6c7-kras cells or $0.5 * 10^4$ Panc1 cells were seeded into the cavities of 6-well-plates whereas transwell-inserts containing M1-4HSC were prepared in line with the descriptions in **Chapter 3.3.3**.

After 6 days of coculture, the transwell-inserts were removed and substituted by fresh transwell-inserts comprising $5 * 10^5$ M1-4HSC or $5 * 10^5$ M-HT. Latter ones were seeded and prepared one day before substitution as described in **Chapter 3.3.3**. For the duration of coculture, the respective 6-well-plate was placed in a JuLI$^{TM}$ Br Live Cell Analyser and surveilled by using a 4x objective and maximum digital zoom. PDECs showing a flattened, enlarged morphology (**cf. Chapter 4.3**) were thereby particularly focussed. Images were recorded all 10 min for a total duration of 144 h. After completed coculture,

the surveillance was stopped and an AVI-Video was rendered and converted into the mpeg4-format using VideoLAN-software 2.2.4. The initial resolution of 2560 $*$ 1920 pixels was thereby cropped to a resolution of 640 $*$ 480 pixels. PDECs exhibiting a flattened, enlarged morphology were counted and the ratio of proliferating versus non-proliferating cells in this population was determined. Additionally, PDECs were characterized regarding their Ki67-status by immunocytochemical stainings performed and quantified after 6 days and 12 days cocultures according to **Chapter 3.3.4**. The experimental setting is summarized and schematically depicted in **Figure 3.5**.

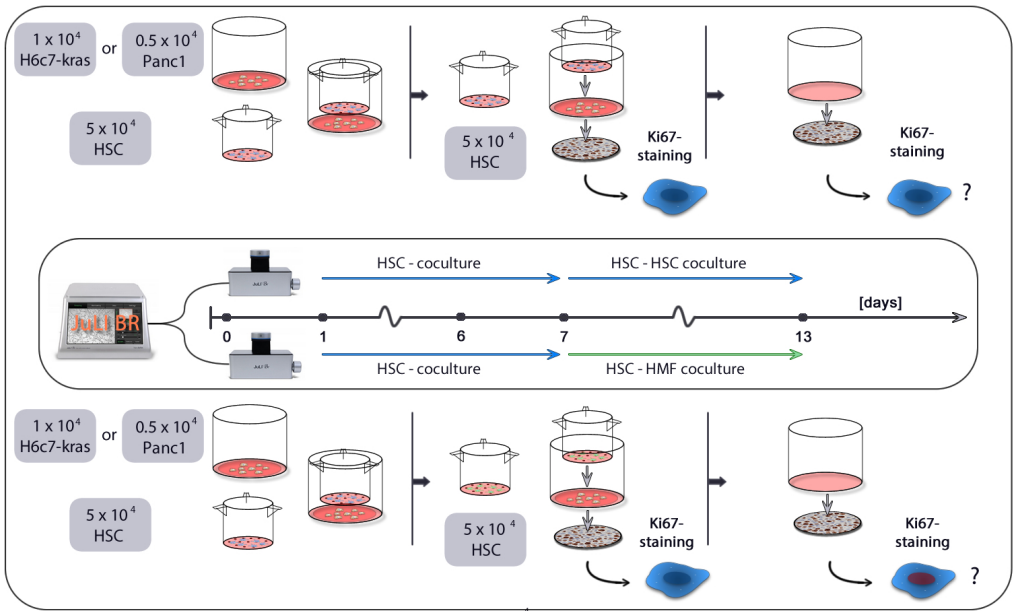


**Figure 3.5.: Experimental setting for an extended coculture system.** $1 * 10^4$ H6c7-kras cells or $0.5 * 10^4$ Panc1 cells were cultured in the presence of $5 * 10^4$ M1-4HSC (HSC) for 6 days. Transwells were substituted after 6 days for transwells with $5 * 10^4$ fresh M1-4HSC (HSC-HSC coculture) or M-HT (HSC-HMF coculture). M1-4HSC and M-HT used in the second coculture period were prepared one day prior to application. H6c7-kras and Panc1 cells were observed using a JuLI$^{TM}$ Br Live Cell Analyser during coculture with particular regard to cells exhibiting a flattened and enlarged morphology (**cf. Chapter 4.3**). After completion of the first and the second coculture period, cells grown on coverslips were examined for their Ki67-status via immunocytochemical staining as described in **Chapter 3.3.4**.

## 3.3.8. Quantification of soluble factors in cocultures

An indirect coculture system allows mutual influence of two cocultured cell entities via soluble factors. In order to identify and quantify soluble factors sequestered by PDECs and hepatic stromal cells, supernatants obtained from cocultures were examined via Multiplex analysis. Multiplex is a high-throughput immunoassay combining the principles of enzyme-linked immunosorbent Assay (ELISA) and flow cytometry, allowing the simultaneous quantification of a variety of different protein and peptide targets from a small probe amount. The

utilization of a murine-human coculture system thereby facilitates the identification of the origin compartment of the particular factor via application of species specific antibodies.
In this work, the Bio-Plex® Multiplex Immunoassay System was applied. It makes use of polystyrol beads, which contain different combinations of two fluorochromes allowing the discrimination of 500 different bead groups by a green laser in a flow cytometer. The beads are coated with monoclonal antibodies specific to a particular protein and peptide which bind the target of interest. After recognition by biotinylated secondary antibodies, the generated complexes can be visualized using a streptavidin-phycoerythrin solution which is detected in the red laser channel of a flow cytometer. In brief, a flow cytometer can recognize the analyte of interest in the green laser channel while the red laser channel allows its quantification.
H6c7-kras and Panc1 cells were cultured in the presence of M1-4HSC or M-HT for 6 days as described in **Chapter 3.3.3**. After completed coculture, supernatants were removed and transferred into centrifugation tubes in which they were centrifuged for 5 min at 400 xg and stored at -80 °C until further analysis. The respective blank medium was incubated in parallel and used as control. For the detection and quantification of protein and peptide targets the Bio-Plex® Pro Assay was utilized following the manufacturer's guidelines. Six murine and 27 human targets were thereby analyzed. Fluorometric measurements were carried out in a Bio-Plex® 200 reader using the corresponding Bio-Plex® manager software. Measurements were carried out in the Department of Immunobiology, Research Center Borstel (Borstel, Germany). Protein values of simultaneously cultured medium controls were subtracted from protein values of coculture supernatants.

### 3.3.9. Blocking of soluble factors under coculture conditions

In order to examine the impact of factors analyzed and quantified via Multiplex analysis on PDEC growth behavior, the signaling of particular factors of interest was blocked or neutralized under coculture conditions. The blocking agent was thereby pipetted into the medium of cocultures set up as described in **Chapter 3.3.3**. First, the respective blocking agent was prediluted in the corresponding coculture medium and pipetted into the coculture upon gentle shaking of the culture plate. The procedure was then iterated after 72 h. In case of SDF-1α-blocking a final concentration of 1 mM blocking agent was applied. IL-8 signaling was blocked using 2.5 µg/ml of respective antibody while agents for blocking IL-6 and VEGF signaling were applied at final concentrations of 10 µg/ml. As a control treatment, corresponding amounts of isotype control antibody were applied under equal conditions. In case of VEGF neutralization approaches in

extended cocultures (**cf. Chapter 3.3.7**), the administration of the blocking agent was carried out upon start of the second coculture period and repeated after 72 h while PDECs were observed in a JuLI$^{TM}$ Br Live Cell Analyser (**cf. Chapter 3.3.7**).

### 3.3.10. Stimulation with exogenous factors

To investigate the impact of factors identified and quantified in the Multiplex analysis on PDEC growth behavior, Panc1 cells were stimulated with the respective protein under monoculture conditions. Therefore, $1 * 10^4$ Panc1 cells were seeded as described in **Chapter 3.3.3** and cultured for 1 week. One day after seeding, cells were stimulated with the respective factor and again on day 4. Recombinant murine (m) IL-6, human (h) IL-6, h IL-8, h SDF-1$\alpha$ and h VEGF were diluted in culture medium, respectively, and pipetted into the medium of the cultured cells to reach a final concentration of 10 ng/ml. The corresponding plates were gently pivoted upon stimulation and subsequently incubated at 37 °C, 86 % humidity and 5% $CO_2$. As a control treatment, Panc1 cells were treated with corresponding amounts of the respective protein solvent.

## 3.4. Biochemical methods

### 3.4.1. Isolation and purification of proteins

To obtain and purify protein lysates from cultured cells the NucleoSpin® RNA/Protein extraction kit was utilized according to manufacturer's instructions. The culture medium was aspirated from the the 6-well-cultivation vessel and replaced by 2 ml of PBS. After 5 min incubation, the cells were detached applying 1 ml Accutase for 20 min at 37 °C. The protease reaction was stopped by transferring the obtained suspension into a 2 ml reaction tube containing 1 ml PBS and subsequent vortexing. After 5 min centrifugation at 400 xg, the obtained cell pellet was resuspended in 1 ml PBS and again spinned down 5 min at 400 xg. The cell pellet was then lysed in 80 - 200 µl 2 x Laemmli buffer corresponding to the amount of cells. The buffer was supplied with 1 mM sodium orthovanadate to inhibit the activity of cell endogenous phosphatases. In the following, the lysate was homogenized via 4 pulses of 1 sec in a sonicator. Completed lysates were stored at -20 °C.

### 3.4.2. Determination of protein concentration

The concentration of proteins in a cell lysate was determined applying the DC$^{TM}$ Protein Assay following the manufacturer's instructions. The corresponding pho-

tometric measurement was done using a translucent 96-well flat-bottom plate in an Infinite® 200 PRO Microplate Reader after 15 min incubation. The total amount of protein per probe was calculated based on a reference serial dilution with known concentrations of bovine γ-globulin.

### 3.4.3. Sodium dodecyl sulfate polyacrylamide gel electrophoresis (SDS-PAGE)

For the vertical separation of proteins in a cell lysate a SDS-PAGE was carried out. For this procedure, protein lysates containing 5 µg - 15 µg protein in 20 µl - 40 µl volume were generated by dilution of cell lysates with 2 x Laemmli buffer. The probes were then mixed 1:4 with loading dye and heated for 5 min at 95°C. After cooling on ice, the samples were loaded onto a polyacrylamide gel prepared of the compounds listed in the tables below. The protein separation ensued by applying a voltage of 95 mV until the probes had reached the separation gel and was then increased to 140 mV until completed segregation.

| **Separation gel (10 %)** | |
|---|---|
| 2.5 ml | $ddH_2O$ |
| 1.5 ml | Tris buffer (pH 6.8) |
| 2 ml | bis-acrylamide 40 % |
| 22 µl | APS 10 % (w/v) |
| 4.4 µl | TEMED |

| **Stacking gel** | |
|---|---|
| 750 µl | $ddH_2O$ |
| 312.5 µl | Tris buffer (pH 6.8) |
| 162.5 µl | bis-acrylamide 40 % |
| 6.75 µl | APS 10 % (w/v) |
| 1.25 µl | TEMED |

### 3.4.4. Protein transfer

After completed SDS-PAGE, the proteins were transferred onto a polyvinylidene fluoride (PVDF) membrane utilizing the semidry blotting technique. The PVDF membrane was activated by 1 min incubation in 100% methanol and subsequent washing in $ddH_2O$. The SDS-gel was placed on the membrane and stacked between Whatman papers soaked in buffer and arranged as depicted in **Figure 3.6**.

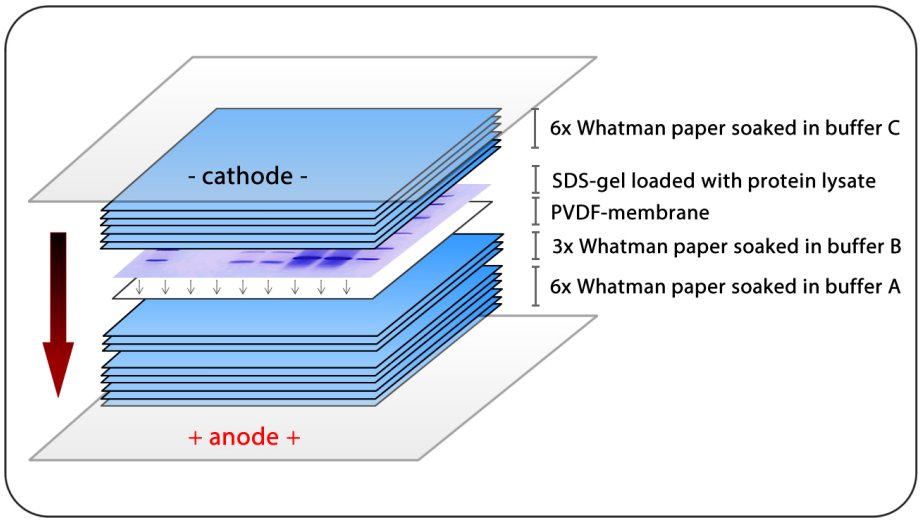


**Figure 3.6.: Protein transfer setup.** The SDS-gel containing the protein lysate separated by protein weight was transferred onto a PVDF-membrane via the semidry blotting procedure. Therefore, the gel was placed on the membrane and stacked between whatman papers soaked in either buffer A, buffer B or buffer C.

After setting up the blotting stack, the transfer was carried out in a blotting chamber by applying an electric current of 1.25 $mA/cm^2$ for 60 min.

### 3.4.5. Immunodetection of proteins

After disassembling the blotting chamber, the immunodetection of the proteins of interest was performed. The PVDF membrane was therefore washed in $ddH_2O$ and incubated in Blotto for 2 h at RT or overnight at 4 °C under gentle pivoting. Next, specific antibodies diluted according to **Chapter 2.9.1** were applied by incubating the membrane overnight at 4°C in a 50 ml centrifugation tube on a roll mixer. The next day, membranes were washed 3 times 10 min in TBS-T before the secondary antibody, prepared according to **Chapter 2.9.1**, was applied for 1 h at RT. After 3 further 10 min washing steps in TBS-T, horseradish-peroxidase (HRP) conjugated secondary antibodies were visualized by 5 min incubation in Clarity ECL substrate at RT. The resulting chemiluminescence signal was recorded via exposure in a Fusion SL detection system using the Fusion Capt Software 16.06.

### 3.4.6. Densitometric quantification of western blot signals

Signals measured in western blot analysis can be measured via semi-quantitative densitometry allowing conclusions on the amount of a particular protein in a lysate. The ratio of phosphorylated-ERK (p-ERK) to phosphorylized p38 (p-p38) was determined using the ImageJ 1.47v software which interprets measured grey scale signals of protein bands as signal peaks. The area under the curve (AUC)

of the peaks was calculated. Heat shock protein 90 (HSP90) was detected as a loading control and the p-ERK or p-p38 signal values divided by the corresponding HSP90 signal value. The normalized p-ERK value was then divided by the p-p38 value to determine the p-ERK/p-p38 ratio.

## 3.5. Statistical analysis

For statistical analysis the SigmaPlot Software 12.5 was used. The Shapiro-Wilk test was applied to test for normal distribution. Parametric data were analyzed by t-test or one-way repeated measures analysis of variance (one-way RM ANOVA) and are presented as mean ± standard deviation (SD). Non-parametric data were analyzed by Kruskal-Wallis one-way ANOVA on ranks test and are represented as medians with 25% and 75% quartiles in box-whisker plots. The statistical significance was determined applying the Student-Newman-Keuls test. P-values $\leq 0.05$ were regarded as statistically significant and are indicated with an asterisk (*).

# 4. Results

## 4.1. Proliferative activity of PDAC cells in liver metastases correlates with the presence of HSCs or HMFs

It is to date poorly established whether the condition of the hepatic microenvironment influences the proliferation and outgrowth of PDAC metastases. To address the question how the hepatic microenvironment may impact on the outgrowth of metastatic lesions, the well established KPC mouse model was utilized. KPC mice carry pancreas duct specific mutations in the *KRAS* and *TP53* genes which together potently induce PDAC formation and metastatic progression [176]. FFPE liver tissues of KPC mice were immunohistologically processed and metastases evaluated considering their proliferation with particular regard to metastasis size. Staining for cytokeratin-19 (CK-19) was performed to detect micrometastases (lesion diameter $\leq$ 200 µm) and macrometastases (lesion diameter $>$ 200 µm) originating from the pancreas duct, while Ki67 was stained in order to determine their corresponding proliferation status. The condition of the surrounding tumor stroma was characterized via desmin staining to detect HSCs and α-SMA staining to visualize HMFs.

Merging of the obtained immunstainings show the occurrence of micrometastases with a low proliferative activity of PDAC cells (Median score 2 $\widehat{=}$ 10% - 50% Ki67-positive cells) predominantly in areas with a low ratio of HMF to HSC (Median α-SMA/Desmin ratio score = 1) (**Figure 4.1 A & B, Supplementary Figure A.1**). Concurrently, macrometastases containing a significantly higher amount of proliferative CK-19-positive cells (Median score 3 $\widehat{=}$ 50% - 100% Ki67-positive cells; p = 0.016) were mostly detected in liver areas with a high presence of HMF (Median α-SMA/Desmin ratio score = 3)(**Figure 4.1 A & B, Supplementary Figure A.2**). Taken together these results indicate the correlation of stroma activation and the proliferative activity of PDAC liver metastases. Moreover, the high abundance of HMFs in the stroma of macrometastases indicate a correlation of inflammatory processes and metastatic outgrowth.

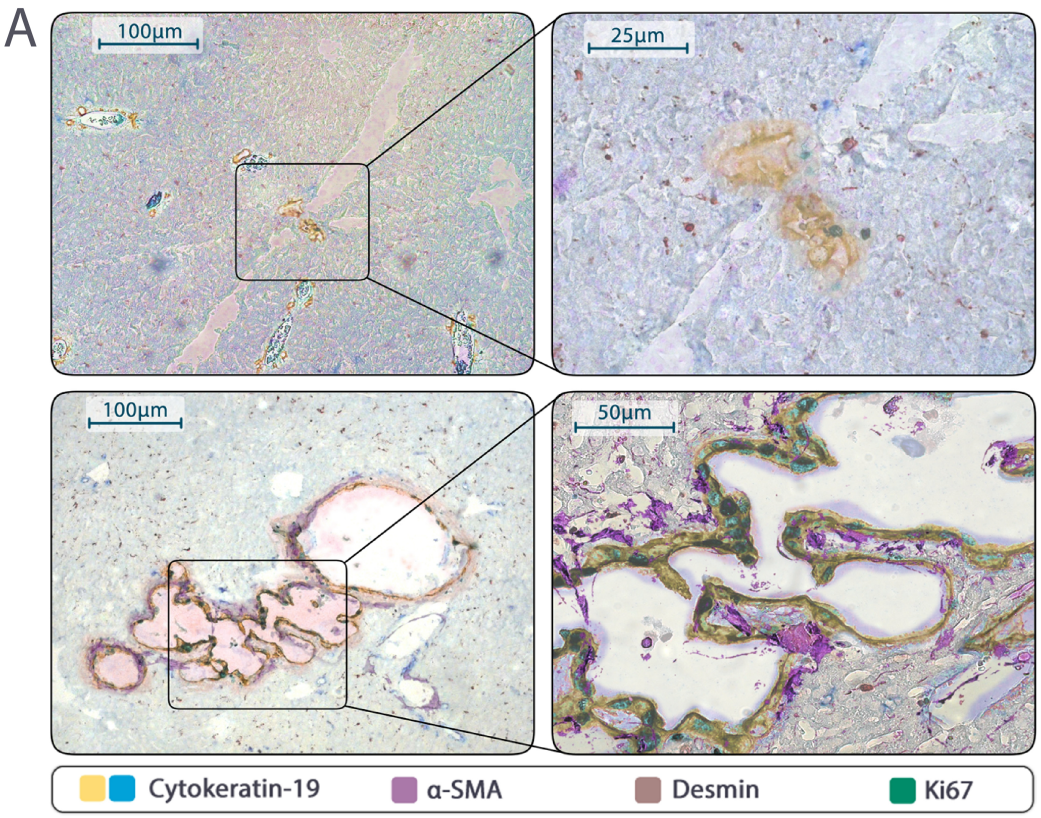


**Figure 4.1.: Proliferative activity of PDAC cells in liver metastases correlates with the presence of hepatic stellate cells (HSC) or hepatic myofibroblasts (HMF).** Liver sections of mice harboring advanced PDAC (n=13) were examined for the presence of micrometastases (lesion diameter $\leq$ 200 µm) and macrometastases (lesion diameter $>$ 200 µm) by staining of cytokeratin-19 (CK-19; to visualize PDAC cells), Ki67 (to detect proliferating cells), α-SMA (for detection of HMF) and desmin (for detection of HSC). **A**) Representative images show the overlay of CK-19, Ki67, desmin and α-SMA stainings obtained by costainings of serial sections. **B**) Scoring of Ki67 and determination of the α-SMA/desmin score in micro- and macrometastases. Data represent median values with quartiles ($Q_{0,75}$ as upper, $Q_{0.25}$ as lower deviation) of 7 micro- and 9 macrometastases. * = p <0.05.

## 4.2. Aged livers exhibit enhanced inflammation and outgrowth of PDAC metastases

The correlation of the desmoplastic reaction and metastatic growth pointed out in **4.1** raised the question if PDAC cells were attracted by the activated, HMFs-rich stroma or if the tumor cells themselves induced the observed inflammation. Hence, an *in vivo* model exhibiting different hepatic conditions regarding the inflammation status was utilized to elucidate whether a persisting liver inflammation fosters the outgrowth of PDAC cells to metastasis.

Aging represents one of the few ensured risc factors for PDAC development. Accordingly, the median age of patients upon PDAC diagnosis is 71 years [2]. Aging wash shown to promote inflammatory processes in the liver which in turn cause remodelling of the hepatic microenvironment, including HSC activation [103, 177, 190, 191]. Thus, aging was chosen as a clinically relevant inflammation-causing trigger to study the impact of liver inflammation on PDAC metastases formation.

For this purpose, wild type-C57BL/6 mice of different age were injected orthotopically with $3 * 10^4$ KPC mouse derived R254 PDAC cells and surveilled for 2 and 4 weeks, respectively [184]. Upon inoculation, mice were either 8 weeks or 52 weeks of age, the latter being equivalent to 65 human years and therefore approximately corresponding to the median age of PDAC patients at the time of diagnosis. Before sacrifice, *in vivo* imaging was performed to measure primary and secondary tumor growth before pancreata and livers were extracted and analyzed via immunhistological and PCR-based methods.

Two weeks after tumor cell injection both groups showed a similar extend of primary tumor growth in the pancreas. While 8 weeks old mice exposed a median tumor volume of 7.2 $mm^3$, 52 weeks old mice exhibited pancreatic tumors with a similarly low median volume of 6.0 $mm^3$ as determined via ultrasound imaging (**Figure 4.2 A, B & C**). The ultrasound analysis did not show the occurrence of tumorous lesions in the liver. Subsequently, sonographic measurements were validated via bioluminescence quantification in a NightOwl imaging system. The whole-animal bioluminescence *in vivo* analysis yielded comparable results showing similarly small tumors in young and old mice (83.6 av. ph/s in young mice versus 106.1 av. ph/s in aged mice)(**Figure 4.3 A**). Again, no animal showed a distinct bioluminescence signal in the hepatic region (**Figure 4.3 B**). In control animals which either received abdominal surgery or were left untreated no tumorous tissue was detectable via both imaging modalities (data not shown).

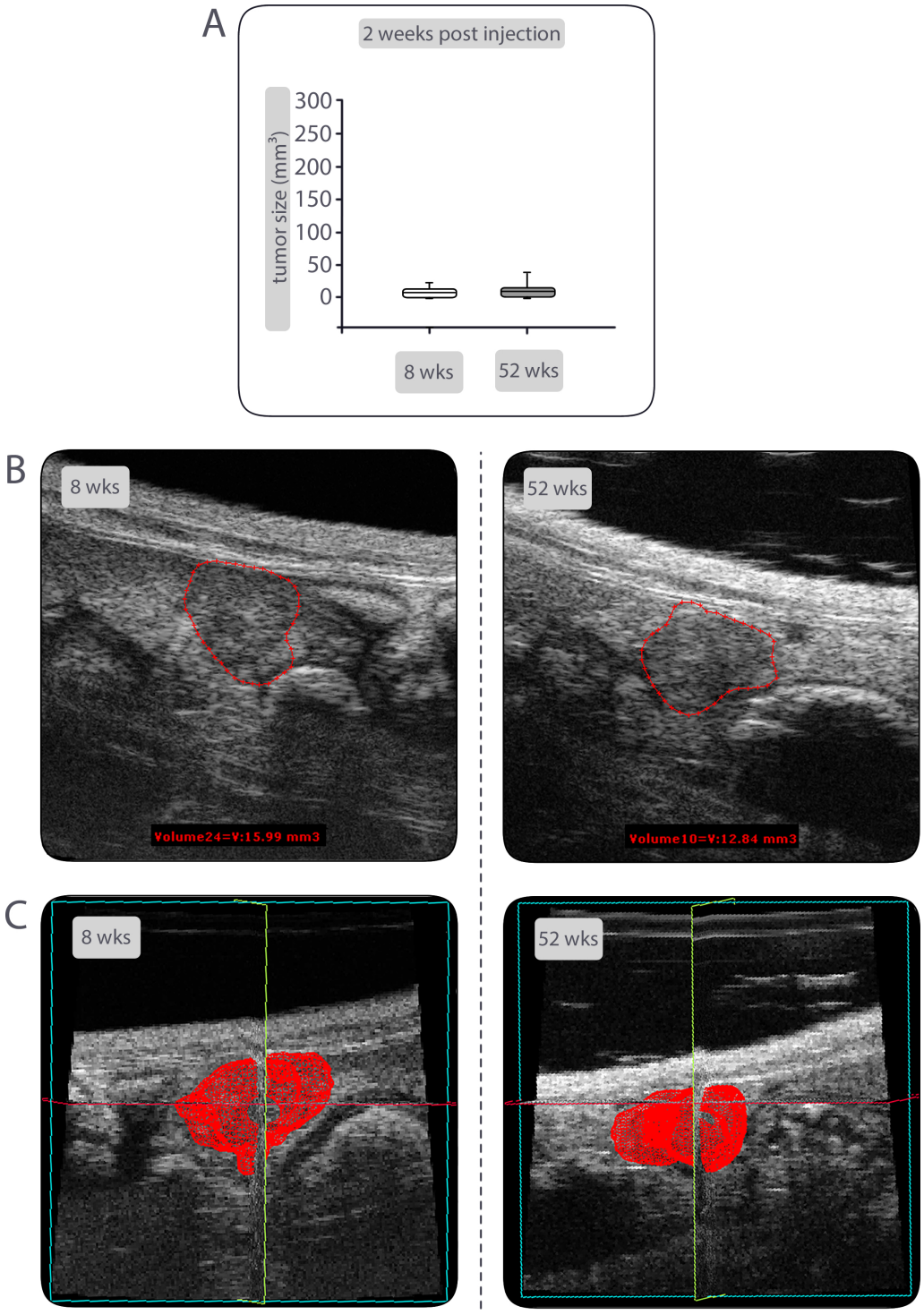


**Figure 4.2.: Sonographic tumor detection in young and aged mice 2 weeks post-injection.** Two weeks after injection of R254 cells, mice were examined considering primary tumor growth via ultrasound imaging with a resolution of 30 µm (**A**). Data represent the median values with quartiles ($Q_{0,75}$ as upper, $Q_{0.25}$ as lower deviation) of 20 animals/group. Representative ultrasound images of PDAC tissue (outlined in red) within the pancreas (**B**) and corresponding 3-dimensional recapitulation of the tumor (**C**) are depicted. wks = weeks

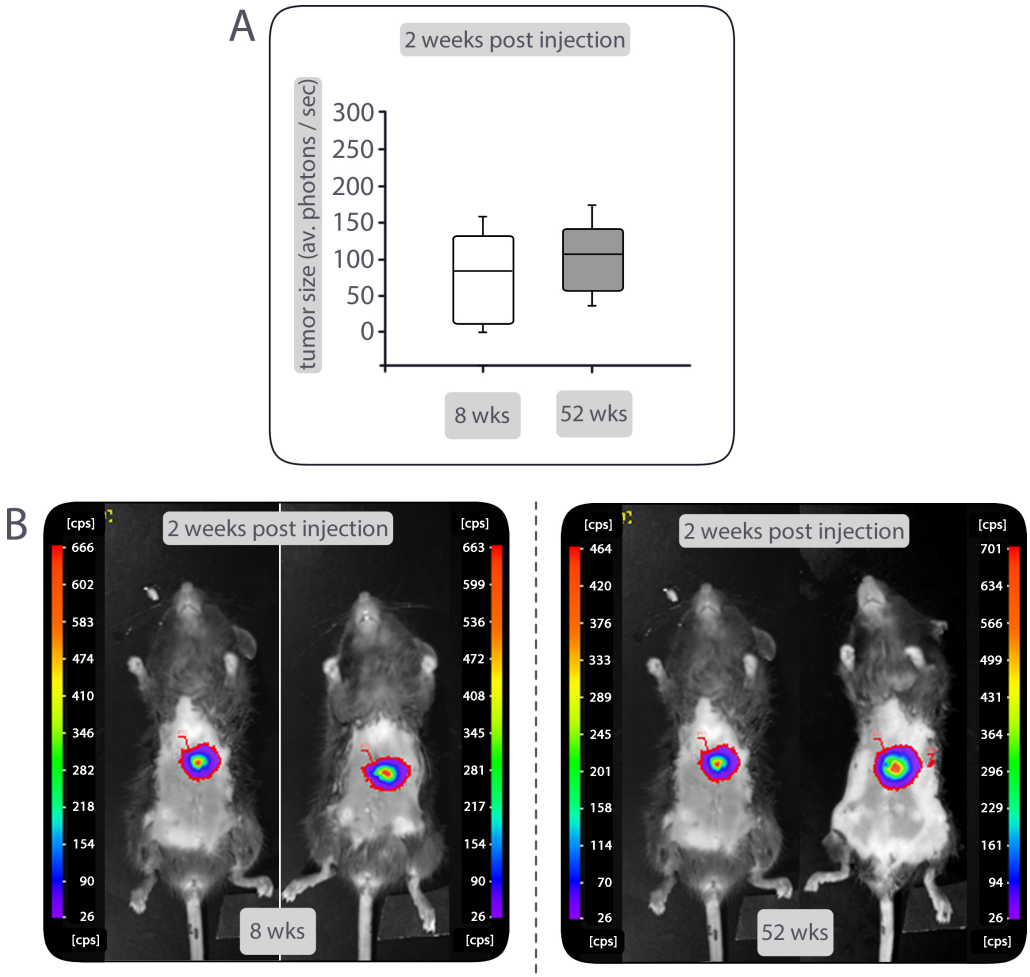


**Figure 4.3.: Tumor detection in young and aged mice 2 weeks post-injection via bioluminescence measurement.** Two weeks after injection of R254 cells, 8 weeks and 52 weeks old mice were examined for tumor growth via bioluminescence imaging (**A**). Animals were placed in a NightOwl *in vivo* imaging system and bioluminescence signals were measured for 300s. Data represent the median values with quartiles ($Q_{0,75}$ as upper, $Q_{0.25}$ as lower deviation) of 20 animals/group. Representative images of two mice, respectively, show bioluminescence signals within the abdomen (**B**) representing tumorous tissue. wks = weeks; cps = counts per second.

Since metastatic lesions were neither detected by ultrasound nor bioluminescence imaging, immunofluorescence stainings of GFP were performed in liver sections of 8 weeks old mice and 52 weeks old mice. Whereas livers of young and old mice did not expose GFP positive metastatic lesions, single disseminated PDAC cells were detectable in liver tissues of both groups. In line with the observed minor primary tumor growth, both groups exhibited similarly low numbers of GFP positive DTCs in the liver (0.4 DTCs per view field in young mice versus 0.5 DTCs per view field in aged mice)(**Figure 4.4 A & B**). Interestingly, DTCs detected in livers of aged mice showed a significantly higher percentage of Ki67-positive DTCs. Livers of 52 weeks old mice exposed 62.1 % Ki67-positive DTCs whereas in livers of 8 weeks old mice only 23.2 % of DTCs were Ki67-positive ($p = 0.001$)(**Figure 4.4 C & D**).

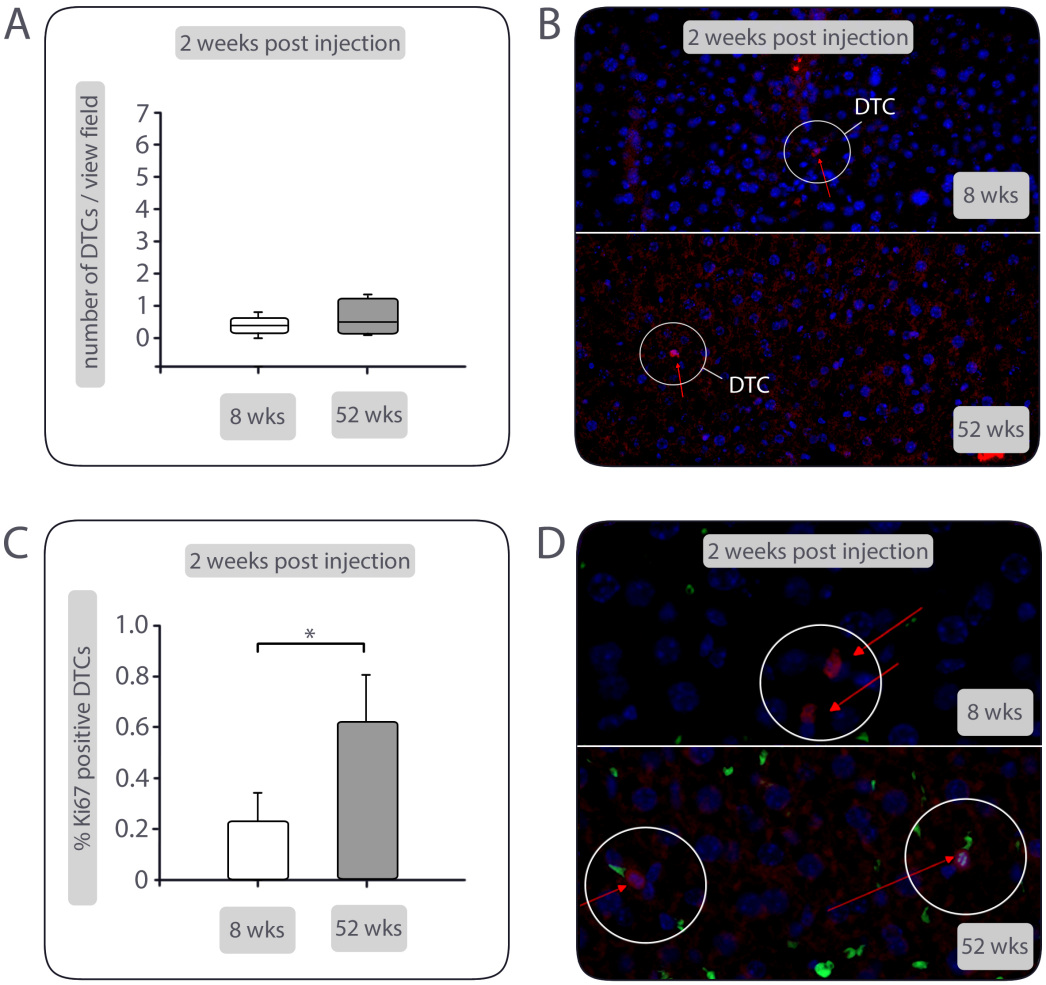


**Figure 4.4.: Immunofluorescence detection of PDAC cells in young and aged mice 2 weeks post-injection.** Following *in vivo* imaging, animals were sacrificed and pancreata as well as livers were resected and analyzed via immunofluorescence staining of GFP (to detect GFP-positive R254 cells) and Ki67 (to detect proliferating cells). Whole liver sections were photographed at 200-fold magnification and the median number of DTCs per view field in whole liver sections was determined (**A**) as well as their corresponding Ki67 status (**C**). Data represent the median values with quartiles ($Q_{0,75}$ as upper, $Q_{0.25}$ as lower deviation) or mean ± SD of 10 animals/group. * = p <0.05. Representative images of GFP positive DTCs in livers of 8 weeks and 52 weeks are depicted in (**B**) at 200-fold magnification. In (**D**) GFP-positive DTCs in livers of 8 weeks and 52 weeks after Ki-67 staining are shown at 400-fold magnification. DTCs are encircled in white, respectively.

Next, liver tissues of 8 weeks and 52 weeks old mice obtained two weeks after injection of R254 PDAC cells were characterized with respect to their inflammatory status. Due to the low abundance of DTCs in livers of young and old mice, it was assumed that these had a negligible impact on the hepatic microenvironment at this time point and that potential inflammatory alterations can be considered as aging-related. For the characterization of liver tissues, total-RNA of mouse livers was isolated and transcribed into cDNA before qRT-PCR-analysis was performed to quantify the expression of HSC and HMF-related genes as well as inflammation-related genes.

The qRT-PCR based analysis revealed a slightly elevated aSMA/desmin ratio of

17.7 % in livers of 52 weeks old mice (1,655) compared to livers of 8 weeks old animals (1,406)(**Figure 4.5 A**). However, livers of young and old mice exposed similar expression levels of collagen-1A1 (col-1A1; 0,0227 in 8 weeks old mice versus 0,0205 in 52 weeks old mice)(**Figure 4.5 B**).

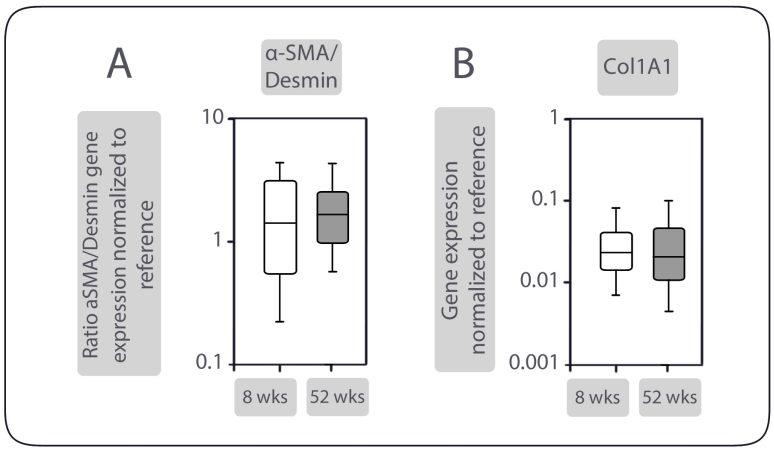


**Figure 4.5.: qRT-PCR based characterization of HSC and HMF-related genes 2 weeks post-injection.** Two weeks after injection of R254 cells, 8 weeks and 52 weeks old mice underwent hepatectomy and snap-frozen liver tissue specimens were subjected to gene expression analysis via qRT-PCR. The ratio of the relative gene expression of α-SMA and desmin was calculated (**A**) and the relative gene expression of collagen-1 (Col1A1) was determined (**B**). GAPDH and β-actin were used as housekeeping-controls. Data represent the median values with quartiles ($Q_{0,75}$ as upper, $Q_{0.25}$ as lower deviation) of 10 animals/group.

Furthermore, the gene expression of a variety of cytokines, involved in activation of HSCs as well as inflammation was examined. Whereas no differences in relative gene expression were detected for the pro-inflammatory cytokines interleukin-6 (IL-6; $0.965e^4$ in 8 weeks old mice versus $0.717e^4$ in 52 weeks old mice)(**Figure 4.6 A**) as well as tumor necrosis factor-α (TNF-α; 0.00236 versus 0.00258)(**Figure 4.6 B**), livers of 52 weeks old mice exhibited higher mRNA levels of fibroblast growth factor-2 (FGF-2; $2.18e^4$ versus $3.53e^4$)(**Figure 4.6 C**), IL-1β (0.0532 versus 0.0926)(**Figure 4.6 D**) and keratinocyte chemoattractant (KC; 0.00623 versus 0.0178)(**Figure 4.6 E**) than livers of 8 weeks old mice. Furthermore, higher mRNA levels of TGF-β1 were detected in livers of 52 weeks old mice (0.104 in livers of 8 weeks old mice versus 0.128 in livers of 52 weeks old mice)(**Figure 4.6 F**). Of note, livers of aged mice showed a significant, 1.7-fold increase in the relative gene expression of VEGF-A compared to livers of young mice (0.0374 versus 0.0211; $p = 0.009$)(**Figure 4.6 G**). By way contrast, a higher relative gene expression of macrophage inflammatory protein-2 (MIP-2)(0.0275 in 8 weeks old mice versus 0.00450 in 52 weeks old mice)(**Figure 4.6 H**) and lipopolysaccharide-induced CXC chemokine (LIX)(0.103 versus 0.00545)(**Figure 4.6 I**), two murine functional homologues to human IL-8, was observed in livers of young mice.

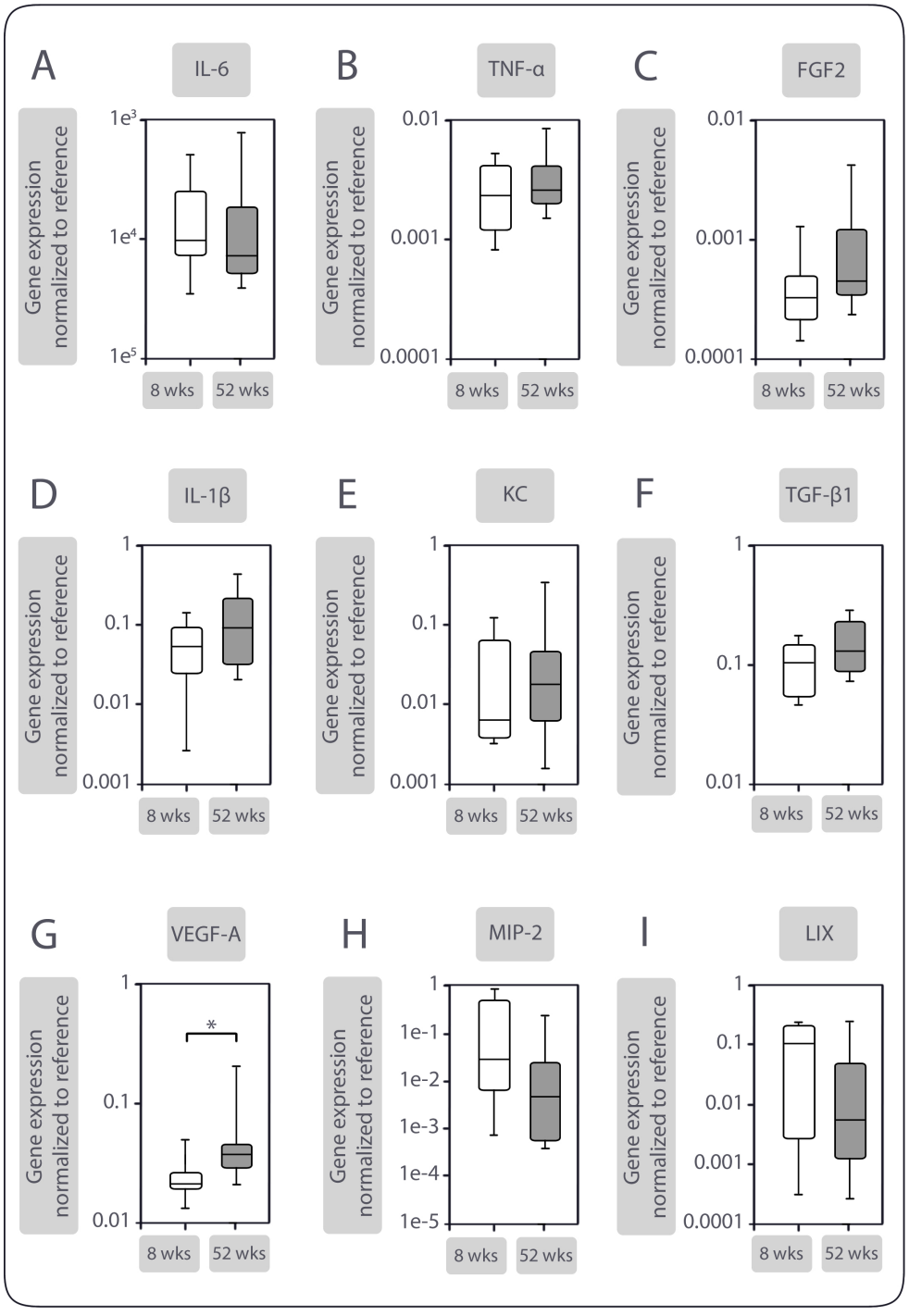


**Figure 4.6.: qRT-PCR based determination of inflammatory cytokines in liver tissues 2 weeks post-injection.** Two weeks after injection of R254 cells, 8 weeks and 52 weeks old mice underwent hepatectomy and snap-frozen tissues were subjected to gene expression analysis via qRT-PCR. The relative gene expression of the proinflammatory cytokines IL-6 (**A**), TNF-α (**B**), FGF2 (**C**), IL-1β (**D**) and KC (**E**) was detected. Furthermore, relative gene expression levels of TGF-β (**F**), VEGF-A (**G**) MIP-2 (**H**) as well as LIX (**I**) were measured. GAPDH and β-actin were used as housekeeping-controls. Data represent the median values with quartiles ($Q_{0,75}$ as upper, $Q_{0.25}$ as lower deviation) of 10 animals/group. * = $p < 0.05$.

Overall these data show a differential expression pattern of inflammatory cytokines in livers of young and aged mice. Importantly, most of the genes which

were upregulated in aged livers are known to be involved in the transdifferentiation of HSCs into HMFs, namely IL-1β [192, 193], FGF2 [194], TGF-β1 [195] and VEGF [196].

To follow the metastatic progression of PDAC in an age-related context for a longer period, corresponding parameters regarding primary and secondary tumor growth were examined in young and old mice four weeks after inoculation of R254 cells.
Animals sacrificed 4 weeks after tumor cell inoculation showed detectable, but not significant differences in primary tumor growth. Ultrasound imaging showed a median tumor size of 35,8 $mm^3$ in 8 weeks old mice while 52 weeks old mice exhibited a median tumor size of 86,5 $mm^3$ (**Figure 4.7 A, B & C**). Subsequent bioluminescence signal quantification showed corresponding results and a visible but not significant increase of primary tumor growth in aged mice compared to young mice (295,455 ph/s in 52 weeks old mice versus 173,880 ph/s in 8 weeks old mice)(**Figure 4.8 A & B**). By way of contrast, mice 8 weeks and 52 weeks of age presented distinct differences concerning metastatic outgrowth. Aged livers exhibited a significantly higher median number of DTCs per view field compared to livers of young mice (4 DTCs per view field in livers of 52 weeks old mice versus 2.1 DTCs per view field in livers of 8 weeks old mice; $p < 0.001$)(**Figure 4.9 A**). The proliferation rate of detected DTCs in livers of both groups was comparable (54% Ki67-positive cells in 8 weeks old mice versus 52% Ki67-positve cells in 52 weeks old mice)(**Figure 4.9 B**). However, micrometastases defined as clusters of more than 5 DTCs were exclusively found in livers of aged mice (0 micrometastasis per liver in young mice versus 3 micrometastasis per liver in aged mice; $p = 0.001$) (**Figure 4.9 C**).

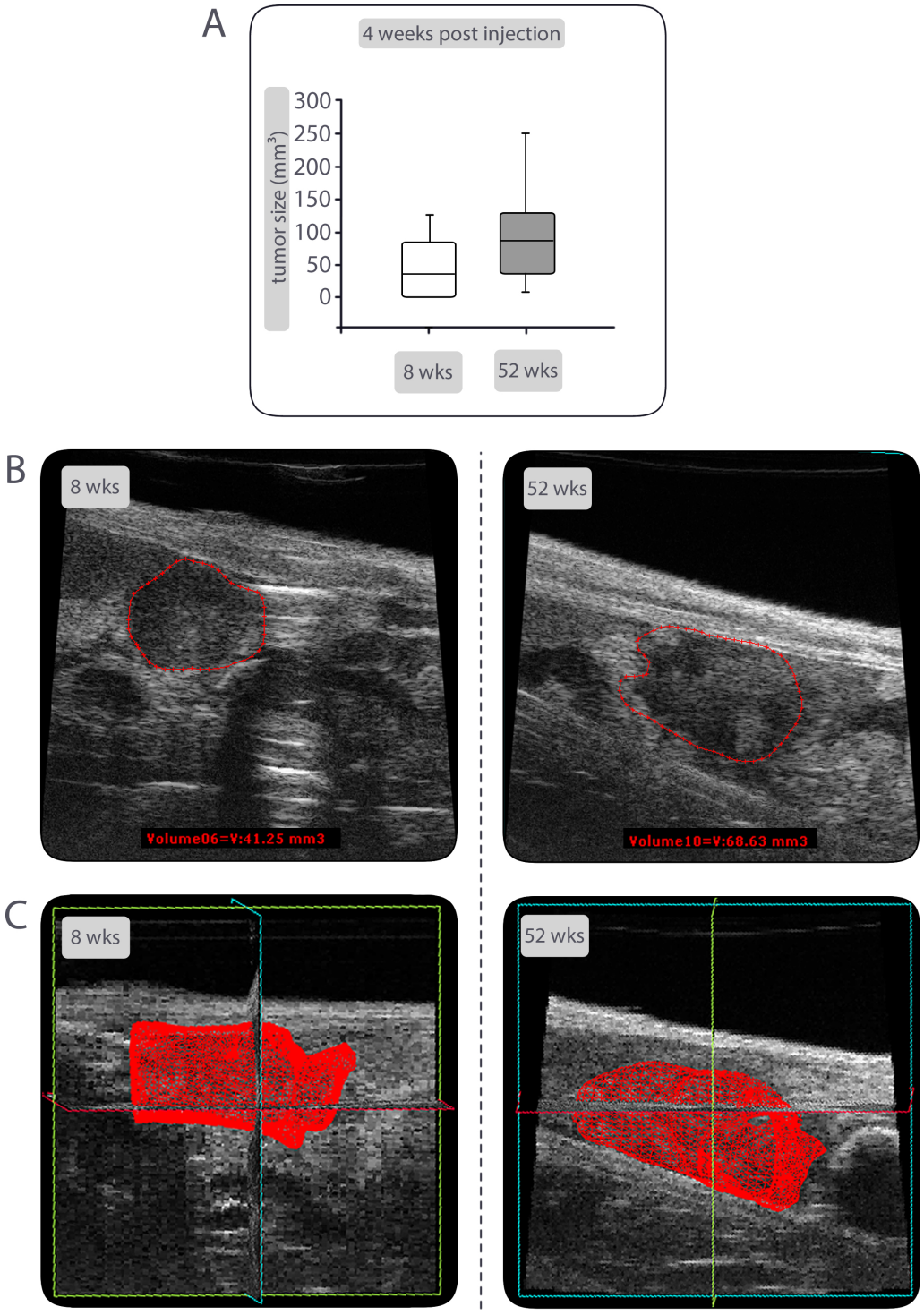


**Figure 4.7.: Sonographic tumor detection in young and aged mice 4 weeks post-injection.** Four weeks after injection of R254 cells, mice were examined for primary tumor growth via ultrasound imaging with a resolution of 30 µm (**A**). Data represent the median values with quartiles ($Q_{0,75}$ as upper, $Q_{0.25}$ as lower deviation) of 10 animals/group. Representative ultrasound images of tumorous tissue (outlined in red) within the pancreas (**B**) and corresponding 3-dimensional recapitulation of the tumor (**C**) are depicted. wks = weeks

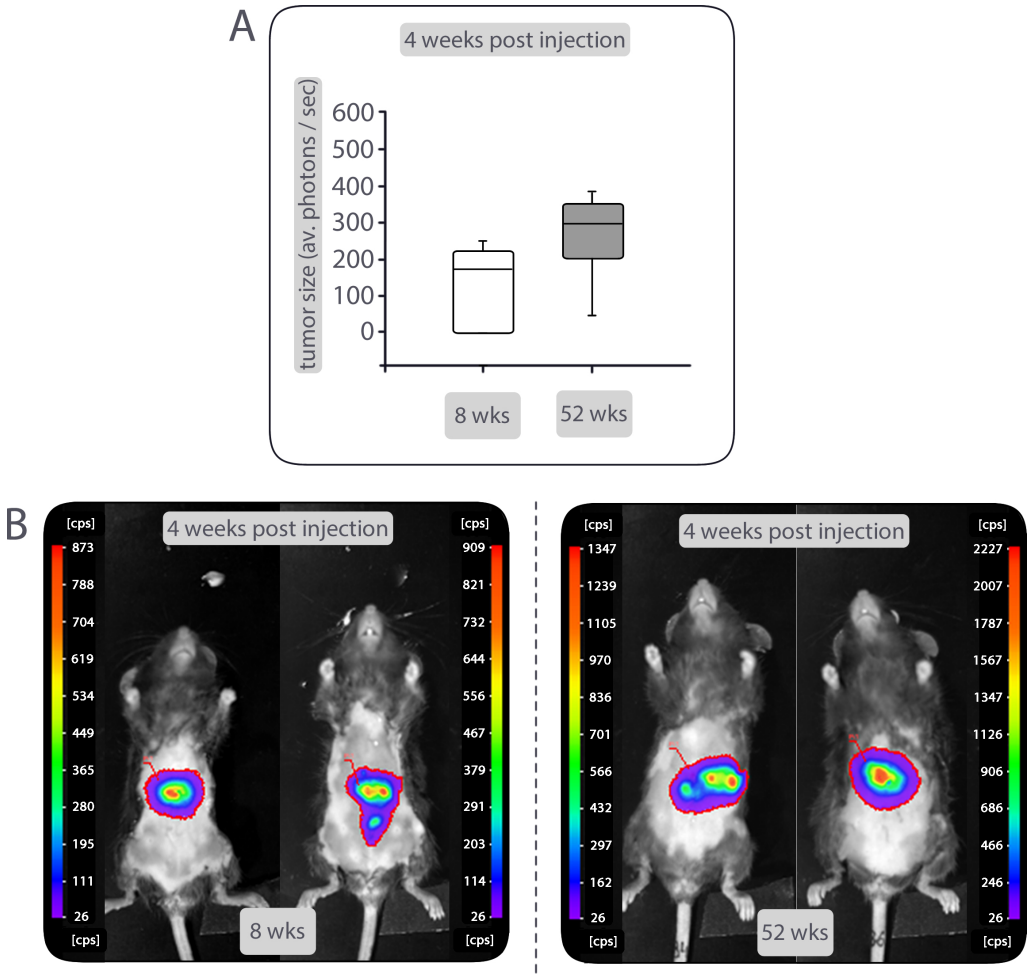


**Figure 4.8.: Tumor detection in young and aged mice 4 weeks post-injection via bioluminescence measurement.** Four weeks after injection of R254 cells, 8 weeks and 52 weeks old mice were examined for tumor growth via bioluminescence imaging (**A**). Animals were placed in a NightOwl *in vivo* imaging system and bioluminescence signals were measured for 300s. Data represent the median values with quartiles ($Q_{0,75}$ as upper, $Q_{0.25}$ as lower deviation) of 10 animals/group. Representative images of two mice, respectively, show bioluminescence signals within the abdomen (**B**) representing tumorous tissue. wks = weeks; cps = counts per second.

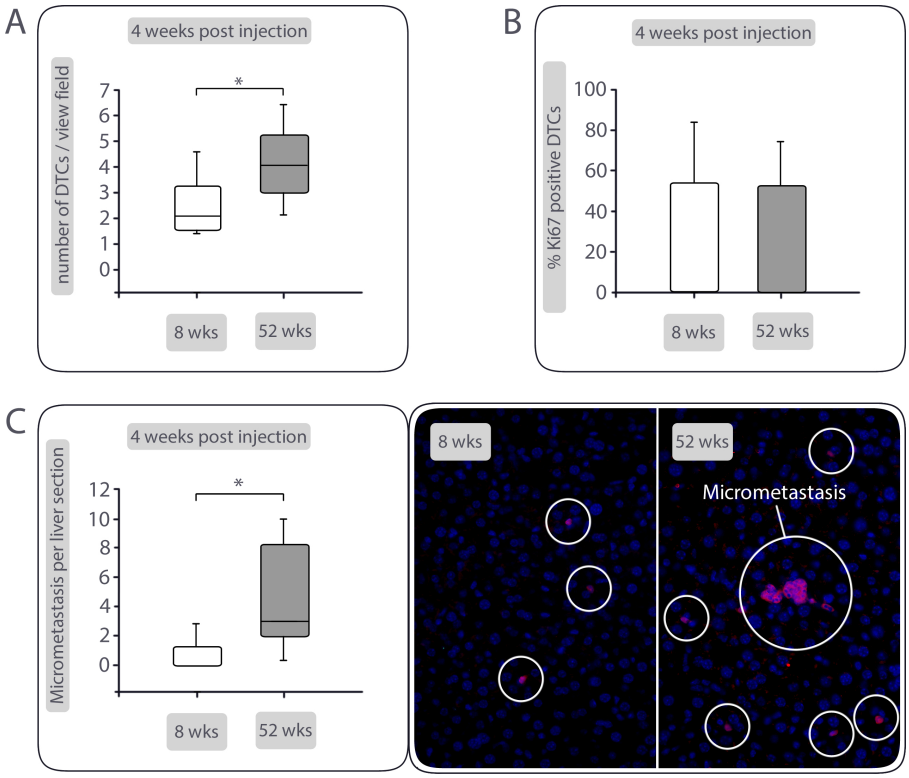


**Figure 4.9.: Immunofluorescence detection of PDAC cells in young and aged mice 4 weeks post-injection.** Following *in vivo* imaging, animals were sacrificed and pancreata as well as livers were resected and analyzed via immunofluorescence staining of GFP (to detect GFP-positive R254 cells) and Ki67 (to detect proliferating cells). Whole liver sections were photographed at 400-fold magnification and the median number of DTCs per view field in whole liver sections was determined (**A**) as well as their corresponding Ki67 status (**B**). **C**) shows the quantification of micrometastases, defined as clusters of 5 or more GFP-positive R254 cells as well as representative images of GFP-positive R254 cells and micrometastases (encircled in white) at 200-fold magnification. Data represent median values with quartiles ($Q_{0,75}$ as upper, $Q_{0.25}$ as lower deviation) or mean ± SD of 10 animals/group. * = $p < 0.05$.

Taken together, the results shown in this chapter demonstrate a marked impact of aging-related inflammation on the metastatic progression of PDAC. Whereas young and aged mice exposed visible but not significant differences in primary PDAC growth, distinct effects could be observed in the hepatic microenvironment and with respect to micrometastases. Two weeks after orthotopical injection of R254 cells, a higher state of inflammation and level of HMFs-related genes were detected in livers of 52 weeks old mice concomitantly with a higher number of Ki67-positive DTCs compared to 8 weeks old mice. Accordingly, significantly higher amounts of GFP-positive DTCs and micrometastases were detected in livers of 52 weeks old mice four weeks after PDAC cell inoculation.

## 4.3. The presence of HSC promotes the enrichment of PDECs with a quiescence-associated phenotype (QAP)

To further unravel the mechanisms by which HSCs and their transdifferentiated inflammatory counterpart HMFs impact on growth behavior of disseminated PDECs in different steps of malignant progression, an indirect coculture system was applied. In this setting, premalignant H6c7-kras or malignant Panc1 PDECs were cultivated in the presence of either M1-4HSC cells (HSC) or M-HT cells (HMF) for 6 days. HSC (**Figure 4.10 A & C**) were transdifferentiated to HMF (**Figure 4.10 B & C**) via administration of exogenous TGF-β1 which allowed the examination of HSC at different grades of activation with the same genetic background [182]. HSC were utilized to model a physiologic liver microenvironment while HMF were used representative for an inflamed hepatic microenvironment.

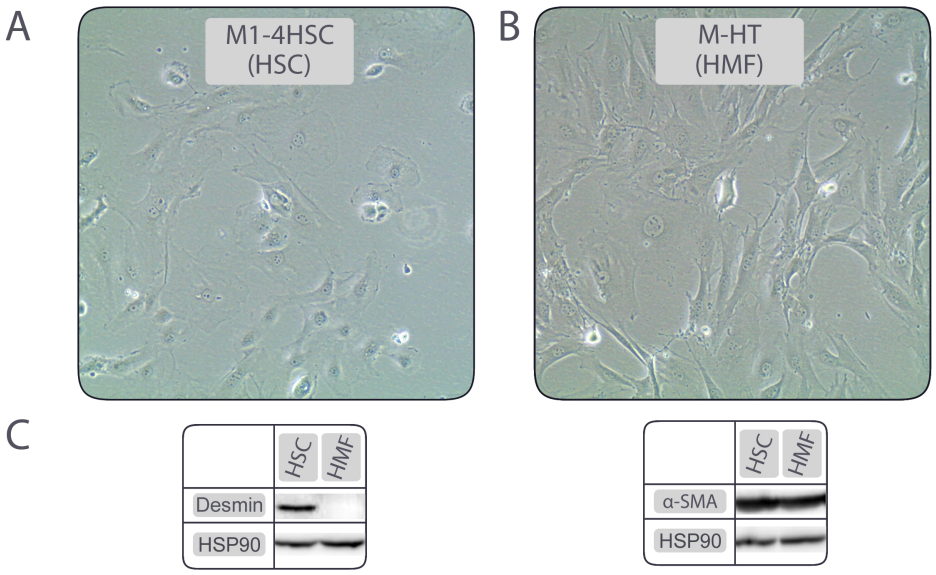


**Figure 4.10.: The hepatic stromal cell lines M1-4HSC and M-HT. A**) M1-4HSC (HSC) grown on plastic expose a characteristic stellate cell morphology. **B**) After 3 weeks of continuous administration of recombinant TGF-β1, M1-4HSC (HSC) acquired a spindle-shaped morphology which is a hallmark of myofibroblasts, the generated cell line is termed M-HT (HMF)[182]. Depicted are representative phase contrast images of both cell lines in monoculture. In (**C**) representative western blots of HSC and HMF lysates are depicted which show a lower ratio of desmin to α-smooth muscle actin (α-SMA) in HMF in accordance with the initial description of the cell system [182]. Heat shock protein-90 (HSP90) was used as loading control.

The coculture of H6c7-kras and Panc1 cells with HSC and HMF, respectively, exposed a differential impact of HSC and HMF on growth of PDECs. Both, H6c7-kras and Panc1 cells exhibited markedly decreased vital cell numbers after 6d coculture with HSC compared to HMF coculture ($9.65*10^4$ versus $15.18*10^4$ for H6c7-kras; $p < 0.05$ and $15.75*10^4$ versus $28.37*10^4$ for Panc1 cells; $p = 0.01$)(**Figure 4.11 A**)*.

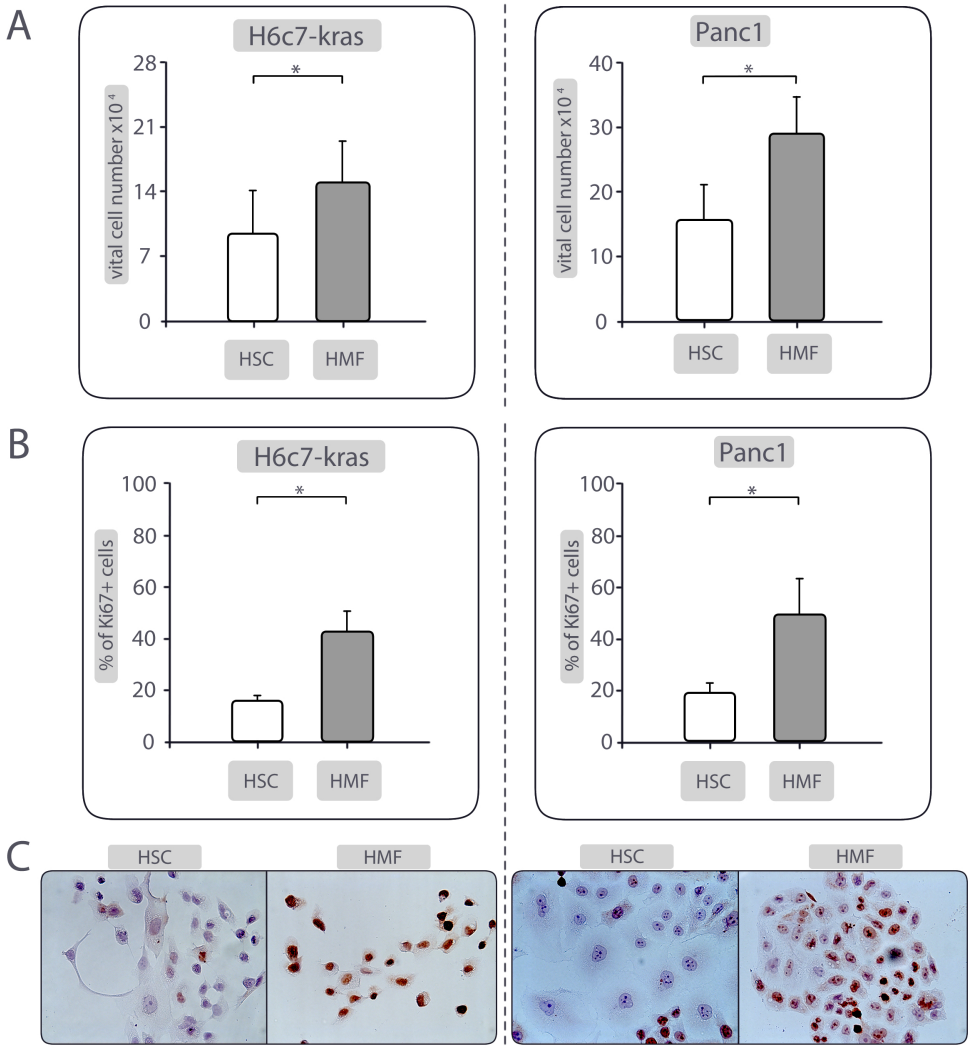


**Figure 4.11.: PDECs exhibit a reduced proliferative activity in the presence of HSC compared to HMF coculture.** H6c7-kras and Panc1 cells were cocultured with HSC or HMF. After 6 days, vital cell numbers (**A**) and percentage of Ki67-positive cells (**B**) were determined. Depicted data represent the mean values ± SD of at least 5 independent experiments. * = $p < 0.05$. **C**) shows representative images of Ki67 immunostainings in H6c7-kras and Panc1 cells after respective coculture in 200-fold magnification.

In line with their vital cell count, HSC cocultured H6c7-kras and Panc1 cells showed a significantly lower amount of Ki67-positive cells than HMF cocultured

*Vital cell counts for H6c7-kras and Panc1 cocultures with HSC or HMF were previously shown in the own Master's thesis [180] and the Master's thesis of Maren Pein [181] and validated in independent experiments.

PDECs (15.9% versus 42.9% Ki67-positive cells for H6c7-kras; $p < 0.001$ and 19.2% versus 49.8% Ki67-positive cells for Panc1; $p = 0.001$)(**Figure 4.11 B & C**). This indicates that the observed differences in PDEC vital cell count were a result of stroma-mediated alterations in PDEC proliferation behavior.

The monitoring of both PDEC lines after Ki67 immunostainings at 400-fold magnification revealed that predominantly HSC coculture conditions led to the emergence of a high number of Ki67-negative PDECs with a flattened, enlarged cytoplasm and nucleus (**Figure 4.12 A**).

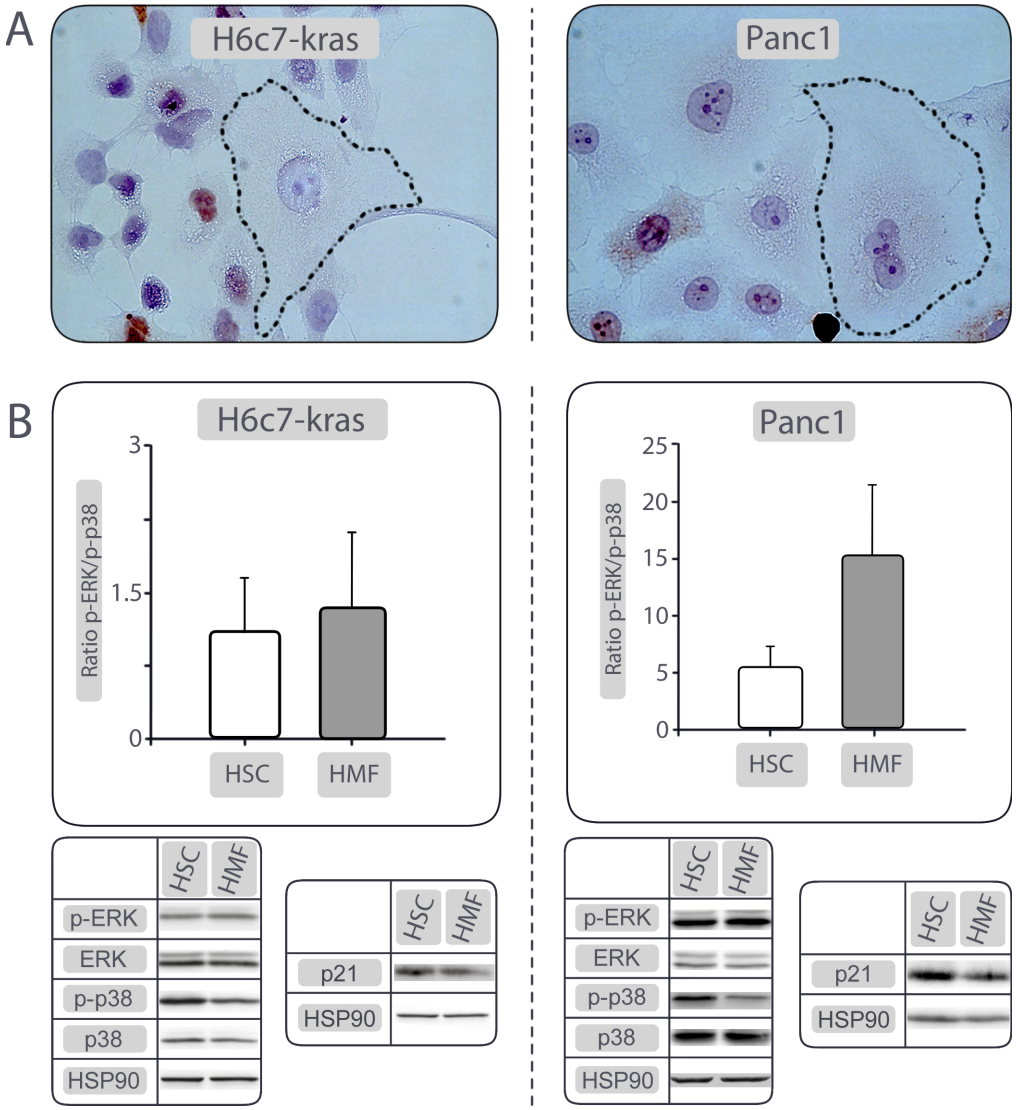


**Figure 4.12.: HSC coculture fosters the manifestation of a QAP in PDECs.** H6c7-kras and Panc1 cells were cocultured with HSC or HMF for 6 days, respectively. **A**) Representative images of Ki67 stainings in H6c7-kras and Panc1 cells after HSC coculture conditions shown at 400-fold magnification (encircled: PDECs exhibiting flattened enlarged morphology). **B**) Representative western blots showing the abundance of total and phosphorylated Erk (Erk/p-Erk) and p38 (p38/p-p38) as well as p21. Hsp90 was used as loading control. Data of densitometric analysis of the ratio of p-Erk and p-p38 expression are presented as mean ± SD of 4 independent experiments. Data represent the median values with quartiles ($Q_{0,75}$ as upper, $Q_{0.25}$ as lower deviation) of 5 independent experiments. * = $p < 0.05$.

Since these observed morphologic features were previously described to be associated with either cellular quiescence, cellular dormancy and cellular senescence [125, 136, 197], a deepened characterization of proliferation-associated features of PDECs under the influence of HSC or HMF was conducted. Western blot analysis of PDEC lysates obtained after coculture showed a lower ratio of p-ERK to p-p38 after HSC coculture compared to HMF coculture which was weakly pronounced in H6c7-kras cells (1.1 after HSC coculture versus 1.3 after HMF coculture) and significantly pronounced in Panc1 cells (5.4 after HSC coculture versus 15.5 after HMF coculture)(**Figure 4.12 B**). Accordingly, protein levels of the cell cycle inhibitor p21 were found to be weakly higher in HSC cocultivated H6c7-kras cells and markedly elevated in Panc1 cells compared to HMF cocultured PDECs (**Figure 4.12 B**). Moreover HSC and HMF cocultured H6c7-kras and Panc1 cells were analyzed with regard to the activity of the senescence marker SABG. Both PDEC lines exhibited distinctly and significantly higher SABG-activity after HSC coculture compared to HMF cocultured H6c7-kras and Panc1 cells (69.2% versus 30.2% SABG-positive H6c7-kras cells; $p < 0.05$ and 45.3% versus 12.3% SABG-positive Panc1 cells; $p = 0.013$)(**Figure 4.13 A & B**).

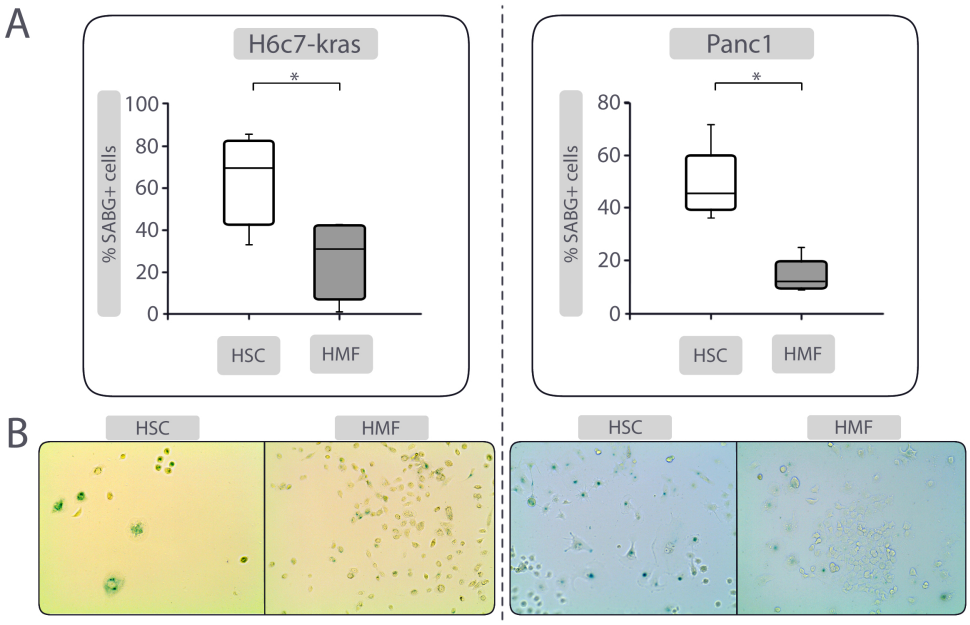


**Figure 4.13.: PDECs exhibit enhanced senescence-associated β-galactosidase (SABG) acivity in the presence of HSC compared to HMF coculture.** H6c7-kras and Panc1 cells were cocultured with HSC or HMF. After 6 days, SABG activity was measured (**A**). Depicted data represent the mean values ± SD of at least 5 independent experiments. * = $p < 0.05$. **B**) shows representative images of SABG stainings in H6c7-kras and Panc1 cells after respective coculture in 200-fold magnification.

Overall, these results show a significant impact of HSC and HMF on the proliferation features of premalignant and malignant PDECs. Compared to HMF coculture conditions, the presence of HSC led to a marked proliferation reduction

in H6c7-kras and Panc1 cells. This manifested by the emergence of features which are associated with quiescence, dormancy and senescence like Ki67 negativity, a flattened and enlarged morphology, a low p-ERK/p-p38 ratio and an increase in p21 and SABG-activity. This manifestation of growth arrest in PDECs is hereafter referred to as quiescence-associated phenotype (QAP).

## 4.4. Human HSCs foster QAP emergence in PDECs similar to murine HSC

A variety of chemokines and cytokines show a species-specific efficacy and may hence not cross-react in a mouse-human coculture system. Therefore, a human-human coculture system was established to validate key findings from mouse-human coculture systems.

This approach aimed at coculturing H6c7-kras and Panc1 cells with human hepatic stromal cells equivalent to HSC and HMF. After a first comparative analysis of different available human HSCs with particular regard to their activation status and transdifferentiability, commercially obtainable HHSteC cells were selected for further experiments. Since HHSteC cells appeared to exhibit an advanced state of transdifferentiation, characterized by a spindle shaped morphology, weak expression of collagen-1A1, α-SMA and desmin, pretreatments with different factors were carried out to obtain characteristics corresponding to HSC and HMF. To generate HHSteCs with an HSC like phenotype (HHSteC-HSC), cells were cultured in medium containing 2.5 µl all-trans-retinoic acid (ATRA) while an HMF-like phenotype (HHSteC-HMF) was generated applying medium with 1 ng/ml TGF-β1 for two weeks, respectively. Afterwards, cells were characterized via immunofluorescence stainings and western blot analysis. Immunofluorescence stainings revealed a distinctly lower ratio of α-SMA to desmin in HHSteC-HSC compared to HHSteC-HMF (**Figure 4.14 A**). Direct comparison of untreated HHSteC cells with HHSteC-HSC and HHSteC-HMF showed highest levels of collagen-1A1 and α-SMA in HHSteC-HMF while the highest level of desmin was found in HHSteC-HSC (**Figure 4.14 B**). Overall these results indicate the successful generation of human HSCs with phenotypes corresponding to murine HSC and HMF.

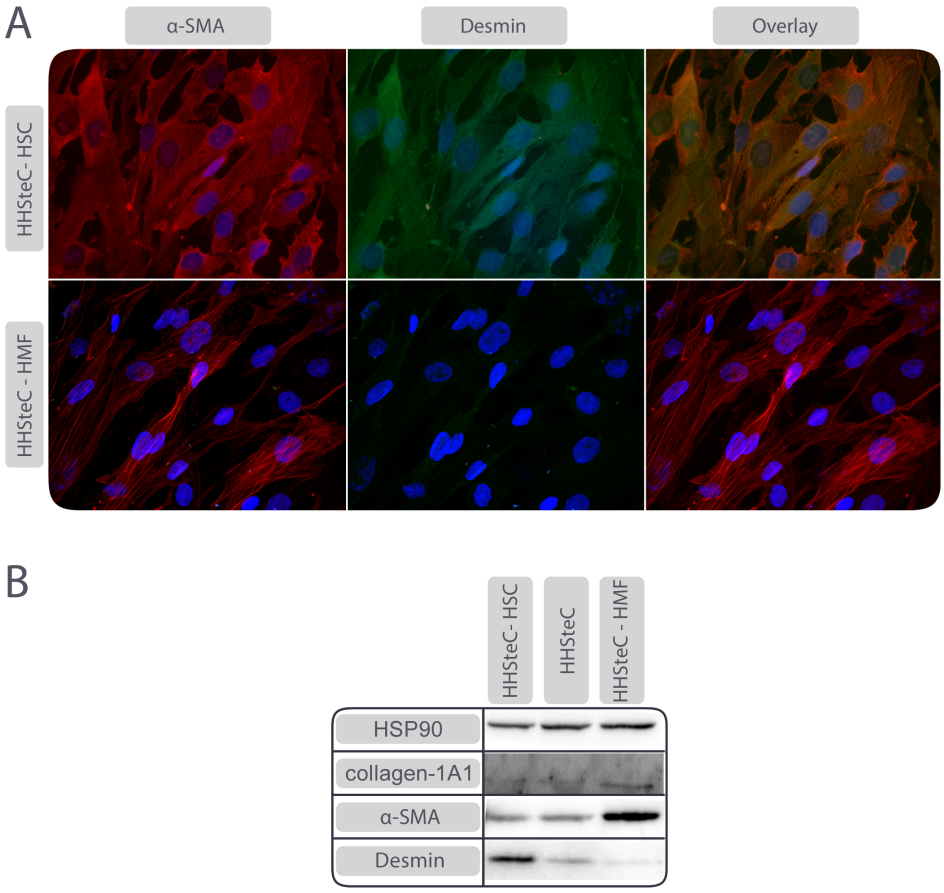


**Figure 4.14.: Generation of HSC and HMF like phenotypes in HHSteC.** In order to generate human hepatic stromal cells with characteristics equivalent to HSC and HMF, HHSteC were pretreated with medium containing either 2.5 µl all-trans-retinoic acid (ATRA) and 1 ng/ml TGF-β1 for 2 weeks, respectively. Cells were characterized via immunofluorescence stainings of α-SMA and desmin (**A**) and detection of collagen-1A1, α-SMA and desmin via western blot (**B**) HSP90 was used as loading control. Representative results of 4 respective independent experiments are shown, immunofluorescence stainings are depicted in 400-fold magnification.

In line with the preceding chapter, HHSteC-HSC and HHSteC-HMF were set in coculture with H6c7-kras and Panc1 cells for 6 days, respectively. HHSteC-HSC coculture resulted in a lower vital cell number of H6c7-kras and Panc1 cells than the corresponding HHSteC-HMF coculture (1.96-fold increase in vital cells in H6c7-kras and 1.48-fold increase in Panc1 cells)(**Figure 4.15 A**). Accordingly, a significantly lower percentage of Ki67-positive PDECs was found after HHSteC-HSC coculture conditions (31,8% versus 51,0% Ki67-positive cells in H6c7-kras (p=0.004) and 33.2% versus 62.5% Ki67-positive cells in Panc1 (p=0.016))(**Figure 4.15 B**). Furthermore, H6c7-kras cells and Panc1 cells co-cultured with HHSteC-HSC showed a markedly higher number of SABG-positive cells than HHSteC-HMF cocultured PDECs (48.6% versus 40.2% SABG-positive H6c7-kras cells (p=0.039) and 35.6% versus 16.2% SABG-positive Panc1 cells)(**Figure 4.15 C**). Taken together, these results show differential effects of human HSCs and HMFs on proliferation thereby validating key findings

obtained in the HSC/HMF coculture system. Moreover, an induction of QAP in H6c7-kras and Panc1 cells by human HSCs, similar to the QAP promoting effect of HSC could be observed.

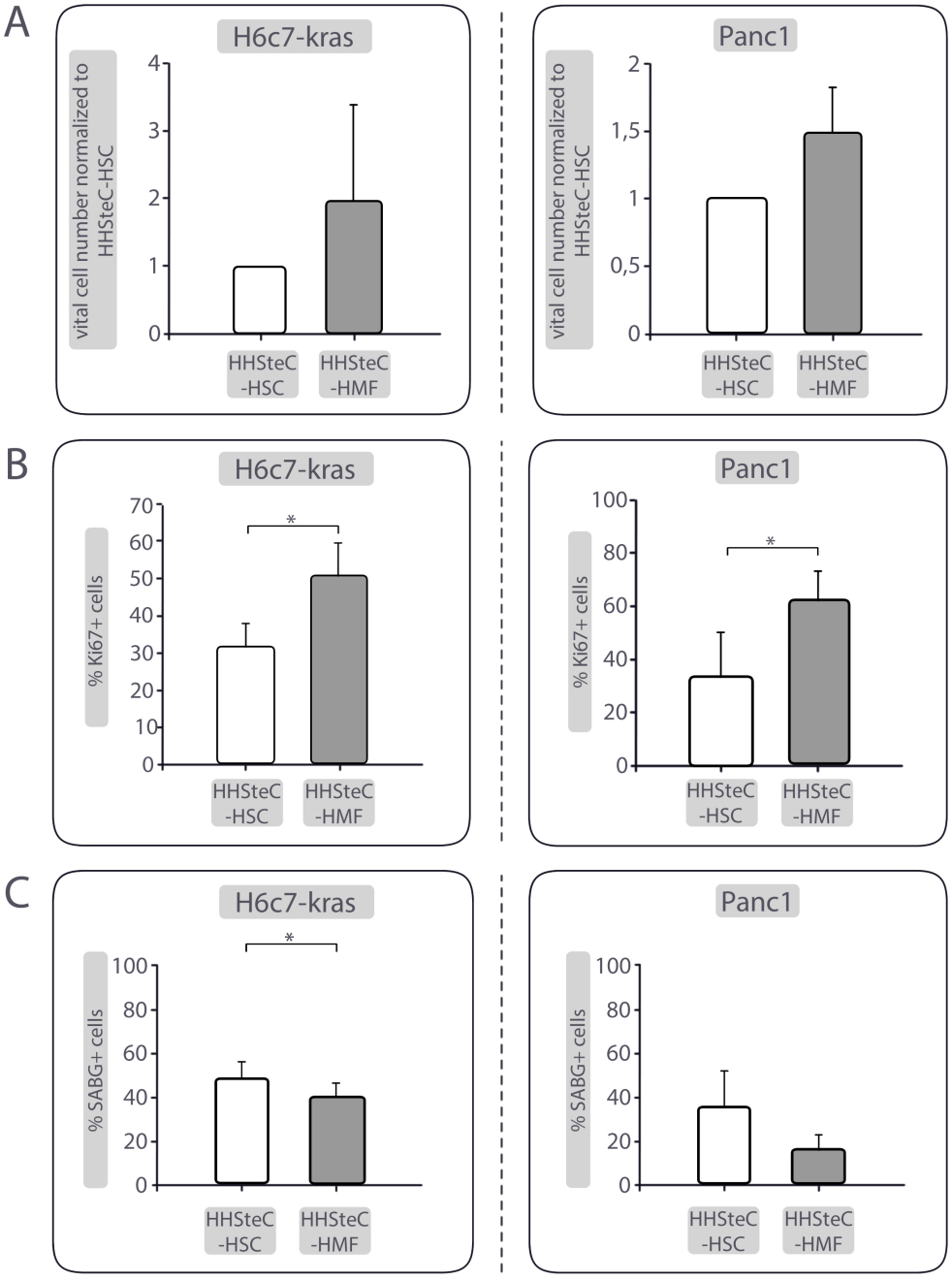


**Figure 4.15.: HHSteC-HSC induce QAP in H6c7-kras and Panc1 cells.** HHSteC were pretreated with medium containing either 2.5 µl all-trans-retinoic acid (ATRA) or 1 ng/ml TGF-β1 and set in coculture with either H6c7-kras or Panc1 cells for 6 days. Vital cell numbers were determined (**A**) as well as the percentage of Ki67-positive cells after immunostainings (**B**). Moreover, H6c7-kras and Panc1 cells were examined for their SABG-activity (**C**). Data represent the mean values ± SD of 4 independent experiments. * = $p < 0.05$.

## 4.5. The presence of HMF reverts QAP in PDECs

Recent studies suggest that during early carcinogenesis PDECs may disseminate and seed the liver, even before a primary tumor is fully established [88, 89, 117]. It is, however, assumed that the accumulation of several genetic alterations or environmental stimuli is mandatory for successful metastatic outgrowth [89, 117, 119]. Thus, the prevalent condition in the microenvironment DTCs are facing may represent a crucial factor for their fate and determine if they either persist in a resting, non-proliferative state or alternatively start to divide and form metastasis [71]. In the preceding chapters it was emphasized that HSC potently induced a state of growth arrest in premalignant and malignant PDECs. On the opposite, the presence of HMF led to a marked acceleration of PDEC proliferation. To elucidate if HMF, modelling an inflamed hepatic stroma, may revert HSC-driven QAP induction and reactivate proliferation in growth arrested PDECs, an extended coculture system was established.

In this setting, QAP was induced in H6c7-kras and Panc1 cells by 6 days of HSC coculture, before HSC were substituted for either newly seeded HSC (HSC-HSC coculture) or HMF (HSC-HMF coculture) and cocultured in their presence for further 6 days. During coculture, H6c7-kras and Panc1 cells showing a flattened, enlarged morphology of QAP were particularly surveilled via realtime Life Cell Imaging. Since HSC- and HMF-mediated effects were more pronounced in Panc1 cells, experiments were first conducted with this cell line.

After extended HSC coculture, the vast majority of Panc1 cells exhibiting a QAP morphology showed no signs of cytokinesis, indicating that the permanent presence of HSC fostered not only the induction, but also the maintenance of QAP in Panc1 cells (**Figure 4.16 A**). In the rare case of Panc1 cells reacquiring proliferative capacity in the presence of HSC, these cell divisions occurred notably slower or were directly followed by cell death (**Figure 4.16 A**, **Supplementary Video 1(HSC-HSC)**).

By way of contrast, the presence of HMF led to a high number of proliferating Panc1 cells despite persisting QAP morphology (**Figure 4.16 A**, **Supplementary Video 2 (HSC-HMF)**). While only 19 % of Panc1 cells with a QAP morphology proliferated after HSC-HSC-coculture, a significantly higher amount of 70 % Panc1 cells with QAP morphology regained proliferative capacity after HSC-HMF coculture ($p=0.008$)(**Figure 4.16 B**). Accordingly, HSC-HMF coculture resulted in a significantly higher number of Ki67-positive Panc1 cells with morphologic features of QAP (27.5 % Ki67-positive Panc1 cells with QAP morphology after HSC-HSC-coculture versus 41.5 % Ki67-positive Panc1 cells with QAP morphology after HSC-HMF coculture; $p=0.047$)(**Figure 4.16 C & D**)

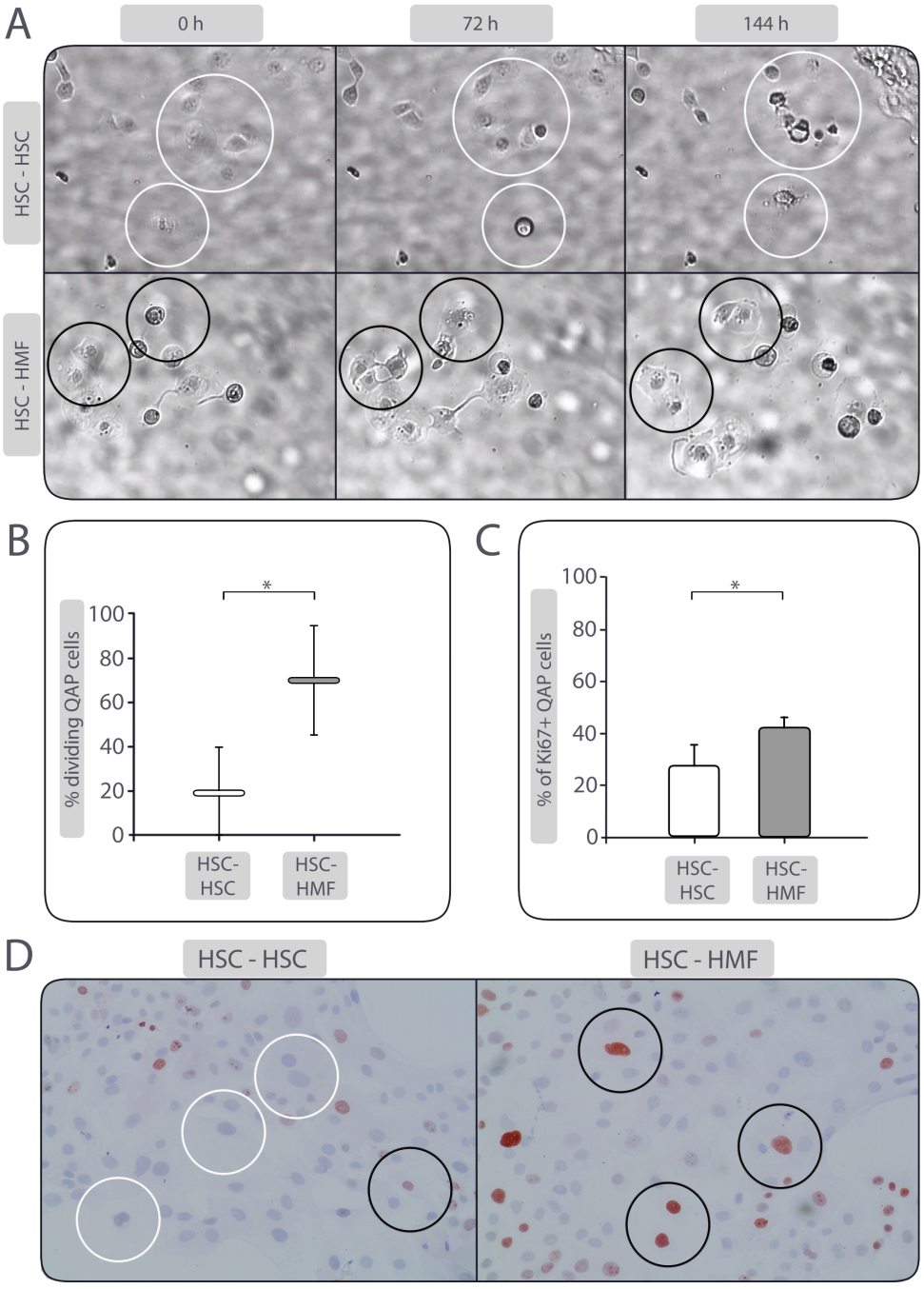


**Figure 4.16.: The quiescence-associated phenotype (QAP) of Panc1 cells can be reversed in the presence of HMF.** Panc1 cells were cocultured with HSC for 6 days. Subsequently, coculture was extended with freshly seeded HMF (HSC-HMF). During the second period of coculture, Panc1 cells were surveilled via realtime Life Cell Imaging with particular focus on cells with morphologic features of QAP. **A**) shows representative images of Panc1 cells during respective coculture in 400-fold magnification after 0 hours (h), 72 hours and 144 hours. Encircled in white are non- or unsuccessfully dividing Panc1 cells with QAP morphology, while Panc1 cells with QAP morphology successfully undergoing cytokinesis are encircled in black. After completed coculture, the number of dividing (**B**) as well as the percentage of Ki67-positive (**C**) Panc1 cells with QAP morphology was determined. Data represent the median values with quartiles ($Q_{0,75}$ as upper, $Q_{0.25}$ as lower deviation) or mean ± SD of 3-5 independent experiments * = $p < 0.05$. Representative images of Ki67 stainings in Panc1 cells after HSC-HSC- or HSC-HMF coculture, obtained in 400-fold magnification are depicted in (**D**) with Ki67-negative Panc1 cells with QAP morphology encircled in white and Ki67-positive Panc1 cells with QAP morphology encircled in black.

Furthermore, Panc1 cells which were surveilled via realtime Life Cell Imaging were examined for their SABG-activity after coculture extended in presence of HMF. Interestingly, Panc1 cells which still exhibited morphologic features of QAP but evidently fulfilled successful cytokinesis during HSC-HMF coculture stained positive for SABG (**Figure 4.17**).

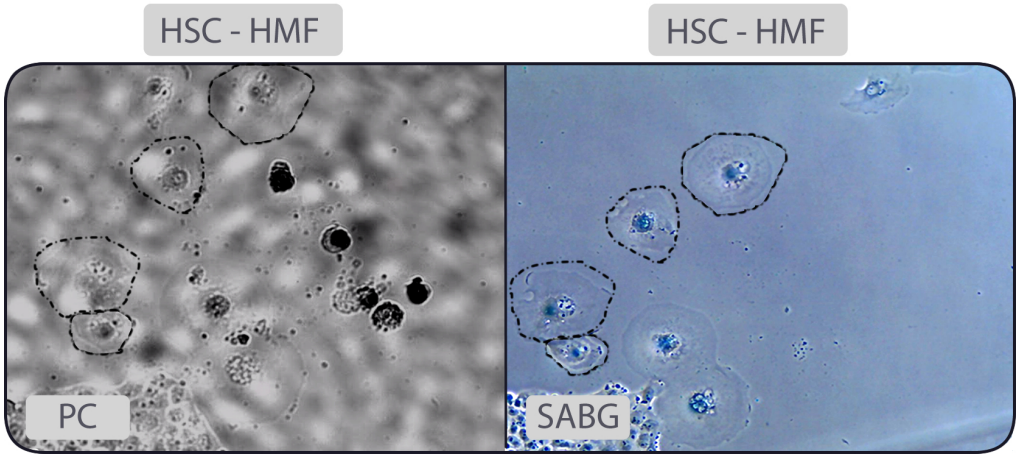


**Figure 4.17.: Panc1 cells with QAP morphology maintain their SABG-activity after HMF-mediated proliferation.** Panc1 cells were cocultured with HSC for 6 days. Subsequently, coculture was extended with either freshly seeded HSC (HSC-HSC) or HMF (HSC-HMF). During the second period of coculture, Panc1 cells were surveilled via realtime Life Cell Imaging with particular focus on cells with morphologic features of QAP (left). An SABG-staining in corresponding observed cells was affiliated (right). Depicted are representative phase contrast (PC) images of Panc1 cells with QAP morhology after HSC-HMF coculture in 400-fold magnification. Panc1 cells with QAP morphology which underwent successful division are encircled in black.

In summary, these results show an HSC-driven induction of QAP as well as an HMF-mediated QAP reversion in Panc1 cells. The fact that HSC-induced growth arrest can be reversed by HMF suggests that the observed QAP can be interpreted as tumor cell dormancy. Furthermore, these results indicate that the condition of the hepatic microenvironment determines the dormancy status of disseminated PDECs. However, the preservation of QAP features like flattened, enlarged morphology as well as persistent SABG-positivity despite proliferative activity indicate that HMF revert the QAP of Panc1 cells only partially.

To validate if the above mentioned effects of hepatic stromal cells on maintenance and reversion of QAP noticed in Panc1 cells are equally observable in premalignant cells, corresponding extended coculture experiments were conducted with H6c7-kras cells.
In line with the effects observed in Panc1 cells, the extended presence of HSC resulted in the maintenance of QAP in cocultured H6c7-kras cells. Only a minority of 17.4 % H6c7-kras cells exhibiting morphologic features of QAP regained

proliferative activity after HSC-HSC coculture (**Figure 4.18 A**).

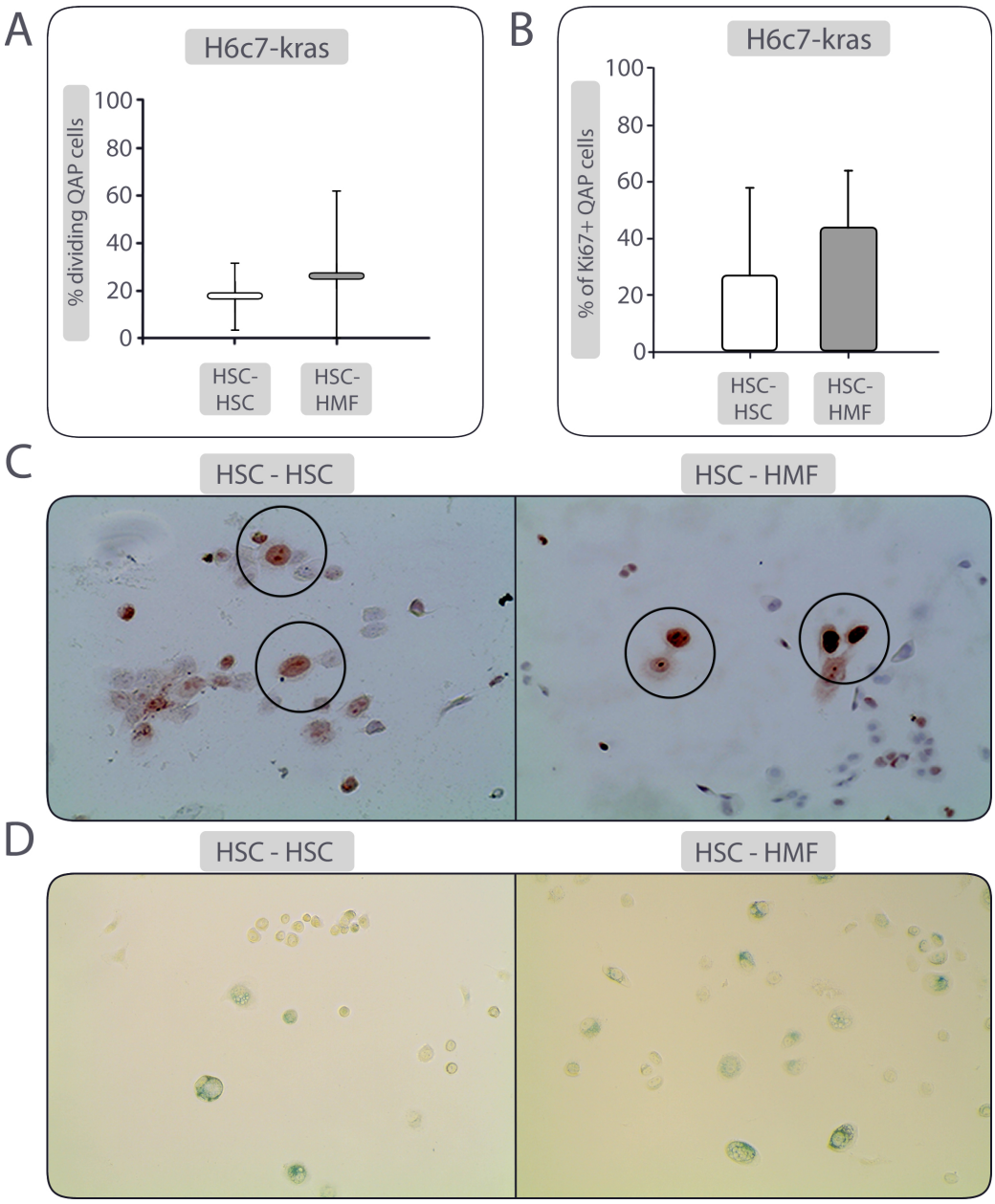


**Figure 4.18.: H6c7-kras cells maintain a QAP after extended coculture.** H6c7-kras cells were cocultured with HSC for 6 days. Subsequently, coculture was extended with either freshly seeded HSC (HSC-HSC) or HMF (HSC-HMF). During the second period of coculture, H6c7-kras cells were surveilled with a realtime Life Cell Imaging device with particular focus on cells with morphologic features of QAP. After completed coculture, the number of dividing (**A**) as well as the percentage of Ki67-positive (**B**) H6c7-kras cells with QAP morphology was determined. Data represent the median values with quartiles ($Q_{0,75}$ as upper, $Q_{0.25}$ as lower deviation) or mean ± SD of 5 independent experiments * = p <0.05. Representative images of Ki67-stainings in H6c7-kras cells after HSC-HSC or HSC-HMF coculture are depicted in **C** with Ki67-positive cells exposing QAP morphology encircled in black. **C** shows representative images of H6c7-kras cell after SABG stainings carried out after HSC-HSC or HSC-HMF coculture.

However, in contrast to the effect observed in Panc1 cells, HMF had a minor impact on cell division in H6c7-kras cells. While 41.5% Panc1 cells with QAP morphology regained proliferative activity, only 25.9% of the observed H6c7-kras

cells with QAP morphology showed proliferative activity after HSC-HMF coculture (**Figure 4.18 A**). Interestingly, subsequent Ki67 stainings showed a visible though not statistically relevant increase in Ki67-positive cells with QAP morphology after HSC-HMF coculture (26.7% Ki67-positive cells with QAP morphology versus 44.1% Ki67-positive cells with QAP morphology)(**Figure 4.18 B & C**). This points to an HMF-driven proliferation induction in H6c7-kras cells with QAP morphology on the one hand which does not lead to a successful cytokinesis on the other hand.

Similar to observations from Panc1 cells, H6c7-kras cells stained positive for SABG after HSC-HSC as well as HSC-HMF coculture (**Figure 4.18 D**).

Overall, the extended cocultures of Panc1 cells and H6c7-kras cells with HSC or HMF indicate a significant role of the hepatic microenvironment on maintenance and reversion of dormancy in PDECs. The attendance of HMF represents a potent stimulus in dormancy reversion and outgrowth of Panc1 cells whereas this effect is markedly less pronounced in H6c7-kras cells.

## 4.6. Identification of factors involved in hepatic stroma-mediated effects on PDECs growth behavior.

To identify factors involved in the stroma-mediated growth behavior of PDECs, supernatants of HSC or HMF cocultures were analyzed for the abundance of soluble inflammatory mediators by Multiplex assay. Therefore, Panc1 cells showing the most pronounced effects under coculture conditions were incubated in the presence of HSC or HMF for 6 days before supernatants were harvested and soluble factors of murine and human origin were quantified. Under 27 human and 6 murine cytokines, factors differentially released under HSC coculture or HMF coculture were identified.

Factors showing a considerably higher abundance in supernatants of HSC cocultured Panc1 cells were murine (m) IL-6 (1000.4 pg/ml under HSC versus 124.8 pg/ml under HMF coculture; p=0.005)(**Figure 4.19 A**) and human (h) IL-8 (244.8 pg/ml under HSC coculture versus 192.5 pg/ml under HMF coculture)(**Figure 4.19 B**). Furthermore, higher levels of m IL-12 were detected in Panc1 supernatants after HSC coculture compared to HMF coculture (34.0 pg/ml under HSC coculture versus 13.0 pg/ml under HMF coculture)(**Figure 4.19 C**). The higher abundance of m IL-6, h IL-8 and m IL-12 in Panc1-HSC coculture supernatants indicates that these factors may possess QAP promoting potential.

In contrast, protein levels of m VEGF (722.4 pg/ml under HSC coculture versus 1049.8 pg/ml under HMF coculture)(**Figure 4.19 D**), h VEGF (348.8 pg/ml under HSC coculture versus 594.2 pg/ml under HMF coculture)(**Figure 4.19 E**) and h SDF-1$\alpha$ (1761.1 pg/ml under HSC coculture versus 2739.1 pg/ml under HMF coculture; p=0.012)(**Figure 4.19 F**) were detected at higher levels in supernatants of Panc1 cells cocultured with HMF compared to HSC suggesting that these factors might be responsible for increased proliferation and QAP reversal under these conditions.

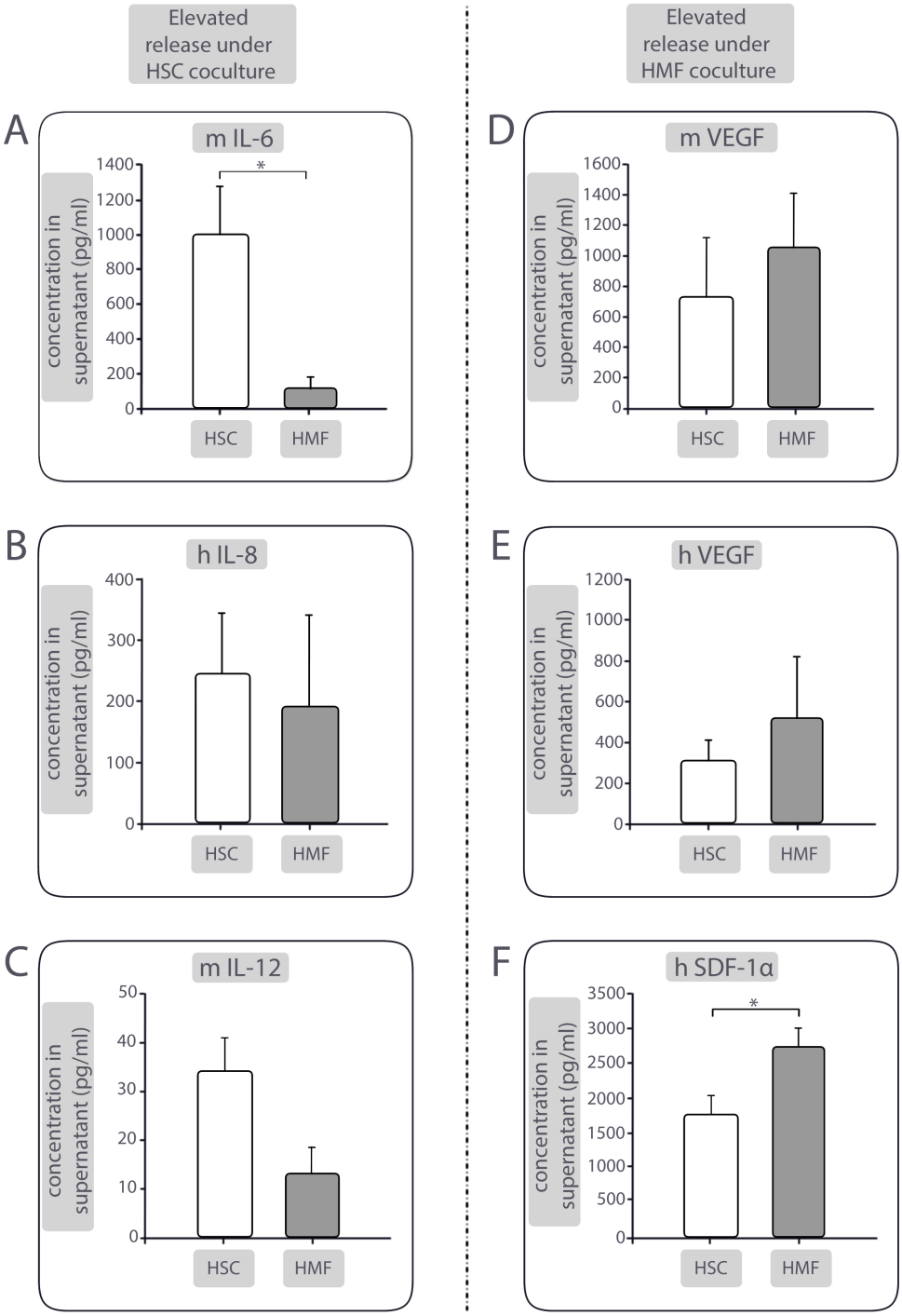


**Figure 4.19.: Identification of factors involved in hepatic stroma-mediated effects on PDECs growth behavior.** Supernatants of Panc1 cells cocultured either in the presence of HSC or HMF for 6 days were analyzed by Multiplex analysis. Murine (m) Interleukin-6 (IL-6) **(A)**, human (h) IL-8 **(B)** and m IL-12 **(C)** were found at higher levels under HSC coculture compared to HMF coculture. M VEGF **(D)**, h VEGF **(E)** and h SDF-1α **(F)** were detected at higher levels in supernatants of HMF cocultures. Data are presented as mean concentration (in pg/ml) ± SD 3 - 5 independent experiments * = p <0.05.

## 4.7. IL-6 is not an inducer of QAP in PDECs

Up to this point, it could be emphasized, that the presence of HSC induces the emergence of QAP in PDECs, while HMF coculture conditions promote proliferation of PDECs **(cf. Chapter 3.3 & 3.5)**. Factors with either a higher release in Panc1/HSC cocultures or Panc1/HMF cocultures were thereby identified. Hence, the next step was to evaluate a causal involvement of soluble factors with a differential release under the respective coculture conditions in the mediation of the observed differences in PDEC growth behavior. Since the most pronounced differential stroma-mediated effects were determined in Panc1 cells, corresponding blocking and induction experiments were conducted in this cell line.

First, candidate cytokines with a possible relevance in QAP induction were examined. Murine IL-6 showed the plainest release in Panc1/HSC cocultures. The role of IL-6 in PDAC progression is to date insufficiently elucidated. A senescence promoting and tumor suppressing effect has been reported for IL-6, while other studies support a tumor promoting role of IL-6 [136, 198]. IL-6 can fulfill its function in two different fashions: classic cis-signaling or trans-signaling. IL-6 cis-signaling works through binding of soluble IL-6 to a membrane-anchored IL-6 receptor (IL-6R) on the cell surface. This complex formation causes the recruitment and homodimerization of gp130, which exerts signal transduction via the JAK/STAT and RAS/MAPK-pathways [199]. While the occurrence of IL-6R is limited to lymphocyte lineages, neutrophils, hepatocytes and monocytes, gp130 is expressed ubiquitously [200]. Cells lacking IL-6R are hence receptive to IL-6 via IL6-trans-signaling, exerting its function via a soluble IL-6R (sIL-6R)[200]. The sIL-6R emerges by translation of a differentially spliced IL-6R mRNA or cleavage of IL-6R on the cell surface by ADAM17 and is released into the intercellular space [201]. Here it can interact with IL-6 and the formed complex may bind to gp130 and exert the above mentioned effects. While IL-6 cis-signaling exclusively functions intraspecifically, IL-6 trans-signaling may also be initiated species-overlapping [200].

To identify a possible role of IL-6 in HSC-driven induction of QAP, IL-6 signaling was blocked under HSC coculture conditions. Both, cis- and trans-signaling modes were thereby examined. First, the clinically approved antibody Tocilizumab was utilized. Tocilizumab is a h IL-6R-antagonist and thus blocks cis- and trans-signaling of IL-6. As a control treatment, 10 mg/ml Rituximab, a humanized monoclonal anti-CD20 antibody of the IgG1κ subclass was applied. Panc1 cells were cocultured with HSC for 6 days and concurrently treated with 10 mg/ml of Tocilizumab and Rituximab, respectively.

The treatment of Panc1/HSC cocultures with Tocilizumab led to a visible, but insignificant increase of vital Panc1 cells of 20.6% ($3.2*10^4$ vital Panc1 cells

after Rituximab treatment versus $3.9*10^4$ vital Panc1 cells after Tocilizumab treatment)(**Figure 4.20 A**), which, moreover, did not induce QAP features in Panc1 cells (data not shown). To examine effects of IL-6 trans-signaling blockade, the fusion protein sgp130Fc was utilized. The sgp130Fc protein unites the extracellular unit of gp130 fused to the Fc domain of a human IgG1 antibody and blocks IL-6 trans-signaling without affecting IL-6 cis-signaling [200]. As a control, the corresponding IgG1-Fc-domain (control-Fc) was utilized. The blockade of IL-6 trans-signaling under HSC coculture conditions had no clear effect on the vital cell count of Panc1 cells ($11.75*10^4$ vital Panc1 cells after control-Fc treatment versus $9.6*10^4$ vital Panc1 cells after gp130Fc treatment)(**Figure 4.20 B**), underlining a minor role of classic IL-6 signaling in HSC-mediated QAP induction in Panc1 cells.

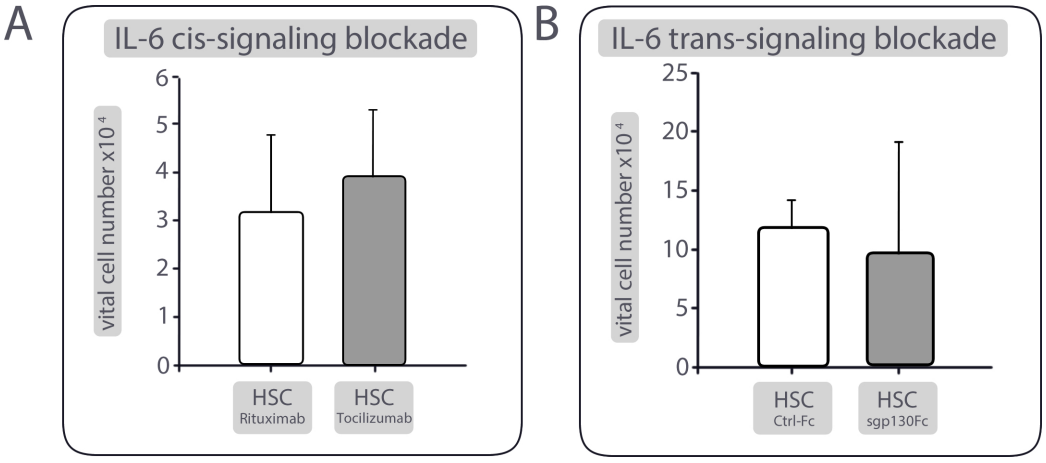


**Figure 4.20.: IL-6 is not important for HSC-mediated QAP in Panc1 cells.** Panc1 cells were indirectly cocultured with HSC for 6 days. Upon start of culture and again after 3 days, cocultures were treated with 10 µg/ml of IL-6 signaling blocking or agents. After 6 days, vital cells were counted. **A)** Vital cell numbers of Panc1 cells upon HSC coculture and application of a Rituximab control or IL-6R antagonist Tocilizumab. **B)** Vital cell numbers of Panc1 cells upon HSC coculture and application of a Ctrl-Fc-antibody or IL-6 trans-signaling blocking sgp130Fc. Values are depicted as mean ± SD of 4 independent experiments.

In order to substantiate these findings, monocultured Panc1 cells were treated with 10 ng/ml recombinant (r) human (h) IL-6 (r h IL-6) and compared to untreated cells. Since murine (m) IL-6 exhibits a negligible affinity towards the human IL-6R, r m IL-6 was utilized as a control. In comparison to untreated Panc1 cells and Panc1 cells exposed to r m IL-6, treatment with r h IL-6 led to a clear but not significant increase of vital cells ($4.2*10^4$ vital Panc1 cells after untreated monoculture versus $7.9*10^4$ vital Panc1 cells after r h IL-6-treatment versus $3.8*10^4$ vital Panc1 cells after r m IL-6 treatment)(**Figure 4.21**). This indicates a proliferation-inducing effect of h IL-6.

In summary, these results exclude murine and human IL-6 alone as crucial fac-

tors in HSC-driven proliferation inhibition and hence promote the view that these proteins are not causally involved in QAP induction in Panc1 cells.

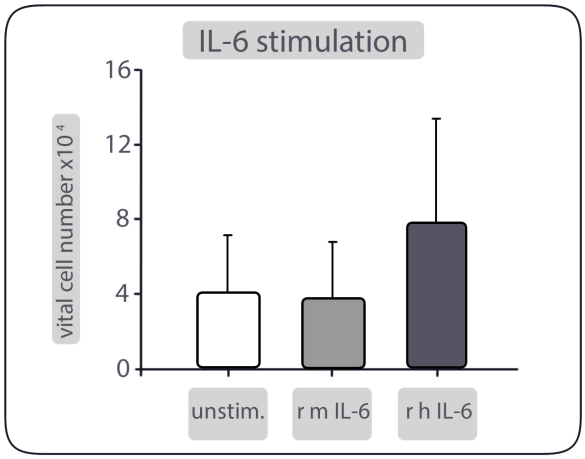


**Figure 4.21.: Human IL-6 increases cell growth of Panc1 cells.** Panc1 cells were monocultivated for 6 days. Cells were either left untreated (unstim.) or treated with 10 ng/ml IL-6 signaling inducing agents upon start of culture and again after 3 days. Depicted is the vital cell count of monocultivated Panc1 cells, either left untreated or stimulated with recombinant (r) murine (m) IL-6 (r m IL-6) or r human IL-6 (r h IL-6). Values are depicted as mean ± SD of 4 independent experiments.

## 4.8. IL-8 is important for HSC-mediated QAP in PDECs

Next, a possible involvement of h IL-8, also known as CXCL8, in HSC-mediated QAP induction was verified. A differential release of h IL-8 of 244.8 pg/ml under HSC coculture versus 192.5 pg/ml under HMF coculture was measured (**cf. Chapter 3.6**). IL-8 has already been reported to prevent tumor cell proliferation and to exhibit senescence-inducing potency [136]. Therefore, in line with IL-6 blocking experiments, h IL-8 was blocked under HSC coculture conditions and QAP features of Panc1 cells were examined. For this approach, Panc1 cells were cocultured with HSC for 6 days, while IL-8 signaling was compromised by application of 2.5 µg/ml neutralizing human CXCL8/IL-8 antibody. As a control, corresponding concentrations of monoclonal mouse IgG1-antibody were utilized. The neutralization of h IL-8 under HSC coculture resulted in an increase of vital Panc1 cells by 31% compared to control treated cells ($19.37*10^4$ Panc1 cells after h IL-8 blockade versus $13.33*10^4$ vital Panc1 cells after control treatment)(**Figure 4.22 A**).

Since the blockade of h IL-8 exposed a marked increase in vital Panc1 cells, further proliferation-associated features were examined in Panc1 cells after h IL-8 blockade to examine a potential QAP promoting role of IL-8. In line with the elevated vital cell count, SABG stainings showed that h IL-8 blockade led to a

significant decrease in SABG-positive Panc1 cells by 35% (26.7% SABG-positive Panc1 cells after h IL-8 blockade versus 40.9% SABG-positive Panc1 cells after control treatment; p = 0.008)(**Figure 4.22 B**). Accordingly, the p-ERK/p-p38 ratio of HSC cocultured Panc1 cells was clearly increased after h IL8 blockade, compared to HSC cocultured cells treated with control antibodies (p-ERK/p-p38 ratio = 0.84 in Panc1 cells after control treatment versus p-ERK/p-p38 ratio = 1.1 in Panc1 cells after h IL-8-blockade)(**Figure 4.22 C**).

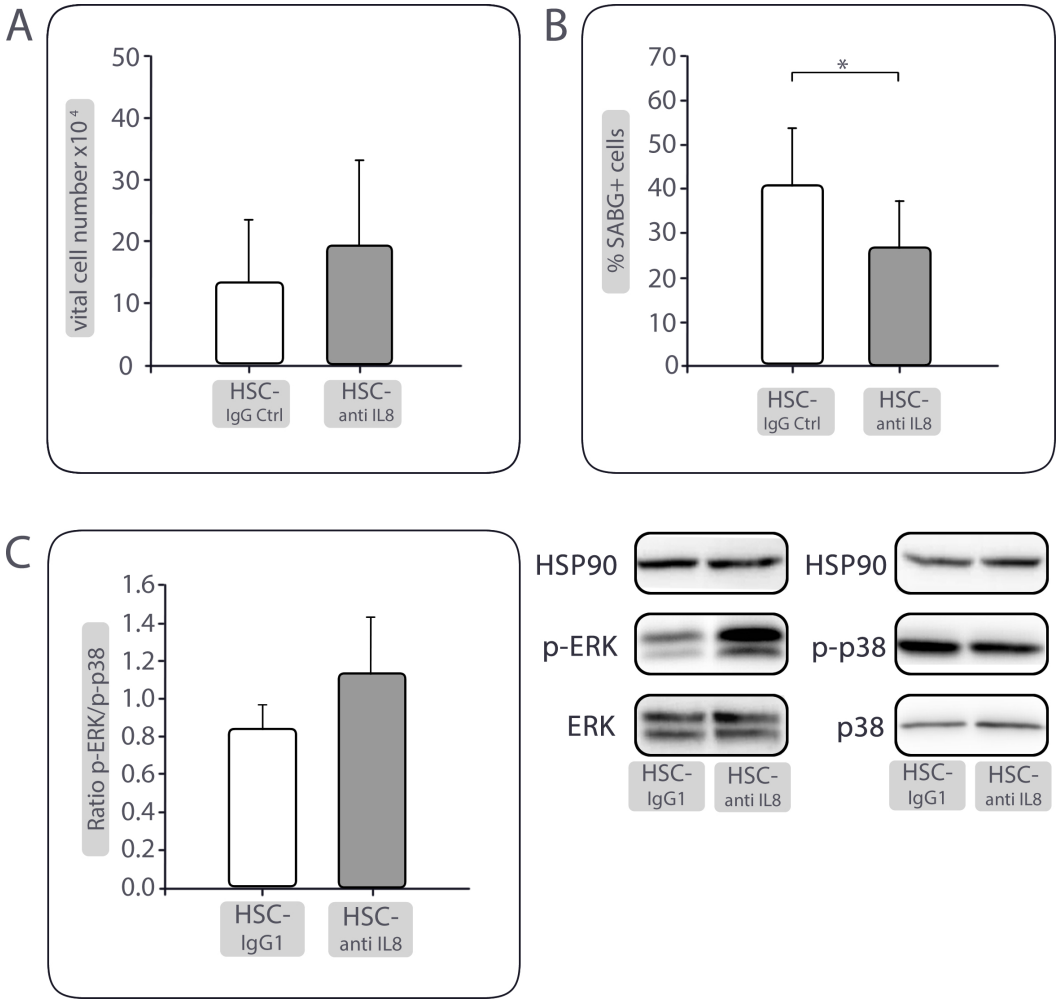


**Figure 4.22.: IL-8 is important for HSC-mediated QAP in PDECs.** Panc1 cells were indirectly cocultured with HSC and either treated with control IgG (2.5 µg/ml) or an anti-IL-8 antibody (2.5 µg/ml)(A-C). After 6 days, vital cell numbers **(A)** and the percentage of SABG-positive cells **(B)** were determined. **C)** shows representative western blots of phosphorylated-ERK (p-ERK) and ERK as well as phosphorylated-p38 (p-p38) and p38. Furthermore, the corresponding p-ERK/p-p38 ratio, determined via densitometric quantification is depicted. HSP90 was used as loading control. Values are presented as mean ± SD of 4 independent experiments. * = p <0.05.

To further substantiate these findings, monocultured Panc1 cells were stimulated with r h IL-8. In accordance with the blockade of IL-8 under HSC coculture conditions, the stimulation of Panc1 cells with r h IL-8 resulted in a mild decrease of vital cells by 14.9% ($6.7*10^4$ vital Panc1 cells after stimulation with recombinant h IL-8 versus $7.7*10^4$ vital Panc1 cells after control treatment)(**Figure 4.23**).

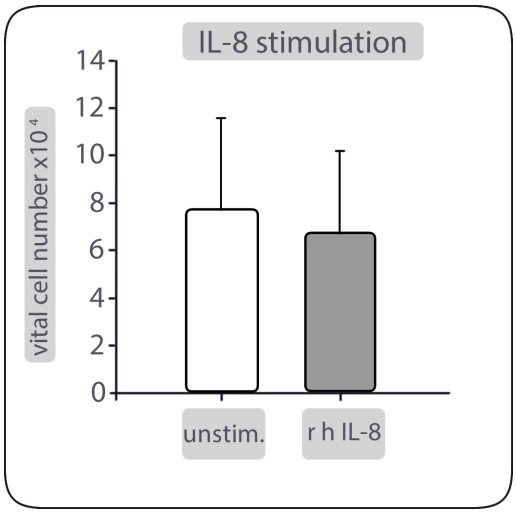


**Figure 4.23.: Human IL-8 decreases cell growth of Panc1 cells.** Panc1 cells were monocultivated for 6 days and either left untreated (unstim.) or treated with 10 ng/ml recombinant human IL-8 (r h IL-8) upon start of culture and again after 3 days. Depicted are mean vital cell counts ± SD of 4 independent experiments.

In summary, blockade of IL-8 showed an increase in vital cell number and p-ERK/p-p38-ratio in line with a significantly decreased SABG-activity of HSC cocultured Panc1 cells. Taken together with the reduced vital cell count determined after stimulation with r h IL-8, these results identify IL-8 as a QAP promoting factor in Panc1 cells.

## 4.9. SDF-1$\alpha$ is not a proliferation promoting factor under HMF coculture.

HMF coculture of H6c7-kras and Panc1 cells led to a higher proliferation and the absence of QAP features, compared to HSC cocultured PDECs (**cf. Chapter 3.3**). Accordingly, factors associated with proliferation and cell growth were detected in higher abundance in Panc1/HMF coculture compared to Panc1/HSC coculture. Hence, the next step was to investigate whether these cytokines with elevated release under Panc1/HMF coculture were causally responsible for the observed accelerated proliferation of Panc1 cells under these conditions.
The most striking and significant differences between Panc1/HSC and Panc1/HMF cocultures concerning cytokine release were found for h SDF-1$\alpha$ (1761.1 pg/ml under HSC coculture versus 2739.1 pg/ml under HMF coculture; p=0.012)(**cf. Chapter 3.6**). Hence, corresponding loss and gain of function experiments were conducted to validate the significance of h SDF-1$\alpha$ in HMF-driven proliferation of PDECs. SDF-1$\alpha$ preferably binds to the receptor CXCR4 (SDF-1$\alpha$ receptor) on the cell surface and induces signaling via G-protein recruitment and activation [202]. In order to block SDF1-$\alpha$ signaling, the clinically approved CXCR4-receptor antagonist AMD3100 (Plerixafor) was applied under HMF coculture conditions. Panc1 cells were cultured in the presence of HMF for 6 days. Upon start of the coculture and again on day 4, coculture medium was supplied with 1 $\mu$M AMD3100 [203]. As a control treatment, DMSO was added to Panc1/HMF cocultures in corresponding amounts. After 6 days, Panc1 cells were examined for proliferation-associated features. The blockade of CXCR4 signaling led to a minor increase in vital Panc1 cell numbers by 20% ($25.9*10^4$ vital Panc1 cells under HMF coculture and DMSO application versus $32.6*10^4$ vital Panc1 cells under HMF coculture and AMD3100 application)(**Figure 4.24 A**), indicating that CXCR4 signaling is not involved in HMF-driven proliferation of Panc1 cells.
To validate this finding, recombinant (r) h SDF-1$\alpha$ was added to monocultured Panc1 cells. This resulted in a nearly unaltered number of vital Panc1 cells ($7.5*10^4$ vital cells in untreated Panc1 monocultures versus $6.5*10^4$ vital Panc1 cells after r h SDF-1$\alpha$ application)(**Figure 4.24 B**).
In summary, these results show a negligible impact of h SDF-1$\alpha$ on proliferation of Panc1 cells under HMF coculture.

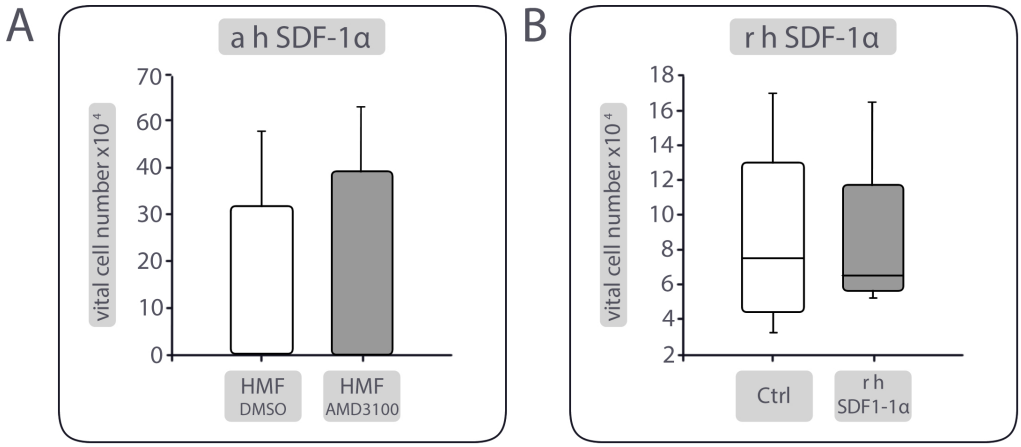


**Figure 4.24.: SDF-1α is not a proliferation promoting factor under HMF coculture. A)** Panc1 cells were indirectly cocultured with HMF and either treated with DMSO or 1 µM AMD3100 upon start and again on day 4 of coculture. After 6 days, vital cell numbers were determined. **B)** Panc1 cells were monocultured and either left untreated or treated with 10 ng/ml recombinant human SDF-1α (r h SDF-1α upon start and again on day 4 of coculture and the vital cell number was measured. Data represent the median values with quartiles ($Q_{0,75}$ as upper, $Q_{0.25}$ as lower deviation) or mean ± SD of 4 independent experiments.

## 4.10. HMF promote proliferation in Panc1 cells via VEGF.

Beyond SDF-1α, both, murine and human VEGF isoforms were found in higher concentrations in Panc1/HMF coculture supernatants (722.4 pg/ml under HSC coculture versus 1049.8 pg/ml under HMF coculture for m VEGF and 348.8 pg/ml under HSC coculture versus 594.2 pg/ml under HMF coculture for h VEGF). Furthermore, in the utilized age-related syngenic mouse model VEGF expression correlated with mouse-age and metastatic outgrowth (**cf. Chapter 3.2**). Moreover, VEGF has already been shown to foster the onset of colorectal cancer cells [204]. Thus, VEGF was adjudged as likely mediator of HMF-driven PDEC proliferation and corresponding blocking experiments were conducted.
VEGF was first described as a crucial molecule in angiogenesis [205]. Currently the VEGF family is composed of five structurally related factors: VEGF-A,VEGF-B,VEGF-C,VEGF-D and placenta growth factor (PGF), which all excert their effects by binding to receptor tyrosine kinases (RTK) [205]. In order to verify a possible proliferation inducing role of VEGF under HMF coculture, Panc1 cells were cocultured with HMF and either 10 µg/ml VEGF blocking antibodies or control antibodies were added into the medium. In a first approach, the h VEGF-A neutralizing antibody Bevacizumab was utilized to block VEGF signaling in Panc1/HMF cocultures. As a control, the anti-CD20 antibody Rituximab was applied under equal conditions. Bevacizumab application had no

impact on vital cell count of Panc1 cells under HMF coculture ($14.8*10^4$ vital Panc1 cells after Bevacizumab application versus $14.0*10^4$ vital Panc1 cells after control treatment)(**Figure 4.25 A**).

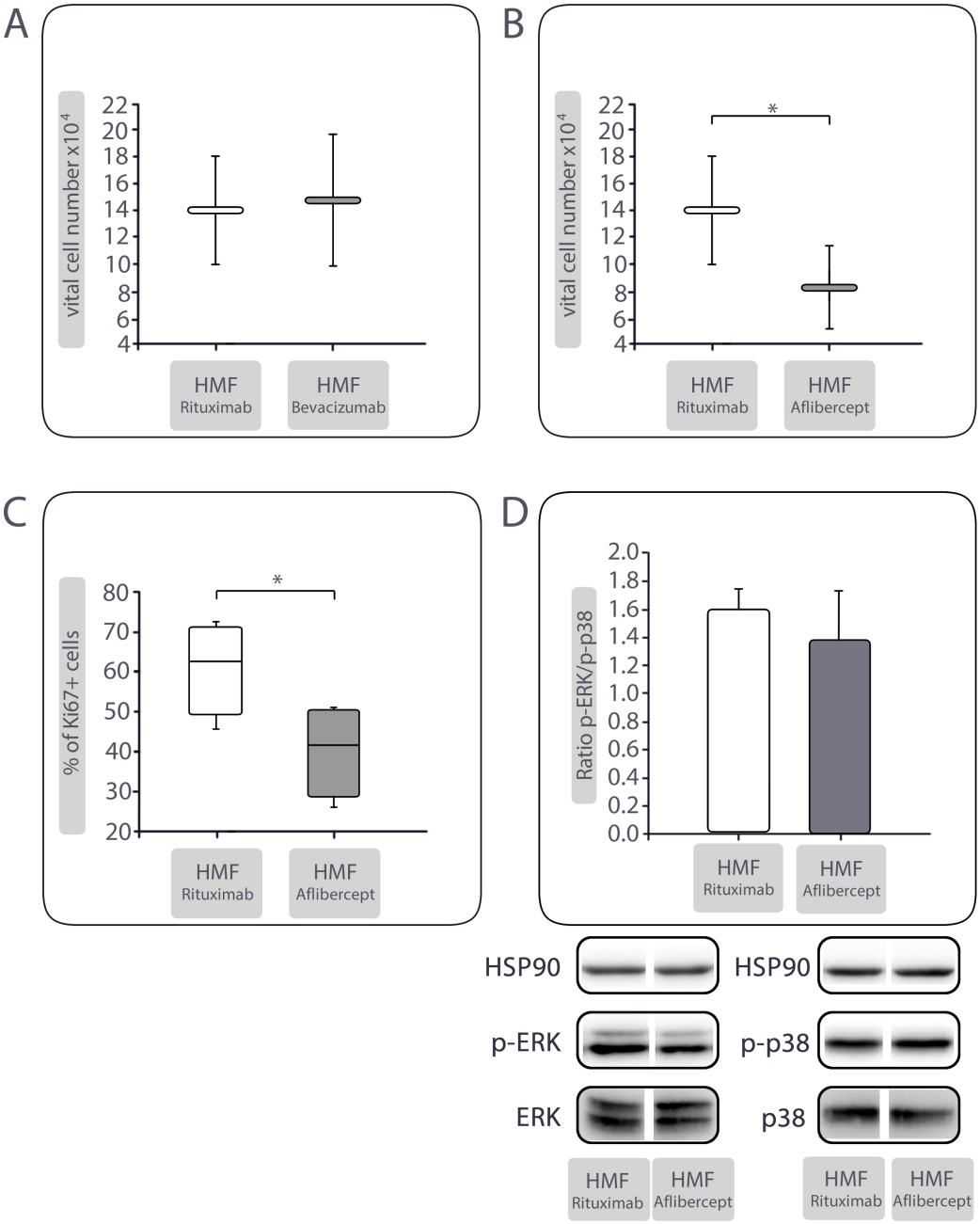


**Figure 4.25.: VEGF is a proliferation promoting factor under HMF coculture.** Panc1 cells were indirectly cocultured with HMF and either treated with 10 µg/ml Bevacizumab **(A)** or Aflibercept **(B-D)** upon start and again on day 4 of coculture. Rituximab, applied in corresponding conditions, was used as respective istotype control-antibody **(A-D)**. After 6 days, vital cell numbers after VEGF blockade via Bevacizumab **(A)** or Aflibercept **(B)** and respective control treatment were determined. Furthermore, the number of Ki67-positive Panc1 cells after Aflibercept treatment versus control treatment was calculated **(C)**. **D)** shows representative western blots of phosphorylated-ERK (p-ERK) and ERK as well as phosphorylated-p38 (p-p38) and p-38. Moreover, the corresponding p-ERK/p-p38 ratio, determined via densitometric quantification is depicted. HSP90 was used as loading control. Data represent the median values with quartiles ($Q_{0,75}$ as upper, $Q_{0.25}$ as lower deviation) or mean ± SD of 3-5 independent experiments * = p <0.05. experiments.

This either indicates a neglectable role of h VEGF-A in HMF-mediated proliferation acceleration or that the blockade of h VEGF alone is not sufficient to completely prohibit HMF-mediated VEGF signaling since m VEGF is not affected by Bevacizumab [206]. Hence, Aflibercept, an antibody that targets not only VEGF-A but also VEGF-B of human as well as murine origin was applied to neutralize VEGF in Panc1/HMF cocultures.

In contrast to treatment with Bevacizumab, application of Aflibercept led to a significant decrease of Panc1 cell growth and proliferation under HMF influence by 41.5% compared to control treatment ($8.2*10^4$ vital Panc1 cells after Aflibercept-application versus $14.0*10^4$ vital Panc1 cells after control treatment; $p = 0.035$)(**Figure 4.25 B**). In line with this finding, a marked and significant reduction of Ki67-positive Panc1 cells by 33% was observed (62.5% Ki67-positive Panc1 cells after control treatment versus 41.4% Ki67-positive Panc1 cells after application of Aflibercept; $p = 0.030$)(**Figure 4.25 C**). Finally, a corresponding lower p-ERK/p-p38 ratio after Aflibercept treatment was determined (p-ERK/p-p38 ratio = 1.60 after HMF-Rituximab control treatment versus p-ERK/p-p38 ratio = 1.38 after HMF-Aflibercept treatment)(**Figure 4.25 D**).

To examine the impact of exogenous VEGF on Panc1 cells, monocultured Panc1 cells were stimulated with r h VEGF-A. Contrary to the negligible impact of Bevacizumab blockade under HMF coculture, administration of exogenous VEGF-A resulted in a visible increase in vital Panc1 cells ($7.9*10^4$ vital Panc1 cells after stimulation with recombinant h VEGF versus $11.6*10^4$ vital Panc1 cells after control treatment)(**Figure 4.26**). This indicates a proliferation promoting impact of VEGF-A on Panc1 cells.

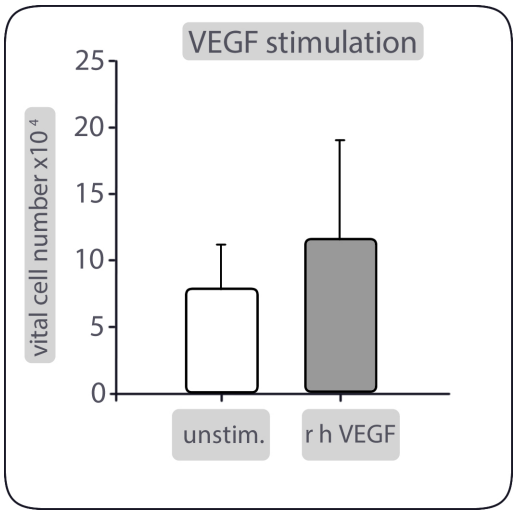


**Figure 4.26.: VEGF-A promotes Panc1 cell growth.** Panc1 cells were monocultivated for 6 days and either left untreated (unstim.) or treated with 10 ng/ml recombinant human VEGF-A (r h VEGF) upon start of culture and again after 3 days. Depicted are mean vital cell counts ± SD of 4 independent experiments.

Taken together, these results emphasize a crucial role of VEGF in HMF-driven acceleration of proliferation in Panc1 cells.

## 4.11. VEGF-neutralization reverts HSC-mediated QAP in Panc1 cells.

In a previous chapter it was shown that the presence of HMF reverts HSC-driven induction of QAP (**cf. Chapter 3.5**). Since VEGF was identified as factor by which HMF induce proliferation in Panc1 cells (**cf. Chapter 4.10**), the question arose whether VEGF may also be causally involved in HMF-mediated QAP reversion of Panc1 cells. In accordance with corresponding extended coculture experiments (**cf. Chapter 3.5**), Panc1 cells were therefore first cultured in presence of HSC for 6 days before coculture conditions were changed to HMF for further 6 days during which 10 µg/ml Aflibercept were applied in order to block VEGF-signaling, while Rituximab was used as an isotype control.
The determination of vital Panc1 cells after HSC-HMF coculture exhibited a mild decrease of vital cells by 14% after VEGF blockade via Aflibercept ($65.3*10^4$ vital Panc1 cells after HSC-HMF coculture and Rituximab application versus $56.1*10^4$ vital Panc1 cells after HSC-HMF coculture and Aflibercept application)(**Figure 4.27 A**). In addition, Aflibercept treatment under HMF coculture conditions following HSC coculture resulted in a clear and significant reduction of Ki67-positive Panc1 cells by 23% (50.0% Ki67-positive Panc1 cells after Rituximab treatment versus 38.4% Ki67-positive cells after Aflibercept application under respective HSC-HMF coculture conditions)(**Figure 4.27 B**). Realtime Life Cell Imaging with particular focus on cells showing morphologic features of QAP, however, detected equal amounts of successful proliferations in Panc1 cells exhibiting QAP morphology after HSC-HMF coculture irrespective of the applied antibody treatment (36.7% proliferating Panc1 cells with QAP morphology after HSC-HMF coculture and Rituximab treatment versus 43.0% proliferating Panc1 cells with QAP morphology after HSC-HMF coculture and Aflibercept treatment)(**Figure 4.27 C**). By way of contrast, the decrease of the p-ERK/p-p38 ratio by 22.4% indicates a striking effect of VEGF neutralization on the reversal of QAP in Panc1 cells (1.318 after HSC-HMF coculture and Rituximab application versus 1.023 after HSC-HMF coculture and Aflibercept application)(**Figure 4.27 D**). Taken together, whereas Aflibercept treatment under HSC-HMF coculture did not impact on the number of dividing Panc1 cells with QAP morphology within the time of observation, the decreased vital cell number, amount of Ki67-positive cells and diminished p-ERK/p-P38 ratio as compared to control treatment, point to a distinct role of VEGF in HMF-mediated dormancy reversion of growth ar-

rested Panc1 cells.

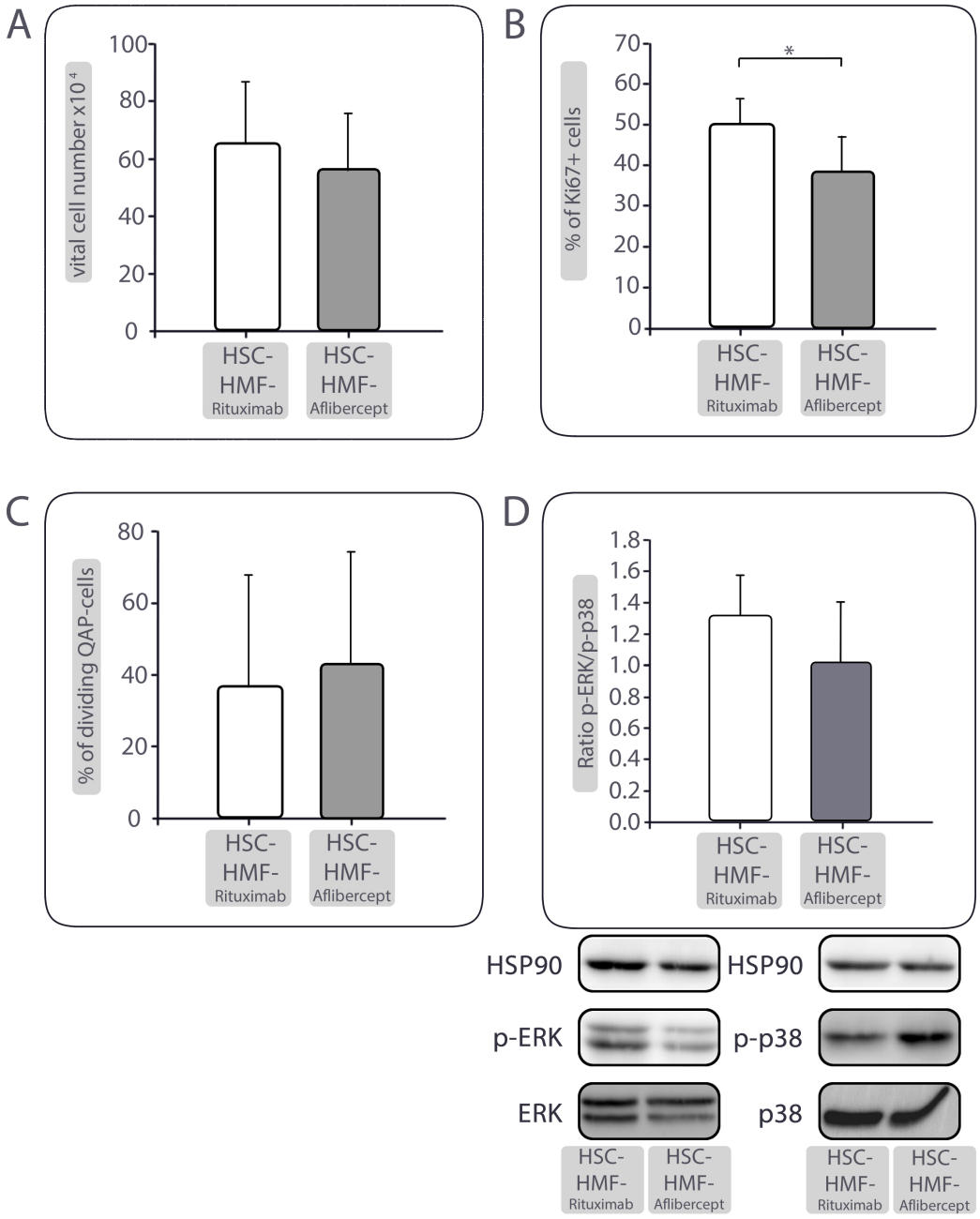


**Figure 4.27.: VEGF neutralization reverts HSC-mediated QAP in Panc1 cells.** Panc1 cells were indirectly cocultured with HSC for 6 days. Subsequently, coculture was extended with freshly seeded HMF (HSC-HMF). During the second period of coculture, cocultures were either treated with 10 µg/ml Aflibercept upon start and again on day 4. Rituximab, applied in corresponding concentrations, was used as respective isotype control antibody. The vital cell number was determined **(A)** as well as the number of Ki67-positive cells **(B)**. During Aflibercept or Rituximab treatment, Panc1 cells were surveilled via realtime Life Cell Imaging with particular focus on cells showing morphologic features of QAP and successful proliferations were quantified **(C)**. Furthermore, phosphorylated (p)-ERK and ERK as well as phosphorylated (p)p-38 and p-38 were detected via western blot analysis and the p-ERK/p-p38 ratio was determined via densitometric measurement **(D)**. HSP90 was used as loading control. Data represent the mean ± SD of 3-5 independent experiments * = $p < 0.05$.

# 5. Discussion

## 5.1. Inflammatory conditions in the hepatic microenvironment foster the outgrowth of disseminated PDECs in the liver

The first aim of this study was to gain a better image of PDAC liver metastases at different stages of progression and detect possible coherences with the prevalent conditions in the respective microenvironment. Due to their plasticity and particular involvement in different inflammatory processes in the liver, HSCs and their transdifferentiated counterpart HMF were detected representative of the inflammatory status of the hepatic microenvironment. Liver metastases were identified in FFPE liver tissues of KPC mice via immunohistochemistry and characterized with regard to their size, proliferation status as well as $\alpha$-SMA/desmin ratio in the direct surrounding representative for HSC and HMF abundance. This initial screening unveiled the emergence of micrometastases with a low amount of proliferating tumor cells in unobtrusive, HSCs-rich microenvironments whereas macrometastases with a significantly higher amount of proliferating tumor cells were mostly detected in HMFs-rich areas (**cf. Figure 4.1**). These findings imply that the condition of the microenvironment determines the growth behavior of PDAC metastasis and support the view that HMFs generate a growth permissive microenvironment for PDAC metastasis in the liver. Supporting this view, Aiello *et al.* recently observed that the development of liver metastases is associated with dynamic changes in the microenvironment and that HMFs represent an essential component of this process [207]. Using the KPC-related PKCY mouse model (Pdx1-Cre; Kras LSL-G12D/+; P53fl/+; Rosa26 LSL-YFP/+ [89]), they showed how the amount of $\alpha$-SMA positive HMFs in the stroma of PDAC liver metastases increased with advancing lesion size. HMFs thereby appeared in direct contact to metastatic lesions as early as these were 6-7 cells in scale. Accompanying growth, secondary lesions acquired a morphology and fibrotic degree similar to primary PDAC lesions. However, in contrast to the results presented in this thesis, in their study the observed changes in $\alpha$-SMA positive cells in the microenvironment did not correlate with

the proliferation status of metastatic lesions. In a further study, applying a model of experimental metastasis based on intrasplenic injection of KPC mouse derived PDAC cells Nielsen *et al.* showed that the deposition of ECM molecules, mainly periostin, by HMFs promoted the progression of PDAC metastases in the liver [208]. Both studies accordingly emphasized that HMFs emerged early around DTCs after their engraftment, supporting the view that the high number of HMFs detected in proximity to proliferating macrometastases of KPC mice arose concomitantly with lesion growth. Importantly, in line with the study at hand, both reports promote the view that stroma activation and inflammatory processes in the liver generate a metastatic niche that fosters the outgrowth of PDAC metastases. However, neither of the two studies nor the applied KPC mouse model allowed conclusions regarding a potential metastasis promoting effect of inflammatory alterations in the liver devoid of disseminated PDAC cells. It was therefore sought to examine the behavior of malignant PDECs that encounter a physiological, HSCs-rich liver versus an inflamed liver exposing a higher abundance of HMFs. A syngeneic mouse model utilizing aging as inflammatory trigger allowed a clearer distinction of a physiological versus an inflamed hepatic microenvironment. C57BL/6J mice, either 8 weeks or 52 weeks of age, were orthotopically injected with KPC mouse-derived R254 PDAC cells. Two weeks and four weeks after injection, 10 animals per group were sacrificed, respectively, and pancreatic tumor growth and metastatic burden were examined. Indeed, higher age was associated with elevated growth of disseminated PDAC cells in the liver. Whereas primary tumors of 8 weeks and 52 weeks old mice were comparably small two weeks after tumor cell injection (**cf. Figure 4.2 & 4.3**), older mice presented with a significantly higher number of Ki67-positive DTCs in the liver (**cf. Figure 4.4**). Concordantly, four weeks after injection, primary tumors were visibly but not statistically enlarged in 52 weeks old mice, whereas only these mice harbored micrometastases (**cf. Figure 4.9**), indicating that proliferating DTCs observed after two weeks indeed progressed to metastatic lesions. Moreover, to detect aging-related inflammatory alterations in the liver, the expression of various pro-inflammatory cytokines was measured. Indeed, most of the genes found upregulated in 52 weeks old mice represented factors which are reported to expose a higher expression in HMFs than HSCs or to be involved in HSC-activation (**cf. Figure 4.5**)[192–196]. Accordingly, a slightly higher $\alpha$-SMA/desmin-ratio could be detected in livers of these mice, indicating an elevated amount of HMFs in aged livers which supports the view that aging is a stimulus for HSC activation (**cf. Figure 4.6**). These observations strongly promote the view that inflammatory processes in the liver and the concomitant emergence of HMFs occurring prior to metastatic spread provide a more growth

permissive microenvironment for malignant PDECs that encounter the organ. Supporting these results, an experimental study of breast cancer recently showed increased seeding and proliferation of DTCs in the pulmonary microenvironment after lungs were challenged with injury stimuli which caused the emergence of myofibroblasts and concomitantly enhanced deposition of collagen-1 and fibronectin [209]. Concordantly, more recent studies provided compelling evidence for the involvement of HMFs in processes preceding metastatic spread of PDAC and showed their role in the establishment of a pre-metastatic niche. In experiments conducted by Costa-Silva *et al.*, HMFs deposed fibronectin in the hepatic microenvironment prior to DTC engraftment. Bone-marrow derived macrophages and granulocytes accumulated in fibronectin-rich areas and in turn provided a favorable niche for PDAC liver metastasis formation. In their model, the emergence of HMFs was promoted by tumor derived exosomes containing migration inhibitory factor-1 (MIF-1). Injected exosomes were incorporated by Kupffer cells which in turn activated quiescent HSCs in a TGF-β1 dependent fashion [110]. Studies by Grünwald *et al.* showed corresponding results and found that HMFs attracted neutrophils via release of SDF-1α [111]. Furthermore, this study emphasizes the role of tissue inhibitor of metalloproteinases-1 (TIMP-1) which is also a prognostic factor for PDAC patient survival and was shown to activate HSCs via CD63 signaling [111, 210]. Both, MIF-1 bearing exosomes and TIMP-1, rendered livers more susceptible to DTC engraftment and specifically directed PDECs to the liver, indicating that HMFs may also be effective in processes promoting DTC homing [110, 111, 210, 211]. Homing in the context of cancer describes the phenomenon that cells of certain tumor entities specifically seed in particular target organs [212]. Interestingly, in the experiments conducted in this work, the proliferation state of detected DTCs was altered whereas the number of DTCs in the liver was comparable in young and aged mice two weeks after PDAC cell injection (**cf. Figure 4.4**). This observation indicates that aging-related inflammation in the liver has a minor impact on the homing of disseminated PDECs to the organ but rather determines their survival and growth in the hepatic microenvironment in the earliest steps of metastasis. In contrast, a higher amount of DTCs was observed in livers of aged mice four weeks after injection of R254 cells compared to livers of young mice (**cf. Figure 4.9**), indicating that homing processes may have played a more important role at this time point. However, it has to be taken into consideration that primary tumors of old mice were visibly larger than PDAC tumors of younger animals four weeks after tumor cell injection although this effect was not statistically significant. The size of a primary tumor was shown to correlate with the number of CTCs in the circulation and also with the amount of DTCs in secondary

organs [213]. It would therefore be reasonable to detect CTCs in the blood of young and old mice which was also sampled within experiments conducted in this work. This approach would allow to exclude that differences in the amount of DTCs observed four weeks post injection are due to larger primary tumors determined in 52 weeks old mice.

Of note, the pre-metastatic niche is defined as metastasis promoting alterations in a secondary environment devoid of tumor cells that are elicited by factors that derive from primary lesions [214]. In the above mentioned studies, MIF-1 containing exosomes and TIMP-1 which were shown to cause the activation of HSCs originated from PDAC cells or corresponding pre-conditioned culture media and can hence be regarded as tumor derived factors [110, 111, 210]. In contrast, differences in the conditions of the hepatic microenvironment as exposed in the syngeneic mouse model applied here were most likely provoked by aging-related inflammatory processes indicating that the dominance of HSC or HMF prevalent in a hepatic microenvironment vastly devoid of primary tumor derived factors may already determine the permissiveness for growth of disseminated PDECs in the liver. Accordingly, while tumor derived factors like TIMP-1 and MIF-1 containing exosomes form a pre-metastatic niche that promotes attraction of PDECs to the liver, aging may represent a tumor cell-independent promoter for conditions corresponding to a pre-metastatic niche in the liver by providing a proliferation and survival conductive microenvironment in dependence of HMF.

Aging is a systemic process, therefore causing inflammation not only in the liver but also in other organs and tissues of the body including the pancreas [177, 215, 216]. Hence, it was assumed that aging-related inflammation also significantly impacts on primary tumor growth. Surprisingly, in the aging-related syngeneic mouse model utilized here, primary tumors were comparably small two weeks after tumor cell inoculation whereas significant distinctions concerning DTC proliferation in the liver were already detectable at this time point (**cf. Figure 4.2 & 4.4**). Furthermore, four weeks after tumor cell injection, aging-associated differences in tumor growth detected livers were more pronounced than distinctions of tumor size in the pancreas (**cf. Figure 4.7 & 4.9**). This indicates that in the utilized model inflammaging did not affect tumor growth in all organs to the same extend and has a higher impact on secondary tumor growth in the liver than on primary tumor growth. It can also be hypothesized that aging represents a particular trigger for inflammatory processes and tumor cell proliferation in the hepatic microenvironment. To conclude whether aging-associated inflammatory alterations impact stronger on metastatic outgrowth in the liver than in other organs, further studies should aim to examine DTC proliferation in e.g. the lungs which are also a common

target of PDAC metastasis [92]. Similar to pancreata and livers, lungs were extracted from corresponding animals from the aging-related syngeneic mouse model and will be subject of further immunohistological analysis.

Due to the inaccessibility of tissue samples from PDAC patients in general and in particular in the early clinical course of the disease, the examination of PDAC metastases at different stages of progression demands the utilization of sophisticated animal models. For the initial screening of metastatic lesions and inflammation in the corresponding microenvironment the KPC mouse model was chosen as it represents a well-established PDAC model which recapitulates the human disease process. KPC mice expose metastatic spread via the portal circulation and predominantly to the liver [176, 217, 218]. Various studies aiming at elucidating processes of metastatic progression in PDAC are based on xenograft approaches comprising the application of human cancer cells into immunodeficient host animals [219]. While a great advantage of these models lies in the facilitated identification of tumor cells via human specific antibodies, the validity of findings obtained from such model systems may be questioned owed to species specific restrictions in the efficacy of potentially relevant factors [220]. Furthermore, xenograft models generally demand the injection of high numbers of tumor cells or the utilization of immunedeficient mice whereas an intact immune response is one of the crucial determinants for the inefficiency of metastasis so that its significance may not be neglected [221]. However, the KPC-model also revealed certain limitations which exacerbated the evaluation of experimental metastases. Due to the lack of unambiguous markers for PDAC cells, their detection can solely be carried out by immunohistological staining of cytokeratins. In the present study, CK-19 was utilized as marker to detect DTCs in mouse livers which is, however, also present in bile duct tissue [222]. This circumstance aggravated the identification of metastasis and rendered the evaluation of metastases via HE staining mandatory. Particularly single DTCs and DTC clusters were due to their minor size only detectable in one or two serial sections. However, 4 serial sections were necessary for staining of the complete marker set and thorough characterization. Hence, morphologically ambiguous potential micrometastases were excluded from the analysis to prevent false positive evaluations. Of note, the examined liver tissue specimens were extracted after PDAC primary tumor growth was well advanced. Matched primary tumors which were also immunohistologically examined, occupied the majority of the KPC mouse pancreas and showed a high degree of dedifferentiation (data not shown). Consequently, micrometastases were only rarely found and conclusions regarding early events in the malignant progression of PDAC were hard to draw.

Moreover, some micrometastases exposed particularly high proliferation despite the presence of desmin in the surrounding microenvironment, indicating certain heterogeneity and a potential role of further intrinsic and extrinsic cues that determine metastasis proliferation. The aging-related syngeneic mouse model used in this study helped overcoming most of these issues and allowed a more detailed analysis of early occurring events in metastases formation. Importantly, injected R254 cells were supplied with GFP and Luciferase reporter constructs [184]. This facilitated the surveillance of primary and secondary tumor growth with non-invasive imaging modalities and the distinct identification of disseminated PDAC cells in the FFPE liver via GFP-Tag antibodies. Moreover, utilized C57/Bl6 mice possess an intact adaptive immune system with various immune cell subsets [223]. Since R254 PDAC cells expose the same genetic background, a natural immune response in the vicinity of primary and disseminated R254 cells can be expected. The syngeneic mouse model system allowed the examination of metastasis formation processes in the earliest steps of metastatic spread. However, targeted injection of R254 PDAC cells into the pancreas head rendered abdominal surgery mandatory. Hence, it is possible that differential regulation of inflammation-associated genes was a result of an aging-related response to surgery itself. Elevated levels of IL-1, IL-6, TNF-$\alpha$ and VEGF have been detected after major abdominal surgery in the peripheral blood of mice and men [224–227]. Although these levels commonly decrease in the days after surgery, it may well be that the decline of pro-inflammatory mediators proceeds notably slower in elder patients and accordingly in older mice [228]. The longer persistence of pro-inflammatory cytokines in the circulation could accordingly represent a HSC-activating stimulus. Likewise this option involves significant clinical relevance since also the curative treatment of PDAC comprises severe surgical intervention. Interestingly, the observed gene expression profile of pro-inflammatory cytokines in livers of old mice is partially in line with previous reports which showed that several cytokines associated with inflammation expose a dynamic expression pattern altering with proceeding age of mice. Foremost the observed higher expression of IL-1$\beta$ in livers of aged mice was in accordance with findings of previous studies identifying higher levels of IL-1$\beta$ in aged C57BL/6J mice in comparison to younger individuals [190, 191]. Moreover, elevated levels of TGF-$\beta$1 were previously detected in livers of 24 months old animals compared to younger mice similar to the results presented here [191]. Importantly, a further study confirmed the finding that livers of young mice exhibit higher levels of the functional murine IL-8 homologue MIP-1. Guo *et al.* found a more than 2.5 times higher level of MIP-1 in 24 months old mice than 6 months old mice [229]. This accordance with previous observations from unoperated mice indicates that

the differential gene expression level of pro-inflammatory cytokines in 8 weeks versus 52 weeks old animals may indeed be due to aging-related processes. To further validate the relevance of an aging-related response to surgical processes in the utilized model a higher amount of young and old animals which solely undergo sham surgery will be included in future studies.
Importantly, although most of the factors found upregulated in livers of 52 weeks old mice are reported to be highly expressed in HMFs or involved in the activation of HSCs, it cannot be ruled out that the observed aging-related effects on DTC proliferation are also caused by other cell entities apart from HSCs or HMFs. For example, macrophages which were shown to play a crucial role in the initial and final steps of metastatic niche formation in PDAC are reported to release various of the here detected pro- and anti-inflammatory cytokines e.g. IL-1β, IL-6, FGF, TGF-β and VEGF [110, 208, 230]. Furthermore, it is reported that HSCs and HMFs differentially impact on other cell entities e.g. T-lymphocytes and neutrophils [105]. It would therefore be reasonable to examine the role of further hepatic stromal cell entities in the applied models. For example, the detection of neutrophils via Ly6G staining or macrophages via F4/80 staining in livers of young and old mice could clarify a potential impact of these cell entities on the proliferation of disseminated PDECs [231][186]).

Combined, the mentioned studies and the results presented here outline a rough picture of how HMFs as a characteristic of inflammatory conditions in the hepatic microenvironment contribute to engraftment and outgrowth of disseminated PDECs and support the view that HMFs are involved in the early steps of metastatic outgrowth of PDAC liver metastases. HMFs are critically involved in events that precede DTC engraftment in the liver as they support the attraction of CTCs to the liver specifically [110, 111, 210]. These studies demonstrate that HMFs participate in establishing and maintaining growth permissive conditions after engraftment of disseminated PDECs. The results presented here promote the view that aging may be regarded as an additional process for HMFs emergence which supports the proliferation of disseminated PDECs in the liver despite tumor derived cues, thereby further fuelling metastatic growth. Hence, the data presented here deliver a further explanation how elevated age increases the risk to develop metastatic PDAC.

## 5.2. A physiological hepatic microenvironment hampers outgrowth of PDAC liver metastasis by promoting dormancy in disseminated PDECs.

Whereas several previous studies and the results obtained from the mouse models applied in this thesis accordingly report a PDAC metastasis promoting effect of inflammatory conditions in the liver, to date no study examined if physiological conditions in the hepatic microenvironment may act to hamper the engraftment and onset of PDAC metastasis in the liver. The observation that micrometastases with a significantly lower amount of Ki67-positive tumor cells were located in areas with a low α-SMA/desmin ratio (**cf. Figure 4.1**), allows the conclusion that the predominance of HSC in the microenvironment may diminish the likelihood of metastatic outgrowth of disseminated PDECs. Furthermore, the minor degree of DTC proliferation detected in younger mice compared to old mice two weeks after tumor cell injection (**cf. Figure 4.4**) was accompanied by higher expression levels of the pro-inflammatory mediators MIP-1 and LIX (**cf. Figure 4.6**), which is most likely due to stromal cells with a higher presence in the less inflamed hepatic microenvironment of young mice. Since HSCs are a crucial component of a physiological microenvironment, this correlation may accordingly represent a further indication that a high abundance of HSCs represents hostile conditions for disseminated PDEC and hampers their outgrowth to overt metastases in contrast to HMF which are a characteristic of an inflamed liver. However, the applied mouse model systems did not allow conclusions regarding a potential direct proliferation inhibiting effect of HSCs on PDECs by e.g. paracrine signaling. The utilization of an indirect coculture system allowed investigations on the proliferation of PDECs and underlying mechanisms in dependence of HSC or HMF in a system devoid of other hepatic stromal cells. Furthermore, using H6c7-kras and Panc1 cells the behavior of PDECs at different stages of malignant progression was examined [180, 181, 232]. Representative for disseminated PDECs encountering a physiological hepatic microenvironment, H6c7-kras and Panc1 cells were cocultured with the murine cell line M1-4HSC (HSC) or human HHSteC pretreated with ATRA (HHSteC-HSC). Modelling the dissemination of PDECs that face an inflamed hepatic microenvironment, H6c7-kras and Panc1 cells were cultured in the presence of the murine cell line M-HT (HMF) or human HHSteC pre-treated with TGF-β1 (HHSteC-HMF). Indeed, the presence of HSC resulted in a significantly lower number of vital cells and Ki67-positive cells in both PDEC

lines compared to HMF cocultured H6c7-kras and Panc1 cells (**cf. Figure 4.11**). Similar results were obtained when comparing HHSteC-HSC and HHSteC-HMF cocultured H6c7-kras and Panc1 cells (**cf. Figure 4.15**). Interestingly, unlike HMF coculture, HSC coculture resulted in the emergence of Ki67-negative cells with a flattened, enlarged morphology. These features of growth arrested cells were validated by further analysis which showed that HSC coculture led to a higher p-ERK/p-p38 ratio, concomitantly with a higher level of the cell cycle inhibitor p21 and a significantly greater SABG-activity than in HMF cocultured PDECs. Accordingly, a corresponding QAP in H6c7-kras and Panc1 cells was obtained in the presence of HHSteC-HSC but not HHSteC-HMF coculture. These results unveil a distinct impact of HSCs and HMFs on the proliferation of disseminated PDECs and, moreover, show a growth arrest promoting effect of HSCs. This is a remarkable finding, since there are only a few indications in the literature that describe a proliferation inhibiting effect of isolated fibroblastoid cells, like a pioneering experimental study from 1966 in which normal fibroblasts inhibited the growth of polyoma-transformed baby hamster kidney cells [233]. Importantly, in experiments conducted in this work the observed QAP of pre-malignant and malignant PDECs was reversed when exchanging the coculture from HSC to HMF after 6 days. A majority of H6c7-kras and Panc1 cells with a QAP-morphology was Ki67-positive after HMF coculture. Accordingly, realtime Life Cell Imaging showed that PDECs with a QAP-morphology reacquired their proliferative capacity in the presence of HMF which hardly occurred in HSC-HSC cocultures. Latter effect was more pronounced in Panc1 than in H6c7-kras cells. These findings identified QAP as a reversible state of growth arrest and that its manifestation is dependent on the presence of HSC or HMF in the microenvironment. Hence, QAP can be regarded as an expression of cellular dormancy in PDECs. To this end, this work contributes to the issue which factors may induce and restrain cellular dormancy in metastases. It has already been proposed that factors of a physiological tissue may promote metastatic dormancy [119]. However, to date only a few of such stimuli were identified. Interestingly, several of these stimuli can be related to fibroblasts at different stages of activation. For instance, Kobayashi *et al.* found a phenotype similar to the HSC-driven QAP of PDECs in prostate cancer cells in dependence on the osteal microenvironment [169]. In their study, bone morphogenetic protein-7 (BMP-7), a member of the TGF-β protein family activated p38 and p21, resulting in the induction of growth arrest and a high SABG-activity in PC3 prostate cancer cells. BMP-7 was shown to be released from fibroblasts and osteoblasts from the bone stroma. Deprivation of BMP-7 reversed the dormant phenotype and reinduced proliferation of PC3 cells *in vitro* and *in*

*vivo*. Bragado *et al.* found that lungs which comprise lower amounts of TGF-β II promote homing and outgrowth of breast cancer cells [171]. In PDAC, the clinical significance of dormancy processes, in particular in metastatic processes, has been regarded as circumstantial due to the short time span from diagnosis of PDAC to the decease of the patient to metastatic disease. Accordingly, only few environmental dependent signaling cues crucial for dormancy processes in PDAC cells were so far identified. Using a model of reversible PDAC, Lin *et al.* demonstrated that dormant cancer cells contribute to residual disease in PDAC in a MYC dependent fashion. Pancreas specific expression of MYC resulted in the formation of PDAC and sporadic metastasis formation in the liver. While ablation of MYC resulted in apoptosis of the majority of PDAC cells, few cells persisted in pancreas and liver in a growth arrested state and could be reinduced to proliferate after re-expression of the MYC oncogene [166]. Interestingly, in their experiments residual dormant tumor cells were always detected in close proximity to or entirely embedded in the fibrotic stroma of pancreata and livers. They consequently hypothesized that signaling cues from the microenvironment represent an essential component of dormancy processes [234]. The observation that H6c7-kras and Panc1 cells are driven into cellular dormancy by HSC and subsequently reacquire proliferative capacity mediated by HMF support these findings and indicate that the condition of the microenvironment – physiologic tissue homoestasis versus inflamed state – determines if and when PDECs may outgrow to metastases. Further evidence for this hypothesis was previously brought forward by experimental models of breast cancer metastasis. Barkan *et al.* provoked fibrosis of the lungs via adenoviral vectors expressing active TGF-β1. The subsequent deposition of collagen-1A1 induced dormant breast cancer cells to form proliferative metastatic lesions via β1-integrin signaling [173, 174]. More recently, DeCock *et al.* described how inflammation promotes the escape from growth arrest of dormant breast cancer cells in the lung. The group generated dormant cells via *in vivo* passaging and *in vitro* expansion of slow-cycling mammary carcinoma cells. Inflammatory conditions in the pulmonary microenvironment were induced by challenging BALB/c mice with lipopolysaccharide and reinduced proliferation in dormant cancer cells in a neutrophil dependent fashion [235]. These results may also to some extend apply for PDAC metastases as these also occur in the lung. However, since PDECs most commonly spread to the liver, inflammatory processes in this organ may be more significant for PDAC and other cancer entities exposing predominant spread to the liver. To this end, the reversion of QAP in PDECs in presence of HMF may deliver corresponding evidence for a dormancy restrictive impact provided by inflammatory conditions in the liver.

However, it has to be emphasized that H6c7-kras and Panc1 cells did not regain proliferative activity in presence of HMF to a same extend, indicating differences in premalignant and malignant PDECs concerning the ability to leave the state of dormancy (**cf. Figure 4.16 & 4.18**). This supports the hypothesis that beyond environmental cues, cell intrinsic traits e.g. acquired mutations, genetic stability and epigenetic configuration critically determine the fate of disseminated PDEC in the secondary environment. Several reports showed that distant metastases derive from a unique subclone of the primary tumor and that most of the mutations prevalent in metastases correspond to genetic alterations in the primary context [87, 236, 237]. Hence, the mutational pattern a potential DTC exposes by the time of dissociation from the primary context is likely to be the most important determinant for its capacity to colonize the liver. With respect to PDAC-associated mutations, H6c7-kras cells harbor only a mutation in the KRAS oncogene while Panc1 cells among others carry a mutation in TP53 which emerges later in clonal evolution of PDAC [38]. Hence, differences in the mutational status of TP53 may harbor the explanation for the different proliferation behavior of H6c7-kras and Panc1 cells with QAP traits in presence of HMFs. This hypothesis is supported by findings from corresponding experiments conducted in the TP53 wildtype PDAC cell line Colo357 which was isolated from a PDAC lymph node metastasis [238]. In line with findings from H6c7-kras cells, Colo357 cells with HSC-mediated QAP-morphology did not regain proliferative activity but exposed a higher amount of Ki67-positive cells after HSC-HMF coculture compared to HSC-HSC coculture (data not shown). The utilization of H6c7-kras and Panc1 cells may allow conclusions which mutations are necessary to survive and proliferate in the hepatic microenvironment. It was previously shown that a mutation in KRAS is sufficient for PDECs to induce survival pathways which may foster their persistence in unfavorable conditions. For instance, oncogenic KRAS activates the kinase Mirk/Dyrk1B in growth arrested PDECs [239]. A 7-fold increase of Mirk was detected in PDAC cells which were arrested in the G0-phase and was shown to lower intracellular levels of noxious ROS (reactive oxygen species)[240]. This mechanism is of particular interest for the applied setting since the utilized cell line HSC is reported to expose and release higher amounts of ROS than HMF [182]. Further reports show that survival mechanisms of dormant cancer cells do not necessarily rely on oncogenic drivers. With autocrine IGF1/AKT signaling, a survival pathway for dormant PDECs independent of KRAS and MYC was lately identified [241]. Accordingly, both, premalignant PDECs carrying only a KRAS mutation, as well as further transformed PDECs which also acquired mutations in TP53 may survive in the hepatic microenvironment. Moreover, the observation that a distinct amount of

H6c7-kras cells were Ki67-positive after extended coculture with HMF indicates that these cells might harbor the capacity to regain proliferative activity when further extending HMF coculture. Consequently, it can be concluded that the outgrowth of both, KRAS mutated as well as KRAS and TP53 mutated disseminated PDECs in the liver is potentially possible. Importantly, however, in the studies performed by Rhim *et al.*, the number of CTC derived from PanIN lesions was significantly lower than the amount of CTCs that descended from established PDAC tumors [89]. Furthermore, due to various rate limiting steps in metastasis, only a very low percentage of DTCs successfully outgrows to a macroscopical lesion [242]. Adding the observation that only 25.9 % of H6c7-kras cells with QAP-morphology proliferated in presence of HMFs (**cf. Figure 4.18**), it may be concluded that PDECs which disseminate prior to establishment of PDAC primary tumor have a significantly lower chance to colonize the liver than PDAC cells that fully underwent malignant transformation. This view is supported by further results from the Rhim study which showed that DTCs derived from PanIN mice did not form overt metastasis in the hepatic microenvironment [89]. Importantly, however, the data shown in this thesis promote the view that inflammatory conditions in the liver may significantly enhance the chance of metastasis formation by premalignant PDECs.

The observation that subpopulation of both PDEC lines maintained their proliferative capacity despite the acquisition of growth arrest and re-entered the cell cycle in presence of HMFs led to the view that QAP can be regarded as a manifestation of cellular dormancy. However, SABG-activity is a feature of QAP that was present in a high percentage of HSC cocultured H6c7-kras and Panc1 cells (**cf. Figure 4.17 & 4.18**). It must therefore be argued that the state of growth arrest described by QAP could also represent a form of reversible senescence. To date, SABG is regarded as the only valid marker for senescence. However, the inclusion of further markers is recommended to detect senescent cells more specifically [243]. DNA microarray analysis predicted DEC1 and decoy receptor 2 as potential novel markers for senescent cells [243]. However, in stainings both markers failed to unambiguously identify a subpopulation of H6c7-kras and Panc1 cells exposing features of QAP (data not shown) indicating that DEC1 and decoy receptor 2 are not adequate markers for senescent PDECs. It can be argued that the markers applied here are not sufficient to describe senescent cells. To this end, cells with QAP do not expose phenotypical features apart from SABG activity that would represent a detectable distinction to a state of cellular dormancy. Therefore, a senescence phenotype may represent a feature or a subpopulation of dormant cells. Stainings of SABG in liver tissue

resected from the applied mouse models could be performed to identify the role of such a subpopulation *in vivo*.

Most of the own findings discussed in this chapter were generated in an indirect *in vitro* coculture which was used in order to model a physiological or an inflamed hepatic microenvironment. Self-evidently, an *in vitro* coculture model system is not sufficient to recapitulate the complexity of the human disease. However, it represents one of the few options to identify a mutual influence of two cell compartments in an isolated fashion. The MI1-4HSC/M-HT (HSC/HMF) cell system was utilized, as it represents HSCs at different degrees of transdifferentiation with the same genetic background [182]. However, studies with HSCs *in vitro* comprise certain general limitations since HSCs are easily activated and transdifferentiated upon isolation. Accordingly, most described immortalized HSCs lines expose an advanced stage of activation indicated by increased expression of $\alpha$-SMA [244]. Activated HSCs differ from quiescent HSCs by enhanced proliferation and migratory potential as well as unbalanced ECM deposition [245]. HSC which were applied in this study also show increased amounts of $\alpha$-SMA (**cf. Figure 4.1**)[182]. However, HSC but not HMF concomitantly expose high amounts of the intermediate filament desmin (**cf. Figure 4.1**) which is regarded as the "gold standard" for HSC characterization. Their phenotype may hence be considered as an early stage of activation and transdifferentiation. Accordingly, HSC had to be treated carefully and not be cultivated for more than ten passages to maintain a constant phenotype. Other often utilized cell lines with an HSCs-like phenotype e.g. LX-2 cells expose a more transdifferentiated profile (data not shown) and were hence not utilized in the study at hand. An *in vitro* cell system that fully recapitulates the traits of quiescent HSCs has yet to be established and would represent an interesting extension for further studies. However, HHSteC-HSC which were generated by treating HHSteC with ATRA may come close to such a phenotype, since ATRA has proven as a compound that reprograms activated HSCs to quiescent HSCs [189]. Importantly, when using the HSC/HMF system to examine the impact of different cell lineages on the proliferation of tumor cells in a comparative manner, potential differences in the proliferation or FCS uptake of the stromal cells have to be taken into consideration. Accordingly, it could be argued that the diminished proliferative activity of H6c7-kras and Panc1 cells after HSC coculture compared to HMF coculture could be based on a higher proliferation and FCS consumption of HSC compared to HMF. However, vital cell numbers of HSC and HMF isolated after completed coculture were principally comparable whereas growth of H6c7-kras and Panc1 cells was

unaltered in media with different FCS amounts (data not shown). Hence, it can be assumed that the differences of PDEC growth under HSC or HMF coculture were indeed due to soluble factors derived of respective hepatic stromal cells and not owed to differences in the proliferation of HSC and HMF. Of note, key findings from HSC/HMF coculture experiments were validated in a second coculture system comprising only human cells. HHSteC-HSC and HHSteC-HMF exposed phenotypes comparable to their respective murine counterpart HSC and HMF (**cf. Figure 4.14**) and showed a comparable differential impact on H6c7-kras and Panc1 cells (**cf. Figure 4.15**). Hence, albeit its limitations the HSC/HMF system represents a useful tool to backup findings from *in vivo* models and to determine underlying mechanisms by which these hepatic stromal cells impact on the proliferation of disseminated PDECs.
A further important issue in the context of proliferation is the validity of Ki67 as a proliferation marker. Ki67-positivity is regarded as strictly associated with proliferation since nuclear Ki67 is detectable in cells during all active phases of the cell cycle and absent in resting cells [246]. Therefore, Ki67 is a widely applied marker which is also used in clinical routine. However, cells that entered the cell cycle but became growth arrested in phases apart from G0 may also stain positive for Ki67. Accordingly, Ki67 stainings may have stained PDECs which were actually captured in growth arrest. This would explain the emergence of Ki67-positive H6c7-kras and Panc1 cells after HSC-HSC coculture. Thus, other methods to unambiguously discriminate proliferative and non-proliferative cells could be included in further studies. As such, BrdU-labeling or carboxyfluorescein succinimidyl ester (CFSE) stainings could be deployed.

Taken together, the results discussed so far clearly indicate that inflammatory conditions in hepatic microenvironment, characterized by the presence of HMFs, represent growth permissive conditions for PDEC that encounter the liver. HSC as integral component of a physiological microenvironment may act to the restrain the progression of disseminated PDECs to overt metastases by inhibiting their proliferation. Accordingly, the conditions of the hepatic microenvironment can be regarded as a dynamic factor determining the likelihood of metastatic outgrowth in the liver and may represent a switch from a dormancy permissive to a dormancy restrictive microenvironment.

## 5.3. Growth arrest and progression of disseminated PDECs is determined by proinflammatory mediators.

Remodelling of the hepatic microenvironment within inflammatory processes in the liver is accompanied by altered release of various chemokines, cytokines and growth factors [247]. Accordingly, distinct alterations were found when comparing the expression of inflammatory mediators in livers of 8 weeks and 52 weeks old mice (**cf. Figure 4.6**). Furthermore, the indirect coculture of PDECs with HSC or HMF facilitated the identification of soluble factors of a physiological or inflamed hepatic microenvironment which may act to promote or to revert QAP in PDECs.

First, stroma derived factors potentially involved in the induction of dormancy in PDECs were examined. A significantly higher concentration of m IL-6 was found in supernatants of Panc1 cells which were cocultured with HSC in comparison to Panc1 cells cocultured with HMF (**cf. Figure 4.19**). The circumstance that only IL-6 of murine origin was detected in higher amounts indicates that IL-6 derived from the HSC compartment. Due to these findings and previous studies which showed a quiescence and senescence promoting effect of IL-6 [136], it was suggested that HSC-mediated IL-6 signaling may be responsible for the observed QAP induction in Panc1 cells under HSC coculture. However, neither the blockade of the IL-6 receptor via Tocilizumab nor the inhibition of IL-6 trans-signaling via sgp130fc impacted on the vital cell count of Panc1 cells under HSC coculture (**cf. Figure 4.20**) or affected the morphology of Panc1 cells regarding a potential QAP emergence to a visible extent (data not shown). Concomitantly, h IL-6 stimulated Panc1 cells showed an increased vital cell number compared with control stimulated cells (**cf. Figure 4.21**). These data validated previous experiments conducted in the workgroup with H6c7-kras cells [181] and indicate that IL-6 signaling is not causally involved in stroma-mediated QAP promotion in both, H6c7-kras and Panc1 cells. M IL-6 was exclusively detected in coculture supernatants while monocultured HSC and HMF did not release detectable amounts of this cytokine. Hence, the measured levels of m IL-6 were probably a consequence of the vice versa communication of HSC or HMF with Panc1 cells. In contrast to m IL-6, which shows no affinity to h IL-6R, the human isoform of IL-6 binds both, the m IL-6R and h IL-6R [200]. Accordingly, the elevated release of m IL-6 may have represented a secondary effect initiated by Panc1 cells. IL-6 was reported to be a major component of the SASP [136, 152]. It is hence possible that Panc1 cells which acquired a QAP elicited senescence-associated signaling in HSC which manifested in

a distinct SASP and subsequent elevated IL-6 release. Accordingly, HSC exposed an increased SABG-activity after coculture with Panc1 cells (data not shown). It could not be clarified, whether the application of Tocilizumab or sgp130fc fully neutralized IL 6 signaling which should be validated in further experiments. However, IL-6 showed no aging-related differential gene expression in the livers of C57Bl/J6 mice (**cf. Figure 4.6**) indicating that this molecule also plays a minor role in stroma-mediated differences in DTC proliferation between young and old mice in the applied mouse model. A previous study showed increased levels of IL-6 in livers of 18 months old C57Bl6/J mice compared to 6 months old animals which indicates that altered IL-6 signaling may rather emerge at advanced age as an expression of an aging-related SASP [152, 190]. Furthermore, IL-6 is considered one of the main signaling pathways that mediate chronic morbidity in aging patients [248]. In line with the growth promoting effect of h IL-6 on Panc1 cells shown in this study, several reports provided evidence that IL-6 fosters the development of PDAC in the primary and secondary context [198, 249]. These data promote the view that IL-6 signaling may have a proliferation promoting impact and plays a minor role in HSCs-mediated dormancy induction and maintenance in disseminated PDECs.

A more significant role in the maintenance of QAP can be accredited to IL-8. In *in vitro* coculture experiments, IL-8 was detected at higher levels in supernatants of HSC cocultured Panc1 than supernatants obtained from Panc1/HMF coculture (**cf. Figure 4.19**). In order to examine the role of IL-8 signaling in cellular dormancy of PDECs, h IL-8 was blocked in Panc1 cells following an approach similar to the blockade of IL-6 signaling. However, in contrast to the blockade of IL-6, the neutralization of IL-8 via monoclonal anti IL-8 antibodies resulted in a clear increase of vital cell Panc1 cells after 6 days of HSC coculture (**cf. Figure 4.22**). Moreover, the neutralization of h IL-8 resulted in a visibly elevated p-ERK/p-p38 ratio in HSC cocultured Panc1 cells accompanied by a significant decrease of SABG activity and a decreased number of cells with a QAP-morphology (**cf. Figure 4.22**). These findings indicate that IL-8 is a critical mediator of HSC-mediated dormancy of PDECs. IL-8 signaling was reported to be altered in various cancer entities [250]. However, the role of IL-8 signaling on tumor promotion is discussed controversially. Several studies recognize IL-8 as a tumor promoting molecule as it among other functions exposes potent pro-angiogenic potential and shows a marked upregulation in chronic inflammation [251–253]. Accordingly, some reports showed a direct impact of IL-8 on the proliferation of tumor cells of different cancer entities including PDAC [254–257]. By way of contrast, other studies report that IL-8

signaling dictates growth arrest in PDAC upon inflammation-mediated OIS [136, 258]. The circumstance that IL-8 was shown to increase both, ERK as well as p38 signaling, leads to the assumption that the functions and effects of IL-8 signaling are context dependent [259]. HSCs and HMFs both are among the cell entities which are known to release IL-8 (Weiskirchen & Tacke 2014). Importantly, IL-8 has also been shown to promote cancer stem cell-like properties in PDAC cells. The administration of recombinant h IL-8 resulted in the formation of mammaspheres in Capan-1 cells [260]. In a further study, the blockade of IL-8 signaling increased the effectiveness of AC (cyclophosphamide, doxorubicin) chemotherapy [261]. Accordingly, previous reports from the work group showed that H6c7-kras and Panc1 cells acquire stem cell features under HSC coculture including enhanced colony formation ability and clonogenicity as well as the induction of stem cell markers nanog and nestin [232]. Hence, it is possible that IL-8 works to induce stemness in disseminated PDECs in dependence on the hepatic microenvironment. A recent study supports this hypothesis and unveiled a link between IL-8 and cellular dormancy. In a 3d coculture, MDA breast cancer cells and Panc1 cells engulfed mesenchymal stromal cells (MSCs) and acquired various features of dormancy and cancer stemness, respectively. After engulfment of MSCs, MDA cells exposed a strong upregulation of pro-inflammatory mediators including IL-8 and IL-6 among other molecules which are reported to be part of the SASP [262].

So far, only functional homologues of h IL-8 but no sequence identical homologues of h IL-8 were identified in mice [263]. Since HSC and HMF are murine cell lines, the detected and neutralized IL-8 could only originate from Panc1 cells. Hence, elevated IL-8 release by Panc1 cells under HSC coculture is probably dependent on another HSC-derived factor which remains to be identified. This factor may induce an IL-8 feedback loop in Panc1 cells which manifests in QAP. Accordingly, the neutralization of IL-8 may hamper this feedback loop and allow the induction of proliferation in Panc1 cells with a QAP. It is hence possible that the absence of IL-8 fostered the proliferation of PDAC cells, which may harbor an explanation for the observed reversion of QAP under HMF coculture. Since the presence of HHSteC-HSC resulted in QAP in Panc1 cells similar to HSC coculture conditions further experiments should aim to neutralize IL-8 in the human-human coculture system. Importantly, young C57Bl/6J mice exposed higher expression levels of the murine chemokines MIP-2 and LIX (**cf. Figure 4.6**) which are recognized as functional homologues of IL-8 [263]. The higher expression of these cytokines correlated with a lower proliferation of disseminated PDECs. Like IL-8, MIP-2 and LIX fulfill their effect by binding to the CXCR1/2 receptor complex [263]. A knockdown of CXCR1/CXCR2 in PDECs in the

applied *in vitro* and *in vivo* systems would therefore help to further validate the role of IL-8 as a QAP promoting factor.

The applied system also allowed identifying candidate cytokines by which an inflamed hepatic microenvironment, and therefore HMFs, may promote reversion of dormancy in disseminated PDECs. Molecules detected in significantly higher levels in Panc1/HMF cocultures than Panc1/HSC cocultures were h SDF-1$\alpha$, h VEGF and m VEGF (**cf. Figure 4.19**). As a first step to test a potential involvement of these factors in the reversion of dormancy, their impact on the proliferation of Panc1 cells in dependence on the microenvironment was examined. For this approach, the respective cytokine of interest was blocked under Panc1/HMF coculture conditions or monocultured Panc1 cells were exposed to the respective recombinant protein. Human SDF-1$\alpha$ exposed the most distinct differential release between Panc1/HSC and Panc1/HMF cocultures (**cf. Figure 4.19**). Furthermore, a proliferation promoting effect of SDF-1$\alpha$ released by CAFs had previously been reported [264]. However, blockade of SDF-1$\alpha$ signaling via the CXCR4 antagonist AMD3100 did not affect the vital cell count of Panc1 cells to a visible extent (**cf. Figure 4.24**). Alternatively to CXCR4 signaling, SDF1-$\alpha$ may also work by binding CXCR7 [265]. However, stimulation of Panc1 cells with r h SDF-1$\alpha$ had a similar minor impact on the vital cell number of Panc1 cells, implying a negligible role of SDF-1$\alpha$ in the HMF-mediated proliferation induction. The SDF-1$\alpha$/CXCR4 axis is mostly known for its involvement in chemotactic processes [266]. SDF-1$\alpha$ attracts CXCR4 expressing cells and is as such involved in processes promoting cell trafficking of stem and progenitor cells e.g. hemato- and lymphopoietic cells to their corresponding target organs. Furthermore, SDF1-$\alpha$ was shown to promote the formation of a pre-metastatic niche in PDAC via neutrophil attraction [111, 210]. It can thus be assumed that SDF-1$\alpha$ may impact Panc1 cells in cellular processes apart from proliferation which were not particularly addressed in the applied indirect coculture system. However, SDF-$\alpha$ expression could be examined in the aging-related syngeneic mouse model to validate the observed minor impact of inflammaging on homing of disseminated PDECs to the liver.

A differential cytokine release between Panc1/HSC and Panc1/HMF cocultures was also detected for VEGF. Of note, in case of VEGF, however, both the human and the murine homologue of the cytokine were detected at higher levels in Panc1/HMF coculture supernatants compared to supernatants obtained from Panc1/HSC coculture (**cf. Figure 4.19**). Moreover, VEGF-A showed the most striking differential gene expression between livers of 8 weeks and livers of 52

weeks animals (**cf. Figure 4.6**). Consequently, VEGF-signaling was blocked under HMF coculture conditions using different antibodies which are also applied in clinical routine. The neutralisation of VEGF-A via Bevacizumab had no visible impact on the vital cell count of Panc1 cells compared to Panc1 cells which were treated with the control antibody Rituximab (**cf. Figure 4.25**). By way of contrast, the stimulation with recombinant h VEGF-A resulted in a clear increase of vital Panc1 cells (**cf. Figure 4.26**). This validated a proliferation promoting effect of VEGF-A on Panc1 cells and indicated that the neutralization of h VEGF-A alone was not sufficient to entirely compromise VEGF-signaling. In contrast, the consequent neutralization of VEGF-A and VEGF-B of murine and human origin via Aflibercept led to a significant decrease of vital Panc1 cells under HMF coculture and number of Ki67-positive cells accompanied by a diminished p-ERK/p-p38 ratio (**cf. Figure 4.25**). Since these observations clearly pointed to the involvement of VEGF in the HMF-mediated proliferation induction, it was also examined if the blockade of VEGF may restrain the observed HMF-mediated dormancy reversal of Panc1 cells. The administration of Aflibercept under HMF coculture following HSC coculture decreased the number of vital and proliferative Panc1 cells as well as the p-ERK/p-p38 ratio (**cf. Figure 4.27**). Together, these results identify VEGF as a crucial factor in the HMF-mediated promotion of proliferation. Furthermore, they imply that HMF revert dormancy of Panc1 cells in a VEGF dependent manner. A significant role of VEGF signaling in escape of tumor dormancy is well appreciated. However, this effect is mostly based on the role of VEGF as a pro-angiogenic factor as which it was first described [267]. VEGF supports the pro-angiogenic switch which is necessary for growing tumors to overcome insufficient blood and nutrient supply and concerns the phenomenon of tumor mass dormancy [118]. Due to this function, VEGF plays a fundamental role in various cancer entities and is a common target of chemotherapy approaches [268]. However, to date all clinical phase-III trials which included anti-VEGF treatment showed no survival benefit in PDAC patients which is also believed to be due to the profound tumor stroma and the observation that tumors expose a strong hypovascularity [219, 269]. In this context, recent studies indicate that the pro-angiogenic switch is dispensable for the progression from micrometastases to macrometastases in PDAC [207]. However, VEGF was shown to directly accelerate the growth of different PDAC cells [270]. Furthermore, it was reported that the inhibition of VEGF induces cellular senescence in colorectal cancer cells [204]. Yet, a direct dormancy reverting effect of VEGF on tumor cells has not been shown. Of note, in a study by Tang *et al.* the enzyme 15-lipoxygenase-2 induced dormancy in prostate cancer cells which correlated

with a diminished VEGF-A expression [271]. In line with the results presented in the study at hand, HMFs were reported to expose higher levels of VEGF than HSCs [106]. Accordingly, VEGF-signaling is also critically involved in inflammatory and fibrotic processes [272]. Furthermore, the observation that h VEGF and m VEGF were similarly elevated in HMF cocultures compared to HSC cocultures (**cf. Figure 4.19**) indicates that VEGF was indeed released by HMFs in the coculture setting. Concomitantly, the observation that livers of 52 weeks old mice exposed significantly higher expression levels of VEGF-A then livers 8 weeks old animals (**cf. Figure 4.6**) represents a further strong indicator that VEGF may promote growth of disseminated PDECs *in vivo*. Importantly, failing clinical phase III trials testing the effect of Bevacizumab or Aflibercept as Gemcitabine additives were conducted in advanced stage, metastasized PDAC patients [273, 274]. Therefore, anti-VEGF therapy aiming at preventing the outgrowth of PDAC metastases might represent a more promising approach for the treatment of early stage PDAC patients. This motivates further endeavors seeking to identify novel mechanisms for earlier detection of PDAC.

Some cytokines, e.g. IL-6 expose species specific efficacy [275]. Hence, results from an *in vitro* coculture system based on cell lines of two different species as given in the applied HSC/HMF coculture system have to be regarded with care. Concomitantly, this coculture system harbors a crucial advantage as it enables the identification of a cytokine's respective origin compartment. To fully examine the mutual impact of stroma and tumors cells via soluble factors, the role of cytokines has to be validated in a one-species coculture system. The established HHSteC coculture system allows this approach and will be used for further corresponding studies. Moreover, this system could be used to conduct a further Luminex assay. This would represent a feasible way to validate factors that may be effective in induction and reversion of dormancy. Furthermore, stromal cells and tumor cells may also communicate via direct contact apart from soluble factors. A feasible way to examine the straight impact of HSCs and HMFs on PDECs would be a direct coculture system. Such a system could recapitulate the architectural traits of the liver and would be an interesting approach for future studies. In some blocking strategies applied in this work, the validation of the blockade of respective factors failed. Hence, the full inhibition of chemokines and cytokines is not ensured to a similar extend in all experiments. This may comprise the explanation why no differences in the reversion of QAP in Panc1 were observed in realtime Life Cell Imaging upon Aflibercept and Rituximab treatment during respective HMF coculture (**cf. Figure 4.27**). However, importantly, the role of factors like VEGF and IL-8 could be validated in

the syngeneic mouse model, promoting the validity of the applied *in vitro* system.

Taken together, the murine/human and human/human coculture system in combination with the applied mouse models identified conditions and factors as well as underlying mechanisms by which the hepatic microenvironment may promote or revert dormancy in disseminated premalignant and malignant PDECs. The data presented in this thesis promote the hypothesis that the hepatic microenvironment and the disseminated PDEC itself represent dynamic and variable systems. Their condition and interplay determine the fate of the disseminated PDEC and their likelihood to progress to overt metastasis in the liver (**Figure 5.1**).

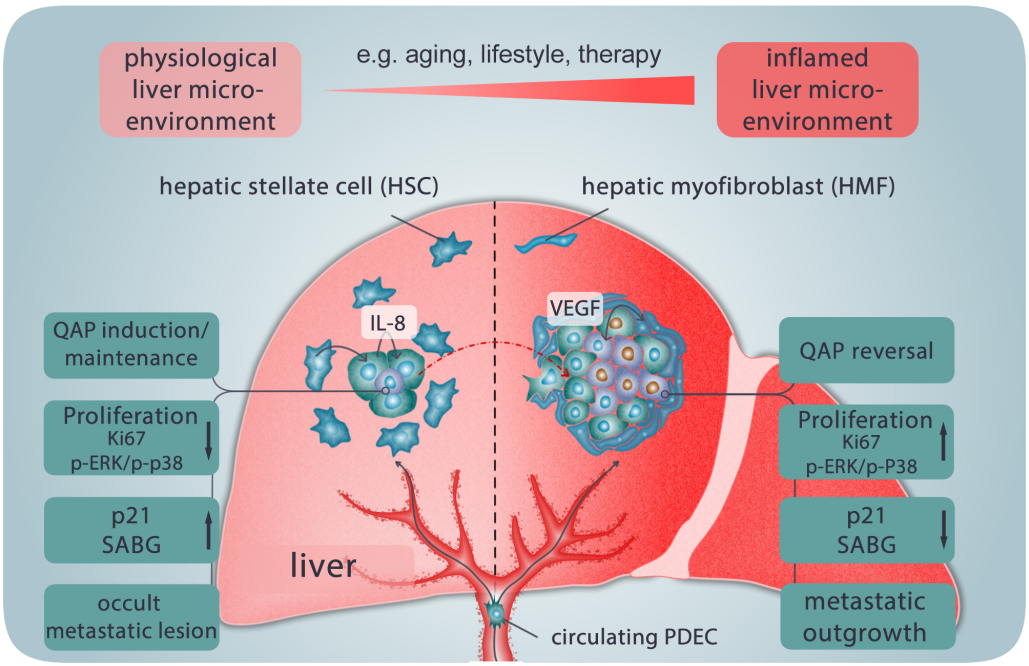


**Figure 5.1.: Model of how the condition of the hepatic microenvironment determines the growth behavior of disseminated PDECs.** A physiological microenvironment, characterized by high abundance of HSCs, prevents the outgrowth of disseminated pancreatic ductal epithelial cells (PDECs) to overt metastases. HSCs induce and maintain a quiescence-associated phenotype (QAP) in PDECs that encounter the organ, manifesting in Ki67-negativity, low phosphorylated (p)-ERK/p-p38 ratio, accompanied by high levels of p21 and senescence-associated β-galactosidase (SABG) acitivity. This QAP is induced and maintained via IL-8. Aging processes, lifestyle factors or therapy promote inflammation and the emergence of HMFs in the hepatic microenvironment. As a consequence, disseminated PDECs escape dormancy in dependence on VEGF released by HMFs. In this fashion, an inflamed hepatic microenvironment promotes the progression of PDAC metastasis.

Analogous to Stephen Paget's theory, the disseminated PDEC can be regarded as a dynamic seed. The mutations PDECs acquired by the time of spreading to the liver determine its plasticity as well as its ability to survive and proliferate in the secondary microenvironment. Whereas both, premalignant and malignant disseminated PDECs can persist in the liver in a dormant state, cells with mutated TP53 may harbor a markedly higher capability to outgrow to overt metastases.

This further promotes the view that PDECs which disseminate lately during PDAC pathogenesis may form metastasis notably faster. The hepatic microenviroment can be seen as a dynamic soil. A physiological microenvironment may act to restrain the progression of disseminated DTCs to overt metastasis and hence represent a dormancy permissive microenvironment. The results presented here indicate that IL-8 which is elevated in an HSCs-rich, physiological microenvironment embodies a factor which acts to induce and maintain a state of dormancy in disseminated PDECs. In contrast, inflammatory conditions in the liver, manifesting in the emergence of HMFs, may represent a switch to a rather dormancy restrictive microenvironment and promote the growth of disseminated PDECs that encounter the liver or persist in the organ in a growth arrested state. These alterations may be triggered by aging processes and lifestyle factors like smoking and alcoholic abuse, but potentially also by therapy procedures like abdominal surgery or chemotherapy. Therefore, the data presented here may comprise an explanation for the emergence of metastases in patients even after R0 resection [7]. Based on the findings from this thesis, VEGF represents a potential factor by which HMFs promote the escape from dormancy in disseminated PDECs. Altogether this thesis shows a marked impact of the hepatic microenvironment on the proliferation behavior of disseminated premalignant and malignant PDECs. Furthermore, they promote the view that dormancy processes play a crucial role in PDAC metastasis. The results from this study encourage undertakings aiming at early diagnosis and prevention of metastasis in PDAC to eradicate this devastating disease.

# 6. Outlook

This study showed for the first time how aging-related inflammatory alterations in the liver promote growth of dormant disseminated PDECs. It thereby provides the foundation for further studies on the impact of inflammatory processes on PDAC metastasis formation. The applied syngeneic mouse model can be used to validate the role of the factors IL-8 and VEGF in induction and reversion of dormancy in disseminated PDECs *in vivo*. A feasible way to test a PDAC proliferation promoting role of VEGF on disseminated PDECs would be to intraperitoneally inject VEGF neutralizing Aflibercept in 8 weeks and 52 two weeks old mice. This could be performed two weeks after orthotopic injection of R254 cells, a time point at which metastatic lesions are still relatively small. Four weeks after tumor cell injection, primary and secondary tumor growth can be examined as well as the regulation of inflammation-associated genes in the liver, further organs and systemically. In a similar approach, a dormancy promoting effect of IL-8 could be validated. For this purpose, antibodies recognizing IL-8 or its murine homologues can be deployed to block tumor cell and stroma-mediated IL-8 signaling, respectively. Furthermore, the syngeneic model can be extended for a premalignant PDEC line in order to examine the role of mutated TP53 in disseminated PDECs *in vivo* in dependence on different conditions in the hepatic microenvironment. Regarding PDAC relevant mutations, the KC mouse derived cell line 8182 harbors only a KRAS mutation but beyond that possesses the same detection modalities as the R254 cell line [184]. Accordingly, differences between premalignant and malignant PDECs concerning stroma-mediated QAP reversion detected *in vitro* could be validated in an *in vivo* setting.

The results from this thesis promote the view that a physiological tissue homeostasis restrains the outgrowth of disseminated PDECs. This view is in line with studies concerning primary PDAC [276, 277]. Sherman et al. showed how treatment with the vitamin D receptor (VDR) ligand calcipotriol reduced inflammation and fibrosis in the PDAC stroma as well as growth of primary PDAC. It would be interesting to examine if corresponding effects can be obtained in the hepatic microenvironment in the context of liver metastasis.

The presence of HSC resulted in enhanced SABG activity in H6c7-kras and Panc1 cells. However, additional markers failed to further characterize and identify

senescence in the applied PDEC lines. The characterization of senescent PDAC cells, especially *in vivo*, may represent a worthwhile approach, since senescent PDECs may embody a particularly hazardous cell subpopulation due to their SASP. The SASP of senescent cells stimulates cells in the surrounding, causing an immunotolerant milieu via recruitment of immunosuppressive myeloid cells [278]. Furthermore, the SASP is reported to stimulate senescent fibroblasts to pro-inflammatory cells [152]. A further fibrotic remodelling of the microenvironment can be the consequent result which may attract or promote the outgrowth of further DTCs. Studies on therapy induced senescence showed the emergence and significance of such a phenotype in lymphoma cells [279]. A promising approach to further characterize potentially senescent cells are peculiarities in their metabolism which will be examined in further studies in the group of inflammatory carcinogenesis.

# References


[1] Peter Kaatsch, Claudia Spix, Alexander Katalinic, Stefan Hentschel, Sabine Luttmann, Christa Stegmaier, Sandra Caspritz, Monika Christ, Anke Ernst, Juliane Folkerts, Jutta Hansmann, Stefanie Klein, Kristine Kranzhöfer, Beatrice Kunz, Katrin Manegold, Andrea Penzkofer, Kornelia Treml, Susanne Weg-Remers, Kerstin Wittenberg, Nadia Baras, Benjamin Barnes, Joachim Bertz, Nina Buttmann-Schweiger, Stefan Dahm, Julia Fiebig, Manuela Franke, Jörg Haberland, Klaus Kraywinkel, Antje Wienecke, and Ute Wolf. *Beiträge zur Gesundheitsberichterstattung des Bundes - Krebs in Deutschland 2011/2012*. Gesundheitsberichterstattung für Deutschland. Robert Koch-Institut, Berlin, 10., ausgabe edition, 2015.

[2] Rebecca L. Siegel, Kimberly D. Miller, and Ahmedin Jemal. Cancer statistics, 2016. *CA: a cancer journal for clinicians*, 66(1):7–30, 2016.

[3] Angel Cid-Arregui and Victoria Juarez. Perspectives in the treatment of pancreatic adenocarcinoma. *World journal of gastroenterology*, 21(31):9297–9316, 2015.

[4] Lola Rahib, Benjamin D. Smith, Rhonda Aizenberg, Allison B. Rosenzweig, Julie M. Fleshman, and Lynn M. Matrisian. Projecting cancer incidence and deaths to 2030: the unexpected burden of thyroid, liver, and pancreas cancers in the united states. *Cancer research*, 74(11):2913–2921, 2014.

[5] Andrew E. Becker. Pancreatic ductal adenocarcinoma: Risk factors, screening, and early detection. *World journal of gastroenterology*, 20(32):11182, 2014.

[6] Hanno Riess, Andrea Goerke, and Helmut Oettle. *Pancreatic Cancer*, volume 177 of *Recent Results in Cancer Research*. Springer-Verlag, Berlin, Heidelberg, 2008.

[7] Cosimo Sperti, Claudio Pasquali, Antonio Piccoli, and Sergio Pedrazzoli. Recurrence after resection for ductal adenocarcinoma of the pancreas. *World Journal of Surgery*, 21(2):195–200, 1997.

[8] Neoptolemos John P., Stocken Deborah D., Friess Helmut, Bassi Claudio, Dunn Janet A., Hickey Helen, Beger Hans, Fernandez-Cruz Laureano, Dervenis Christos, Lacaine François, Falconi Massimo, Pederzoli Paolo, Pap Akos, Spooner David, Kerr David J., and Büchler Markus W. A randomized trial of chemoradiotherapy and chemotherapy after resection of pancreatic cancer. *New England Journal of Medicine*, 351(7):726, 2004.

[9] Haiyong Han and Daniel D. von Hoff. Snapshot: pancreatic cancer. *Cancer cell*, 23(3):424–424.e1, 2013.

[10] Daniel Ansari, Adam Gustafsson, and Roland Andersson. Update on the management of pancreatic cancer: surgery is not enough. *World journal of gastroenterology*, 21(11):3157–3165, 2015.

[11] Simona Iodice, Sara Gandini, Patrick Maisonneuve, and Albert B. Lowenfels. Tobacco and the risk of pancreatic cancer: a review and meta-analysis. *Langenbeck's archives of surgery*, 393(4):535–545, 2008.

[12] C. Bosetti, E. Lucenteforte, D. T. Silverman, G. Petersen, P. M. Bracci, B. T. Ji, E. Negri, D. Li, H. A. Risch, S. H. Olson, S. Gallinger, A. B. Miller, H. B. Bueno-de Mesquita, R. Talamini, J. Polesel, P. Ghadirian, P. A. Baghurst, W. Zatonski, E. Fontham, W. R. Bamlet, E. A. Holly, P. Bertuccio, Y. T. Gao, M. Hassan, H. Yu, R. C. Kurtz, M. Cotterchio, J. Su, P. Maisonneuve, E. J. Duell, P. Boffetta, and C. La Vecchia. Cigarette smoking and pancreatic cancer: an analysis from the international pancreatic cancer case-control consortium (panc4). *Annals of oncology : official journal of the European Society for Medical Oncology*, 23(7):1880–1888, 2012.

[13] Irene Tramacere, Lorenza Scotti, Mazda Jenab, Vincenzo Bagnardi, Rino Bellocco, Matteo Rota, Giovanni Corrao, Francesca Bravi, Paolo Boffetta, and Carlo La Vecchia. Alcohol drinking and pancreatic cancer risk: a meta-analysis of the dose-risk relation. *International journal of cancer*, 126(6):1474–1486, 2010.

[14] Eric J. Duell. Epidemiology and potential mechanisms of tobacco smoking and heavy alcohol consumption in pancreatic cancer. *Molecular carcinogenesis*, 51(1):40–52, 2012.

[15] Ilya Gukovsky, Ning Li, Jelena Todoric, Anna Gukovskaya, and Michael Karin. Inflammation, autophagy, and obesity: common features in the pathogenesis of pancreatitis and pancreatic cancer. *Gastroenterology*, 144(6):1199–209.e4, 2013.

[16] R. Huxley, A. Ansary-Moghaddam, A. Berrington de Gonzalez, F. Barzi, and M. Woodward. Type-ii diabetes and pancreatic cancer: a meta-analysis of 36 studies. *British journal of cancer*, 92(11):2076–2083, 2005.

[17] R. J. Stevens, A. W. Roddam, and V. Beral. Pancreatic cancer in type 1 and young-onset diabetes: systematic review and meta-analysis. *British journal of cancer*, 96(3):507–509, 2007.

[18] Eugenia E. Calle, Carmen Rodriguez, Kimberly Walker-Thurmond, and Michael J. Thun. Overweight, obesity, and mortality from cancer in a prospectively studied cohort of u.s. adults. *New England Journal of Medicine*, 348(17):1625–1638, 2003.

[19] F. M. Giardiello, J. D. Brensinger, A. C. Tersmette, S. N. Goodman, G. M. Petersen, S. V. Booker, M. Cruz-Correa, and J. A. Offerhaus. Very high risk of cancer in familial peutz-jeghers syndrome. *Gastroenterology*, 119(6):1447–1453, 2000.

[20] Marcia S. Brose, Timothy R. Rebbeck, Kathleen A. Calzone, Jill E. Stopfer, Katherine L. Nathanson, and Barbara L. Weber. Cancer risk estimates for brca1 mutation carriers identified in a risk evaluation program. *Journal of the National Cancer Institute*, 94(18):1365–1372, 2002.

[21] Ying Bao and Dominique S. Michaud. Physical activity and pancreatic cancer risk: a systematic review. *Cancer epidemiology, biomarkers & prevention : a publication of the American Association for Cancer Research, cosponsored by the American Society of Preventive Oncology*, 17(10):2671–2682, 2008.

[22] Marinos Pericleous, Roberta Elisa Rossi, Dalvinder Mandair, Tara Whyand, and Martyn Evan Caplin. Nutrition and pancreatic cancer. *Anticancer research*, 34(1):9–21, 2014.

[23] J. M. Slack. Developmental biology of the pancreas. *Development (Cambridge, England)*, 121(6):1569–1580, 1995.

[24] Jurij Dolenšek, Marjan Slak Rupnik, and Andraž Stožer. Structural similarities and differences between the human and the mouse pancreas. *Islets*, 7(1):e1024405, 2015.

[25] L. R. Engelking. Physiology of the endocrine pancreas. *Seminars in veterinary medicine and surgery (small animal)*, 12(4):224–229, 1997.

[26] E. T. Sternheim, J. Voigt, W. Kaspar, and W. G. Dippold. Das pankreaskarzinom. *Der Internist*, 41(9):848–859, 2000.

[27] Tanaka, Tako Ohtsuka and Masao. Intraductal papillary mucinous neoplasm of the pancreas; characteristics, diagnosis, and management based on the fukuoka consensus guidelines 2012. *Pancreapedia: The Exocrine Pancreas Knowledge Base*, 2014.

[28] M. Distler, D. Aust, J. Weitz, C. Pilarsky, and Robert Grutzmann. Precursor lesions for sporadic pancreatic cancer: Panin, ipmn, and mcn. *BioMed research international*, 2014:474905, 2014.

[29] Stefano La Rosa, Fausto Sessa, and Carlo Capella. Acinar cell carcinoma of the pancreas: Overview of clinicopathologic features and insights into the molecular pathology. *Frontiers in medicine*, 2:41, 2015.

[30] Maximilian Reichert, Karin Blume, Alexander Kleger, Daniel Hartmann, and Guido von Figura. Developmental pathways direct pancreatic cancer initiation from its cellular origin. *Stem cells international*, 2016:9298535, 2016.

[31] R. H. Hruban, N. V. Adsay, J. Albores-Saavedra, C. Compton, E. S. Garrett, S. N. Goodman, S. E. Kern, D. S. Klimstra, G. Kloppel, D. S. Longnecker, J. Luttges, and G. J. Offerhaus. Pancreatic intraepithelial neoplasia: A new nomenclature and classification system for pancreatic duct lesions. *The American journal of surgical pathology*, 25(5):579–586, 2001.

[32] Ralph H. Hruban, Kyoichi Takaori, David S. Klimstra, N. Volkan Adsay, Jorge Albores-Saavedra, Andrew V. Biankin, Sandra A. Biankin, Carolyn Compton, Noriyoshi Fukushima, Toru Furukawa, Michael Goggins, Yo Kato, Gunter Kloppel, Daniel S. Longnecker, Jutta Luttges, Anirban Maitra, G. Johan A. Offerhaus, Michio Shimizu, and Suguru Yonezawa. An illustrated consensus on the classification of pancreatic intraepithelial neoplasia and intraductal papillary mucinous neoplasms. *The American journal of surgical pathology*, 28(8):977–987, 2004.

[33] Giuseppe Zamboni, Kenichi Hirabayashi, Paola Castelli, and Anne Marie Lennon. Precancerous lesions of the pancreas. *Best practice & research. Clinical gastroenterology*, 27(2):299–322, 2013.

[34] C. Almoguera, D. Shibata, K. Forrester, J. Martin, N. Arnheim, and M. Perucho. Most human carcinomas of the exocrine pancreas contain mutant c-k-ras genes. *Cell*, 53(4):549–554, 1988.

[35] R. H. Hruban, A. D. van Mansfeld, G. J. Offerhaus, D. H. van Weering, D. C. Allison, S. N. Goodman, T. W. Kensler, K. K. Bose, J. L. Cameron,

and J. L. Bos. K-ras oncogene activation in adenocarcinoma of the human pancreas. a study of 82 carcinomas using a combination of mutant-enriched polymerase chain reaction analysis and allele-specific oligonucleotide hybridization. *The American journal of pathology*, 143(2):545–554, 1993.

[36] Mitsuro Kanda, Hanno Matthaei, Jian Wu, Seung-Mo Hong, Jun Yu, Michael Borges, Ralph H. Hruban, Anirban Maitra, Kenneth Kinzler, Bert Vogelstein, and Michael Goggins. Presence of somatic mutations in most early-stage pancreatic intraepithelial neoplasia. *Gastroenterology*, 142(4):730–733.e9, 2012.

[37] M. Spaargaren, J. R. Bischoff, and F. McCormick. Signal transduction by ras-like gtpases: A potential target for anticancer drugs. *Gene expression*, 4(6):345–356, 1995.

[38] R. E. Wilentz, C. A. Iacobuzio-Donahue, P. Argani, D. M. McCarthy, J. L. Parsons, C. J. Yeo, S. E. Kern, and R. H. Hruban. Loss of expression of dpc4 in pancreatic intraepithelial neoplasia: Evidence that dpc4 inactivation occurs late in neoplastic progression. *Cancer research*, 60(7):2002–2006, 2000.

[39] Daniel Zeitouni, Yuliya Pylayeva-Gupta, Channing J. Der, and Kirsten L. Bryant. Kras mutant pancreatic cancer: No lone path to an effective treatment. *Cancers*, 8(4), 2016.

[40] Stephen Pandol, Mouad Edderkaoui, Ilya Gukovsky, Aurelia Lugea, and Anna Gukovskaya. Desmoplasia of pancreatic ductal adenocarcinoma. *Clinical gastroenterology and hepatology : the official clinical practice journal of the American Gastroenterological Association*, 7(11 Suppl):S44–7, 2009.

[41] Murray Korc. Pancreatic cancer-associated stroma production. *American journal of surgery*, 194(4 Suppl):S84–6, 2007.

[42] Stephen Pandol, Mouad Edderkaoui, Ilya Gukovsky, Aurelia Lugea, and Anna Gukovskaya. Desmoplasia of pancreatic ductal adenocarcinoma. *Clinical gastroenterology and hepatology : the official clinical practice journal of the American Gastroenterological Association*, 7(11 Suppl):S44–7, 2009.

[43] Kevin A. Meyer, Christopher K. Neeley, Nicki A. Baker, Alexandra R. Washabaugh, Carmen G. Flesher, Barbara S. Nelson, Timothy L. Frankel, Carey N. Lumeng, Costas A. Lyssiotis, Michelle L. Wynn, Andrew D. Rhim, and Robert W. O'Rourke. Adipocytes promote pancreatic cancer cell proliferation via glutamine transfer. *Biochemistry and biophysics reports*, 7:144–149, 2016.

[44] Max G. Bachem, Marion Schunemann, Marco Ramadani, Marco Siech, Hans Beger, Andreas Buck, Shaoxia Zhou, Alexandra Schmid-Kotsas, and Guido Adler. Pancreatic carcinoma cells induce fibrosis by stimulating proliferation and matrix synthesis of stellate cells. *Gastroenterology*, 128(4):907–921, 2005.

[45] Lisa Hutchinson. Pancreatic cancer: Disrupting the chemokine axis in pdac. *Nature reviews. Clinical oncology*, 13(6):330, 2016.

[46] Anthony Evans and Eithne Costello. The role of inflammatory cells in fostering pancreatic cancer cell growth and invasion. *Frontiers in physiology*, 3:270, 2012.

[47] Berna C. Ozdemir, Tsvetelina Pentcheva-Hoang, Julienne L. Carstens, Xiaofeng Zheng, Chia-Chin Wu, Tyler R. Simpson, Hanane Laklai, Hikaru Sugimoto, Christoph Kahlert, Sergey V. Novitskiy, Ana de Jesus-Acosta, Padmanee Sharma, Pedram Heidari, Umar Mahmood, Lynda Chin, Harold L. Moses, Valerie M. Weaver, Anirban Maitra, James P. Allison, Valerie S. LeBleu, and Raghu Kalluri. Depletion of carcinoma-associated fibroblasts and fibrosis induces immunosuppression and accelerates pancreas cancer with reduced survival. *Cancer cell*, 25(6):719–734, 2014.

[48] Andrew D. Rhim, Paul E. Oberstein, Dafydd H. Thomas, Emily T. Mirek, Carmine F. Palermo, Stephen A. Sastra, Erin N. Dekleva, Tyler Saunders, Claudia P. Becerra, Ian W. Tattersall, C. Benedikt Westphalen, Jan Kitajewski, Maite G. Fernandez-Barrena, Martin E. Fernandez-Zapico, Christine Iacobuzio-Donahue, Kenneth P. Olive, and Ben Z. Stanger. Stromal elements act to restrain, rather than support, pancreatic ductal adenocarcinoma. *Cancer cell*, 25(6):735–747, 2014.

[49] S. Sebens Müerköster, V. Werbing, B. Sipos, M. A. Debus, M. Witt, M. Grossmann, D. Leisner, J. Kötteritzsch, H. Kappes, G. Klöppel, P. Altevogt, U. R. Fölsch, and H. Schäfer. Drug-induced expression of the cellular adhesion molecule l1cam confers anti-apoptotic protection and chemoresistance in pancreatic ductal adenocarcinoma cells. *Oncogene*, 26(19):2759–2768, 2007.

[50] Clifford J. Whatcott, Richard G. Posner, Daniel D. von Hoff, and Haiyong Han. Desmoplasia and chemoresistance in pancreatic cancer, 2012.

[51] Pavan Tummala, Omer Junaidi, and Banke Agarwal. Imaging of pancreatic cancer: An overview. *Journal of Gastrointestinal Oncology*, 2(3):168–174, 2011.

[52] Seiko Hirono, Hiroki Yamaue, Yutaka Hoshikawa, Shinomi Ina, Masaji Tani, Manabu Kawai, Masaru Ushijima, Masaaki Matsuura, Yuriko Saiki, Akio Saiura, Junji Yamamoto, Yoshio Miki, and Tetsuo Noda. Molecular markers associated with lymph node metastasis in pancreatic ductal adenocarcinoma by genome-wide expression profiling. *Cancer science*, 101(1):259–266, 2010.

[53] Anna Melissa Schlitter and Irene Esposito. Definition of microscopic tumor clearance (r0) in pancreatic cancer resections. *Cancers*, 2(4):2001–2010, 2010.

[54] I. E. Demir, C. A. Jäger, H. Friess, and G. O. Ceyhan. The impact of resection margin status on pancreatic cancer-associated survival: A meta-analysis. *HPB*, 18:e130–e131, 2016.

[55] H. A. Burris, M. J. Moore, J. Andersen, M. R. Green, M. L. Rothenberg, M. R. Modiano, M. C. Cripps, R. K. Portenoy, A. M. Storniolo, P. Tarassoff, R. Nelson, F. A. Dorr, C. D. Stephens, and D. D. von Hoff. Improvements in survival and clinical benefit with gemcitabine as first-line therapy for patients with advanced pancreas cancer: a randomized trial. *Journal of clinical oncology : official journal of the American Society of Clinical Oncology*, 15(6):2403–2413, 1997.

[56] Daniel D. von Hoff, Ramesh K. Ramanathan, Mitesh J. Borad, Daniel A. Laheru, Lon S. Smith, Tina E. Wood, Ronald L. Korn, Neil Desai, Vuong Trieu, Jose L. Iglesias, Hui Zhang, Patrick Soon-Shiong, Tao Shi, N. V. Rajeshkumar, Anirban Maitra, and Manuel Hidalgo. Gemcitabine plus nab-paclitaxel is an active regimen in patients with advanced pancreatic cancer: a phase i/ii trial. *Journal of clinical oncology : official journal of the American Society of Clinical Oncology*, 29(34):4548–4554, 2011.

[57] Thierry Conroy, Françoise Desseigne, Marc Ychou, Olivier Bouché, Rosine Guimbaud, Yves Bécouarn, Antoine Adenis, Jean-Luc Raoul, Sophie Gourgou-Bourgade, Christelle de La Fouchardière, Jaafar Bennouna, Jean-Baptiste Bachet, Faiza Khemissa-Akouz, Denis Péré-Vergé, Catherine Delbaldo, Eric Assenat, Bruno Chauffert, Pierre Michel, Christine Montoto-Grillot, and Michel Ducreux. Folfirinox versus gemcitabine for metastatic pancreatic cancer. *The New England journal of medicine*, 364(19):1817–1825, 2011.

[58] Manuel Hidalgo and Daniel D. von Hoff. Translational therapeutic opportunities in ductal adenocarcinoma of the pancreas. *Clinical cancer research*

*: an official journal of the American Association for Cancer Research*, 18(16):4249–4256, 2012.

[59] Ryan M. Carr and Martin E. Fernandez-Zapico. Pancreatic cancer microenvironment, to target or not to target? *EMBO molecular medicine*, 8(2):80–82, 2016.

[60] David A. Tuveson and John P. Neoptolemos. Understanding metastasis in pancreatic cancer: a call for new clinical approaches. *Cell*, 148(1-2):21–23, 2012.

[61] Scott Valastyan and Robert A. Weinberg. Tumor metastasis: molecular insights and evolving paradigms. *Cell*, 147(2):275–292, 2011.

[62] Valerie S. LeBleu, Brian Macdonald, and Raghu Kalluri. Structure and function of basement membranes. *Experimental biology and medicine (Maywood, N.J.)*, 232(9):1121–1129, 2007.

[63] Gaorav P. Gupta and Joan Massagué. Cancer metastasis: building a framework. *Cell*, 127(4):679–695, 2006.

[64] Chrisostomi Gialeli, Achilleas D. Theocharis, and Nikos K. Karamanos. Roles of matrix metalloproteinases in cancer progression and their pharmacological targeting. *The FEBS journal*, 278(1):16–27, 2011.

[65] Evette S. Radisky and Derek C. Radisky. Matrix metalloproteinase-induced epithelial-mesenchymal transition in breast cancer. *Journal of mammary gland biology and neoplasia*, 15(2):201–212, 2010.

[66] Robert A. Weinberg. Mechanisms of malignant progression. *Carcinogenesis*, 29(6):1092–1095, 2008.

[67] Richard C. Bates and Arthur M. Mercurio. Tumor necrosis factor-alpha stimulates the epithelial-to-mesenchymal transition of human colonic organoids. *Molecular biology of the cell*, 14(5):1790–1800, 2003.

[68] Tal Leibovich-Rivkin, Yulia Liubomirski, Biana Bernstein, Tsipi Meshel, and Adit Ben-Baruch. Inflammatory factors of the tumor microenvironment induce plasticity in nontransformed breast epithelial cells: Emt, invasion, and collapse of normally organized breast textures. *Neoplasia (New York, N.Y.)*, 15(12):1330–1346, 2013.

[69] Jian Xu, Samy Lamouille, and Rik Derynck. Tgf-beta-induced epithelial to mesenchymal transition. *Cell research*, 19(2):156–172, 2009.

[70] Isabel Fabregat, Andrea Malfettone, and Jitka Soukupova. New insights into the crossroads between emt and stemness in the context of cancer. *Journal of clinical medicine*, 5(3), 2016.

[71] Johanna A. Joyce and Jeffrey W. Pollard. Microenvironmental regulation of metastasis. *Nature reviews. Cancer*, 9(4):239–252, 2009.

[72] J. A. Nagy, S-H Chang, A. M. Dvorak, and H. F. Dvorak. Why are tumour blood vessels abnormal and why is it important to know? *British journal of cancer*, 100(6):865–869, 2009.

[73] B. Nieswandt, M. Hafner, B. Echtenacher, and D. N. Männel. Lysis of tumor cells by natural killer cells in mice is impeded by platelets. *Cancer research*, 59(6):1295–1300, 1999.

[74] Jae Hong Im, Weili Fu, Hui Wang, Sujata K. Bhatia, Daniel A. Hammer, M. Anna Kowalska, and Ruth J. Muschel. Coagulation facilitates tumor cell spreading in the pulmonary vasculature during early metastatic colony formation. *Cancer research*, 64(23):8613–8619, 2004.

[75] Xiao-Liang Lou, Jian Sun, Shu-Qi Gong, Xue-Feng Yu, Rui Gong, and Huan Deng. Interaction between circulating cancer cells and platelets: clinical implication. *Chinese journal of cancer research = Chung-kuo yen cheng yen chiu*, 27(5):450–460, 2015.

[76] Monika Julia Wolf, Alexandra Hoos, Judith Bauer, Steffen Boettcher, Markus Knust, Achim Weber, Nicole Simonavicius, Christoph Schneider, Matthias Lang, Michael Stürzl, Roland S. Croner, Andreas Konrad, Markus G. Manz, Holger Moch, Adriano Aguzzi, Geert van Loo, Manolis Pasparakis, Marco Prinz, Lubor Borsig, and Mathias Heikenwalder. Endothelial ccr2 signaling induced by colon carcinoma cells enables extravasation via the jak2-stat5 and p38mapk pathway. *Cancer cell*, 22(1):91–105, 2012.

[77] Dianbo Yao, Chaoliu Dai, and Songlin Peng. Mechanism of the mesenchymal-epithelial transition and its relationship with metastatic tumor formation. *Molecular cancer research : MCR*, 9(12):1608–1620, 2011.

[78] Sakari Vanharanta and Joan Massagué. Origins of metastatic traits. *Cancer cell*, 24(4):410–421, 2013.

[79] Mina J. Bissell. The central role of basement membrane in functional differentiation, apoptosis, and cancer. In Jonathan L. Tilly, Jerome F.

Strauss, and Martin Tenniswood, editors, *Cell death in reproductive physiology*, pages 125–140. Springer-Verlag New York, [Place of publication not identified], 2013.

[80] Vicki Plaks, Charlotte D. Koopman, and Zena Werb. Cancer. circulating tumor cells. *Science (New York, N.Y.)*, 341(6151):1186–1188, 2013.

[81] Julio A. Aguirre-Ghiso, Paloma Bragado, and Maria Soledad Sosa. Metastasis awakening: targeting dormant cancer. *Nature medicine*, 19(3):276–277, 2013.

[82] K. J. Luzzi, I. C. MacDonald, E. E. Schmidt, N. Kerkvliet, V. L. Morris, A. F. Chambers, and A. C. Groom. Multistep nature of metastatic inefficiency: dormancy of solitary cells after successful extravasation and limited survival of early micrometastases. *The American journal of pathology*, 153(3):865–873, 1998.

[83] Shapour Omidvari, Seyed Hasan Hamedi, Mohammad Mohammadianpanah, Hamid Nasrolahi, Ahmad Mosalaei, Abdolrasoul Talei, Niloofar Ahmadloo, and Mansour Ansari. Very late relapse in breast cancer survivors: a report of 6 cases. *Iranian journal of cancer prevention*, 6(2):113–117, 2013.

[84] Ann F. Chambers, Alan C. Groom, and Ian C. MacDonald. Dissemination and growth of cancer cells in metastatic sites. *Nature reviews. Cancer*, 2(8):563–572, 2002.

[85] Klaus Pantel and Catherine Alix-Panabières. Real-time liquid biopsy in cancer patients: fact or fiction? *Cancer research*, 73(21):6384–6388, 2013.

[86] Don X. Nguyen, Paula D. Bos, and Joan Massagué. Metastasis: from dissemination to organ-specific colonization. *Nature reviews. Cancer*, 9(4):274–284, 2009.

[87] Shinichi Yachida, Sian Jones, Ivana Bozic, Tibor Antal, Rebecca Leary, Baojin Fu, Mihoko Kamiyama, Ralph H. Hruban, James R. Eshleman, Martin A. Nowak, Victor E. Velculescu, Kenneth W. Kinzler, Bert Vogelstein, and Christine A. Iacobuzio-Donahue. Distant metastasis occurs late during the genetic evolution of pancreatic cancer. *Nature*, 467(7319):1114–1117, 2010.

[88] Hiroshi Haeno, Mithat Gonen, Meghan B. Davis, Joseph M. Herman, Christine A. Iacobuzio-Donahue, and Franziska Michor. Computational model-

ing of pancreatic cancer reveals kinetics of metastasis suggesting optimum treatment strategies. *Cell*, 148(1-2):362–375, 2012.

[89] Andrew D. Rhim, Emily T. Mirek, Nicole M. Aiello, Anirban Maitra, Jennifer M. Bailey, Florencia McAllister, Maximilian Reichert, Gregory L. Beatty, Anil K. Rustgi, Robert H. Vonderheide, Steven D. Leach, and Ben Z. Stanger. Emt and dissemination precede pancreatic tumor formation. *Cell*, 148(1-2):349–361, 2012.

[90] Andrew D. Rhim, Fredrik I. Thege, Steven M. Santana, Timothy B. Lannin, Trisha N. Saha, Shannon Tsai, Lara R. Maggs, Michael L. Kochman, Gregory G. Ginsberg, John G. Lieb, Vinay Chandrasekhara, Jeffrey A. Drebin, Nuzhat Ahmad, Yu-Xiao Yang, Brian J. Kirby, and Ben Z. Stanger. Detection of circulating pancreas epithelial cells in patients with pancreatic cystic lesions. *Gastroenterology*, 146(3):647–651, 2014.

[91] Renata D'Alpino Peixoto, Caroline Speers, Colleen E. McGahan, Daniel J. Renouf, David F. Schaeffer, and Hagen F. Kennecke. Prognostic factors and sites of metastasis in unresectable locally advanced pancreatic cancer. *Cancer medicine*, 4(8):1171–1177, 2015.

[92] Christine A. Iacobuzio-Donahue, Baojin Fu, Shinichi Yachida, Mingde Luo, Hisashi Abe, Clark M. Henderson, Felip Vilardell, Zheng Wang, Jesse W. Keller, Priya Banerjee, Joseph M. Herman, John L. Cameron, Charles J. Yeo, Marc K. Halushka, James R. Eshleman, Marian Raben, Alison P. Klein, Ralph H. Hruban, Manuel Hidalgo, and Daniel Laheru. Dpc4 gene status of the primary carcinoma correlates with patterns of failure in patients with pancreatic cancer. *Journal of clinical oncology : official journal of the American Society of Clinical Oncology*, 27(11):1806–1813, 2009.

[93] Fernando Vidal-Vanaclocha. The prometastatic microenvironment of the liver. *Cancer microenvironment : official journal of the International Cancer Microenvironment Society*, 1(1):113–129, 2008.

[94] Keith L. Moore, Arthur F. Dalley, and A. M. R. Agur. *Clinically oriented anatomy*. Wolters Kluwer/Lippincott Williams & Wilkins Health, Philadelphia, 7th ed. edition, 2014.

[95] J. K. Corless and H. M. Middleton. Normal liver function. a basis for understanding hepatic disease. *Archives of internal medicine*, 143(12):2291–2294, 1983.

[96] Pnina Brodt, editor. *Liver metastasis: Biology and clinical management*, volume v. 16 of *Cancer Metastasis - Biology and Treatment*. Springer, Dordrecht and New York, 2011.

[97] Robert R. Langley and Isaiah J. Fidler. The seed and soil hypothesis revisited–the role of tumor-stroma interactions in metastasis to different organs. *International journal of cancer*, 128(11):2527–2535, 2011.

[98] I. Fidler and M. Kripke. Metastasis results from preexisting variant cells within a malignant tumor. *Science*, 197(4306):893–895, 1977.

[99] Murli Krishna. Microscopic anatomy of the liver. *Clinical Liver Disease*, 2(S1):S4–S7, 2013.

[100] Makoto Naito, Go Hasegawa, and Kiyoshi Takahashi. Development, differentiation, and maturation of kupffer cells. *Microscopy Research and Technique*, 39(4):350–364, 1997.

[101] R. S. McCuskey and P. A. McCuskey. Fine structure and function of kupffer cells. *Journal of electron microscopy technique*, 14(3):237–246, 1990.

[102] A. Geerts. History, heterogeneity, developmental biology, and functions of quiescent hepatic stellate cells. *Seminars in liver disease*, 21(3):311–335, 2001.

[103] Scott L. Friedman. Hepatic stellate cells: protean, multifunctional, and enigmatic cells of the liver. *Physiological reviews*, 88(1):125–172, 2008.

[104] Florian Winau, Guido Hegasy, Ralf Weiskirchen, Stephan Weber, Cecile Cassan, Peter A. Sieling, Robert L. Modlin, Roland S. Liblau, Axel M. Gressner, and Stefan H. E. Kaufmann. Ito cells are liver-resident antigen-presenting cells for activating t cell responses. *Immunity*, 26(1):117–129, 2007.

[105] Ralf Weiskirchen and Frank Tacke. Cellular and molecular functions of hepatic stellate cells in inflammatory responses and liver immunology. *Hepatobiliary surgery and nutrition*, 3(6):344–363, 2014.

[106] Yi Zhao, Yanqing Wang, Qiang Wang, Zhengrong Liu, Qingfeng Liu, and Xin Deng. Hepatic stellate cells produce vascular endothelial growth factor via phospho-p44/42 mitogen-activated protein kinase/cyclooxygenase-2 pathway. *Molecular and cellular biochemistry*, 359(1-2):217–223, 2012.

[107] Chunyue Yin, Kimberley J. Evason, Kinji Asahina, and Didier Y. R. Stainier. Hepatic stellate cells in liver development, regeneration, and cancer. *The Journal of clinical investigation*, 123(5):1902–1910, 2013.

[108] Vinicio Carloni, Tu Vinh Luong, and Krista Rombouts. Hepatic stellate cells and extracellular matrix in hepatocellular carcinoma: more complicated than ever. *Liver international : official journal of the International Association for the Study of the Liver*, 34(6):834–843, 2014.

[109] Ramón Bataller and David A. Brenner. Liver fibrosis. *The Journal of clinical investigation*, 115(2):209–218, 2005.

[110] Bruno Costa-Silva, Nicole M. Aiello, Allyson J. Ocean, Swarnima Singh, Haiying Zhang, Basant Kumar Thakur, Annette Becker, Ayuko Hoshino, Milica Tesic Mark, Henrik Molina, Jenny Xiang, Tuo Zhang, Till-Martin Theilen, Guillermo Garcia-Santos, Caitlin Williams, Yonathan Ararso, Yujie Huang, Goncalo Rodrigues, Tang-Long Shen, Knut Jorgen Labori, Inger Marie Bowitz Lothe, Elin H. Kure, Jonathan Hernandez, Alexandre Doussot, Saya H. Ebbesen, Paul M. Grandgenett, Michael A. Hollingsworth, Maneesh Jain, Kavita Mallya, Surinder K. Batra, William R. Jarnagin, Robert E. Schwartz, Irina Matei, Hector Peinado, Ben Z. Stanger, Jacqueline Bromberg, and David Lyden. Pancreatic cancer exosomes initiate premetastatic niche formation in the liver. *Nature cell biology*, 17(6):816–826, 2015.

[111] Barbara Grunwald, Veronika Harant, Susanne Schaten, Monika Fruhschutz, Ria Spallek, Bastian Hochst, Katharina Stutzer, Sonja Berchtold, Mert Erkan, Olga Prokopchuk, Marc Martignoni, Irene Esposito, Mathias Heikenwalder, Aayush Gupta, Jens Siveke, Paul Saftig, Percy Knolle, Dirk Wohlleber, and Achim Kruger. Pancreatic premalignant lesions secrete tissue inhibitor of metalloproteinases-1, which activates hepatic stellate cells via cd63 signaling to create a premetastatic niche in the liver. *Gastroenterology*, 151(5):1011–1024.e7, 2016.

[112] Douglas Hanahan and Robert A. Weinberg. The hallmarks of cancer. *Cell*, 100(1):57–70, 2000.

[113] D. Amadori, A. Volpi, R. Maltoni, O. Nanni, L. Amaducci, A. Amadori, D. C. Giunchi, A. Vio, A. Saragoni, and R. Silvestrini. Cell proliferation as a predictor of response to chemotherapy in metastatic breast cancer: a prospective study. *Breast cancer research and treatment*, 43(1):7–14, 1997.

[114] A. A. Ross. Minimal residual disease in solid tumor malignancies: a review. *Journal of hematotherapy*, 7(1):9–18, 1998.

[115] David Liu, Julio Aguirre Ghiso, Yeriel Estrada, and Liliana Ossowski. Egfr is a transducer of the urokinase receptor initiated signal that is required for in vivo growth of a human carcinoma. *Cancer cell*, 1(5):445–457, 2002.

[116] Tsukasa Shibue and Robert A. Weinberg. Integrin beta1-focal adhesion kinase signaling directs the proliferation of metastatic cancer cells disseminated in the lungs. *Proceedings of the National Academy of Sciences of the United States of America*, 106(25):10290–10295, 2009.

[117] Filippo G. Giancotti. Mechanisms governing metastatic dormancy and reactivation. *Cell*, 155(4):750–764, 2013.

[118] Julio A. Aguirre-Ghiso. Models, mechanisms and clinical evidence for cancer dormancy. *Nature reviews. Cancer*, 7(11):834–846, 2007.

[119] Maria Soledad Sosa, Paloma Bragado, and Julio A. Aguirre-Ghiso. Mechanisms of disseminated cancer cell dormancy: an awakening field. *Nature reviews. Cancer*, 14(9):611–622, 2014.

[120] Hilary A. Coller, Liyun Sang, and James M. Roberts. A new description of cellular quiescence. *PLoS biology*, 4(3):e83, 2006.

[121] Rosana Pelayo, Kozo Miyazaki, Jiaxue Huang, Karla P. Garrett, Dennis G. Osmond, and Paul W. Kincade. Cell cycle quiescence of early lymphoid progenitors in adult bone marrow. *STEM CELLS*, 24(12):2703–2713, 2006.

[122] Guang Yao. Modelling mammalian cellular quiescence. *Interface focus*, 4(3):20130074, 2014.

[123] Erika L. Pearce and Edward J. Pearce. Metabolic pathways in immune cell activation and quiescence. *Immunity*, 38(4):633–643, 2013.

[124] Tom H. Cheung and Thomas A. Rando. Molecular regulation of stem cell quiescence. *Nature reviews. Molecular cell biology*, 14(6):329–340, 2013.

[125] Mikhail V. Blagosklonny. Cell cycle arrest is not senescence. *Aging*, 3(2):94–101, 2011.

[126] Claire Attwooll, Eros Lazzerini Denchi, and Kristian Helin. The e2f family: specific functions and overlapping interests. *The EMBO journal*, 23(24):4709–4716, 2004.

[127] David Cobrinik. Pocket proteins and cell cycle control. *Oncogene*, 24(17):2796–2809, 2005.

[128] J. R. Nevins. The rb/e2f pathway and cancer. *Human Molecular Genetics*, 10(7):699–703, 2001.

[129] Guang Yao, Tae Jun Lee, Seiichi Mori, Joseph R. Nevins, and Lingchong You. A bistable rb-e2f switch underlies the restriction point. *Nature cell biology*, 10(4):476–482, 2008.

[130] Koji Itahana, Goberdhan P. Dimri, Eiji Hara, Yoko Itahana, Ying Zou, Pierre-Yves Desprez, and Judith Campisi. A role for p53 in maintaining and establishing the quiescence growth arrest in human cells. *The Journal of biological chemistry*, 277(20):18206–18214, 2002.

[131] Yan Liu, Shannon E. Elf, Yasuhiko Miyata, Goro Sashida, Yuhui Liu, Gang Huang, Silvana Di Giandomenico, Jennifer M. Lee, Anthony Deblasio, Silvia Menendez, Jack Antipin, Boris Reva, Andrew Koff, and Stephen D. Nimer. p53 regulates hematopoietic stem cell quiescence. *Cell stem cell*, 4(1):37–48, 2009.

[132] G. H. Stein, L. F. Drullinger, A. Soulard, and V. Dulic. Differential roles for cyclin-dependent kinase inhibitors p21 and p16 in the mechanisms of senescence and differentiation in human fibroblasts. *Molecular and cellular biology*, 19(3):2109–2117, 1999.

[133] Paola Perucca, Ornella Cazzalini, Mark Madine, Monica Savio, Ronal Alfred Laskey, Vanio Vannini, Ennio Prosperi, and Lucia Anna Stivala. Loss of p21 cdkn1a impairs entry to quiescence and activates a dna damage response in normal fibroblasts induced to quiescence. *Cell cycle (Georgetown, Tex.)*, 8(1):105–114, 2009.

[134] Ingmar Glauche, Kateri Moore, Lars Thielecke, Katrin Horn, Markus Loeffler, and Ingo Roeder. Stem cell proliferation and quiescence–two sides of the same coin. *PLoS computational biology*, 5(7):e1000447, 2009.

[135] Robert H. te Poele, Andrei L. Okorokov, Lesley Jardine, Jeffrey Cummings, and Simon P. Joel. Dna damage is able to induce senescence in tumor cells in vitro and in vivo. *Cancer research*, 62(6):1876–1883, 2002.

[136] Thomas Kuilman, Chrysiis Michaloglou, Liesbeth C. W. Vredeveld, Sirith Douma, Remco van Doorn, Christophe J. Desmet, Lucien A. Aarden, Wolter J. Mooi, and Daniel S. Peeper. Oncogene-induced senescence relayed

by an interleukin-dependent inflammatory network. *Cell*, 133(6):1019–1031, 2008.

[137] Jonathan A. Ewald, Joshua A. Desotelle, George Wilding, and David F. Jarrard. Therapy-induced senescence in cancer. *Journal of the National Cancer Institute*, 102(20):1536–1546, 2010.

[138] J. W. Shay and W. E. Wright. Hayflick, his limit, and cellular ageing. *Nature reviews. Molecular cell biology*, 1(1):72–76, 2000.

[139] C. B. Harley, A. B. Futcher, and C. W. Greider. Telomeres shorten during ageing of human fibroblasts. *Nature*, 345(6274):458–460, 1990.

[140] Maria Pia Longhese. Dna damage response at functional and dysfunctional telomeres. *Genes & development*, 22(2):125–140, 2008.

[141] Chanhee Kang, Qikai Xu, Timothy D. Martin, Mamie Z. Li, Marco Demaria, Liviu Aron, Tao Lu, Bruce A. Yankner, Judith Campisi, and Stephen J. Elledge. The dna damage response induces inflammation and senescence by inhibiting autophagy of gata4. *Science (New York, N.Y.)*, 349(6255):aaa5612, 2015.

[142] Luis I. Toledo, Matilde Murga, Paula Gutierrez-Martinez, Rebeca Soria, and Oscar Fernandez-Capetillo. Atr signaling can drive cells into senescence in the absence of dna breaks. *Genes & development*, 22(3):297–302, 2008.

[143] Arishya Sharma, Kamini Singh, and Alexandru Almasan. Histone h2ax phosphorylation: a marker for dna damage. *Methods in molecular biology (Clifton, N.J.)*, 920:613–626, 2012.

[144] Jan M. van Deursen. The role of senescent cells in ageing. *Nature*, 509(7501):439–446, 2014.

[145] Fabrizio Di d'Adda Fagagna, Philip M. Reaper, Lorena Clay-Farrace, Heike Fiegler, Philippa Carr, Thomas von Zglinicki, Gabriele Saretzki, Nigel P. Carter, and Stephen P. Jackson. A dna damage checkpoint response in telomere-initiated senescence. *Nature*, 426(6963):194–198, 2003.

[146] Pierpaola Davalli, Tijana Mitic, Andrea Caporali, Angela Lauriola, and Domenico D'Arca. Ros, cell senescence, and novel molecular mechanisms in aging and age-related diseases. *Oxidative medicine and cellular longevity*, 2016:3565127, 2016.

[147] R. Wadhwa, T. Sugihara, K. Taira, and S. C. Kaul. The arf-p53 senescence pathway in mouse and human cells. *Histology and histopathology*, 19(1):311–316, 2004.

[148] Hani Rayess, Marilene B. Wang, and Eri S. Srivatsan. Cellular senescence and tumor suppressor gene p16. *International journal of cancer*, 130(8):1715–1725, 2012.

[149] J. Cisowski, V. I. Sayin, M. Liu, C. Karlsson, and M. O. Bergo. Oncogene-induced senescence underlies the mutual exclusive nature of oncogenic kras and braf. *Oncogene*, 35(10):1328–1333, 2016.

[150] Jennifer P. Morton, Paul Timpson, Saadia A. Karim, Rachel A. Ridgway, Dimitris Athineos, Brendan Doyle, Nigel B. Jamieson, Karin A. Oien, Andrew M. Lowy, Valerie G. Brunton, Margaret C. Frame, T. R. Jeffry Evans, and Owen J. Sansom. Mutant p53 drives metastasis and overcomes growth arrest/senescence in pancreatic cancer. *Proceedings of the National Academy of Sciences of the United States of America*, 107(1):246–251, 2010.

[151] Ewa Sikora, Grazyna Mosieniak, and Malgorzata Alicja Sliwinska. Morphological and functional characteristic of senescent cancer cells. *Current drug targets*, 17(4):377–387, 2016.

[152] Jean-Philippe Coppe, Pierre-Yves Desprez, Ana Krtolica, and Judith Campisi. The senescence-associated secretory phenotype: the dark side of tumor suppression. *Annual review of pathology*, 5:99–118, 2010.

[153] Florence Debacq-Chainiaux, Jorge D. Erusalimsky, Judith Campisi, and Olivier Toussaint. Protocols to detect senescence-associated beta-galactosidase (sa-betagal) activity, a biomarker of senescent cells in culture and in vivo. *Nature protocols*, 4(12):1798–1806, 2009.

[154] Christian M. Beausejour, Ana Krtolica, Francesco Galimi, Masashi Narita, Scott W. Lowe, Paul Yaswen, and Judith Campisi. Reversal of human cellular senescence: roles of the p53 and p16 pathways. *The EMBO journal*, 22(16):4212–4222, 2003.

[155] Hannah E. Walters, Sylwia Deneka-Hannemann, and Lynne S. Cox. Reversal of phenotypes of cellular senescence by pan-mtor inhibition. *Aging*, 8(2):231–244, 2016.

[156] J. Wang. Global analysis of dauer gene expression in caenorhabditis elegans. *Development*, 130(8):1621–1634, 2003.

[157] Leónie Bentsink and Maarten Koornneef. Seed dormancy and germination. *The Arabidopsis book*, 6:e0119, 2008.

[158] E. Yefenof, L. J. Picker, R. H. Scheuermann, T. F. Tucker, E. S. Vitetta, and J. W. Uhr. Cancer dormancy: isolation and characterization of dormant lymphoma cells. *Proceedings of the National Academy of Sciences of the United States of America*, 90(5):1829–1833, 1993.

[159] Yuval Shaked, Sandra McAllister, Ofer Fainaru, and Nava Almog. Tumor dormancy and the angiogenic switch: possible implications of bone marrow-derived cells. *Current pharmaceutical design*, 20(30):4920–4933, 2014.

[160] J. A. Aguirre-Ghiso, D. Liu, A. Mignatti, K. Kovalski, and L. Ossowski. Urokinase receptor and fibronectin regulate the erk(mapk) to p38(mapk) activity ratios that determine carcinoma cell proliferation or dormancy in vivo. *Molecular biology of the cell*, 12(4):863–879, 2001.

[161] Xin Lu, Euphemia Mu, Yong Wei, Sabine Riethdorf, Qifeng Yang, Min Yuan, Jun Yan, Yuling Hua, Benjamin J. Tiede, Xuemin Lu, Bruce G. Haffty, Klaus Pantel, Joan Massagué, and Yibin Kang. Vcam-1 promotes osteolytic expansion of indolent bone micrometastasis of breast cancer by engaging $\upalpha4\upbeta$1-positive osteoclast progenitors. *Cancer cell*, 20(6):701–714, 2011.

[162] Aguirre-ghiso.2003 - erkmapk activity as a determinant of tumor growth and dormancy; regulation by p38sapk.

[163] Thea D. Tlsty and Lisa M. Coussens. Tumor stroma and regulation of cancer development. *Annual review of pathology*, 1:119–150, 2006.

[164] Hua Gao, Goutam Chakraborty, Ai Ping Lee-Lim, Qianxing Mo, Markus Decker, Alin Vonica, Ronglai Shen, Edi Brogi, Ali H. Brivanlou, and Filippo G. Giancotti. The bmp inhibitor coco reactivates breast cancer cells at lung metastatic sites. *Cell*, 150(4):764–779, 2012.

[165] P. Kienle and M. Koch. Minimal residual disease in gastrointestinal cancer. *Seminars in surgical oncology*, 20(4):282–293, 2001.

[166] Wan-Chi Lin, Nirakar Rajbhandari, Chengbao Liu, Kazuhito Sakamoto, Qian Zhang, Aleata A. Triplett, Surinder K. Batra, Rene Opavsky, Dean W. Felsher, Dominick J. DiMaio, Michael A. Hollingsworth, John P. Morris, 4th., Matthias Hebrok, Agnieszka K. Witkiewicz, Jonathan R. Brody, Hallgeir Rui, and Kay-Uwe Wagner. Dormant cancer cells contribute to resid-

ual disease in a model of reversible pancreatic cancer. *Cancer research*, 73(6):1821–1830, 2013.

[167] Sten Friberg and Andreas Nystrom. Cancer metastases: Early dissemination and late recurrences. *Cancer growth and metastasis*, 8:43–49, 2015.

[168] J. A. Aguirre Ghiso, K. Kovalski, and L. Ossowski. Tumor dormancy induced by downregulation of urokinase receptor in human carcinoma involves integrin and mapk signaling. *The Journal of cell biology*, 147(1):89–104, 1999.

[169] Aya Kobayashi, Hiroshi Okuda, Fei Xing, Puspa R. Pandey, Misako Watabe, Shigeru Hirota, Sudha K. Pai, Wen Liu, Koji Fukuda, Christopher Chambers, Andrew Wilber, and Kounosuke Watabe. Bone morphogenetic protein 7 in dormancy and metastasis of prostate cancer stem-like cells in bone. *The Journal of experimental medicine*, 208(13):2641–2655, 2011.

[170] Yusuke Shiozawa, Elisabeth A. Pedersen, Aaron M. Havens, Younghun Jung, Anjali Mishra, Jeena Joseph, Jin Koo Kim, Lalit R. Patel, Chi Ying, Anne M. Ziegler, Michael J. Pienta, Junhui Song, Jingcheng Wang, Robert D. Loberg, Paul H. Krebsbach, Kenneth J. Pienta, and Russell S. Taichman. Human prostate cancer metastases target the hematopoietic stem cell niche to establish footholds in mouse bone marrow. *The Journal of clinical investigation*, 121(4):1298–1312, 2011.

[171] Paloma Bragado, Yeriel Estrada, Falguni Parikh, Sarah Krause, Carla Capobianco, Hernan G. Farina, Denis M. Schewe, and Julio A. Aguirre-Ghiso. Tgf-beta2 dictates disseminated tumour cell fate in target organs through tgf-beta-riii and p38alpha/beta signalling. *Nature cell biology*, 15(11):1351–1361, 2013.

[172] Younghun Jung, Ann M. Decker, Jingcheng Wang, Eunsohl Lee, Lulia A. Kana, Kenji Yumoto, Frank C. Cackowski, James Rhee, Peter Carmeliet, Laura Buttitta, Todd M. Morgan, and Russell S. Taichman. Endogenous gas6 and mer receptor signaling regulate prostate cancer stem cells in bone marrow. *Oncotarget*, 7(18):25698–25711, 2016.

[173] Dalit Barkan, Lara H. El Touny, Aleksandra M. Michalowski, Jane Ann Smith, Isabel Chu, Anne Sally Davis, Joshua D. Webster, Shelley Hoover, R. Mark Simpson, Jack Gauldie, and Jeffrey E. Green. Metastatic growth from dormant cells induced by a col-i-enriched fibrotic environment. *Cancer research*, 70(14):5706–5716, 2010.

[174] Dalit Barkan, Jeffrey E. Green, and Ann F. Chambers. Extracellular matrix: a gatekeeper in the transition from dormancy to metastatic growth. *European journal of cancer (Oxford, England : 1990)*, 46(7):1181–1188, 2010.

[175] Colin William Steele, Nina Angharad Kaur Gill, Nigel Balfour Jamieson, and Christopher Ross Carter. Targeting inflammation in pancreatic cancer: Clinical translation. *World journal of gastrointestinal oncology*, 8(4):380–388, 2016.

[176] Sunil R. Hingorani, Lifu Wang, Asha S. Multani, Chelsea Combs, Therese B. Deramaudt, Ralph H. Hruban, Anil K. Rustgi, Sandy Chang, and David A. Tuveson. Trp53r172h and krasg12d cooperate to promote chromosomal instability and widely metastatic pancreatic ductal adenocarcinoma in mice. *Cancer cell*, 7(5):469–483, 2005.

[177] Carlos Lopez-Otin, Maria A. Blasco, Linda Partridge, Manuel Serrano, and Guido Kroemer. The hallmarks of aging. *Cell*, 153(6):1194–1217, 2013.

[178] Evelin Grage-Griebenow, Elfi Jerg, Artur Gorys, Daniel Wicklein, Daniela Wesch, Sandra Freitag-Wolf, Lisa Goebel, Ilka Vogel, Thomas Becker, Michael Ebsen, Christoph Röcken, Peter Altevogt, Udo Schumacher, Heiner Schäfer, and Susanne Sebens. L1cam promotes enrichment of immunosuppressive t cells in human pancreatic cancer correlating with malignant progression. *Molecular oncology*, 8(5):982–997, 2014.

[179] Ole Helm, Janka Held-Feindt, Evelin Grage-Griebenow, Norbert Reiling, Hendrik Ungefroren, Ilka Vogel, Uwe Kruger, Thomas Becker, Michael Ebsen, Christoph Rocken, Dieter Kabelitz, Heiner Schafer, and Susanne Sebens. Tumor-associated macrophages exhibit pro- and anti-inflammatory properties by which they impact on pancreatic tumorigenesis. *International journal of cancer*, 135(4):843–861, 2014.

[180] Lennart Lenk. Einfluss hepatischer sternzellen und myofibroblasten auf den phänotyp und das verhalten von pankreasadenokarzinomzellen: Master's thesis. 2013.

[181] Maren Pein. Impact of hepatic stromal cells on the phenotype and behavior of pancreatic ductal epithelial cells in dependence on the k-ras g12v oncogene: Master's thesis. 2014.

[182] Verena Proell, Mario Mikula, Eva Fuchs, and Wolfgang Mikulits. The plasticity of p19 arf null hepatic stellate cells and the dynamics of activation. *Biochimica et biophysica acta*, 1744(1):76–87, 2005.

[183] Jiaying Qian, Jiangong Niu, Ming Li, Paul J. Chiao, and Ming-Sound Tsao. In vitro modeling of human pancreatic duct epithelial cell transformation defines gene expression changes induced by k-ras oncogenic activation in pancreatic carcinogenesis. *Cancer research*, 65(12):5045–5053, 2005.

[184] Johannes von Burstin, Stefan Eser, Mariel C. Paul, Barbara Seidler, Martina Brandl, Marlena Messer, Alexander von Werder, Annegret Schmidt, Jorg Mages, Philipp Pagel, Angelika Schnieke, Roland M. Schmid, Gunter Schneider, and Dieter Saur. E-cadherin regulates metastasis of pancreatic cancer in vivo and is suppressed by a snail/hdac1/hdac2 repressor complex. *Gastroenterology*, 137(1):361–71, 371.e1–5, 2009.

[185] Michael Lieber, Joann Mazzetta, Walter Nelson-Rees, Michael Kaplan, and George Todaro. Establishment of a continuous tumor-cell line (panc-1) from a human carcinoma of the exocrine pancreas. *International Journal of Cancer*, 15(5):741–747, 1975.

[186] Ole Helm, Ruben Mennrich, Domantas Petrick, Lisa Goebel, Sandra Freitag-Wolf, Christian Roder, Holger Kalthoff, Christoph Rocken, Bence Sipos, Dieter Kabelitz, Heiner Schafer, Hans-Heinrich Oberg, Daniela Wesch, and Susanne Sebens. Comparative characterization of stroma cells and ductal epithelium in chronic pancreatitis and pancreatic ductal adenocarcinoma. *PloS one*, 9(5):e94357, 2014.

[187] Jurgen Tepel, Marie-Luise Kruse, Christina March, Alexander Fiedler, Matthias Kapischke, Thomas Ketterer, Bence Sipos, Bernd Kremer, and Holger Kalthoff. Terminally modified oligodeoxynucleotides directed against p53 in an orthotopic xenograft model: a novel adjuvant treatment strategy for pancreatic ductal carcinoma. *Pancreas*, 28(1):1–12, 2004.

[188] Mario Mikula, Eva Fuchs, Heidemarie Huber, Hartmut Beug, Rolf Schulte-Hermann, and Wolfgang Mikulits. Immortalized p19arf null hepatocytes restore liver injury and generate hepatic progenitors after transplantation. *Hepatology (Baltimore, Md.)*, 39(3):628–634, 2004.

[189] Antonios Chronopoulos, Benjamin Robinson, Muge Sarper, Ernesto Cortes, Vera Auernheimer, Dariusz Lachowski, Simon Attwood, Rebeca García, Saba Ghassemi, Ben Fabry, and Armando Del Río Hernández. Atra mechanically reprograms pancreatic stellate cells to suppress matrix remodelling and inhibit cancer cell invasion. *Nature communications*, 7:12630, 2016.

[190] Bui Thanh Tung, Elisabeth Rodriguez-Bies, Elena Talero, Enrique Gamero-Estevez, Virginia Motilva, Placido Navas, and Guillermo Lopez-Lluch. Anti-inflammatory effect of resveratrol in old mice liver. *Experimental gerontology*, 64:1–7, 2015.

[191] Pallavi Singh, Zeynep Z. Coskun, Catriona Goode, Adam Dean, LuAnn Thompson-Snipes, and Gretchen Darlington. Lymphoid neogenesis and immune infiltration in aged liver. *Hepatology (Baltimore, Md.)*, 47(5):1680–1690, 2008.

[192] Roben G. Gieling, Karen Wallace, and Yuan-Ping Han. Interleukin-1 participates in the progression from liver injury to fibrosis. *American journal of physiology. Gastrointestinal and liver physiology*, 296(6):G1324–31, 2009.

[193] Yuan-Ping Han, Ling Zhou, Jiaohong Wang, Shigang Xiong, Warren L. Garner, Samuel W. French, and Hidekazu Tsukamoto. Essential role of matrix metalloproteinases in interleukin-1-induced myofibroblastic activation of hepatic stellate cell in collagen. *The Journal of biological chemistry*, 279(6):4820–4828, 2004.

[194] Justin D. Schumacher and Grace L. Guo. Regulation of hepatic stellate cells and fibrogenesis by fibroblast growth factors. *BioMed research international*, 2016:8323747, 2016.

[195] Claus Hellerbrand, Branko Stefanovic, Frank Giordano, Elmar R. Burchardt, and David A. Brenner. The role of tgf-$\upbeta$1 in initiating hepatic stellate cell activation in vivo. *Journal of Hepatology*, 30(1):77–87, 1999.

[196] H. Yoshiji, S. Kuriyama, J. Yoshii, Y. Ikenaka, R. Noguchi, D. J. Hicklin, Y. Wu, K. Yanase, T. Namisaki, M. Yamazaki, H. Tsujinoue, H. Imazu, T. Masaki, and H. Fukui. Vascular endothelial growth factor and receptor interaction is a prerequisite for murine hepatic fibrogenesis. *Gut*, 52(9):1347–1354, 2003.

[197] Julio A. Aguirre-Ghiso, Yeriel Estrada, David Liu, and Liliana Ossowski. Erk(mapk) activity as a determinant of tumor growth and dormancy; regulation by p38(sapk). *Cancer research*, 63(7):1684–1695, 2003.

[198] Freya A. Goumas, Reinhild Holmer, Jan-Hendrik Egberts, Artur Gontarewicz, Carola Heneweer, Ulf Geisen, Charlotte Hauser, Maria-Margarete Mende, Karen Legler, Christoph Rocken, Thomas Becker, Georg H. Waetzig, Stefan Rose-John, and Holger Kalthoff. Inhibition of

il-6 signaling significantly reduces primary tumor growth and recurrencies in orthotopic xenograft models of pancreatic cancer. *International journal of cancer*, 137(5):1035–1046, 2015.

[199] P. C. Heinrich, I. Behrmann, G. Müller-Newen, F. Schaper, and L. Graeve. Interleukin-6-type cytokine signalling through the gp130/jak/stat pathway. *The Biochemical journal*, 334 ( Pt 2):297–314, 1998.

[200] Stefan Rose-John. Il-6 trans-signaling via the soluble il-6 receptor: importance for the pro-inflammatory activities of il-6. *International journal of biological sciences*, 8(9):1237–1247, 2012.

[201] J. C. Galicia, H. Tai, Y. Komatsu, Y. Shimada, K. Akazawa, and H. Yoshie. Polymorphisms in the il-6 receptor (il-6r) gene: strong evidence that serum levels of soluble il-6r are genetically influenced. *Genes and immunity*, 5(6):513–516, 2004.

[202] Clare Yellowley. Cxcl12/cxcr4 signaling and other recruitment and homing pathways in fracture repair. *BoneKEy reports*, 2:300, 2013.

[203] Kirsten Hattermann, Eric Holzenburg, Friederike Hans, Ralph Lucius, Janka Held-Feindt, and Rolf Mentlein. Effects of the chemokine cxcl12 and combined internalization of its receptors cxcr4 and cxcr7 in human mcf-7 breast cancer cells. *Cell and tissue research*, 357(1):253–266, 2014.

[204] Mohammad R. Hasan, Shirley H. Y. Ho, David A. Owen, and Isabella T. Tai. Inhibition of vegf induces cellular senescence in colorectal cancer cells. *International journal of cancer*, 129(9):2115–2123, 2011.

[205] Hira Lal Goel and Arthur M. Mercurio. Vegf targets the tumour cell. *Nature reviews. Cancer*, 13(12):871–882, 2013.

[206] Lanlan Yu, Xiumin Wu, Zhiyong Cheng, Chingwei V. Lee, Jennifer LeCouter, Claudio Campa, Germaine Fuh, Henry Lowman, and Napoleone Ferrara. Interaction between bevacizumab and murine vegf-a: a reassessment. *Investigative ophthalmology & visual science*, 49(2):522–527, 2008.

[207] Nicole M. Aiello, David L. Bajor, Robert J. Norgard, Amine Sahmoud, Neha Bhagwat, Minh N. Pham, Toby C. Cornish, Christine A. Iacobuzio-Donahue, Robert H. Vonderheide, and Ben Z. Stanger. Metastatic progression is associated with dynamic changes in the local microenvironment. *Nature communications*, 7:12819, 2016.

[208] Sebastian R. Nielsen, Valeria Quaranta, Andrea Linford, Perpetua Emeagi, Carolyn Rainer, Almudena Santos, Lucy Ireland, Takao Sakai, Keiko Sakai, Yong-Sam Kim, Dannielle Engle, Fiona Campbell, Daniel Palmer, Jeong Heon Ko, David A. Tuveson, Emilio Hirsch, Ainhoa Mielgo, and Michael C. Schmid. Macrophage-secreted granulin supports pancreatic cancer metastasis by inducing liver fibrosis. *Nature cell biology*, 18(5):549–560, 2016.

[209] Thomas R. Cox, Demelza Bird, Ann-Marie Baker, Holly E. Barker, Melisa W-Y Ho, Georgina Lang, and Janine T. Erler. Lox-mediated collagen crosslinking is responsible for fibrosis-enhanced metastasis. *Cancer research*, 73(6):1721–1732, 2013.

[210] Bastian Seubert, Barbara Grunwald, Julia Kobuch, Haissi Cui, Florian Schelter, Susanne Schaten, Jens T. Siveke, Ngee H. Lim, Hideaki Nagase, Nicole Simonavicius, Mathias Heikenwalder, Thomas Reinheckel, Jonathan P. Sleeman, Klaus-Peter Janssen, Percy A. Knolle, and Achim Kruger. Tissue inhibitor of metalloproteinases (timp)-1 creates a premetastatic niche in the liver through sdf-1/cxcr4-dependent neutrophil recruitment in mice. *Hepatology (Baltimore, Md.)*, 61(1):238–248, 2015.

[211] B. T. Sher, R. Bargatze, B. Holzmann, W. M. Gallatin, D. Matthews, N. Wu, L. Picker, E. C. Butcher, and I. L. Weissman. Homing receptors and metastasis. *Advances in cancer research*, 51:361–390, 1988.

[212] Ayuko Hoshino, Bruno Costa-Silva, Tang-Long Shen, Goncalo Rodrigues, Ayako Hashimoto, Milica Tesic Mark, Henrik Molina, Shinji Kohsaka, Angela Di Giannatale, Sophia Ceder, Swarnima Singh, Caitlin Williams, Nadine Soplop, Kunihiro Uryu, Lindsay Pharmer, Tari King, Linda Bojmar, Alexander E. Davies, Yonathan Ararso, Tuo Zhang, Haiying Zhang, Jonathan Hernandez, Joshua M. Weiss, Vanessa D. Dumont-Cole, Kimberly Kramer, Leonard H. Wexler, Aru Narendran, Gary K. Schwartz, John H. Healey, Per Sandstrom, Knut Jorgen Labori, Elin H. Kure, Paul M. Grandgenett, Michael A. Hollingsworth, Maria de Sousa, Sukhwinder Kaur, Maneesh Jain, Kavita Mallya, Surinder K. Batra, William R. Jarnagin, Mary S. Brady, Oystein Fodstad, Volkmar Muller, Klaus Pantel, Andy J. Minn, Mina J. Bissell, Benjamin A. Garcia, Yibin Kang, Vinagolu K. Rajasekhar, Cyrus M. Ghajar, Irina Matei, Hector Peinado, Jacqueline Bromberg, and David Lyden. Tumour exosome integrins determine organotropic metastasis. *Nature*, 527(7578):329–335, 2015.

[213] M. Katoh, M. Neumaier, R. Nezam, J. R. Izbicki, and U. Schumacher.

Correlation of circulating tumor cells with tumor size and metastatic load in a spontaneous lung metastasis model. *Anticancer research*, 24(3a):1421–1425, 2004.

[214] Hector Peinado, Haiying Zhang, Irina R. Matei, Bruno Costa-Silva, Ayuko Hoshino, Goncalo Rodrigues, Bethan Psaila, Rosandra N. Kaplan, Jacqueline F. Bromberg, Yibin Kang, Mina J. Bissell, Thomas R. Cox, Amato J. Giaccia, Janine T. Erler, Sachie Hiratsuka, Cyrus M. Ghajar, and David Lyden. Pre-metastatic niches: organ-specific homes for metastases. *Nature reviews. Cancer*, 2017.

[215] Generoso Uomo. Inflammatory pancreatic diseases in older patients: recognition and management. *Drugs & aging*, 20(1):59–70, 2003.

[216] Daniel Baylis, David B. Bartlett, Harnish P. Patel, and Helen C. Roberts. Understanding how we age: insights into inflammaging. *Longevity & healthspan*, 2(1):8, 2013.

[217] Elizabeth C. Little, Cindy Wang, Patricia M. Watson, Dennis K. Watson, David J. Cole, and E. Ramsay Camp. Novel immunocompetent murine models representing advanced local and metastatic pancreatic cancer. *The Journal of surgical research*, 176(2):359–366, 2012.

[218] Chetana Lim, Francois Cauchy, Daniel Azoulay, Olivier Farges, Maxime Ronot, and Marc Pocard. Tumour progression and liver regeneration–insights from animal models. *Nature reviews. Gastroenterology & hepatology*, 10(8):452–462, 2013.

[219] Pawel K. Mazur and Jens T. Siveke. Genetically engineered mouse models of pancreatic cancer: unravelling tumour biology and progressing translational oncology. *Gut*, 61(10):1488–1500, 2012.

[220] J. Mestas and C. C. W. Hughes. Of mice and not men: Differences between mouse and human immunology. *Journal of immunology (Baltimore, Md. : 1950)*, 172(5):2731–2738, 2004.

[221] B. S. Mitchell and U. Schumacher. Use of immunodeficient mice in metastasis research. *British journal of biomedical science*, 54(4):278–286, 1997.

[222] Richa Jain, Sandra Fischer, Stefano Serra, and Runjan Chetty. The use of cytokeratin 19 (ck19) immunohistochemistry in lesions of the pancreas, gastrointestinal tract, and liver. *Applied immunohistochemistry & molecular morphology : AIMM*, 18(1):9–15, 2010.

[223] R. S. Sellers, C. B. Clifford, P. M. Treuting, and C. Brayton. Immunological variation between inbred laboratory mouse strains: points to consider in phenotyping genetically immunomodified mice. *Veterinary pathology*, 49(1):32–43, 2012.

[224] J. M. Badia, S. A. Whawell, D. M. Scott-Coombes, P. D. Abel, R. C. N. Williamson, and J. N. Thompson. Peritoneal and systemic cytokine response to laparotomy. *British Journal of Surgery*, 83(3):347–348, 1996.

[225] S. Aosasa, S. Ono, H. Mochizuki, H. Tsujimoto, S. Osada, E. Takayama, S. Seki, and H. Hiraide. Activation of monocytes and endothelial cells depends on the severity of surgical stress. *World Journal of Surgery*, 24(1):10–16, 2000.

[226] Avraham Belizon, Emre Balik, Daniel L. Feingold, Marc Bessler, Tracey D. Arnell, Kenneth A. Forde, Patrick K. Horst, Suvinit Jain, Vesna Cekic, Irena Kirman, and Richard L. Whelan. Major abdominal surgery increases plasma levels of vascular endothelial growth factor: open more so than minimally invasive methods. *Annals of surgery*, 244(5):792–798, 2006.

[227] Jan-Hendrik Egberts, Vera Cloosters, Andreas Noack, Bodo Schniewind, Lutz Thon, Stefanie Klose, Bastian Kettler, Corinna von Forstner, Christian Kneitz, Jurgen Tepel, Dieter Adam, Harald Wajant, Holger Kalthoff, and Anna Trauzold. Anti-tumor necrosis factor therapy inhibits pancreatic tumor growth and metastasis. *Cancer research*, 68(5):1443–1450, 2008.

[228] Barba Resnick, Lisa P. Gwyther, and Karen A. Roberto, editors. *Resilience in aging: Concepts, research, and outcomes*. Springer, New York and Dordrecht and Heidelberg and London, 2011.

[229] Minglei Guo, Lei Gong, Lin He, and Lois Lehman-McKeeman. The expression of cancer-related genes in aging mouse liver is rxr-alpha and gender dependent. *Advanced Studies in Biology, Vol. 1, 2009,*, (2):61–83, 2009.

[230] Antonio Sica, Tiziana Schioppa, Alberto Mantovani, and Paola Allavena. Tumour-associated macrophages are a distinct m2 polarised population promoting tumour progression: potential targets of anti-cancer therapy. *European journal of cancer (Oxford, England : 1990)*, 42(6):717–727, 2006.

[231] Shawn Rose, Alexander Misharin, and Harris Perlman. A novel ly6c/ly6g-based strategy to analyze the mouse splenic myeloid compartment. *Cytometry. Part A : the journal of the International Society for Analytical Cytology*, 81(4):343–350, 2012.

[232] Fabrice Viol. Mechanisms of liver metastases in pancreatic ductal adenocarcinoma: Analysis of cancer stem cell properties in pancreatic ductal epithelial cells in dependence on the hepatic microenvironment: Master's thesis. 2015.

[233] M. G. P. STOKER, MOIRA SHEARER, and C. O'NEILL. Growth inhibition of polyoma-transformed cells by contact with static normal fibroblasts. *Journal of Cell Science*, (1/3), 1966.

[234] Wan-Chi Lin, Nirakar Rajbhandari, and Kay-Uwe Wagner. Cancer cell dormancy in novel mouse models for reversible pancreatic cancer: a lingering challenge in the development of targeted therapies. *Cancer research*, 74(8):2138–2143, 2014.

[235] Jasmine M. de Cock, Tsukasa Shibue, Anushka Dongre, Zuzana Keckesova, Ferenc Reinhardt, and Robert A. Weinberg. Inflammation triggers zeb1-dependent escape from tumor latency. *Cancer research*, 76(23):6778–6784, 2016.

[236] Li Ding, Matthew J. Ellis, Shunqiang Li, David E. Larson, Ken Chen, John W. Wallis, Christopher C. Harris, Michael D. McLellan, Robert S. Fulton, Lucinda L. Fulton, Rachel M. Abbott, Jeremy Hoog, David J. Dooling, Daniel C. Koboldt, Heather Schmidt, Joelle Kalicki, Qunyuan Zhang, Lei Chen, Ling Lin, Michael C. Wendl, Joshua F. McMichael, Vincent J. Magrini, Lisa Cook, Sean D. McGrath, Tammi L. Vickery, Elizabeth Appelbaum, Katherine Deschryver, Sherri Davies, Therese Guintoli, Li Lin, Robert Crowder, Yu Tao, Jacqueline E. Snider, Scott M. Smith, Adam F. Dukes, Gabriel E. Sanderson, Craig S. Pohl, Kim D. Delehaunty, Catrina C. Fronick, Kimberley A. Pape, Jerry S. Reed, Jody S. Robinson, Jennifer S. Hodges, William Schierding, Nathan D. Dees, Dong Shen, Devin P. Locke, Madeline E. Wiechert, James M. Eldred, Josh B. Peck, Benjamin J. Oberkfell, Justin T. Lolofie, Feiyu Du, Amy E. Hawkins, Michelle D. O'Laughlin, Kelly E. Bernard, Mark Cunningham, Glendoria Elliott, Mark D. Mason, Dominic M. Thompson, JR, Jennifer L. Ivanovich, Paul J. Goodfellow, Charles M. Perou, George M. Weinstock, Rebecca Aft, Mark Watson, Timothy J. Ley, Richard K. Wilson, and Elaine R. Mardis. Genome remodelling in a basal-like breast cancer metastasis and xenograft. *Nature*, 464(7291):999–1005, 2010.

[237] Marco Gerlinger, Andrew J. Rowan, Stuart Horswell, James Larkin, David Endesfelder, Eva Gronroos, Pierre Martinez, Nicholas Matthews, Aengus

Stewart, Patrick Tarpey, Ignacio Varela, Benjamin Phillimore, Sharmin Begum, Neil Q. McDonald, Adam Butler, David Jones, Keiran Raine, Calli Latimer, Claudio R. Santos, Mahrokh Nohadani, Aron C. Eklund, Bradley Spencer-Dene, Graham Clark, Lisa Pickering, Gordon Stamp, Martin Gore, Zoltan Szallasi, Julian Downward, P. Andrew Futreal, and Charles Swanton. Intratumor heterogeneity and branched evolution revealed by multiregion sequencing. *New England Journal of Medicine*, 366(10):883–892, 2012.

[238] R. T. Morgan, L. K. Woods, G. E. Moore, L. A. Quinn, L. McGavran, and S. G. Gordon. Human cell line (colo 357) of metastatic pancreatic adenocarcinoma. *International journal of cancer*, 25(5):591–598, 1980.

[239] Kideok Jin, Sunju Park, Daina Z. Ewton, and Eileen Friedman. The survival kinase mirk/dyrk1b is a downstream effector of oncogenic k-ras in pancreatic cancer. *Cancer research*, 67(15):7247–7255, 2007.

[240] Xiaobing Deng, Daina Z. Ewton, and Eileen Friedman. Mirk/dyrk1b maintains the viability of quiescent pancreatic cancer cells by reducing levels of reactive oxygen species. *Cancer research*, 69(8):3317–3324, 2009.

[241] Nirakar Rajbhandari, Wan-Chi Lin, Barbara L. Wehde, Aleata A. Triplett, and Kay-Uwe Wagner. Autocrine igf1 signaling mediates pancreatic tumor cell dormancy in the absence of oncogenic drivers. *Cell reports*, 18(9):2243–2255, 2017.

[242] Frank A. W. Coumans, Sabine Siesling, and Leon W. M. M. Terstappen. Detection of cancer before distant metastasis. *BMC cancer*, 13:283, 2013.

[243] Manuel Collado and Manuel Serrano. Senescence in tumours: evidence from mice and humans. *Nature reviews. Cancer*, 10(1):51–57, 2010.

[244] Boris Hinz, Sem H. Phan, Victor J. Thannickal, Andrea Galli, Marie-Luce Bochaton-Piallat, and Giulio Gabbiani. The myofibroblast: one function, multiple origins. *The American journal of pathology*, 170(6):1807–1816, 2007.

[245] Adil El Taghdouini, Mustapha Najimi, Pau Sancho-Bru, Etienne Sokal, and Leo A. van Grunsven. In vitro reversion of activated primary human hepatic stellate cells. *Fibrogenesis & tissue repair*, 8:14, 2015.

[246] T. Scholzen and J. Gerdes. The ki-67 protein: from the known and the unknown. *Journal of cellular physiology*, 182(3):311–322, 2000.

[247] Hermann E. Wasmuth, Frank Tacke, and Christian Trautwein. Chemokines in liver inflammation and fibrosis. *Seminars in liver disease*, 30(3):215–225, 2010.

[248] Marcello Maggio, Jack M. Guralnik, Dan L. Longo, and Luigi Ferrucci. Interleukin-6 in aging and chronic disease: A magnificent pathway. *The journals of gerontology. Series A, Biological sciences and medical sciences*, 61(6):575–584, 2006.

[249] Marina Lesina, Magdalena U. Kurkowski, Katharina Ludes, Stefan Rose-John, Matthias Treiber, Gunter Kloppel, Akihiko Yoshimura, Wolfgang Reindl, Bence Sipos, Shizuo Akira, Roland M. Schmid, and Hana Algul. Stat3/socs3 activation by il-6 transsignaling promotes progression of pancreatic intraepithelial neoplasia and development of pancreatic cancer. *Cancer cell*, 19(4):456–469, 2011.

[250] David J. J. Waugh and Catherine Wilson. The interleukin-8 pathway in cancer. *Clinical cancer research : an official journal of the American Association for Cancer Research*, 14(21):6735–6741, 2008.

[251] D. E. Hu, Y. Hori, and T.-P. D. Fan. Interleukln-8 stimulates angiogenesis in rats. *Inflammation*, 17(2):135–143, 1993.

[252] D. R. Smith, P. J. Polverini, S. L. Kunkel, M. B. Orringer, R. I. Whyte, M. D. Burdick, C. A. Wilke, and R. M. Strieter. Inhibition of interleukin 8 attenuates angiogenesis in bronchogenic carcinoma. *The Journal of experimental medicine*, 179(5):1409–1415, 1994.

[253] A. Harada, N. Mukaida, and K. Matsushima. Interleukin 8 as a novel target for intervention therapy in acute inflammatory diseases. *Molecular medicine today*, 2(11):482–489, 1996.

[254] R. Brew, J. S. Erikson, D. C. West, A. R. Kinsella, J. Slavin, and S. E. Christmas. Interleukin-8 as an autocrine growth factor for human colon carcinoma cells in vitro. *Cytokine*, 12(1):78–85, 2000.

[255] H. Takamori, Z. G. Oades, O. C. Hoch, M. Burger, and I. U. Schraufstatter. Autocrine growth effect of il-8 and groalpha on a human pancreatic cancer cell line, capan-1. *Pancreas*, 21(1):52–56, 2000.

[256] Hidenobu Kamohara, Masashi Takahashi, Takatoshi Ishiko, Michio Ogawa, and Hideo Baba. Induction of interleukin-8 (cxcl-8) by tumor necrosis factor-alpha and leukemia inhibitory factor in pancreatic carcinoma cells:

Impact of cxcl-8 as an autocrine growth factor. *International journal of oncology*, 31(3):627–632, 2007.

[257] F. Luppi, A. M. Longo, W. I. de Boer, K. F. Rabe, and P. S. Hiemstra. Interleukin-8 stimulates cell proliferation in non-small cell lung cancer through epidermal growth factor receptor transactivation. *Lung cancer (Amsterdam, Netherlands)*, 56(1):25–33, 2007.

[258] Juan C. Acosta, Ana O'Loghlen, Ana Banito, Maria V. Guijarro, Arnaud Augert, Selina Raguz, Marzia Fumagalli, Marco Da Costa, Celia Brown, Nikolay Popov, Yoshihiro Takatsu, Jonathan Melamed, Fabrizio Di d'Adda Fagagna, David Bernard, Eva Hernando, and Jesus Gil. Chemokine signaling via the cxcr2 receptor reinforces senescence. *Cell*, 133(6):1006–1018, 2008.

[259] Colin W. Steele, Saadia A. Karim, Joshua D. G. Leach, Peter Bailey, Rosanna Upstill-Goddard, Loveena Rishi, Mona Foth, Sheila Bryson, Karen McDaid, Zena Wilson, Catherine Eberlein, Juliana B. Candido, Mairi Clarke, Colin Nixon, John Connelly, Nigel Jamieson, C. Ross Carter, Frances Balkwill, David K. Chang, T. R. Jeffry Evans, Douglas Strathdee, Andrew V. Biankin, Robert J. B. Nibbs, Simon T. Barry, Owen J. Sansom, and Jennifer P. Morton. Cxcr2 inhibition profoundly suppresses metastases and augments immunotherapy in pancreatic ductal adenocarcinoma. *Cancer cell*, 29(6):832–845, 2016.

[260] Zahidul Islam, Jennifer S. Gray, and James J. Pestka. p38 mitogen-activated protein kinase mediates il-8 induction by the ribotoxin deoxynivalenol in human monocytes. *Toxicology and applied pharmacology*, 213(3):235–244, 2006.

[261] Swarnali Acharyya, Thordur Oskarsson, Sakari Vanharanta, Srinivas Malladi, Juliet Kim, Patrick G. Morris, Katia Manova-Todorova, Margaret Leversha, Nancy Hogg, Venkatraman E. Seshan, Larry Norton, Edi Brogi, and Joan Massague. A cxcl1 paracrine network links cancer chemoresistance and metastasis. *Cell*, 150(1):165–178, 2012.

[262] Thomas J. Bartosh, Mujib Ullah, Suzanne Zeitouni, Joshua Beaver, and Darwin J. Prockop. Cancer cells enter dormancy after cannibalizing mesenchymal stem/stromal cells (mscs). *Proceedings of the National Academy of Sciences of the United States of America*, 113(42):E6447–E6456, 2016.

[263] M. Singer and P. J. Sansonetti. Il-8 is a key chemokine regulating neutrophil

recruitment in a new mouse model of shigella-induced colitis. *Journal of immunology (Baltimore, Md. : 1950)*, 173(6):4197–4206, 2004.

[264] Fei Teng, Wen-Yan Tian, Ying-Mei Wang, Yan-Fang Zhang, Fei Guo, Jing Zhao, Chao Gao, and Feng-Xia Xue. Cancer-associated fibroblasts promote the progression of endometrial cancer via the sdf-1/cxcr4 axis. *Journal of hematology & oncology*, 9:8, 2016.

[265] Jennifer M. Burns, Bretton C. Summers, Yu Wang, Anita Melikian, Rob Berahovich, Zhenhua Miao, Mark E. T. Penfold, Mary Jean Sunshine, Dan R. Littman, Calvin J. Kuo, Kevin Wei, Brian E. McMaster, Kim Wright, Maureen C. Howard, and Thomas J. Schall. A novel chemokine receptor for sdf-1 and i-tac involved in cell survival, cell adhesion, and tumor development. *The Journal of experimental medicine*, 203(9):2201–2213, 2006.

[266] Magda Kucia, Kacper Jankowski, Ryan Reca, Marcin Wysoczynski, Laura Bandura, Daniel J. Allendorf, Jin Zhang, Janina Ratajczak, and Mariusz Z. Ratajczak. Cxcr4-sdf-1 signalling, locomotion, chemotaxis and adhesion. *Journal of molecular histology*, 35(3):233–245, 2004.

[267] M. Clauss. Molecular biology of the vegf and the vegf receptor family. *Seminars in thrombosis and hemostasis*, 26(5):561–569, 2000.

[268] R. R. Somani and U. V. Bhanushali. Targeting angiogenesis for treatment of human cancer. *Indian journal of pharmaceutical sciences*, 75(1):3–10, 2013.

[269] Vito Longo, Oronzo Brunetti, Antonio Gnoni, Stefano Cascinu, Giampietro Gasparini, Vito Lorusso, Domenico Ribatti, and Nicola Silvestris. Angiogenesis in pancreatic ductal adenocarcinoma: A controversial issue. *Oncotarget*, 7(36):58649–58658, 2016.

[270] Min Li, Hui Yang, Hong Chai, William E. Fisher, Xiaoping Wang, F. Charles Brunicardi, Qizhi Yao, and Changyi Chen. Pancreatic carcinoma cells express neuropilins and vascular endothelial growth factor, but not vascular endothelial growth factor receptors. *Cancer*, 101(10):2341–2350, 2004.

[271] Yong Tang, Man-Tzu Wang, Yakun Chen, Dianer Yang, Mingxin Che, Kenneth V. Honn, Gregory D. Akers, Stephen R. Johnson, and Daotai Nie. Downregulation of vascular endothelial growth factor and induction of tumor dormancy by 15-lipoxygenase-2 in prostate cancer. *International journal of cancer*, 124(7):1545–1551, 2009.

[272] Liu Yang, Junghee Kwon, Yury Popov, Gabriella B. Gajdos, Tamas Ordog, Rolf A. Brekken, Debabrata Mukhopadhyay, Detlef Schuppan, Yan Bi, Douglas Simonetto, and Vijay H. Shah. Vascular endothelial growth factor promotes fibrosis resolution and repair in mice. *Gastroenterology*, 146(5):1339–50.e1, 2014.

[273] Hedy Lee Kindler, Donna Niedzwiecki, Donna Hollis, Susan Sutherland, Deborah Schrag, Herbert Hurwitz, Federico Innocenti, Mary Frances Mulcahy, Eileen O'Reilly, Timothy F. Wozniak, Joel Picus, Pankaj Bhargava, Robert J. Mayer, Richard L. Schilsky, and Richard M. Goldberg. Gemcitabine plus bevacizumab compared with gemcitabine plus placebo in patients with advanced pancreatic cancer: phase iii trial of the cancer and leukemia group b (calgb 80303). *Journal of clinical oncology : official journal of the American Society of Clinical Oncology*, 28(22):3617–3622, 2010.

[274] Philippe Rougier, Hanno Riess, Robert Manges, Petr Karasek, Yves Humblet, Carlo Barone, Armando Santoro, Sylvie Assadourian, Laurence Hatteville, and Philip A. Philip. Randomised, placebo-controlled, double-blind, parallel-group phase iii study evaluating aflibercept in patients receiving first-line treatment with gemcitabine for metastatic pancreatic cancer. *European journal of cancer (Oxford, England : 1990)*, 49(12):2633–2642, 2013.

[275] Angus W. Thomson and Michael T. Lotze, editors. *The cytokine handbook*, volume v.1 of *Cytokine Handbook*. Academic Press, Amsterdam and Boston, 4th ed. edition, 2003.

[276] Mara H. Sherman, Ruth T. Yu, Dannielle D. Engle, Ning Ding, Annette R. Atkins, Herve Tiriac, Eric A. Collisson, Frances Connor, Terry van Dyke, Serguei Kozlov, Philip Martin, Tiffany W. Tseng, David W. Dawson, Timothy R. Donahue, Atsushi Masamune, Tooru Shimosegawa, Minoti V. Apte, Jeremy S. Wilson, Beverly Ng, Sue Lynn Lau, Jenny E. Gunton, Geoffrey M. Wahl, Tony Hunter, Jeffrey A. Drebin, Peter J. O'Dwyer, Christopher Liddle, David A. Tuveson, Michael Downes, and Ronald M. Evans. Vitamin d receptor-mediated stromal reprogramming suppresses pancreatitis and enhances pancreatic cancer therapy. *Cell*, 159(1):80–93, 2014.

[277] Cyrus M. Ghajar. Metastasis prevention by targeting the dormant niche. *Nature reviews. Cancer*, 15(4):238–247, 2015.

[278] Megan K. Ruhland, Andrew J. Loza, Aude-Helene Capietto, Xianmin Luo, Brett L. Knolhoff, Kevin C. Flanagan, Brian A. Belt, Elise Alspach, Kathleen Leahy, Jingqin Luo, Andras Schaffer, John R. Edwards, Gregory Longmore, Roberta Faccio, David G. DeNardo, and Sheila A. Stewart. Stromal

senescence establishes an immunosuppressive microenvironment that drives tumorigenesis. *Nature communications*, 7:11762, 2016.

[279] Jan R. Dorr, Yong Yu, Maja Milanovic, Gregor Beuster, Christin Zasada, J. Henry M. Dabritz, Jan Lisec, Dido Lenze, Anne Gerhardt, Katharina Schleicher, Susanne Kratzat, Bettina Purfurst, Stefan Walenta, Wolfgang Mueller-Klieser, Markus Graler, Michael Hummel, Ulrich Keller, Andreas K. Buck, Bernd Dorken, Lothar Willmitzer, Maurice Reimann, Stefan Kempa, Soyoung Lee, and Clemens A. Schmitt. Synthetic lethal metabolic targeting of cellular senescence in cancer therapy. *Nature*, 501(7467):421–425, 2013.

# List of Figures

# A. Appendix

## A.1. Supplementary data

### A.1.1. Liver metastases from PDAC bearing KPC mice

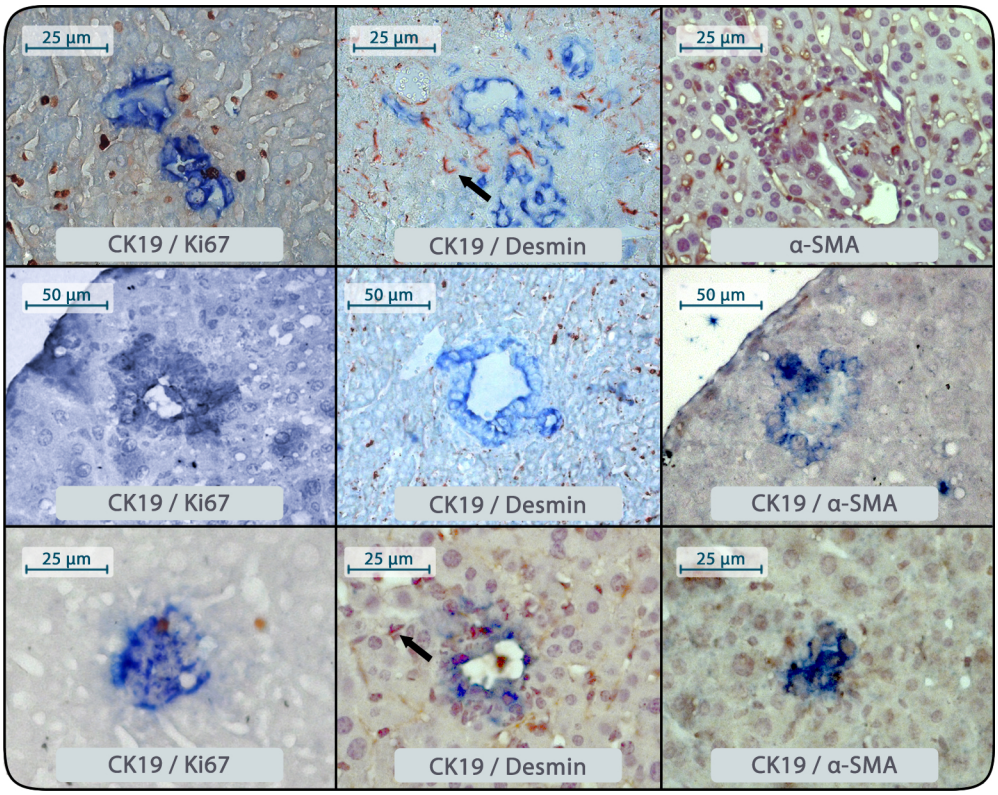


**Figure A.1.: Additional representative images of immunohistochemically stained micrometastases in livers of PDAC bearing KPC mice.** Liver sections of mice harboring endogenous advanced PDAC (n=13) were examined for the presence of micrometastases (lesion diameter $\leq$ 200 µm) and macrometastases (lesion diameter $>$ 200 µm) by staining of Cytokeratin-19, Ki67, α-SMA (for detection of HMFs) and desmin (for detection of HSCs)(**cf. Figure 4.1**). Representative images of serial sections of micrometastases stained in single or double stainings (as indicated) are shown. Black arrows indicate HSCs, representatively.

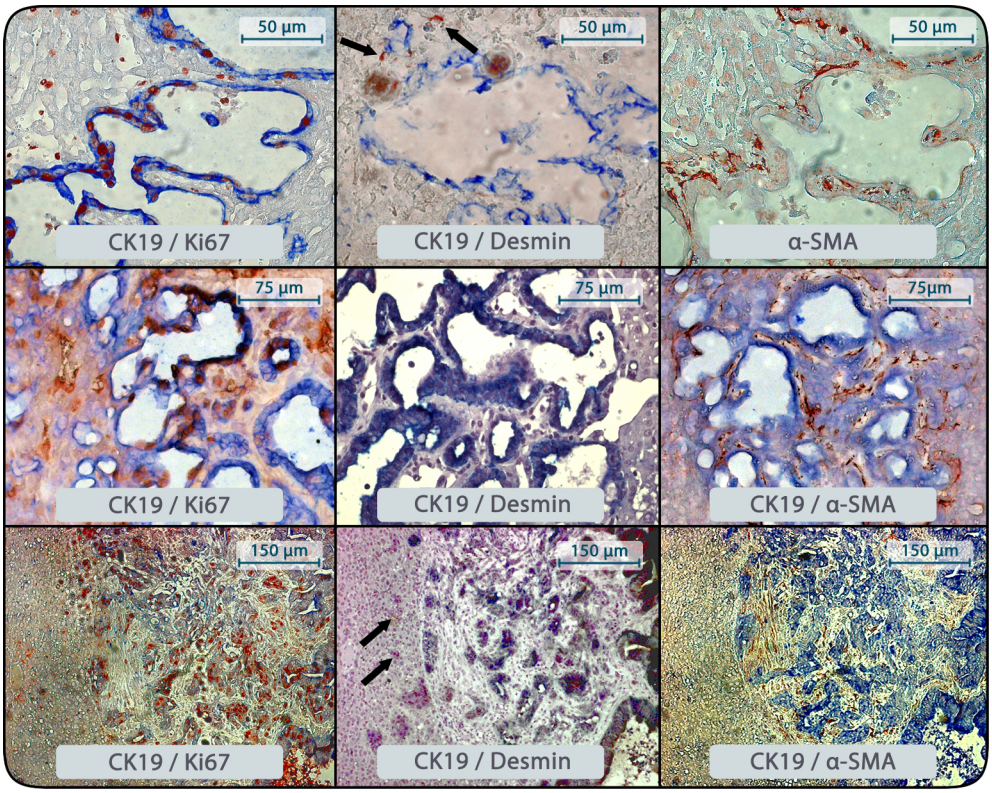


**Figure A.2.: Additional representative images of immunohistochemically stained macrometastases in livers of PDAC bearing KPC mice.** Liver sections of mice harboring endogenous advanced PDAC (n=13) were examined for the presence of micrometastases (lesion diameter $\leq$ 200 µm) and macrometastases (lesion diameter $>$ 200 µm) by staining of Cytokeratin-19, Ki67, α-SMA (for detection of HMFs) and desmin (for detection of HSCs)(**cf. Figure 4.1**). Representative images of serial sections of macrometastases stained in single or double stainings (as indicated) are shown. Black arrows indicate HSCs, representatively.

### A.1.2. Realtime Life Cell Imaging videos

Supplementary Video 1 and 2 are provided on a CD supplied with this work.

### A.1.3. Supplementary Video 1

**Panc1 cells remain non-dividing during prolonged HSC-coculture.** After 6 days coculture with HSC, coculture of Panc1 cells was prolonged for further 6 days in the presence of fresh HSC (HSC-HSC). Growth behavior was monitored by real-time microscopy particularly focusing on cells with QAP-associated enlarged and flattened morphology. Cells with flattened and enlarged QAP morphology remaining non-dividing are encircled in red. The representative video covers 144 hours of coculture recorded at 200-fold magnification.

### A.1.4. Supplementary Video 2

**HSC-mediated QAP in Panc1 cells is reversed in the presence of HMF.** After 6 days coculture with HSC, coculture of Panc1 cells was prolonged for further 6 days in the presence of fresh HMF (HSC-HMF). Growth behavior was monitored by real-time microscopy particularly focusing on cells with the QAP-associated flattened morphology. Cells with enlarged, flattened morphology regaining proliferative activity are encircled in black. The representative video covers 144 hours of coculture recorded at 200-fold magnification.

## A.2. Curriculum vitae

| | |
|---|---|
| **Personal Data** | |
| | Lennart Terje Niklas Lenk<br>Born: 14.07.1987 in Hamburg<br>Nationality: German |
| **Doctoral Studies** | |
| Since Juli 2013 | Doctoral studies (PhD)<br>Group: Inflammatory Carcinogenesis<br>Institute of Experimental Cancer Research<br>Christian-Albrechts-Universität of Kiel<br>within the DFG-Project: SE 1831/2-3<br>Supervisor: Prof. Dr. Susanne Sebens |
| **Studies** | |
| Oct. 2009 - Jun. 2013 | **Studies of biology** (10 semesters)<br>Christian-Albrechts-Universität of Kiel |
| Oct. 2012 - Jun. 2013 | **Master's Thesis**<br>Institute for Experimental Medicine<br>Christian-Albrechts-Universität of Kiel<br>"Einfluss hepatischer Sternzellen und Myofibroblasten auf den Phänotyp und das Verhalten von Pankreasadenokarzinomzellen"<br>Supervisor: Prof. Dr. Susanne Sebens |
| Feb. 2011 - Aug. 2011 | **Bachelor's Thesis**<br>Zoological Institute<br>Christian-Albrechts-Universität of Kiel<br>"Regulation des Lebenszyklus der Ohrenqualle *Aurelia aurita*"<br>Supervisor: Prof. Dr. Dr. Thomas C.G. Bosch |
| **Educational Training** | |
| June 2007 | Abitur<br>Marion-Dönhoff-Gymnasium, Mölln |

## A.3. Publications

### A.3.1. Thesis related publications

**Lenk L**, Pein M, Will O, Gomez B, Viol F, Hauser C, Egberts JH, Gundlach JP, Helm O, Tiwari S, Weiskirchen R, Rose-John S, Röcken C, Mikulits W, Wenzel P, Schneider G, Saur D, Schäfer H, Sebens S. The hepatic microenvironment essentially determines tumor cell dormancy and metastatic outgrowth of pancreatic ductal adenocarcinoma. *OncoImmunology* (In press)

Mußbach F, Ungefroren H, Günther B, Katenkamp K, Henklein P, Westermann M, Settmacher U, **Lenk L**, Sebens S, Müller JP, Böhmer FD, Kaufmann R. Proteinase-activated receptor 2 (PAR2) in hepatic stellate cells - evidence for a role in hepatocellular carcinoma growth in vivo. *Mol Cancer.* 2016 Jul 29;15(1):54.

Genrich G, Kruppa M, **Lenk L**, Helm O, Broich A, Freitag-Wolf S, Röcken C, Sipos B, Schäfer H, Sebens S. The anti-oxidative transcription factor Nuclear factor E2 related factor-2 (Nrf2) counteracts TGF-β1 mediated growth inhibition of pancreatic ductal epithelial cells - Nrf2 as determinant of protumorigenic functions of TGF-β1. *BMC Cancer.* 2016 Feb 25;16:155.

**Lenk L**, Pein M, Mikulits W, Weiskirchen R, Hengstler J, Wenzel P, Schneider G, Sebens S. Alterations of the hepatic microenvironment modulate the phenotype and behavior of disseminated pancreatic ductal epithelial cells. *Clinical and Experimental Metastasis* 2015 32(3):216-217.

Goebel L, Grage-Griebenow E, Gorys A, Helm O, Genrich G, **Lenk L**, Wesch D, Ungefroren H, Freitag-Wolf S, Sipos B, Röcken C, Schäfer H, Sebens S. CD4+ T cells potently induce epithelial-mesenchymal-transition in premalignant and malignant pancreatic ductal epithelial cells - novel implications of CD4+ T cells in pancreatic cancer development. *Oncoimmunology.* 2015 Jan 22;4(4):e1000083.

## A.3.2. Further publications

Schewe DM, Alsadeq A, Sattler C, **Lenk L**, Vogiatzi F, Cario G, Vieth S, Valerius T, Rosskopf S, Meyersieck F, Alten J, Schrappe M, Gramatzki M, Peipp M, Kellner C. An Fc engineered CD19 antibody eradicates MRD in patient-derived MLL-rearranged acute lymphoblastic leukemia xenografts. *Blood*. 2017 Jul 11.

Kreutzer C, Peters S, Schulte DM, Fangmann D, Türk K, Wolff S, van Eimeren T, Ahrens M, Beckmann J, Schafmayer C, Becker T, Kerby T, Rohr A, Riedel C, Heinsen FA, Degenhardt F, Franke A, Rosenstiel P, Zubek N, Henning C, Freitag-Wolf S, Dempfle A, Psilopanagioti A, Petrou-Papadaki H, **Lenk L**, Jansen O, Schreiber S, Laudes M. Hypothalamic Inflammation in Human Obesity is Mediated by Environmental and Genetic Factors. *Diabetes*. 2017 Jun 2

## A.4. Congress presentations and awards

**Lenk L**, Pein M, Knaack H, Viol F, Mikulits W, Weiskirchen R, Hengstler J, Wenzel P, Schneider G, Saur D and Sebens S. Metastasierung des duktalen Pankreasadenokarzinoms - Alterationen der Lebermikroumgebung beeinflussen das Verhalten und den Phänotyp disseminierter Pankreasgangepithelzellen
*35. Jahrestagung des DPC 2015, Rostock* (Oral presentation, awarded with a travel stipend)

**Lenk L**, Viol F, Knaack H, Pein M, Fabian A, Mikulits W, Weiskirchen R, Wenzel P, Schneider G, Saur D and Sebens S. Sleep is the enemy: cellular dormancy and cancer stem cell properties are influenced by hepatic alterations in disseminated pancreatic ductal epithelial cells.
*Pancreatic Cancer Symposium 2015, Marseille* (Oral presentation)

Viol F, **Lenk L**, Knaack H, Pein M, Fabian A, Mikulits W, Weiskirchen R, Wenzel P, Schneider G, Saur D and Sebens S. Cellular dormancy and cancer stem cell properties are influenced by hepatic alterations in disseminated pancreatic ductal epithelial cells.
*DKFZ-ZMBH Alliance FORUM 2015: Tumor Microenvironment, Metabolism and Metastasis, Heidelberg*

Knaack H, Viol F, **Lenk L**, Hengstler J, Will O, Hauser C, Gundlach J.-P and Sebens S. Die hepatische Mikroumgebung beeinflusst das Krebsstammzellpotenzial disseminierter Pankreasgangepithelzellen sowie ihr Wachstumsverhalten in vivo
*37. Jahrestagung des DPC 2017, Greifswald* (awarded best poster)

Tietgen M, Damm T, **Lenk L**, Desel C, Sebens S, Gluer C-C, Tiwari S. Evidence that CD146 positive bone marrow stromal cells in bone metastases have an inhibitory role in regulating tumor growth
*43rd Annual European Calcified Tissue Society Congress 2016, Rom*

Knaack H, **Lenk L**, Viol F, Fabian A, Buttlar J, Mikulits W, Schäfer H and Sebens S. Metastasierung des duktalen Pankreasadenokarzinoms – die hepatische Mikroumgebung beeinflusst Wachstumsverhalten und Krebsstammzelleigenschaften disseminierter Pankreasgangepithelzellen über die Modulation des Metabolismus
*36. Jahrestagung des DPC 2016, München/Freising*

Fabian A, **Lenk L**, Viol F, Mikulits W, Schäfer H, Sebens S. Metastasierung des duktalen Pankreasadenokarzinoms – Alterationen der Lebermikroumgebung beeinflussen den Metabolismus und das Wachstumsverhalten disseminierter Pankreasgangepithelzellen
*70. Jahrestagung der Deutschen Gesellschaft für Gastroenterologie, Verdauungs- und Stoffwechselkrankheiten mit Sektion Endoskopie 2015, Leipzig*

Arfmann-Knübel S, Kruppa M, Großmann M, **Lenk L**, Helm O, Sebens S, Schäfer H. Einfluss des anti-oxidativen Transkriptionsfaktors Nuclear factor E2 related factor-2 (Nrf2) auf die Migration und EMT von benignen und malignen Pankreasgangepithelzellen
*68. Jahrestagung der Deutschen Gesellschaft für Verdauungs- und Stoffwechselkrankheiten mit Sektion Endoskopie 2013, Nürnberg*

## A.5. Acknowledgements

*-As it enables me to be even more sincere, I would like to express my gratitude in my mother tongue-*

Mein ausgesprochener und größter Dank gilt meiner Doktormutter, Prof. Dr. Susanne Sebens. Ich bedanke mich herzlich für eine hervorragende Betreuung, für inspirierende, motivierende und auch kritische Diskussionen und Denkanstöße. Ich danke ihr für die Bereitstellung des Projekts, das in mich gesetzte Vertrauen und das unvergleichliche Arbeitsklima.

Ein großer Dank geht an Prof. Dr. Thomas Röder, der sich als zweiter Gutachter für diese Arbeit zur Verfügung gestellt hat.

Ich möchte mich herzlich bei der Arbeitsgruppe *Inflammatorische Karzinogenese* bedanken. Ich danke Hendrike Knaack, Lauritz Miarka, Beatriz Gomez, Sascha Rahn, Lisa Goebel, Geeske Genrich, Vivien Zimmermann, Marcus Kruppa, Simon Stegner und Jann Buttlar. Ein besonderer Dank gilt Dr. Ole Helm, der mich in die Arbeitsgruppe eingeführt hat, und stets ein toller Kollege war. Besonders hervorgehoben sei auch Dagmar Leisner, die eine unermüdliche, geschickte und außerordentlich liebenswerte technische Unterstützung war. Am Herzen liegt es mir, mich bei den Menschen zu bedanken, an deren Betreuung ich größeren Anteil haben durfte. Es war ein Glück mit solch motivierten, klugen und freundlichen Menschen zusammenarbeiten zu können. Ich danke Maren Pein, Fabrice Viol und Alexander Fabian für die spannenden Tage im Labor und die entstandenen Freundschaften.

Bedanken möchte ich mich auch bei Dr. Olga Will und Dr. Sanjay Tiwari vom MOIN-CC für die Unterstützung und Supervision beim Kleintierimaging. An dieser Stelle sei auch den Chirurgen Prof. Dr. Jan-Hendrik Egberts, Dr. Jan-Paul Gundlach und Dr. Charlotte Hauser gedankt. Auch danke ich den zahlreichen Kooperationspartnern, die einen wichtigen Anteil am Fortschritt dieser Arbeit tragen. Gedankt sei Prof. Dr. Dieter Saur (TU München), Prof. Dr. Heiner Schäfer (Uni Kiel), Prof. Dr. Ralf Weiskirchen (RTWH Aachen), Prof. Dr. Wolfgang Mikulits (Uni Wien) Prof. Dr. Günter Schneider (TU München), Sandra Krüger und Prof. Dr. Christoph Röcken (UKSH Kiel).

Ich danke meinen großartigen Freunden, die immer verständnisvoll waren und mir den Rücken in anstrengenden Zeiten gestärkt haben. Besonders danke ich Stephanie Brombacher.

Ein wichtiges Anliegen ist es mir, meiner Familie zu danken, die es mir ermöglicht hat, diesen Weg zu gehen und mich stets bedingungslos unterstützt hat. Ohne Susann, Andreas, Sinnikka, Målin und Anthony wäre diese Arbeit nicht möglich gewesen. Danke!

## A.6. Erklärung

Hiermit erkläre ich an Eides Statt, dass die vorliegende Dissertation unter Einhaltung der Regeln guter wissenschaftlicher Praxis der Deutschen Forschungsgemeinschaft entstanden ist und ich keine anderen als die angegebenen Hilfsmittel und Quellen benutzt habe. Ich versichere weiterhin, dass ich außer der wissenschaftlichen Beratung durch meine Doktormutter Prof. Dr. Susanne Sebens keine Hilfe in Anspruch genommen habe. Diese Abhandlung hat nicht an anderer Stelle im Rahmen eines Prüfungsverfahrens vorgelegen. Ich erkläre, dass ich noch keinen Promotionsversuch vorgenommen habe. Teile dieser Dissertation wurden bereits zur Publikation eingereicht.

Kiel, den 16. Oktober 2017 Lennart Terje Niklas Lenk